Proteomic Profiling of Animal Models of Motor Neuron Disease and Muscular Dystrophy

Submitted to Maynooth University for the degree of Doctor of Philosophy

Maynooth University
National University of Ireland Maynooth

Ashling Holland, B. Sc

March 2015

Supervisor

Professor Kay Ohlendieck
Department of Biology
Maynooth University
NUI Maynooth
Co. Kildare

Co-Supervisor

Doctor Paul Dowling
Department of Biology
Maynooth University
NUI Maynooth
Co. Kildare

Head of Department

Professor Paul Moynagh
Department of Biology
Maynooth University
NUI Maynooth
Co. Kildare

TABLE OF CONTENTS

LIST OF FIGURES

LIST OF TABLES

PUBLICATIONS

Peer-reviewed papers

Holland A. and Ohlendieck K. 2013. Proteomic profiling of the contractile apparatus from skeletal muscle. *Expert Reviews of Proteomics.* 10, 239-57.

Holland A., Carberry S. and Ohlendieck K. 2013. Proteomics of the dystrophin-glycoprotein complex and dystrophinopathy. *Current Protein & Peptide Science.* 14, 680-697.

Holland A., Dowling P., Zweyer M., Swandulla D., Henry, M., Clynes, M. and Ohlendieck K. 2013. Proteomic profiling of cardiomyopathic tissue from the aged *mdx* model of Duchenne muscular dystrophy reveals a drastic decrease in laminin, nidogen and annexin. *Proteomics.* 15, 2312-23.

Jockusch H., **Holland A.,** Staunton L., Schmitt-John T., Heimann P., Dowling, P. and Ohlendieck K. 2013. Pathoproteomics of testicular tissue deficient in the GARP component VPS54. The wobbler mouse model of globozoospermia. *Proteomics*. 14, 839–852.

Jarmuda, S., McMahon, F., Zaba, R., O'Reilly, N., Jakubowicz, O., **Holland, A.,** Szkaradkiewicz, A. and Kavanagh, K. 2013. Correlation between serum reactivity to Demodex-associated Bacillus oleronius proteins, and altered sebum levels and Demodex populations in erythematotelangiectatic rosacea patients. *Journal of Medical Microbiology.* 63, 258-62.

Holland, A. and Ohlendieck, K. 2014. Proteomic profiling of the dystrophin-deficient *mdx* heart, a phenocopy of dystrophinopathy-associated cardiomyopathy. *BioMed Research International.* Article ID: 24619. 15 pages.

Dowling, P., **Holland, A.** and Ohlendieck, K. 2014. Masss spectrometry-based identification of proteomic biomarkers of dystrophinopathies. *Journal of Neuromuscular Diseases.* 1, 15–40.

Holland, A., Dowling, P. and Ohlendieck, K. 2014. New pathobiochemical insights into dystrophinopathy from the proteomics of senescent *mdx* mouse muscle. *Frontiers in Aging Neuroscience.* 3, 109.

Holland, A., Schmitt-John, T., Dowling, P., Jockusch, H. and Ohlendieck, K. 2014. Intricate effects of primary motor neuropathy on contractile proteins and metabolic muscle enzymes as revealed by label-free mass spectrometry. *Bioscience Reports.* 34, Article ID: e00119.

Holland, A. and Ohlendieck, K. 2014. Proteomic identification of muscle-associated biomarkers of amyotrophic lateral sclerosis using the wobbler mouse model of primary motor neuronopathy. *Journal of Integrated OMICS.* 4, 57-68.

Holland, A. and Ohlendieck, K. 2014. Proteomic profiling of calsequestrin and the Ca^{2+} -related damage pathway in dystrophinopathy. *Calcium Signalling.* 1, 60-69.

Holland, A. and Ohlendieck, K. 2015. Comparative profiling of the sperm proteome. *Proteomics.* 15, 632-648.

Holland, A., Dowling, P., Meleady, P., Henry, M., Zweyer, M., Mundegar, R., Swandulla, D. and Ohlendieck, K. 2015. Label-free mass spectrometric analysis of the *mdx-4cv* diaphragm identifies the matricellular protein periostin as a potential factor involved in the dystrophinopathy-related fibrosis. *Proteomics.* doi: 10.1002/pmic.201400471. In press.

Holland, A. and Ohlendieck, K. 2015. Comparative proteomics for studying muscular dystrophy: Intrinsic biological and analytical issues associated with the systematic utilization of tissue specimens. *Journal of Proteomics and Bioinformatics*. S10, 002. In press.

Holland, A., Henry, M., Meleady, P., Winkler, C.K., Krautwalk, M., Brinkmeier, H. and Ohlendieck, K. 2015. Comparative label-free mass spectrometric analysis of mildly versus severely affect *mdx* mouse skeletal muscle identifies annexin, lamin and vimentin as universal dystrophic markers. *Molecules*. 20, 11317-11344. In press.

Holland, A., Murphy, S., Dowling, P. and Ohlendeick, K. 2016. Pathoproteomic profiling of the skeletal muscle matrisome in dystrophinopathy-associated myofibrsis. *Proteomics*. Invited review for the '*Annual Reviews Issue of Proteomics*' special issue for February 2016. In press.

PRESENTATIONS

Departmental Lab Meeting Series

2013 Proteomic profiling of cardiomyopathic tissue from the *mdx* mouse. **Holland, A.** 2013. Departmental Lab Meeting Series, Maynooth University. **Oral presentation.**

2014 Proteomic profiling of the wobbler mouse model of motor-neuron disease. **Holland, A.** 2014. Departmental Lab Meeting Series, Maynooth University. **Oral presentation.**

Maynooth University Biology Research Day

2012 Comparative biochemical and proteomic analysis of muscle tissue from animal models of neuromuscular disorders. **Holland, A.,** Dowling, P. and Ohlendieck, K. 2012. Maynooth University. **Poster.**

2013 Proteomic profiling of cardiomyopathic tissue from the aged *mdx* model of Duchenne muscular dystrophy. **Holland, A.** and Ohlendieck, K. 2013. Maynooth University. **Poster.**

2014 Proteomic profiling of skeletal muscle from the wobbler mouse model of motor neuron disease using label-free mass spectrometry. **Holland, A.,** Schmitt-John, T., Dowling, P., Meleady, P., Henry, M. and Ohlendieck, K. 2014. Maynooth University. **Poster.**

2015 Establishing a protein biomarker signature for X-linked muscular dystrophy. **Holland, A.** and Ohlendieck, K. 2015. Maynooth University. **Poster.**

BioAT Research Day

2012 Comparative biochemical and proteomic analysis of muscle tissue from animal models of neuromuscular disorders. **Holland, A.,** Dowling, P. and Ohlendieck, K. BioAT Research Day 2012, Royal College of Surgeons Ireland. **Poster.**

2013 Proteomic profiling of cardiomyopathic tissue from the aged *mdx* model of Duchenne muscular dystrophy. **Holland, A.** BioAT Research Day 2013, Maynooth University. **Oral presentation.**

2014 Proteomic profiling of skeletal muscle from the wobbler mouse model of motor neuron disease using label-free mass spectrometry. **Holland, A.,** Dowling, P., Schmitt-John, T., Henry, M., Meleady, M. and Ohlendieck, K. BioAT Research Day 2014, BioAT Research Day 2014, Dublin City University. **Poster.**

2015 Establishing a protein biomarker signature for X-linked muscular dystrophy. **Holland, A.** BioAT Research Day 2013, IT Tallaght. **Abstract.**

International Presentations

2014 Proteomic profiling of the wobbler mouse model of motor-neuron disease. **Holland, A.** 2014. University College London, UCL, London, England, U.K. **Oral presentation.**

National Presentations

2015 Establishment of a proteomic biomarker signature for X-linked muscular dystrophy: Identification of novel integral muscle proteins by mass spectrometry-based proteomics. **Holland, A.** 2015. Muscular Dystrophy Ireland, MDI, Dublin, Ireland. **Oral presentation.**

Conferences

2013 Proteomic analysis of cardiomyopathic tissue from the aged *mdx* model of Duchenne muscular dystrophy. **Holland, A.** and Ohlendieck, K. 2013. International Congress of the World Muscle Society, Asilomar Conference Grounds, California, U.S.A. **Poster.** *Awarded WMS fellowship

2014 Proteomic profiling of skeletal muscle from the wobbler mouse model of motor neuron disease using label-free mass spectrometry. **Holland, A.** and Ohlendieck, K. 2014. European Muscle Conference, Salzburg, Austria. **Poster.**

2015 Irish Mass Spectrometry Society Annual Conference. Dublin, Ireland. **Attended.**

2015 Muscular Dystrophy UK, Cross Border Conference. Belfast, Northern Ireland. **Attended.**

ABSTRACTS

Holland, A. and Ohlendieck, K. 2013. Proteomic analysis of cardiomyopathic tissue from the aged mdx model of Duchenne muscular dystrophy. *Neuromuscular Disorders*. 23, 812–812.

Holland, A. and Ohlendieck, K. 2014. Proteomic profiling of X-linked muscular dystrophy-associated cardiomyopathy. *International Journal of Molecular Medicine.* 34, S6-S6.

Holland, A. and Ohlendieck, K. 2015. Proteomic profiling of skeletal muscle from the wobbler mouse model of motor neuron diseases using label-free mass spectrometry. *Journal of Muscle Research and Cell Motility.* 36, 139-140.

AWARDS

2013 Winner of the Fellowship Prize, from the World Muscle Society

2014 Sponsored by Sigma-Aldrich for conference attendance

CONTRIBUTION TO THE PUBLIC UNDERSTANDING OF SCIENCE

- "Irish research team shines light on male infertility" – Maynooth University, press release, 17th October 2013 (http://communications.nuim.ie/press/17102013.shtml)

- **"**International research collaboration shines light on male infertility, structural and biological changes in sperm identified**"** – article online and in print by Dick Ahlsrom, Irish Times, 17th October 2013 (http://www.irishtimes.com/international-research-collaboration-shines-light-on-male-infertility-1.1563397)

- "Irish researchers discovering more and more about male infertility; Male infertility is responsible for about 50 per cent of infertility in Ireland" – article online by Sinead O'Carroll, thejournal.ie, 18th October 2013 (http://www.thejournal.ie/male-infertility-globozoospermia-1134205-Oct2013/)

- "Researchers uncover how disorder hits male fertility" – article in print, Irish Independent, 13th November 2013

- "Label-free mass spectrometric analysis of the *mdx-4cv* diaphragm identifies the matricellular protein periostin as a potential factor involved in dystrophinopathy-related fibrosis" – 3U Proteomics, press release, 6th March 2015 (http://3u.ie/3u-proteomics/)

- "New knowledge for Duchenne muscular dystrophy" – Bonn University, press release, by John Seiler, 19th March 2015 (http://www3.uni-bonn.de/Pressemitteilungen/052-2015)

- "DMD: periostin is driving scarring" – article online by Geraint Rowland, DocCheck News, 20th March 2015 (http://news.doccheck.com/de/81061/dmd-periostin-treibt-narbenbildung-voran/)

- "New research brings hope for diagnosis and treatment for muscular dystrophy" – Maynooth University, press release, 26th March 2015 (https://www.maynoothuniversity.ie//news-events/new-research-brings-hope-diagnosis-and-treatment-muscular-dystrophy)

- "Protein can help diagnose muscular dystrophy" – article online and in print by Dick Ahlstrom, Irish Times, 26th March 2015 (http://www.irishtimes.com/news/science/protein-can-help-diagnose-muscular-dystrophy-1.2145422)

ACKNOWLEDGMENTS

First and foremost I would like to sincerely thank my supervisor Professor Kay Ohlendieck. Thank you for your guidance, advice, support and encouragement throughout my time as an undergraduate and post-graduate in the Muscle Biology Lab. I could not have imagined achieving so many monumental achievements, including the many papers and exciting press releases, without your continuous drive for science. I will be forever grateful. Danke für alles.

To my co-supervisor Dr. Paul Dowling (DCU initially and now Maynooth University), thank you for your help and advice throughout my PhD.

Thank you to all members of the Muscle Biology Lab, both past and present.

I would like to acknowledge the Irish Higher Education Authority (HEA PRTLI Cycle 5) for funding my research and for giving me the opportunity to participate in the BioAT Programme.

To Muscular Dystrophy Ireland for their generous support of our proteomic research to muscular dystrophy. Thank you to all of the members of MDI who I met at the AGM and who reminded me of the importance of research.

To Dr. Paula Meleady and Prof. Martin Clynes (DCU) for their continued support in our proteomics research initiative, and a special thank you to Mr. Mick Henry, for always helping and answering my many mass spec questions.

To Prof. Dieter Swandulla and Ms. Margit Zweyer (University of Bonn, Germany), Dr. Peter Heimann and Prof. Harald Jockusch (University of Bielefeld, Germany) and Prof. Thomas Schmitt-John (University of Århus, Denmark) for all of the samples and their continuous collaborations.

To all the staff in the Department of Biology at Maynooth University who keep the department running, especially Michelle and Patricia.

To the ex-KK girls, Niamh and Sophie, and the past and present Bioscience girls Helen, Zita, Kate and Pam. Thank you for the many cups of tea, the adventures and the nights out. I will never forget the good times and all the laughs we have had over the years.

To Conor, thank you for being you, even on the days you thought you were George Clooney. You always managed to make things easier and kept me smiling. You are the yin to my yang. Also thank you for bankrupting me with all the trips to London!

Finally, but by no means least, to the most important people in my life, my parents, Ger and Ken, and of course Diego. Thank you for your unwavering support and encouragement, not only throughout this PhD, but in everything I do. For all the early morning and late night lifts to and from the airport and for always babysitting Diego. Mom, thank you for always asking how “my cooking” was going, and Dad, thank you for actually cooking for me! Everyday you both gave me the encouragement and motivation to keep going and I am glad to say, we finally got there. I am eternally grateful for all your love and support, and I dedicate this work to you. We did it!

DECLERATION

This thesis has not been submitted in whole or part to this or any other university for any degree, and is the original work of the author except where stated.

Signed _____

Ashling Holland B. Sc

Date _____

ABBREVIATIONS

1° Ab	Primary Antibody
1D	One dimensional
2° Ab	Secondary Antibody
2D	Two dimensional
2D-DIGE	Two dimensional difference in-gel electrophoresis
2D-GE	Two dimensional gel electrophoresis
Ab	Antibody
ACh	Acetylcholine
AChR	Acetylcholine receptor
ACN	Acetonitrile
ADP	Adenosine diphosphate
AK	Adenylate kinase
ALS	Amyotrophic lateral sclerosis
APS	Ammonium persulphate
ATP	Adenosine triphosphate
Au	Gold
BHD	Hydroxybutyrate dehydrogenase
BMD	Becker muscular dystrophy
Bromophenol Blue	3',3",5',5" tetrabromophenolsulfonphthalien
BSA	Bovine serum albumin
CA	Carbonic Anhydrase
CAL	Calreticulin
CCB	Colloidal Coomassie blue
CHAPS	3-[3-chlolamidopropyl-dimethylammonio-1-propane sulfonate]
Chk	Chicken
CLC-1	Chloride channel
CMD	Congenital muscular dystrophy
CRC	Ca^{2+}-release channel
CSQ	Calsequestrin
Cu/Zn SOD	Copper/zinc superoxide dismutase
cvHSP	Cardio-vascular heat shock protein

Cy	Cyanine
DAGC	Dystrophin associated glycoprotein complex
DAPI	Diamidino-phenylindole
DC	Differential centrifugation
DES	Desmin
DG	Dystroglycan
DGC	Dystrophin-glycoprotein complex
DGP	Dystroglycanopathy
dH_2O	Distilled water
DHPR	Dihydropyridine receptors
DIA	Diaphragm
DIGE	Difference in-gel electrophoresis
DMD	Duchenne muscular dystrophy
DMF	Dimethylformamide
DTT	Dithiothretiol
ECL	Enhanced chemiluminescence
ECM	Extracellular matrix
EDL	*Extensor digitorum longus*
EDTA	Ethylenediamintetraacetic acid
EGTA	Ethylene glycolbis(β-aminoethyl ether)- N, N, N', N'- tetraacetic acid
ELC	Essential light chain
EOM	Extraocular muscle
ER	Endoplasmic Reticulum
ESI	Electrospray ionisation
FABP	Fatty acid binding protein
fALS	Familial amyotrophic lateral sclerosis
FDB	*Flexor digitorum brevis*
FG	Fast glycolytic
FOG	Fast oxidative glycolytic
g	Grams
g	g force
GAPDH	Glyceraldehyde 3-phosphate dehydrogenase
grmd	Golden retriever muscular dystrophy

Gt	Goat
h	Hour(s)
HB	Homogenisation buffer
HCl	Hydrochloric acid
HEPES	(N-[2Hydroxyethyl]piperazine-N'-[2-ethanesulfonic acid])
HLM	Hind limb muscle
HPLC	High performance liquid chromatography
HRC	Histadine-rich Ca^{2+}-binging protein
HRP	Horse radish peroxidase
HSP	Heat shock protein
IB	Immunoblot
ICAT	Isotope-code affinity tag
IEF	Isoelectric focusing
IF	Immunofluorescence microscopy
INT	*Interosseus*
IP	Immunoprecipitation
IPG	Immobilised pH gradient
iTRAQ	Isobaric tags for relative and absolute quantification
JN	Junction
JP	Junctophilin
kDa	Kilo Daltons
L	Litre
LC-MS	Liquid chromatography mass spectrometry
LCM	Laser capture microscopy
LGMD	Limb-girdle muscular dystrophy
LOPIT	Localisation of organelle proteins by isotope tagging
M	Molar
m/z	Mass/ charge (ratio)
mAb	Monoclonal antibody
MBP-C	Myosin binding protein-C
mdx	X-linked muscular dystrophy mouse model (murine X-chromosome linked)

mdx-4cv	X-linked muscular dystrophy mouse model-4cv (murine X-chromosome linked)
MHC	Myosin heavy chain
min	Minute(s)
ml	Milliliter
MLC	Myosin light chain
mM	Milli molar
MS	Mass spectrometry
Ms	Mouse
MW	Molecular weight
Na^+	Sodium ions
NADH	Nicotinamide adenine dinucleotide
ng	Nanograms
NL	Non-linear
OCT	Optimum cutting temperature compound
pAb	Polyclonal antibody
PAGE	Polyacrylamide gel electrophoresis
PBS	Phosphate buffered saline
p*I*	Isoelectric point
PIC	Protease inhibitor cocktail
PMT	Photo multiplier tube
PPD-glycerol	P-Phenylenediamine glycerol
PTM	Post-translational modification
PVA	Parvalbumin
Rb	Rabbit
RGC	Regucalcin
RLC	Regulatory light chain
ROS	Reactive oxygen species
RuBPs	Ruthenium (II) tris-bathophenathroline disulfonate
RyR	Ryanodine receptor
s	Second(s)
sALS	Sporadic amyotrophic lateral sclerosis
SAR	Sarcalumenin

SDH	Succinate dehydrogenase
SDS	Sodium dodecyl sulphate
SERCA	Sarcoplasmic/endoplasmic reticulum Ca^{2+}-ATPase
Shp	Sheep
SILAC	Stable isotope labelling with amino acids in cell culture
SL	Sarcolemma
SO	Slow oxidative
SOD	Superoxide dismutase
SOL	*Soleus*
SR	Sarcoplasmic reticulum
T-Tubules	Transverse tubules
TEMED	N,N,N',N'-tetramethylethylenediamine
TFA	Trifluoroacetic acid
TGF-β	Transforming growth factor beta
TI-DIRT	Transient isotopic differentiation of interactions as random or targeted
Tm	Tropomyosin
Tn	Troponin
TnC	Troponin C
TnI	Troponin I
TnT	Troponin T
TRI	Triadin
TT	Transverse tubules
V	Volt
VDAC	Voltage-dependent anion-selective channel
Vh	Voltage hours
VPS	Vesicular protein-sorting factor
VPS	Vesicle sorting protein
WB	Western blot
WR	Wobbler
WT	Wild-type
XDCM	X-linked dialated cardiomyopathy
XL	Chemical crosslinking
α-DG	Alpha-dystroglycan

β-DG	Beta-dystroglycan
μg	Microgram
μL	Microlitre

ABSTRACT

Proteomic profiling plays a decisive role in the identification of novel biomarkers of neuromuscular disorders and the elucidation of new pathobiochemical mechanisms that underlie these diseases. Detailed mass spectrometry-based analysis of various diseased muscle groups from animal models of motor neuron disease and X-linked muscular dystrophy is presented, in addition to motor neuron disease associated globozoospermia. This research has shown that both gel electrophoresis based and/or liquid chromatography for large-scale protein separation, and label-free mass spectrometry based-proteomics are highly suitable to determine changes in the isoform expression pattern of muscle and testis proteins. The work presented outlines major categories of protein families that have been identified by proteomics-based screening approaches in conjunction with biochemical verification analyses. This research has successfully established comprehensive biomarker signatures that have the potential to be used for the evaluation of new treatments and therapeutics, improve the understanding of pathobiochemical processes of the different diseases under investigation and diagnostics and prognostics of motor neuron disease, impaired spermiogenesis and X-linked muscular dystrophy.

Chapter 1

Introduction

1.1 Muscle Biology

Muscle accounts for approximately 40% of human body weight and is composed of myofibers, nerves and connective tissue (Waterlow, 1976). Muscles are highly complex biological structures and are essential for a range of biological functions including posture, support of the body, locomotion, heat homeostasis and metabolic integration (Ohlendieck, 2011A).

There are four main types of muscle tissues: skeletal, cardiac, smooth and myoepithelial muscle. Skeletal muscle is attached to bones by tendons. They are multi-nucleated, striated in appearance and under voluntary muscle control (Clark *et al.,* 2002). The striated appearance is due to the arrangement of sarcomeres, the contractile units (Rahimov and Kunkel, 2013). The thin muscle filaments and thick muscle filaments in the sarcomere and their banding pattern in longitudinal skeletal muscle sections can be seen under low and high magnification in Figure 1.1 A and B, respectively (Holland and Ohlendieck, 2013). Cardiac muscle is only found in the heart and is responsible for cardiac tissue contraction and distribution of blood through the body. Similar to skeletal muscle, cardiac muscle is striated (Clark *et al.,* 2002). However it contains individual units called intercalated discs, which support synchronised cardiac muscle contractions (Coghlan and Coghlan, 2001). Cardiac muscle functions spontaneously and is involuntary, as it is not controlled by the somatic nervous system. As cardiac tissue is under continuous activity, it has a high concentration of mitochondria making it resistant to fatigue (Lemieux and Hoppel, 2009). The third type of muscle is smooth muscle. In contrast to skeletal or cardiac muscle smooth muscle is non-striated. Like cardiac muscle, smooth muscle is under involuntary control and can sustain longer contractions. It is located in the lining

of blood vessels, urinary bladder, kidneys, oesophagus and small intestines. Finally the fourth type, myoepithelial cells have a similar structure and function to smooth muscle (Hubner *et al.,* 1971). Myoepithelial muscle cells form the basal layer of the epithelium in mammary glans, lactiferous sinuses and ducts. These muscle cells are positive for alpha smooth muscle actin and have the ability to contract and thus expel secretions (Leslie *et al.,* 1990).

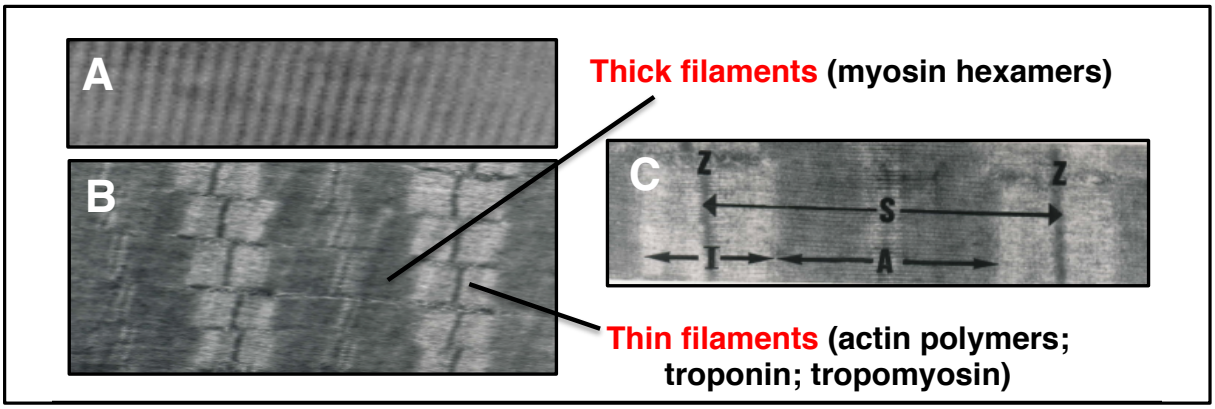

Figure 1.1 Striated skeletal muscle patterns.
Shown are light microscopical (A) and electron microscopical (B) images of longitudinal sections of skeletal muscle to illustrate the histological appearance of the contractile apparatus. Panel (C) outlines the position of A-bands, I-bands, Z-discs and sarcomeres. *Image from Holland and Ohlendieck, 2013

1.1.1 Muscle development

Muscle is formed during embryonic development in a process called myogenesis and almost all muscles are of mesodermal origin (Mok and Sweetman, 2011). Pax-3 and Pax-7 are transcription factors involved in myogenesis and their signalling roles are of crucial importance during differentiation of somites. Further development signalling involving other myogenic transcription factors include MyoD, myf-5, MRF-4 and myogenin (Mok and Sweetman, 2011). Figure 1.2 outlines how myogenesis is composed of a complex series of developmental steps that results in the committal of mesodermal progenitor cells to the skeletal muscle lineage, cellular differentiation, migration, myoblast fusion and fibre maturation (Buckingham *et al.,* 2003).

The expression of a key stimulator of myoblast population differentiation, the MGF, has been shown to be induced by the myofibrillar proteins myomesin, myosin binding protein-C and titin (Kravchenko *et al.,* 2012). This leads to the formation of multi-nucleated myotubes. These myotubes mature into skeletal muscle fibres, which are subsequently innervated to form a functional adult motor unit (Buckingham *et al.,* 2003). The process of muscle maturation involves the expression of muscle specific genes, allowing for the generation of contractile proteins including myosin, actin, troponin and tropomyosin. Adult motor-units are made of many skeletal muscle fibres and are highly plastic (Ohlendieck 2012). Their protein composition can be influenced by changes in neuromuscular activity levels, metabolic fuel source, severely altered innervation patterns, resistance exercise, endurance training, prolonged exposure to microgravity, immobilisation, disuse, trauma, denervation, nerve

crush injury, cycles of muscle regeneration and natural muscle aging causing the neuromuscular system to adapt accordingly (Holland and Ohlendieck, 2013).

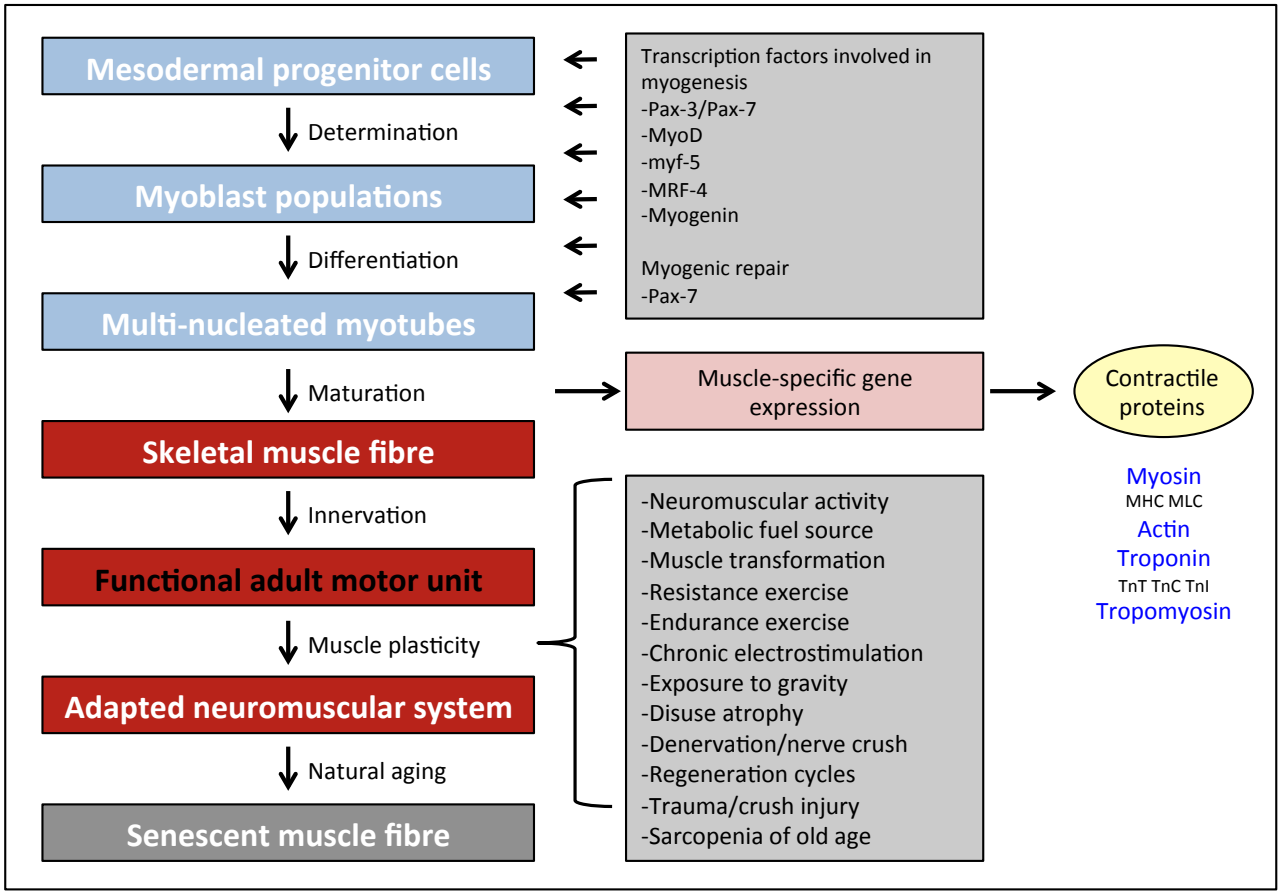

Figure 1.2 Complex changes during development, maturation and adaptions of skeletal muscle.
The various steps that have a profound effect on the dynamics of the skeletal muscle proteome including committal of mesodermal progenitor cells to the skeletal muscle lineage, cellular differentiation, migration, myoblast fusion, fibre maturation, establishment of functional adult motor units, adaptations of the neuromuscular system to changed functional demands and the natural aging process are listed. The drastic increase in muscle-specific gene expression is a characteristic event during maturation of the neuromuscular system and is accompanied by production of large numbers of myosin, actin, troponin and tropomyosin isoforms. Changes in their abundance and isoforms expression patterns paly a role in muscle adaptations and their fibre plasticity. MHC: myosin heavy chain; MLC: myosin light chain; Tn: troponin (subunits I, T, C). *Image from Holland and Ohlendieck, 2013

1.1.2 Muscle regeneration and satellite cells

Skeletal muscle is susceptible to damage caused by overstretching, trauma, day-to-day wear and tear and several degenerative muscle disorders including Duchenne muscular dystrophy (Fu *et al.,* 2015). Satellite cells represent a major group of muscle stem cells that are crucially important mediators of muscle repair through muscle regeneration (Mauro, 1961). Other forms of muscle-resident adult stem cells have recently been identified. These alternative muscle stem cells represent an important part of muscle regeneration, however their regulatory mechanisms require further research (Yin *et al.,* 2013).

Quiescent satellite cells reside between the muscle sarcolemma and the basal lamina of myofibres (Mauro, 1961). They possess the necessary receptors and enzymes required to rapidly activate, process and respond to signalling molecules that result in satellite cell activation in response to injury (Irintchev *et al.,* 1997). Specific gene expression profiles can be seen in quiescent satellite cells as compared to actively proliferating satellite cells. Quiescent satellite cells dominantly express the transcription factors Pax7, Pax3, M-cadherin and CXCR4 (Kuang *et al.* 2006; Alfaro *et al.,* 2011) while MyoD expression is absent (Cornelison and Wold, 1997). Many of these transcription factors are also expressed during normal stages of skeletal muscle determination and differentiation (Figure 1.2).

The number of satellite cells reaches a peak during the neonatal stage and accounts for approximately 30-35% of the total myofibre nuclei. During adulthood this number decreases to 2-7% of the total myofibre nuclei. The reduction in satellite cell population has a direct link with decreased muscle

regeneration capacity in older muscle tissue (Schmalbruch and Hellhammer, 1976). Degenerative muscle disorders such as Duchenne muscular dystrophy experience a progressive depletion of satellite cells and the stem cell pool becomes exhausted, resulting in failure of muscle repair (Jiang *et al.,* 2014).

1.1.3 Muscle structure

Mature skeletal muscle fibres are composed of thousands of multinucleated myofibrils running in parallel of each fibre in a longitudinal orientation (Clark *et al.,* 2002). Myofibrils are made up of sarcomeres, the contractile machinery of voluntary muscles. Figure 1.3 illustrates the position of the sarcomeric units, of approximately 2 μm, located between the two Z-discs (Burkholder and Lieber, 2001) and the typical A-bands and I-bands of skeletal muscles. The thin filaments contain actin polymers, troponin and tropomyosin, and the thick filaments consist of certain arrays of myosin hexamers (Pette and Staron, 2000). Nebulin and titin represent essential non-actin and non-myosin molecules in the thin and think filaments, respectively. Nebulin is an enormous actin-binding protein that spans the entire length of the thin filament, running parallel to the string like titin molecules (Pappas *et al.,* 2011). Titin functions elastic-like during muscle contraction and connects the thick filament to the Z-disc (Ottenheijm and Granzier, 2010).

Figure 1.4 shows the molecular diversity in some of the main contractile apparatus proteins in relation to myosin (A), troponin (B), actin (C) and tropomyosins (Holland and Ohlendieck, 2013). Developing and mature muscles have many different molecular combinations of myosin heavy chains (MHC), myosin light chains (MLC), actins, troponins and tropomyosins. The troponin

complex (Figure 1.4 B) is made up of troponin C (TnC) that is the binding site for calcium ions, Ca^{2+}, troponin T (TnT) that binds strongly to tropomyosin and troponin I (TnI) that inhibits actin-myosin binding (Pette and Staron, 2000).

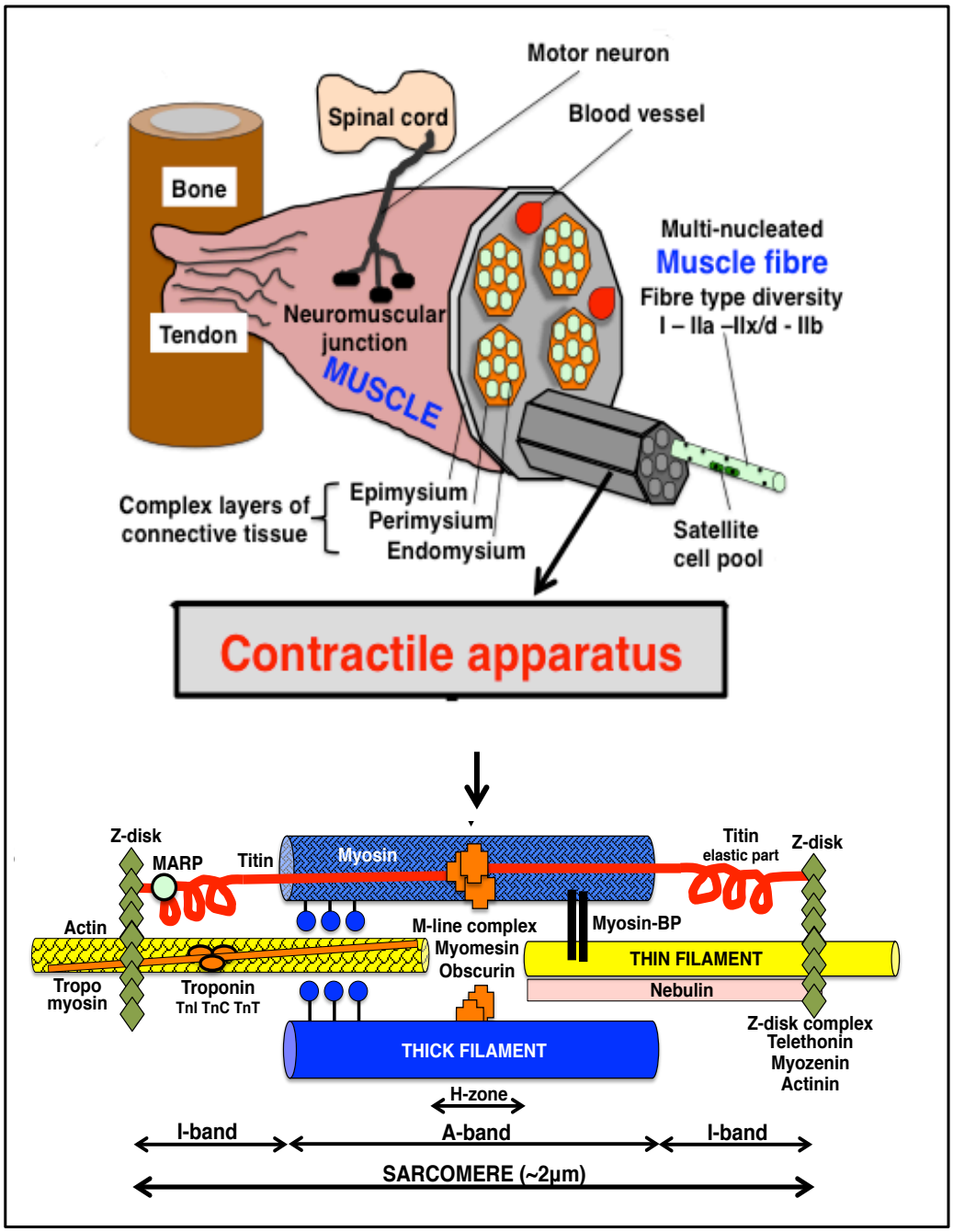

Figure 1.3 The contractile apparatus and sarcomere structure.
Shown on top are the main constituents of the neuromuscular system and surrounding tissue including multinucleated muscle fibres with varying contractile properties (fibre types I, IIA, IIXD and IIB), satellite cells, blood vessels, motor neurons and several layers of connective tissue. Shown below the contractile apparatus is the main structure and components of the sarcomere from skeletal muscle including think filaments, thick filaments, the M-line complex, the titin gap filament and the Z-disk complex. BP: binding protein; Tn: troponin (subunits I, T, C).
*Image from Holland and Ohlendieck, 2013

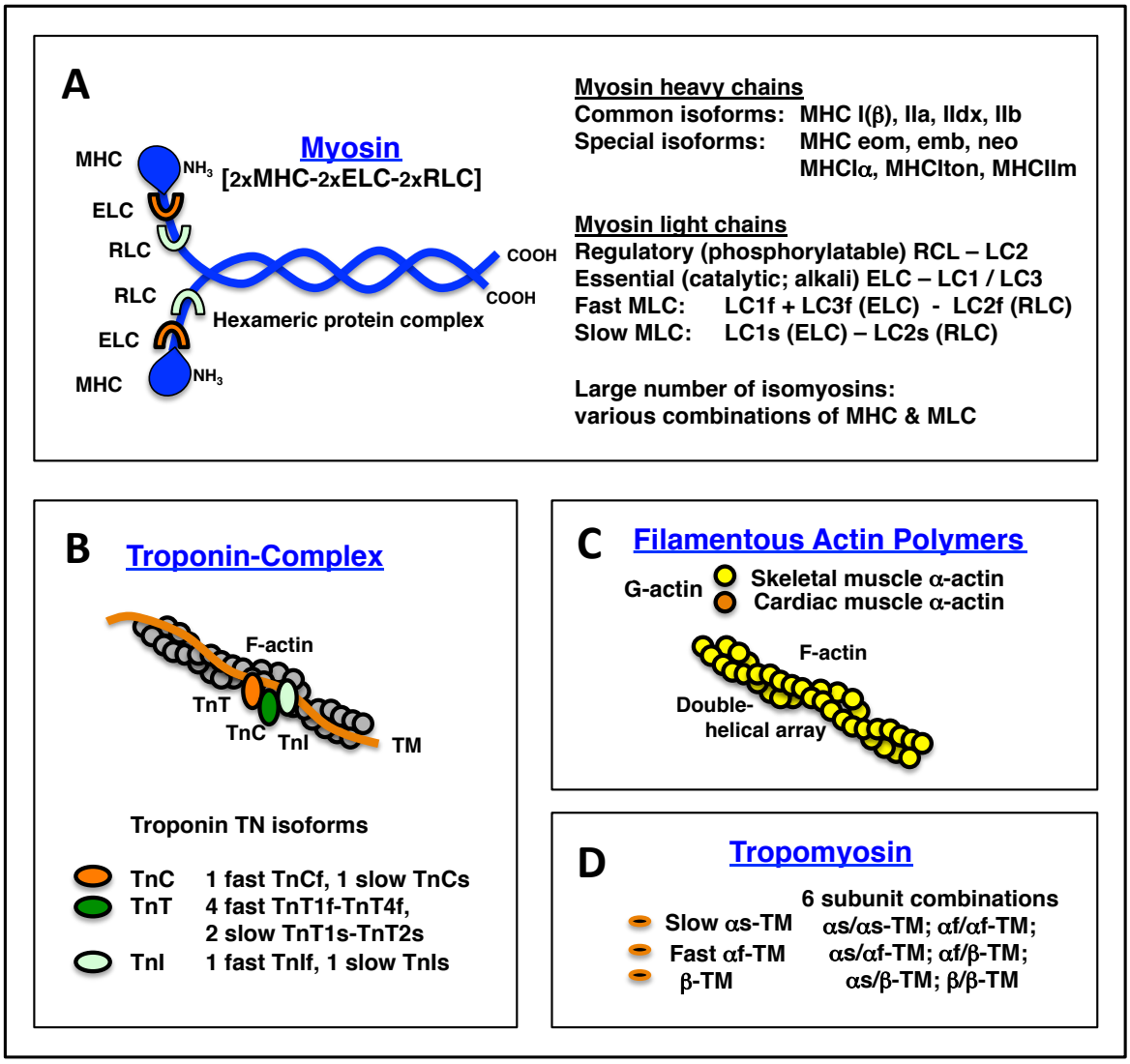

Figure 1.4 Protein composition of the contractile apparatus from skeletal muscle. Shown is the molecular diversity of key proteins of the actomyosin apparatus including myosin heavy and light chains (A), troponins (B), actins (C) and tropomyosins (D). ELC: essential light chain; MHC: myosin heavy chain; MLC: myosin light chain; RLC: regulatory light chain; TM: tropomyosin; Tn troponin (subunits I, T, C).
*Image from Holland and Ohlendieck, 2013

1.1.4 The motor neuron system and muscle contraction

Skeletal muscle contraction begins in the motor cortex of the brain and is conducted though neurons of the somatic nervous system as an electrical signal. Neurons, nerve cells, are the most basic unit of the nervous system. A single neuron contains a cell body with two or more dendrites and axons. Dendrites carry information from their tips to the rest of the neuron, while axons are responsible for rapid transmission of impulses from one neuron to another neuron or an effector muscle cell (Turkheimer *et al.,* 2015).

Thus muscle contraction beings at the neuromuscular junction. The neuromuscular junction connects the nervous system to the muscular system (Figure 1.3). The electrical signal is converted to a chemical signal, in the form of the neurotransmitter acetylcholine, ACh, allowing signal transduction through the synapse of the motor neuron and the muscle. ACh binds to the post-synaptic acetylcholine receptors, AChR, located on the muscle membrane. Activation of the AChR causes a localised depolarisation resulting in the opening of sodium ion and potassium ion channels (Farley and Miles, 1977). More sodium ions, Na^+, enter the cytosol of the muscle sarcolemma than potassium ions, K^+, leave causing depolarisation and this initiates an action potential (Hodgkin and Horowicz, 1960). The action potential travels through the sarcolemma and enters the transverse tubules, T-tubules. The action potential is sensed by the α_{1s}-subunit of the dihydropyridine receptor, DHPR, in the T-tubules (Figure 1.5). This induces a conformational change in DHPR and consequently in the II-III loop of the voltage sensing DHPR allowing it to directly interact with the Ryanodine receptor, RyR1, on the sarcoplasmic reticulum, SR, membrane (Proenza *et al.,* 2002). This triggers the opening of the RyR1 calcium channels

creating an influx of calcium ions, Ca^{2+}, from the SR lumen into the cytoplasm of the muscle cell.

These cytosolic Ca^{2+}-ions bind with TnC causing structural changes to the troponin complex (Figure 1.4 B). TnI can no longer inhibit actin-myosin binding. In the presence of ATP, the myosin head of the think filament (Figure 1.4 A) interacts with the myosin-binding site on actin (Figure 1.4 C) (Holland and Ohlendieck, 2013). ATP is broken down to ADP and P_i, the myosin head is released and moves to the subsequent available actin molecule on the thin filament. As the actin filaments and myosin head structures molecularly couple they cause the sliding of the thin filaments past the thick filaments creating a cross-bridge and a shorted sarcomeric length generating a muscle contraction (Gordon *et al.,* 2000). This is repeated until there is no more Ca^{2+} or ATP.

Depolarisation of the sarcolemma activates chloride and potassium channels and chloride ions, Cl^-, flux into the cell and potassium ions, K^+, flux out. When the sarcolemma returns to its resting potential the DHPR-RyR interaction disassembles causing the RyR1 Ca^{2+}-channel to close and ATPases like sarcoplasmic-endoplasmic reticulum calcium ATPase, SERCA, transport Ca^{2+}-ions back into the SR (Heegaard *et al.,* 1960). This prevents actin-myosin cross bridge formations and the Ca^{2+}-ions bound to troponin are released, tropomyosin uncouples, proteins of the contractile apparatus return to their normal conformation and the muscle relaxes.

The original cross bridge hypothesis of myosin-actin interactions (Sellers, 2004) has evolved into a more precise version known as the swinging lever-arm hypothesis of muscle contraction (Holmes, 1997), as the actomyosin coupling is regulated in a Ca^{2+}-dependent way through the tropomyosin complex and the

inhibitory tropomyosin strands (Gunning *et al.,* 2008).

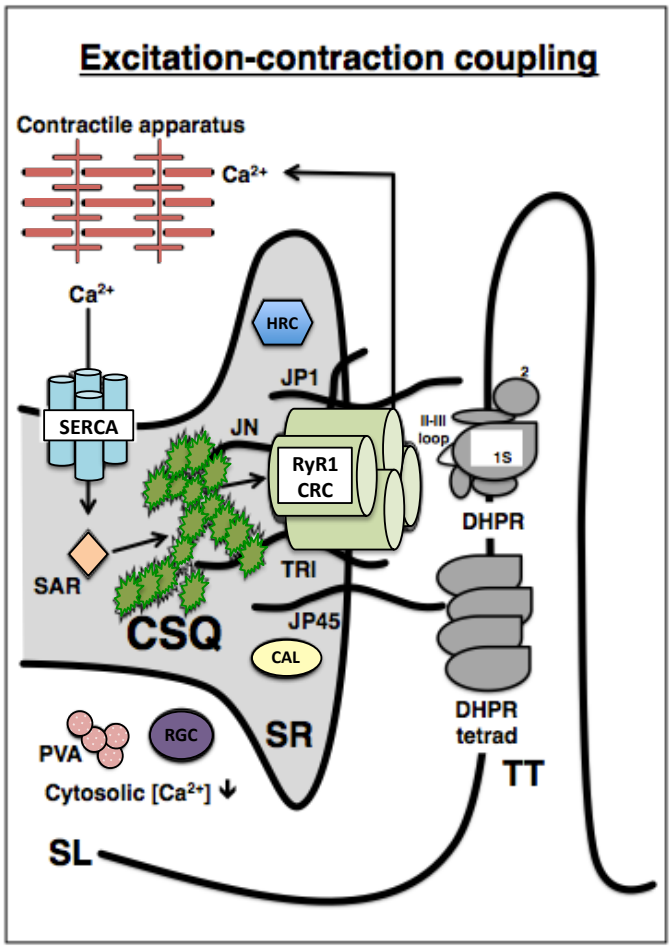

Figure 1.5. The excitation-contraction coupling apparatus from skeletal muscle. Shown is a depiction of the subcellular localisation of key proteins involved in the excitation contraction coupling with respect to the sarcolemma (SL), the transverse tubules (TT) and the sarcoplasmic reticulum (SR). In adult skeletal muscle fibres, excitation contraction coupling is mediated by the direct physical coupling between the II-III loop domain of the α_{1s}-subunit of the voltage sensing dihydropyridine receptor (DHPR), as well as other subunit domains of the DHPR, with corresponding domains in the foot region of the ryanodine receptor-1 (RyR1) isoform of the junctional Ca^{2+}-release channel (CRC) complex. Triad associated proteins such as triadin (TRI), junction (JN) and junctophilin (JP) have been proposed to be involved in the receptor coupling process and ion channelling. SAR: sarcalumenin; CAL: calreticulin; HRC: histadine-rich Ca^{2+}-binding protein; RGC: regucalcin; PVA: parvalbumin.
*Image from Holland and Ohlendieck, 2014D

1.1.5 Muscle fibre classification

The biophysical and metabolic diversity of contractile tissues, in addition to the physiological adaptability of whole skeletal muscles to changed functional demands, is based on the enormous variability in contractile proteins and bioenergetic enzyme isoforms (Pette and Staron, 2001; Greising *et al.,* 2012).

In human skeletal muscles, the main fibre types can be categorized as type I, slow-red oxidative, type IIA, fast-red glycolytic-oxidative, and type IIX/D, fast-white glycolytic, as well as a large number of hybrid fibres (Figure 1.6). Distinct mixtures of fibre types provide the contractile basis of the varying physiological demands of individual skeletal muscles (Schiaffino and Reggiani, 2011). The distribution of fibre type-specific myosins and metabolic enzymes are characteristic of slow-twitching fibres with predominantly oxidative metabolism, fast-twitching fibres with glycolytic-oxidative bioenergetics and fast-twitching fibres with glycolytic metabolism (Pette and Starton, 2000; Holland and Ohlendeick, 2013).

The skeletal muscle continuum of human and rodent fibre types during gradual fast-to-slow or slow-to-fast transformations is diagrammatically presented in Figure 1.6. Different pathological insults and physiological factors can influence fibre type transitions in skeletal muscle tissues. Increased neuromuscular activity and muscle stimulation can cause a fast-to-slow fibre transition, while decreased neuromuscular activity and muscle unloading can cause a slow-to-fast fibre transition (Ohlendieck, 2011).

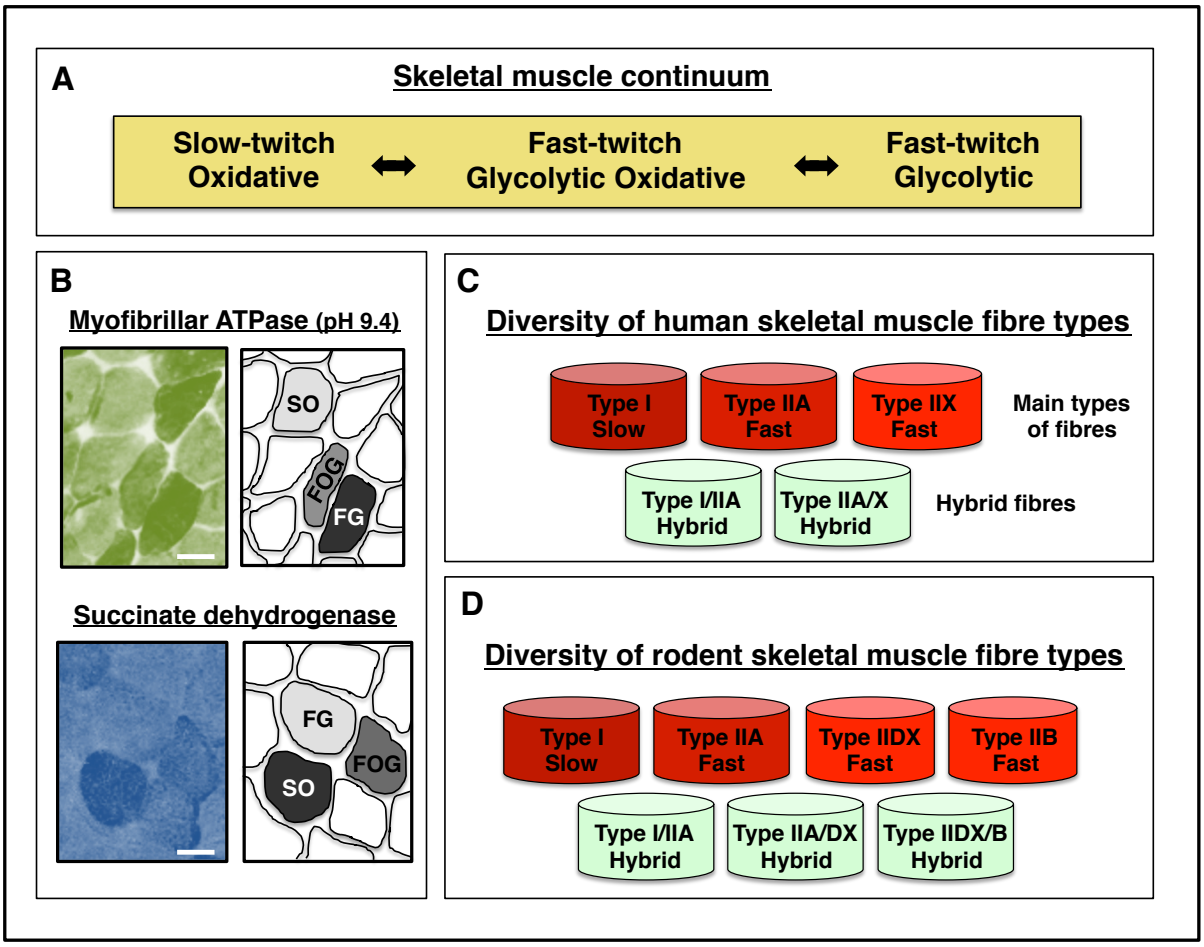

Figure 1.6 Overview of the dynamic range of skeletal muscle fibre types.
Panel (A) shows the main fibre types and panel (B) shows the histochemical labelling of slow-twitch oxidative, fast-twitch glycolytic oxidative and fast-twitch glycolytic fibres using staining and myofibrillar ATPase activity at pH 9.4 and staining of mitochondrial succinate dehydrogenase activity. Panels (C) and (D) show a summary of the main fibre types and hybrid fibres typically found in human skeletal muscle and rodent skeletal muscles, respectively. FG: fast glycolytic; FOG; fast oxidative glycolytic; SO slow oxidative. Bar is 40 µm.
*Image from Holland and Ohlendieck, 2013

1.1.6 Muscle aging

Natural muscle aging is a highly complex and multifactorial process in which significant skeletal muscle mass is lost and muscle contraction function is decreased (Berger and Doherty, 2010). Age-related muscle wasting is associated with the progressive loss of spinal motor neurons as a result of apoptosis, cycles of denervation and defective reinnervation, uncoupling between excitation and muscular contraction, impaired ion homeostasis, perturbed hormonal levels and growth factors, reduced levels of muscle protein synthesis, disturbed regulation of bioenergetics and metabolic pathways, diminished cellular stress responses and an overall reduced regenerative capacity (Edström *et al.,* 2007). There are distinct differences in aging with respect to the severity and onset of aging within the muscular system, and also between individuals. However, the majority of humans experience a progressive loss in muscle tissue mass during the aging process (Faulkner *et al.,* 2007).

Proteome wide changes occur during muscle aging. These broad proteome changes include proteins linked with cellular signaling, glycolysis, mitochondrial metabolism, metabolite transportation, detoxification, the cytoskeleton, the cellular stress response and the general contractile apparatus (Doran *et al.,* 2009A). The alterations experienced in the contractile apparatus during aging are not likely to contribute to the progressive decrease in muscle mass and strength. However, it could be a result of a differential susceptibility of different fibre types to muscular atrophy. Fast-twitch fibres appear to experience an elevated rate of muscular atrophy during aging, resulting in an overall fast-to-slow muscle fibre transformation (Ohlendieck, 2011). A glycolytic-to-oxidative shift is also present in slower-twitching senescent muscles (O'Connell and

Ohlendieck, 2009). These distinct changes in the abundance and/or post-translational modifications of contractile proteins are a good starting point for the identification of novel indicators of muscle sarcopenia. Previous proteomic studies of aging human *vastus lateralis* muscle have shown a distinct shift to a slower muscle fibre population with enhanced oxidative metabolism (Gelfi *et al.,* 2006; Staunton *et al.,* 2012). The distribution pattern of myosin heavy chains, MHC, troponins and actins transforms to a slower isoform phenotype during senescence. Myosin light chain-2, MLC-2, increases during aging. In contrast to this MLC-2f, MLC-2f1 and MLC 2f2 decrease in aged human muscle (Gelfi *et al.,* 2006). This has established MLC isoforms as potential indicators of sarcopenia (Doran *et al.,* 2009). Physiological adaptations and pathological alterations of skeletal muscle during natural aging are outlined in Figure 1.7. The altered isoform expression patterns of contractile proteins mentioned above are a suitable source for the identification of a novel biomarker signature of aging (Holland and Ohlendieck, 2013).

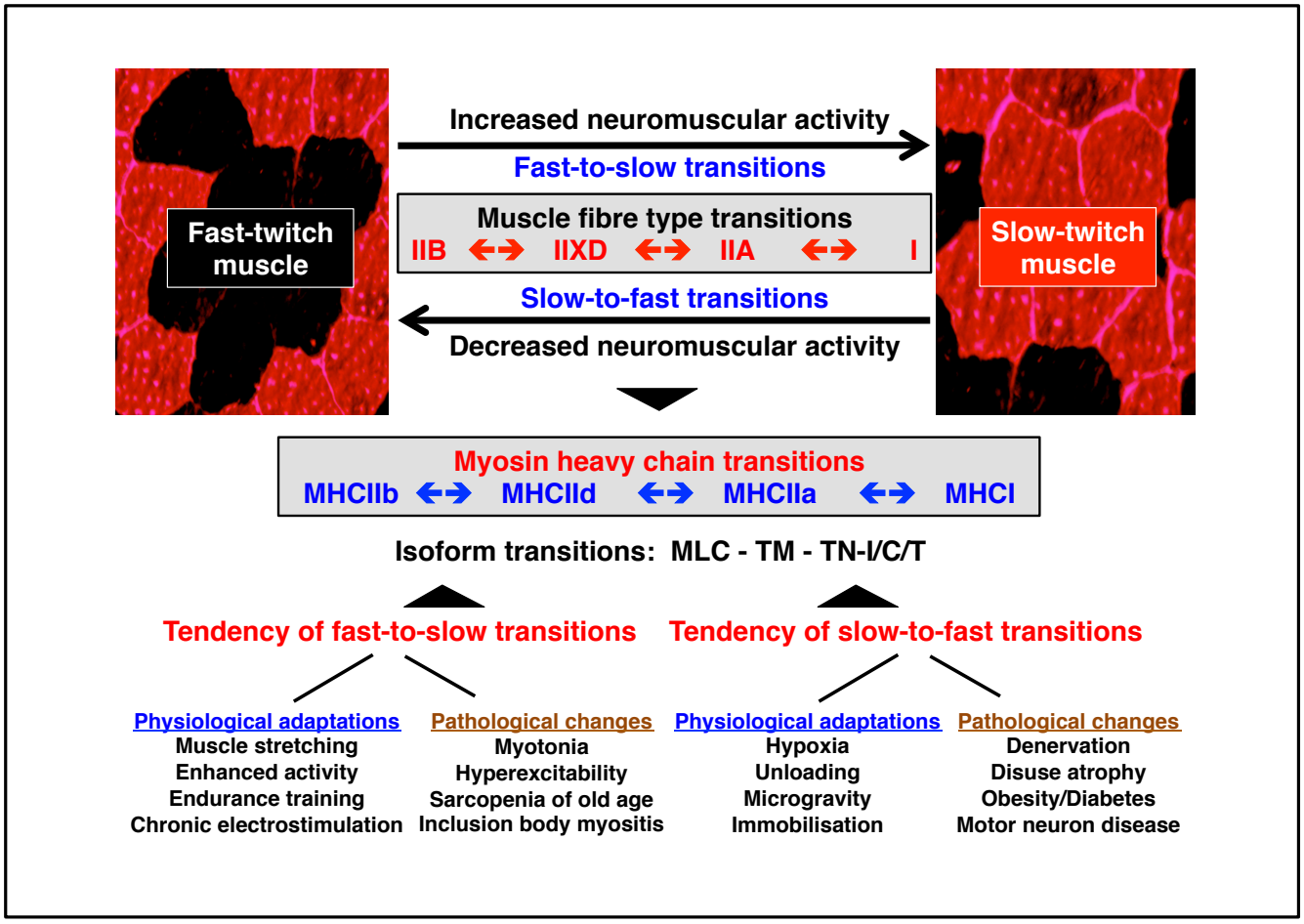

Figure 1.7 Proteome-wide changes during the physiological adaptations and pathological events that result in major myosin heavy chain transitions. Shown is a summary of the effect of fast-to-slow versus slow-to-fast fibre type muscle transitions due to altered neuromuscular activity patterns or pathophysiological changes.
*Image from Holland and Ohlendieck, 2013

1.2 Motor neuron disease

Motor neuron disease, MND, is a heterogeneous group of neurodegenerative syndromes that are highly linked with progressive paralysis due to loss of upper and/or lower motor neurons (Wijesekera and Leigh, 2009). There are many forms of MND including conditions such as spastic paraplegia, spino-bulbar muscular atrophy, hereditary spastic paralysis, primary lateral sclerosis and amyotrophic lateral sclerosis (Shaw and Wood-Allum, 2010).

Enhanced neuromuscular activity results in a fast-to-slow transformation, while slow-to-fast transformations are characteristic of neuromuscular unloading (Pansarasa *et al.,* 2014). As outlined in Figure 1.8, muscle fibre type shifting occurs due to physiological adaptions or pathological insults including MND and disease associated muscular atrophy (Pansarasa *et al.,* 2014; Holland and Ohlendieck, 2014C). MND has been shown to not have a typical clear slow-to-fast transformation, but a more individual disease related complex proteome-wide alteration.

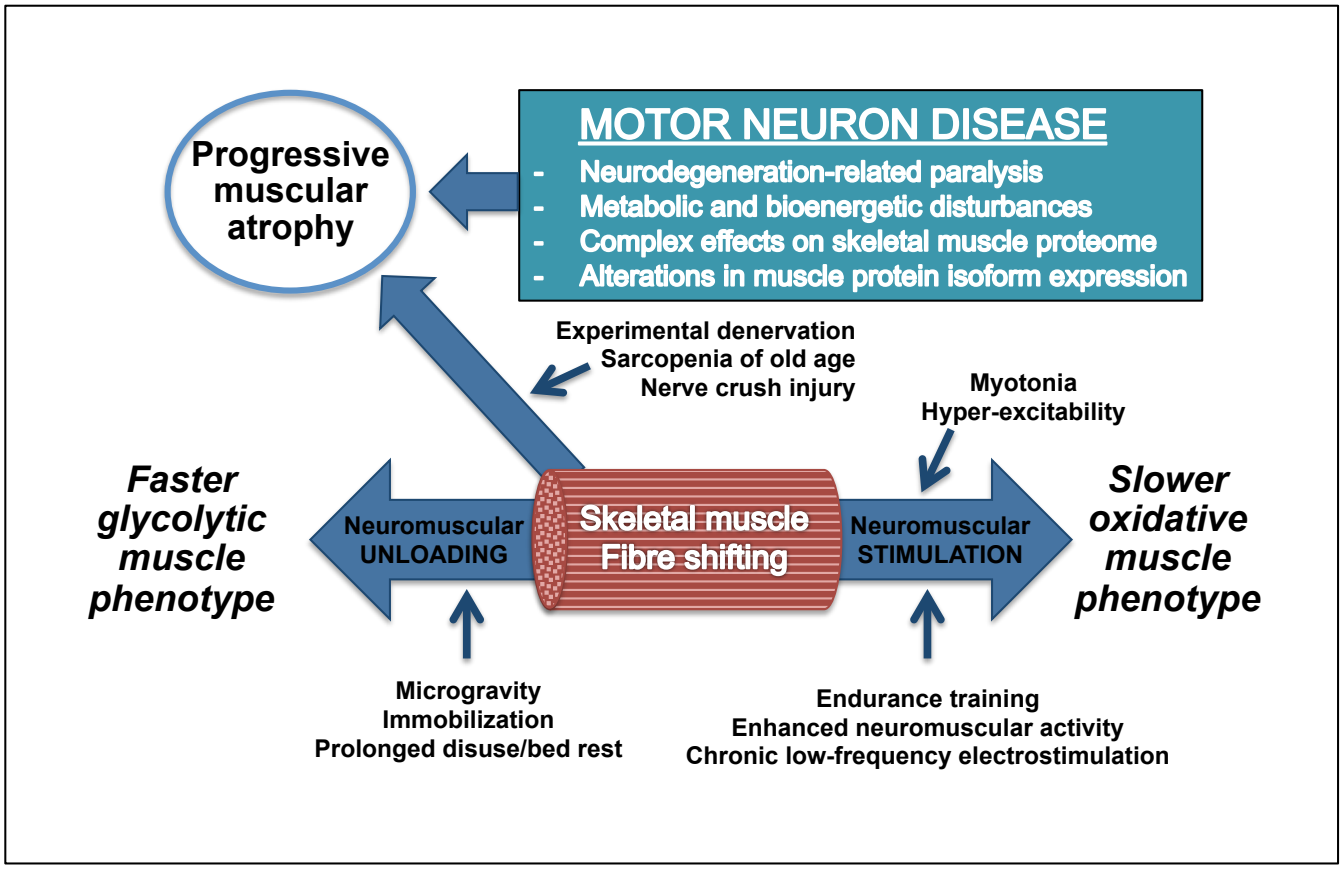

Figure 1.8 Overview of skeletal muscle plasticity and fibre transitions due to physiological adaptations or pathological insults to the neuromuscular system. Motor neuron disease is characterized by progressive muscular atrophy and complex changes in the skeletal muscle proteome.
*Image from Holland and Ohlendieck, 2014C

1.2.1 Amyotrophic lateral sclerosis

In 1869 Jean-Martin Charcot was the first to describe amyotrophic lateral sclerosis, ALS, a highly progressive and rapidly terminal disease. Today, it is the most common form of motorneuron disease (Wijesekera and Leigh, 2009). ALS is typically adult-onset with an average age of onset at 60 years (Musaro, 2013). The loss of upper and lower motor neurons in ALS patients results in muscle weakness, muscular atrophy, spasticity of muscles and ultimately an extremely progressive form of paralysis (Dion *et al.,* 2009). ALS is characterized by death and degeneration of motor neurons in the primary motor cortex, corticospinal tracts, brainstem and spinal cord (Rowland and Shneider, 2001). The term ALS comes from "amyotrophy"; referring to the atrophying muscle fibres (Figure 1.9). Anterior horn cells degenerate causing denervation of muscles creating muscle weakness and fasciculation's. "Lateral sclerosis" refers to the degenerating motor neurons of lateral and anterior corticospinal tracts which being to harden and are replaced by gliosis (Rowland and Shneider, 2001).

The highly progressive nature of this disease leads to death, generally due to degeneration of respiratory muscles inducing respiratory failure (Gros-Louis *et al.,* 2006). This occurs within 2-3 years in bulbar ALS on-set cases and 3-5 years for limb on-set after initial clinical signs manifest (Dion *et al.,* 2009). Patients presenting with bulbar onset ALS experience dysarthria of speech, dysphagia for both liquids and solids and sialorrhoea. Limb symptoms typically occur within 1-2 years, but can develop in tandem with bular symptoms. More than half of ALS suffers have limb on-set; the spinal form ALS (classical 'Charcot ALS'). The symptoms of this form are focal muscle weakness and muscular atrophy. Symptoms can begin proximally or distally in both upper and lower

limbs (Wijesekera and Leigh, 2009). Disease progression can lead to development of spasticity in atrophying limbs leading to complications in dexterity and gait (Wijesekera and Leigh, 2009).

ALS can be sporadic in nature or of genetic origin. Five to ten percent of ALS patients have familial form, fALS, inherited in an autosomal dominant way. Various genes have been shown to be involved in inherited forms of ALS, including *SOD1*, *TARDBP*, *FUS, VCP*, *OPTN*, *ALS2*, *SETX*, *C9ORF72*, *PFN1*, *VAPB*, *UBQLN2* and *ANG* (Kudo *et al.,* 2010; Da Cruz and Cleveland, 2011; Paratore *et al.,* 2012; Pratt *et al.,* 2012). The majority of patients, ninety to ninety five percent, present with no clear family history and this form is considered sporadic ALS, sALS, (Valentine *et al.,* 2005; Wijesekera and Leigh, 2009). All patients experience muscle weakness, atrophy and spasticity meaning fALS and sALS are clinically indistinguishable (Gros-Louis *et al.,* 2006; Baghi *et al.,* 2007).

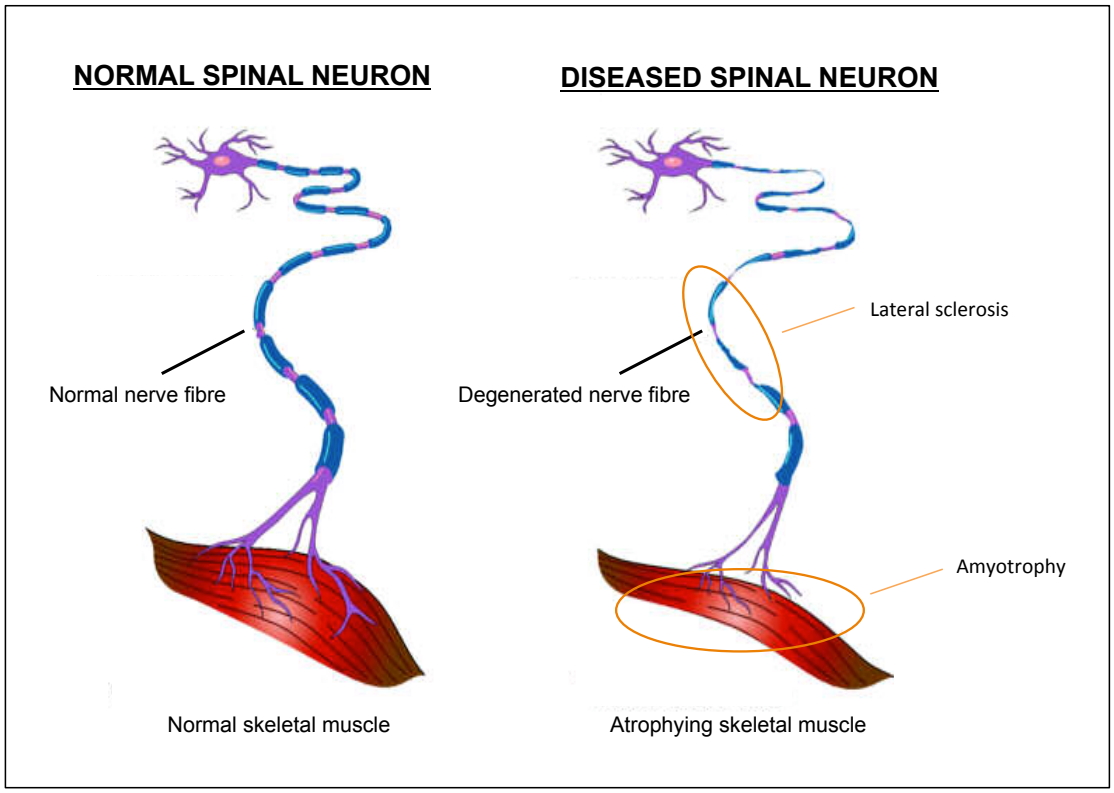

Figure 1.9 Amyotrophic lateral sclerosis.
Shown on the left is a normal spinal neuron, with a normal nerve fibre and normal skeletal muscle. On the right, is a diseased spinal neuron typical of ALS. It demonstrates a degenerated nerve fibre, causing lateral sclerosis. The degenerated nerve fibre leads to a reduction in the communication between the neuron and skeletal muscle resulting in disease induced muscular atrophy.
*Image modified from www.vetnext.com

1.2.2 Treatment of ALS

Genomic, transcriptomic, proteomic and metabolomic screening programs have been initiated to determine global changes in human ALS specimens and animal models of motor neuron disease (Tanaka *et al.,* 2012; Mendonça *et al.,* 2012). The aim of this research is to establish novel biomarkers for diagnostic, prognostic and therapeutic applications (Ekegren *et al.,* 2008; Krüger *et al.,* 2013).

However, at present there is only one FDA approved treatment for ALS. Riluzole was FDA approved in 1995, and licensed in 1996. Riluzole has modest effects on patients with an average life extension of 2-3 months, meaning it's effects on patient survival and function are limited (Wijesekera and Leigh, 2009). For the past 20 years the majority of clinical trials have been disappointing and have been unsuccessful in identifying another neuroprotective agent or finding a mechanism to halt disease progression (Gordon, 2013; Mitsumoto *et al.,* 2014). Currently clinical trials are testing medications focused on interfeering with a known cellular event and to slow disease development (Gordon and Mitsumoto, 2007) and testing chemical compounds (Miller *et al.,* 2007). The wide array of drugs that have been tested for the treatment of ALS only confirm the idea that ALS is a multifactorial disease with a multitude of cellular mechanisms that lead to motor neuron death.

The absence of a treatment for ALS patients and the lethal nature of the disease means the only post-prognosis alternative is disease management. This includes a combination of supportive, palliative and multi-disciplinary care (Gordon, 2013). ALS sufferers can also undergo non-invasive ventilation to assist in prolonging survival and improve their quality of life (Traynor *et al.,* 2003).

1.3 Dystrophinopathies and DMD

Primary genetic abnormalities in the dystrophin gene result in the early onset and debilitating muscle wasting allelic disorder Duchenne muscular dystrophy or the delayed-onset less common and milder form Becker muscular dystrophy, BMD (Koenig *et al.,* 1989). Duchenne muscular dystrophy, DMD, is one of the most frequently inherited lethal neuromuscular diseases of childhood (Muntoni *et al.,* 2003), with a prevalence of approximately 1 in 3,500 live male births (Mah *et al.,* 2014). Regional and national differences in disease frequency have been reported (Moat *et al.,* 2013).

From a young age of approximately 3 years boys exhibit early physical indicators of the disease, including progressive proximal muscle wasting, waddling gait, toe walking, slow running patterns or frequent falls (Chelly and Desguerre, 2013; Rahimov and Kunkel, 2013). At a molecular level, certain typical proteins for this form of inherited muscle disease have drastically increased levels. These include serum creatine kinase, pyruvate kinase and carbonic anhydrase isoform CA-3 (Zatz *et al.,* 1991; Ohta *et al.,* 1991). The rapid progression of symmetrical muscle wasting leads to loss of unassisted ambulation around 12 years of age. The continuous muscle wasting and progressive degeneration of the skeletal musculature leads to weakening of the heart and other respiratory muscles, which in turn triggers lethal cardiac or respiratory failure in mid to late twenties (Bushby *et al.,* 2010; Mosqueira *et al.,* 2013). Some dystrophinopathy cases exhibit scoliosis (Kinali *et al.,* 2006; Hsu *et al.,* 2013), non-progressive forms of mental retardation (Kozicka *et al.,* 1971) and attention deficit hyperactivity disorder (Pane *et al.,* 2012).

Figure 1.10, panels A and B, shows transverse muscle tissue cryosections, stained with haematoxylin and eosin, clearly depicting abnormal variation in muscle fibre diameter in typical dystrophic fibres (B) when compared to age matched normal skeletal muscle fibres (A). Dystrophin deficient skeletal muscles (B) exhibit increased levels of endomyosial fat and connective tissue, in addition to the presence of necrotic and regenerative fibres with central nucleation (Holland *et al.,* 2013A).

DMD results from a primary abnormality in the gene coding for the cytoskeletal protein dystrophin (Hoffman *et al.,* 1987). The dystrophin gene is the largest known gene containing 2.4 million bases and because of its enormous size is highly susceptible to mutations (Tennyson *et al.,* 1995). At the genetic level DMD can be caused due to recessive, frame-shifting deletions and duplications or nonsense mutations resulting in muscle fibres with complete loss of or overexpression of non-functional dystrophin (Monaco *et al.,* 1986; Hoffman *et al.,* 1987; Koeing *et al.,* 1987). Full-length dystrophin isoform (Dp427) is a large membrane cytoskeletal protein, located in the fibre periphery, 427 kDa in size. The full-length dystrophin isoform functions as a molecular anchor that provides an indirect linkage between the basal lamina and the actin membrane cytoskeleton. Deficiency and/or absence of this crucial protein is believed to be the primary cause of the disintegration of the sarcolemmal integrity (Holland *et al.,* 2013A; Rahimov and Kunkel, 2013). This causes the sarcolemma to become more susceptible to contraction induced micro-rupturing. Repair mechanisms to the micro-rupturing seem to induce Ca^{2+}-leak channels in the sarcolemma creating increased levels in Ca^{2+}-levels in the dystrophic cytosol (Alderton and Steinhardt, 2000). Elevated proteolytic activity triggers different direct and

indirect negative effects on energy metabolism, ion handling and the structural integrity of Dp427 deficient muscle. Chronic changes in crucial pathways and cellular mechanisms cause drastic muscle tissue wasting and decreased muscle strength, ultimately leading to end stage contractile failure (Lewis *et al.,* 2009).

In 2014, Wang and colleagues reported that intragenic deletion of the dystrophin-encoding DMD gene is a frequent mechanism that leads to myogenic tumours progressing to high-grade sarcomas that can be fatal. Their work has shown that dystrophin is a tumour suppressor in human cancers with myogenic programs.

The dystrophin isoform Dp427 has an autosomal homologue, utrophin Up395 (Ohlendieck *et al.,* 1991A). Dp427 and Up395 do not exist in isolation; they form high molecular mass complexes with a variety of muscle proteins (Campbell and Kahl, 1989; Matsumura *et al.,* 1992). In some cases of DMD, rare reverting mutants may account for a minor amount of dystrophin-positive muscle fibres (Thanh *et al.,* 1995).

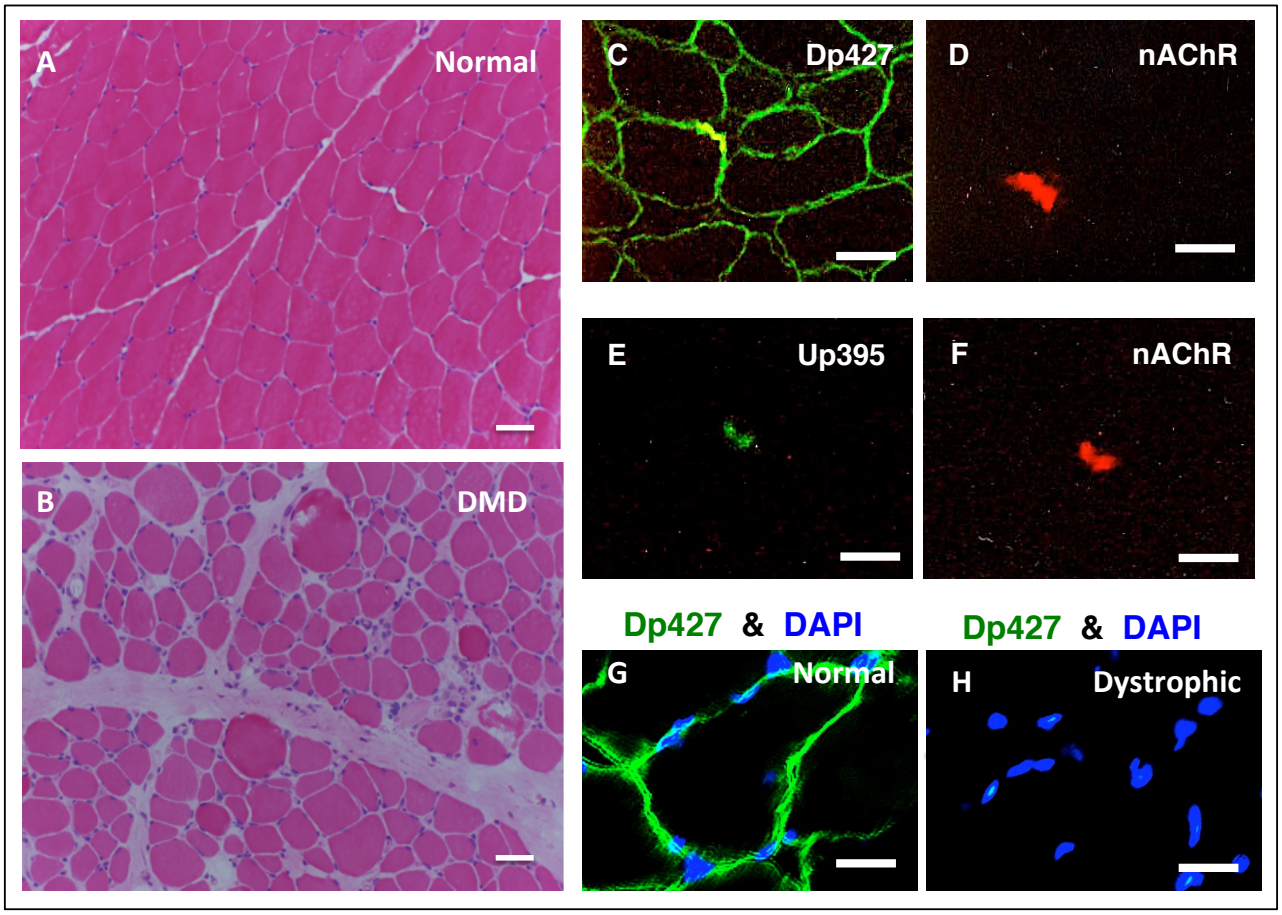

Figure 1.10 Histological hallmarks of dystrophinopathy and immunofluorescence localization of dystrophin and utrophin in skeletal muscle.
Shown is the histological staining of transverse cryosections from normal (A) versus dystrophic (DMD, Duchenne muscular dystrophy) (B) skeletal muscle using haematoxylin and eosin. Immunofluorescence microscopy was employed to demonstrate the surface localization of the full-length dystrophin isoform Dp427 (green) (C) and its autosomal homologue utrophin Up395 (green) (E) in normal muscle, as compared to the position of the neuromuscular junction that has been labeled with α-bungarotoxin (red) (D, F). Panels (G) and (H) illustrate the absence of dystrophin isoform Dp427 (green) in dystrophic skeletal muscle. Nuclei (blue) have been labeled with diamidino-2-phenylindole (DAPI). Bars equal 40 µm.
*Image from Holland *et al.,* 2013A

1.3.1 Dystrophin and its isoforms

The molecular structure of the 427 kDa rod-shaped membrane cytoskeletal protein dystrophin is illustrated in Figure 1.11 A. There are four prominent domains in dystropin. The first is an amino terminal region with 2 calponin homology units that have a strong interaction with the actin membrane cytoskeleton (Norwood *et al.,* 2000). The second domain is a central rod domain containing 24 spectrin-like repeats separated by proline rich hinge regions (H1-4) where the middle domain functions as a second alternative actin-binding site close to the amino-terminus (Broderick and Winder, 2005; Muthu *et al.,* 2012). The third is a cysteine rich domain, pivotal for binding the integral glycoprotein β-dystroglycan and has a WW-domain that binds β-dystroglycan and a ZZ-module that binds syntrophins (Hnia *et al.,* 2007; Ilsley *et al.,* 2002). Finally the fourth domain is a unique carboxy-terminal domain that binds through its coiled-coil protein-binding motifs to dystrobrevins (Sadoulet-Puccio *et al.,* 1997, Le Rumeur *et al.,* 2010).

The dystrophin gene has seven different promoters that express three full-length transcripts and four shorter isoforms in various cellular locations (Muntoni *et al.,* 2003), generated by alternative splicing and post-translational modifications (Sadoulet-Puccio and Kunkel, 1996). These dystrophin specific promoters determine the tissue specific expression of the Dp427 isoforms, as seen in Figure 1.11. Dp427-M, is found in skeletal and cardiac muscle, Dp427-B in the brain and Dp427-P in Purkinje cerebellar cells (Klamut *et al.,* 1990; Nudel *et al.,* 1989; Gorecki *et al.,* 1992).

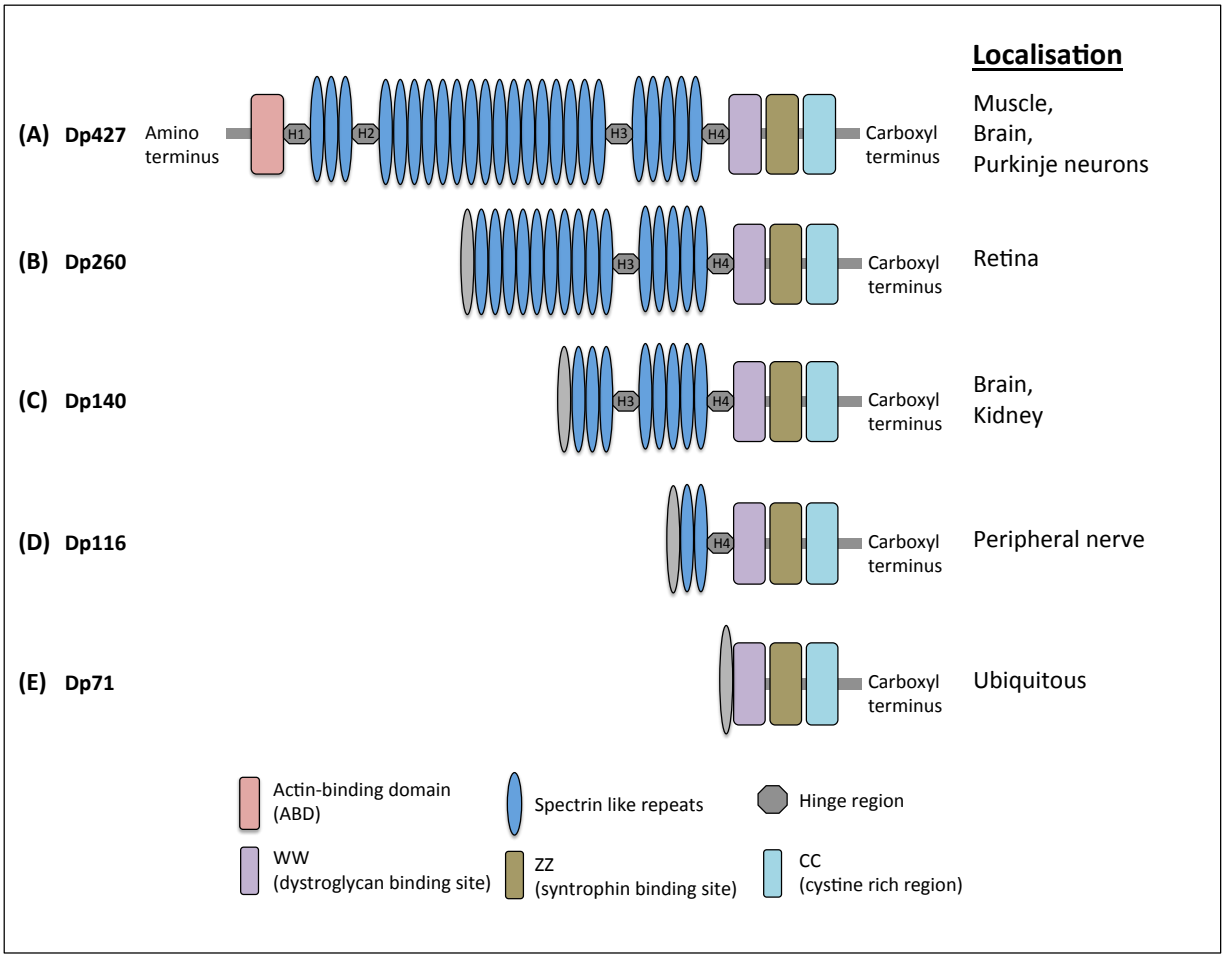

Figure 1.11 Dystrophin and dystrophin isoforms.
Shown is a diagram of the domain structure of the full-length Dp427 isoform of the membrane cytoskeletal protein dystrophin (A), and shorter dystrophin isoforms of relative molecular mass; the retinal isoform Dp260 (B), brain and kidney isoform Dp160 (C), Schwann cell isoform in the peripheral nerves Dp116 (D) and the truncated ubiquitous dystrophin isoform Dp71 (E).
*Image modified from www.medscape.com and Holland and Ohlendieck, 2013

Shorter isoforms of functional dystrophin are also present in other parts of the neuromuscular system. These include the retinal isoform Dp260-R (Figure1.11 B), brain and kidney isoform Dp160-B/K (Figure1.11 C), Schwann cell isoform in the peripheral nerves Dp116-S (Figure1.11 D) and finally the truncated ubiquitous dystrophin isoform Dp71-G (Figure1.11 E) (D'Souza *et al.,* 1995; Lidov *et al.,* 1995; Byers *et al.,* 1993; Bar *et al.,* 1990; Tinslet *et al.,* 1993). In comparison to full-length dystrophin, some of these shorter isoforms lack the actin-binding domain and in-turn function in a significantly different way than Dp427 in skeletal or cardiac muscle or in the central nervous system (Culligan and Ohlendieck, 2002).

1.3.2 Dystrophin-associated glycoprotein complex

The dystrophin-associated glycoprotein complex, DAGC, is a highly complex protein arrangement located at the muscle periphery. The principal elements of the dystrophin-glycoprotein complex, DGC, are associated with the membrane cytoskeleton, sarcolemma, and the extracellular matrix, ECM (Ohlendieck, 1996; Rahimov and Kunkel, 2013).

The membrane cytoskeletal elements of the DGC include the dystrophin isoform Dp427, which is located internally of the sarcolemma membrane and forms a structural network with a variety of non-dystrophin proteins in both skeletal and cardiac muscle fibres, as outlined in Section 1.3.2. (Watkins *et al.,* 1988; Ervasti and Campbell, 1993). Other DGC membrane cytoskeletal components include actin, 43 kDa (Rybakova and Ervasti, 1997), α-dystrobrevin, 94kDa (Sadoulet-Puccio *et al.,* 1997) and α, β_1 and β_2-syntrophin isoforms of 58,

59 and 60 kDa, respectively (Gee *et al.,* 1998).

The integral DGC components of the sarcolemma are represented by the (i) sarcoglycan sub-complex, comprised of 4 different sarcoglycan isoforms of varying molecular masses; α-sarcoglycan, 50 kDa, β-sarcoglycan, 43 kDa, γ-sarcoglycan, 35 kDa, and δ-sarcoglycan, 35 kDa (Roberds *et al.,* 1993; Yoshida *et al.,* 1997) (ii) sarcospan, a highly hydrophobic protein of 25 kDa (Crosbie *et al.,* 2000) and (iii) the core element β-dystroglycan, 43 kDa, the trans-sarcolemmal linker glycoprotein (Ibraghimov-Beskrovnaya *et al.,* 1992). In dystrophin deficient tissue, as seen in DMD patients, the concentration of all sarcolemmal DAGC proteins is drastically reduced (Culligan, 1998).

The ECM proteins are the final group of proteins comprising the DGC. The extracellular proteins are indirectly linked to the muscle isoform Dp427 through α-dystroglycan, 156 kDa (Bozzi *et al.,* 2009; Moore and Winder, 2012) and the basal lamina element laminin-α2, 400 kDa (Ervasti and Campbell, 1993). Further to the above-mentioned fundamental components of the DGC it is important to note that signalling proteins, neuronal nitric oxide synthase (Brenam *et al.,* 1996), and ion channels, voltage gated Na^+-channels (Gee *et al.,* 1998), are indirectly linked to this dystrophin network of biomolecules (Ervasti and Sonnemann, 2008).

Differences in subcellular localisation and protein composition exist between the cardiac and skeletal DGC. The muscle complex is heavily enriched in both the sarcolemma (Ohlendieck, 1991B) and the neuromuscular junction (Ohlendieck, 1991A) and coexist with the utrophin-glycoprotein complex (Matsumura *et al.,* 1992). The cardiac complex is also found in the transverse tubular system (Klietsch *et al.,* 1993) and partially associates with costameric

vinculin (Kaprielian and Severs, 2000). This vinculin association could suggest a physical role in the maintenance of surface membrane integrity and membrane domain organisation (Lapidos *et al.,* 2004). In contrast to the skeletal DGC the cardiac DGC does not appear to interact with the signalling enzyme nNOS, has a different composition in syntrophin and dystrobrevin proteins and shows extra binding partners in cavlin-1, ahnak-1, cypher and cryab (Johnson *et al.,* 2012; Rahimov and Kunkel, 2013).

Figure 1.12 gives a schematic summary of the molecular organisation of the dystrophin-associated glycoprotein complex, DAGC. The primary function of the internal membrane protein Dp427 is providing a stabilising link between the extracellular matrix, ECM, protein laminin and the actin network found inside the muscle (Ervasti and Campbell, 1993; Rahimov and Kunkel, 2013). Dp427 acts as a molecular anchor in such a way that the N-terminus side of Dp427 and the rod domain bind the muscle actin filaments while the other domains on the full-length Dp427 associate indirectly with the α2-chain of laminin via binding to β-dystroglycan. This then secures the position of the peripheral laminin-binding protein α-dystroglycan on the external muscle surface. The DGC provides stability for the structural integrity of the muscle periphery during excitation-contraction-relaxation cycles. It further prevents potentially harmful rupturing of the muscle sarcolemmal membrane system (Gumerson and Michele, 2011). Deficiency or absence in dystrophin is directly linked with an elevated frequency of micro rupturing of the muscle plasma membrane and subsequent repair mechanisms resulting in abnormal Ca^{2+}-handling (Culligan *et al.,* 1998; Vallejo-Illarramendi *et al.,* 2014).

Abnormalities of individual proteins of the DAGC can lead to specific muscle diseases, Figure 1.12 of the DAGC also outlines these pathophysiological linkages (Holland and Ohlendieck, 2013; Shin *et al.,* 2013). Duchenne muscular dystrophy, DMD, Becker muscular dystrophy, BMD, X-linked dilated cardiomyopathy, XDCM, congenital muscular dystrophy, CMD, and different forms of limb-girdle muscular dystrophy, LGMD, are all caused due to primary or secondary alterations in the structure and/or abundance of Dp427 and members of the DGC (Campbell, 1995; Rahimov and Kunkel, 2013).

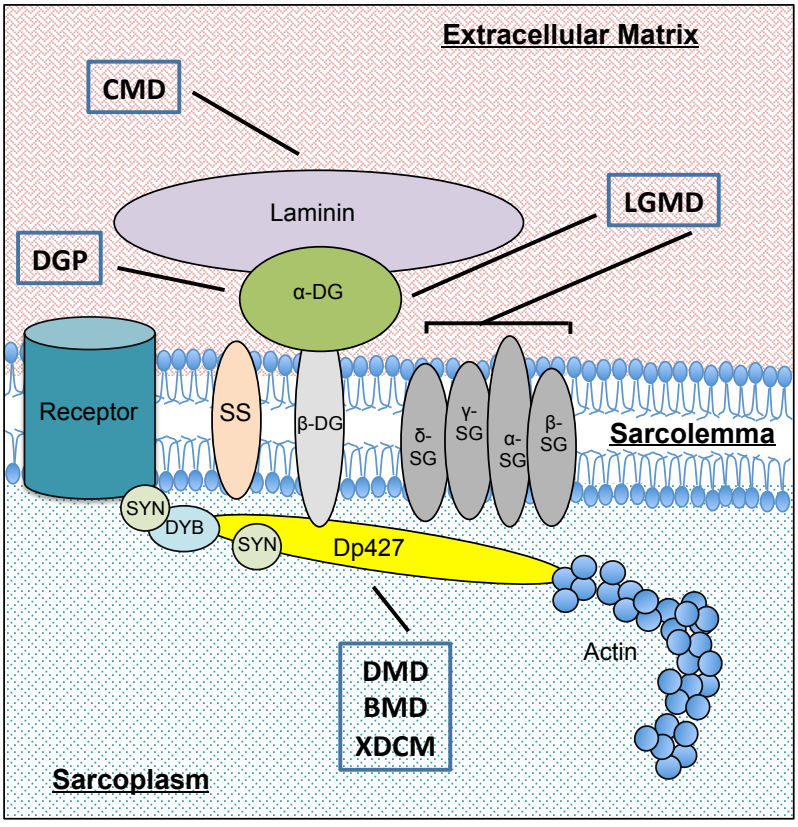

Figure 1.12 The dystrophin-associated glycoprotein complex, DAGC.
Shown is the composition of the core dystrophin-associated glycoprotein complex found in skeletal muscle. The association between primary abnormalities in select individual members of the dystrophin-glycoprotein complex and inherited muscle diseases are indicated. BMD, Becker muscular dystrophy; CMD, congenital muscular dystrophy; DGP, dystroglycanopathy; DMD, Duchenne muscular dystrophy; LGMD, limb-girdle muscular dystrophy; XDCM, X-linked dilated cardiomyopathy.
*Image from Holland *et al.,* 2013A

1.3.3 Cardiomyopathy and DMD

Heart disease plays a prominent role in the aetiology of X-linked muscular dystrophy (Cox and Kunkel, 1997). While dystrophinopathies are primarily considered skeletal muscle disorders that experience progressive muscle wasting (Bradley *et al.,* 1972), at end stages of the disease patients experience serious impairments of the respiratory system and cardiomyopathic complications (Nigro *et al.,* 1990; Fayssoil *et al.,* 2010). During the second decade of life the majority of DMD patients exhibit clinical cardiac symptoms (Finsterer and Stöllberger, 2003), including arrhythmias, cardiomyopathy and regional wall abnormalities (Fayssoil *et al.,* 2010).

Loss of cardiac dystrophin initially leads to changes in dystrophin-associated proteins triggering numerous secondary cellular abnormalities, such as sarcolemmal disintegration, fibrosis, necrosis, adipose tissue replacement and interstitial replacement (Mutoni, 2003). Contractile fibres are gradually replaced with non-contracting cells, such as connective tissue, leading to a major loss of cardiac cellular function (Frankel and Rosser, 1976). Dystrophic cardiac muscle exhibits a limited regenerative capacity, as it does not experience cycles of degeneration and regeneration as seen in skeletal muscle (Finsterer and Stöllberger, 2003). This disease associated degeneration leads to progressive cardiac disease and thus fatal complications in DMD patients (Holland and Ohlendieck, 2014A). Over recent years respiratory care for DMD patients has greatly improved, leading to a more prominent role in cardiomyopathy treatment for the general overall therapy for DMD (Bach and Martinez, 2011; Passamano *et al.,* 2012).

1.3.4 Comparison of sarcopenia of old age versus dystrophic sarcopenia

Natural muscle aging, outlined in Section 1.1.5, and dystrophic muscle aging are both characterised by progressive loss of contractile muscle tissue mass, an increased levels of fibrosis, a reduction in satellite cell populations, a significantly increased stress response and abnormal cellular signalling (Berger and Doherty, 2010; Doran *et al.,* 2006).

The comparison of proteomic data sets from the analysis of muscular dystrophy versus sarcopenia is suggestive that the pathobiochemical signature of certain damage or adaption pathways is comparable, however the molecular pathogenesis of both mechanisms is different in relation to the degree of unilateral shifts in fibre types or energy metabolism. Both natural and dystrophic aging processes exhibit a disturbed abundance of proteins associated with contractile apparatus, muscle metabolism, the cellular stress response, calcium homeostasis, the excitation-contraction coupling, cellular signalling cascades and the cytoskeletal network (Doran *et al.,* 2006B; Doran *et al.,* 2007B; Staunton *et al.,* 2012) as presented in Figure 1.13.

Both forms of age-related muscular atrophy are linked with altered levels of key enzymes of glycolysis, the citric acid cycle and oxidative phosphorylation (Piec *et al.,* 2005; Doran *et al.,* 2006B; Doran *et al.,* 2008). Dystrophic sarcopenia experiences impaired calcium handling with decreased levels in calcium-binding proteins and abnormal calcium-ATPase activity, while normal aging of muscles have a fast-to-slow transformation and normal calcium-ATPase and calcium-binding proteins (Allen *et al.,* 2010). During natural and dystrophic sarcopenia cellular stress response is initiated and both express increased levels of small heat shock proteins, such as αB-crystallin and certain HSPB isoforms (Doran *et*

al., 2006A; Doran *et al.,* 2007B). In contrast, dystrophic aging muscle exhibits generally perturbed levels of metabolic enzymes, while proteomic profiling of normal muscle naturally aging indicates a clear glycolytic-to-oxidative metabolic shift and paralleled fast-to-slow transformation in the actomyosin apparatus (Ohlendieck, 2011A).

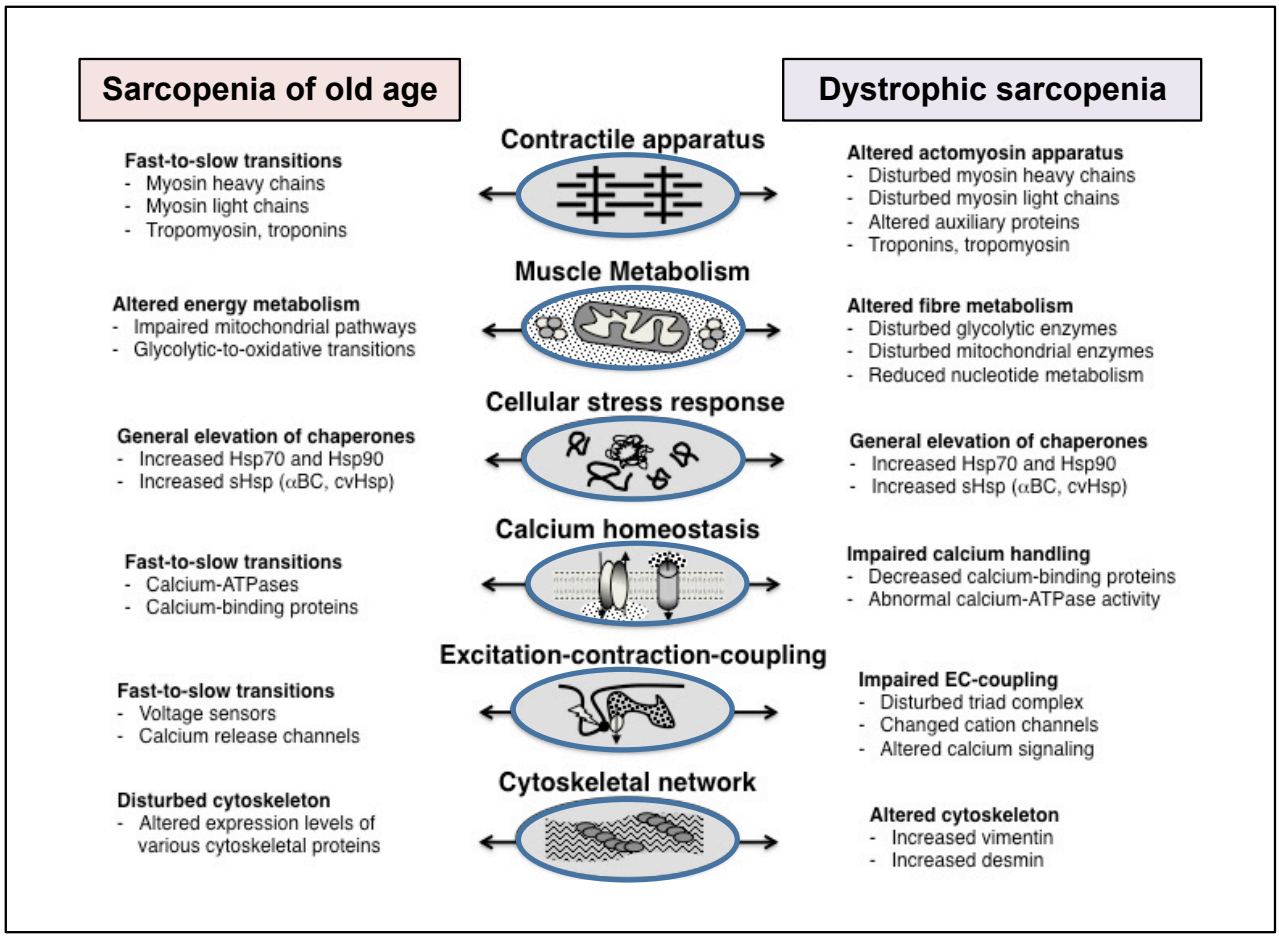

Figure 1.13 Overview of the proteome wide alterations in the muscle tissue during sarcopenia of old age versus dystrophic sarcopenia.
*Image from Holland *et al.,* 2014B

1.4 Animal models and research

The use of animal models in biomedical research is imperative for the investigation of basic aspects of pathophysiology mechanisms and more complex preclinical evaluation of new and potential treatment and therapeutic options (Guenet, 2011). Animal models have been routinely used in neuromuscular research, including proteomic studies of neuromuscular disorders such as ALS and DMD (Vainzof *et al.,* 2008). In order to make biomedical research meaningful and for it to benefit the field, animal models should ideally fulfill certain criteria, including; (i) show closely related genetic abnormalities found in corresponding human disorders, (ii) exhibit similar secondary alterations at the molecular, cellular, tissue and organ level, (iii) illustrate a resemblance to the human pathology in relation to disease onset, progression and severity, (iv) exhibit several of the multi-factorial symptoms seen in human diseases and (v) resemble fundamental physiological, metabolic and immunological features of the human organism (Doran *et al.,* 2007A).

1.4.1 The wobbler mouse

Animal models mimicking the human form of diseases, such as motor neuron disease, play an essential role in ALS research and are routinely used for pathobiochemical studies and for the evaluation of novel pharmacological approaches (McGoldrick *et al.,* 2013). The wobbler, WR, mouse is an established mouse model frequently used in ALS research (Iwamoto *et al.,* 2009; Canzi *et al.,* 2012; De Paola *et al.,* 2012).

1.4.2 Genotype of the wobbler mouse

The wobbler, WR, mouse (genotype *wr/wr*, phenotype WR) (Duchen and Strich, 1968; Moser *et al.,* 2013) has a C57BL/6J background (Leestma *et al.,* 1980; Heimann *et al.,* 1991) and exhibits progressive neurodegeneration and neuroinflammation (Laage *et al.,* 1988; Karlsson *et al.,* 2013; Broch-Lips *et al.,* 2013).

The wobbler mouse exhibits a recessive mutation in the WR genotype on chromosome 11 (Kaupmann *et al.,* 1992). This genetic abnormality has been identified as a missense mutation in the ubiquitously expressed gene *Vps54.* The *Vps54* gene encodes for the vesicular protein-sorting factor VPS-54, an essential component of the hetero-trimeric Golgi-associated retrograde protein (GARP) complex. VPS-54 is a crucial factor for intracellular transport mechanisms (Bonifacino and Hierro, 2011). However no human neurodegenerative disease has been identified that exhibits the same genetic abnormality as seen in the WR mouse (Meisler *et al.,* 2008).

This mutation in the WR mouse genotype leads to an altered primary amino acid sequence, with a leucine-to-glutamine replacement (L967Q) near the C-terminus of the 977 amino acid polypeptide chain of the VPS-54 protein (Schmitt-John *et al.,* 2005). This amino acid exchange causes a destabilization of the tertiary structure of the VPS-54 protein and as a consequence of the hydrophobic-to-hydrophilic amino acid replacement there is a reduction in concentration levels of VPS-54 (Perez-Victoria *et al.,* 2010).

Embryonic lethality occurs in the homozygous knockout of the *Vps54* gene (Schmitt-John *et al.,* 2005). In homozygous mice the *wr* allele is relatively mild, allowing the animals to survive for several months. These mice develop

muscular atrophy at a highly elevated rate (Moser *et al.,* 2013) and have a secondary feature of impaired spermatogenesis (Leestma *et al.,* 1980; Heimann *et al.,* 1991; Paiardi *et al.,* 2011).

1.4.3 Phenotype of the wobbler mouse

Wobbler mice go through 3 phases during their lifecycle; (i) pre-symptomatic phase (0 to 3-weeks old), (ii) evolutionary phase (3-weeks to 3-months old) and (iii) stabilization phase (3-months to death). The pre-symptomatic phase occurs during the first 3-weeks of postnatal life, at which point wobbler mice do not present clinical signs of the disease and appear normal (Boillée *et al.,* 2003). Symptoms begin to manifest in the evolutionary phase at 3 to 4-weeks old during juvenile life stages and continues until mice are 2 to 3-months old. From weeks 3 to 4 wobbler mice are 40-50% smaller than their control littermates and remain smaller throughout their lifespan (Andrews *et al.,* 1974; Bose *et al.,* 1999; Coulpier *et al.,* 1996). Wobbler mice entering the evolutionary phase begin to present with a progressive unsteady gait and a discrete head tremor develops, hence the name “wobbler”. Muscular strength in the forelimbs is decreased at 3-weeks old (Ishiyama *et al.,* 1997; Smith *et al.,* 1997) and muscle tension is affected by the fourth week and decreases with age unlike in healthy control mice where muscle tension increases with age (Ikeda and Mitsumoto, 1993). Muscular weakness of the forelimbs become apparent from ages 4 to 5-weeks old, with noticeable reduced capacity of the fore paws ability to cling. The weakness of the muscles of the forelimbs, head and neck steadily decline over the evolutionary period. However, the hind limb muscles

exhibit a slower functional decline until the mice are 12-weeks old, at which point they progressively lose the ability to extend their forelimbs at the wrists causing difficulty in walking and climbing (Boillée *et al.,* 2003). Several signs of degeneration and notable loss of motor neurons are evident during this time period (Pollin *et al.,* 1990). Following this, the clinical symptoms halt in the progression of motor neuron disease and begin to stabilize in older mice of 3 to 5-months old during the final months of life (Boillée *et al.,* 2003).

1.4.4 Impaired spermatogenesis and the wobbler mouse

The WR mouse demonstrates a defect in sperm assembly. This is linked with a failure to form an acrosome and an elongated sperm head (Leestma *et al.,* 1980; Heimann *et al.,* 1991). Abnormalities such as this are similar to the human globozoospermia form of impaired spermatogenesis (Dam *et al.,* 2007).

The WR mouse has become recognised as an ideal model for studying globozoospermia due to its characteristic abnormally round-headed irregular morphology of sperm cells. This abnormality, in combination with lack of a proper acrosome, prevents sperm penetrating the *zona pellucida* and fusing with oocytes (Leestma *et al.,* 1980; Heimann *et al.,* 1991; Paiardi *et al.,* 2011).

Previous studies of WR spermatids have shown increased concentrations of mouse ubiquitin-specific processing protease mUBPy and differential sorting of this deubiquitinating enzyme (Chianese *et al.,* 2010). Another protein that adds to the reduced fertilizing capacity of WR sperm cells is the oocyte-activating factor phospholipase PLC-zeta due to its abnormal localization (Heytens *et al.,* 2010).

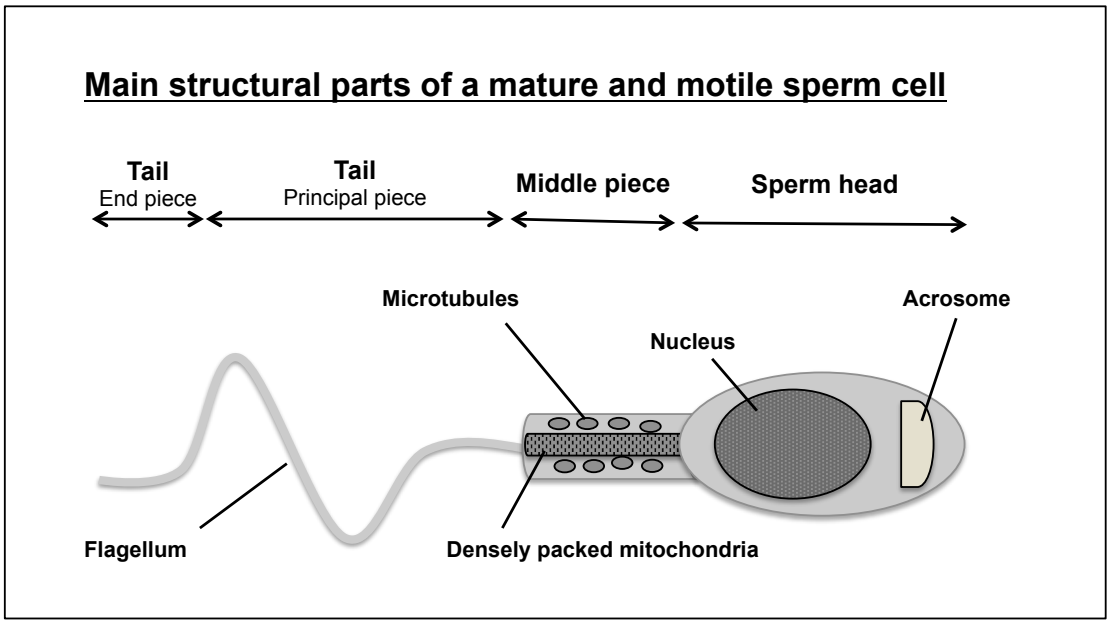

Figure 1.14. Overall general structure of a mature normal sperm cell.
Shown are the main structural parts of a mature and motile sperm cell, including the sperm head, the middle piece and both the principal piece and end piece of the sperm tail.
*Image from Holland and Ohlendieck, 2014B

Electron microscopy imagery on normal intact spermatozoa has demonstrated standard zoning into the head domain and sperm tail, Figure 1.14 (Baker *et al.,* 2005; Holland and Ohlendieck, 2014B). Sperm cells from the WR mouse have an irregularly rounded head structure containing a deformed nucleus and lacking an acrosome, showing a distinct contrast to normal sperm. Furthermore, the majority of wobbler spermatozoa exhibit aberrations in the axoneme structure in the principal piece (Holland and Ohlendieck, 2014B). In combination, these morphological abnormalities of WR sperm cells are highly similar to that of globozoospermia in infertile men (Alvarez Sedo *et al.,* 2012; Dam *et al.,* 2011) and make the testis of the WR mouse a distinctly suitable animal model for assistance in determining the basis of impaired spermatogenesis.

1.4.5 Animal models of X-linked muscular dystrophy

Mammalian animal models are routinely used in muscular dystrophy research (Banks and Chamberlain, 2008), including the established dystrophin-deficient *mdx* mouse (Bulfield *et al.,* 1984), *mdx-4cv* mouse (Banks *et al.,* 2010) and dystrophic breeds of dogs, the *grmd* golden retriever (Kornegay *et al.,* 2012). The *mdx,* murine X-chromosome linked, and *mdx-4cv* mice are fundamental models of dystrophinopathy and crucial for the global strategy to develop new approaches to counter-act muscle wasting in muscular dystrophy. These models have been extensively employed for the evaluation of experimental treatments (Spurney *et al.,* 2009), including gene transfer therapy (Wells and Wells, 2002; Tedesco, 2015), myoblast transfer therapy (Partridge *et al.,* 1989), exon skipping therapy (Doran *et al.,* 2009B), and other pharmacological interventions (Fairclough *et al.,* 2012).

1.4.6 Genotypes of the *mdx* and *mdx-4cv* mice

The *mdx* mouse exhibits dystrophin deficiency due to a single base substitution within exon 23 of the Dp427-encoding gene in the Xp21 region of the X-chromosome. The original and naturally occurring mutation in *mdx* mice is a G to A replacement (Bulfield *et al.,* 1984). This causes a premature protein termination, preventing the coding of the full-length dystrophin polypeptide chain (Sicinski *et al.,* 1989) leading to a truncated protein product of dystrophin that is quickly degraded in dystrophic muscle fibres (Partridge *et al.,* 1989).

Chemical mutagenesis with N-ethylnitrosourea has created four additional *mdx* strains, *2cv*, *3cv, 4cv* and *5cv* (Chapman *et al.,* 1989). The *mdx-4cv*

dystrophic mouse has a C to T transition in exon 53. This genetic base change causes a nonsense codon (Im *et al.,* 1996) leading to the almost complete absence of dystrophin (Banks *et al.,* 2010). Many of the pathological consequences seen in human dystrophic muscle including, elevated levels of the general muscle marker-serum creatine kinase (Torres and Duchen, 1987), increased vulnerability to stretch- and contraction-induced muscle injury (Weller *et al.,* 1990; Lynch *et al.,* 2000) and muscle fibres highly susceptible to osmotic shock (Menke and Jockusch, 1991) are also recognizable in both *mdx* and *mdx-4cv* mouse species.

1.4.7 Phenotypes of the *mdx* and *mdx-4cv* mice

Aged *mdx* muscle exhibit severe disease associated symptoms (Lefaucheur *et al.,* 1995). These symptoms include the presence of branched fibres that can trigger mechanical weakening of the plasmalemma (Head *et al.,* 2010), loss and replacement of myofibres with extensive connective tissue (Pastoret and Sebille, 1995) leading to progressive motor weakness (Lynch *et al.,* 2001), increased susceptibility to spontaneous rhabdomyosarcoma (Chamberlain *et al.,* 2007), reduced structural and functional recovery post-injury (Irintchev *et al.,* 1997) and a major decline in the regenerative potential of affected muscle fibres (Mouisel *et al.,* 2010).

During senescence the *mdx* mouse demonstrates severe muscle wasting and replacement of myofibres with connective tissue (Pastoret and Sebille, 1995), leading to progressive motor weakness (Lynch *et al.,* 2001). During aging the *mdx* phenotype closely resembles the human pathology of

dystrophinopathies, thus indicating the importance of exploiting the model for aging studies to determine age-related changes in dystrophin-deficient fibres (Carberry *et al.,* 2012A; Doran *et al.,* 2006A; Lewis *et al.,* 2010; Holland *et al.,* 2013A).

At the molecular level, *mdx* muscle tissue exhibit significantly reduced levels of dystrophin-associated proteins (Ohlendieck and Campbell, 1991), similar to the human form. In addition *mdx* muscle exhibits elevated cytosolic Ca^{2+}-handling in the sarcoplasmic reticulum (Doran *et al.,* 2004; Culligan *et al.,* 2002; Dowling *et al.,* 2004). The same primary abnormality in this monogenic disorder causes a range of alterations in different subtypes of *mdx* and *mdx-4cv* muscle. Extraocular, *interosseus* and laryngeal *mdx* muscles are minimally effected, indicating a mild phenotype (Dowling *et al.,* 2003; Dowling *et al.,* 2002; Marques *et al.,* 2007), limb muscles including *soleus, gastrocnemius, extensor digitalis longus* and *tibialis anterior* are moderately weakened and experience segmental necrosis (Torres and Duchen, 1987) and the diaphragm undergoes sever fibre degeneration, representing the most severely disturbed skeletal muscle type in the *mdx* mouse (Stedman *et al.,* 1991; Holland *et al.,* 2013A).

The *mdx-4cv* mouse model exhibits very few dystrophin-positive revertant fibres (Danko *et al.,* 2011; Judge *et al.,* 2006), thus making it an excellent pathophysiological system for the evaluation of experimental gene therapies; including exon skipping (Mitrpant *et al.,* 2009), artificial chromosomes (Tedesco, 2015) and viral vector transfer methods (Kimura *et al.,* 2010). However this *mdx-4cv* model is not as well characterized as the more conventional *mdx* mouse.

1.4.8 Cardiomyopathy and *mdx* mice

Besides the skeletal musculature, the *mdx* heart is also affected by a number of cellular, physiological and biochemical abnormalities and cardiorespiratory complications, mirroring frequent symptoms of DMD (Holland and Ohlendieck, 2014A). The lack of cardiac dystrophin is associated with necrotic changes, infiltration of inflammatory cells, elevated levels of adipose tissue, interstitial fibrosis and tachycardia, leading to impaired contractile properties in *mdx* cardiac tissue (Bridges, 1986; Sapp *et al.,* 1996; Bia *et al.,* 1999).

Similar to DMD hearts, *mdx* heart muscle cells have a greatly reduced expression of dystrophin-associated glycoproteins (Lohan *et al.,* 2005) and experiences similar differences between the DAGC in skeletal and cardiac muscle with respect to the human form of the diseases, see Section 1.3.2.

The dystrophic phenotype of the young *mdx* heart does not represent a perfect replica of DMD-related cardiomyopathic complications (Bridges, 1986). Obvious signs of cardiomyopathy are more prominent in aged *mdx* mice as compared to milder cardiac alterations in young mice (van Erp *et al.,* 2010; Verhaart *et al.,* 2012). Senescent *mdx* mice demonstrate elevated levels of widespread and patchy ventricular wall fibrosis (Quinlan *et al.,* 2004) and the basal region shows a higher degree of fibrotic changes than the apex of the dystrophic heart (Cheng *et al.,* 2012). However in the aged *mdx* heart the pathological changes have been deemed to be of considerable clinical relevance (Chu *et al.,* 2002; Quinlan *et al.,* 2004; Khairallah *et al.,* 2007). Cardiac *mdx* fibres are frequently used to evaluate new treatment strategies to counteract cardiomyopathic complications associated to dystrophin deficiency (Yue *et al.,*

2003; Wehking-Hendrick *et al.,* 2005; Wu *et al.,* 2008).

Key luminal Ca^{2+}-binding proteins (Lohan and Ohlendieck, 2004) and abnormal stress-induced Ca^{2+}-influx into the cytosol (Fanchaouy *et al.,* 2009) are some of the secondary abnormalities dystrophic cardiac fibres of the *mdx* mouse experience. Physical exercise and aging appear to speed up the dystrophic process in *mdx* heart muscle (Lefaucheur *et al.,* 1995; Nakamura *et al.,* 2002). In 2008, Spurney and colleagues recognised *mdx* heart dysfunction being most prominent at 9-months of age. The *mdx* mouse is an ideal animal model that can be used to study the proteomic alteration in the dystrophin deficient mouse to help understand the underlying pathophysiological mechanisms of the disease.

1.5 Proteomics

Proteomics is the study of proteins expressed by a cell, and the entire protein complement is known as the proteome (Walther and Mann, 2010). Proteomics aims to study the total proteins expressed in any given system, by abundance, structure, post-translational modification, activity or how certain proteins interact with each other (Wright *et al.,* 2012). Proteomics is an ideal analytical tool for high through put discovery of protein changes in health and disease as it is an unbiased and technology driven approach used for the comprehensive cataloguing of the entire protein complement (Hochstrasser *et al.,* 2002).

The systematic application of large scale-protein separation techniques in combination with mass spectrometry for the identification of unknown proteins has given unprecedented insights into proteome-wide alterations during development, cellular differentiation, physiological adaptions, pathological mechanisms and natural aging (Walther and Mann, 2010; Altelaar *et al.,* 2013; Wang *et al.,* 2014). In 2014 two landmark publications presented the first comprehensive proteome map of over 17,000 distinct proteins encoded by the human genome (Kim *et al.,* 2014; Wilhelm *et al.,* 2014). This first human proteome draft represents the majority of predicted products from the annotated protein coding genes in the human genome (Lander, 2011). However the approximately 20,700 protein coding genes (Lander, 2011; Murgia *et al.,* 2015; Deshmukh *et al.,* 2015) have been estimated to translate into more than 100,000 different protein isoforms as a single gene can often give rise to multiple distinct proteins due to alternative gene splicing, sequence polymorphisms and post-translational modifications (PTMs) (Patel *et al.,* 2009).

Proteomic workflows involve separation of the biological protein sample to order to enhance visualisation and resolution, by gel based or gel free methods, followed by identification of peptide/proteins fragments using mass spectrometry, MS. Bioanalytical software can be used to analyse the MS data and search databases to identify novel targets (Ramasamy *et al.,* 2014).

There are two different approaches that can be used in proteomics. The first is the top-down proteomic approach that analyses the proteome at the intact level. This allows it to preserve any biochemical properties and PTMs of proteins. The alternative is the bottom-up proteomic strategy. This requires enzymatic cleavage of complex proteins samples and heavily relies on chromatography and electrophoretic methods to simplify the peptide fragment populations (Bogdanov and Smith, 2005; Gevaert *et al.,* 2007). Therefore bottom-up proteomics requires accurate, high-speed tandem MS/MS instruments and high throughput database search engines to communicate the mass spectra to peptide sequences, followed by peptides to their parent protein (Lane, 2005).

Proteomics initially strongly relied on two-dimensional gel electrophoresis, 2D-GE, and protein labelling methods (O'Farrell, 1975; Minden *et al.,* 2009). In recent years, proteomics has adapted advanced liquid chromatography and label-free mass spectrometric methods for the comprehensive characterisation of the muscle protein constellation (Walther and Mann, 2010; Ohlendieck, 2011B). 2D-GE can be used in conventional proteomics as it has the ability to study a large portion of muscle-associated proteins including molecular chaperones (Brinkmeier and Ohlendieck, 2014), metabolic enzymes (Ohlendieck, 2010B) and contractile proteins (Holland and Ohlendieck, 2013). However this technique under represents many low-

abundant proteins and large integral membrane proteins, meaning evaluation of potential physiological or pathophysiological effects on these types of proteins require analysis using alternative techniques. Alternative methods include the application of individual or combinations of special protein labelling techniques, organelle proteomics to reduction of sample complexity (Gatto *et al.,* 2010) or the use of one-dimensional, 1D, gradient gels combined with on-membrane digestion prior to MS analysis (Ino and Hirano, 2011).

Skeletal muscle contains protein populations with a broad range of differing physicochemical properties and concentration ranges, making pre-fractionation methods a regular tool to reduce sample complexity and specifically enrich target proteins for subsequent mass spectrometric analysis. Figure 1.15 demonstrates a flowchart how modern proteomics uses standard protein separation approaches and routine protein identification by mass spectrometric analysis.

A crucial part of comparative profiling is the independent verification of proteomic data. Altered abundances of newly identified protein candidates are generally carried out by comparative immunoblotting (Ohlendieck, 2011B). Protein-protein interactions are frequently investigated using co-immuno precipitation assays, chemical crosslinking analysis and biochemical binding experiments. Immunofluorescence microscopy can be employed to investigate subcellular localisation of select proteins and can provide crucial information on fibre type specific expression patterns of newly identified skeletal muscle proteins. In addition to this a variety of biochemical assay, physiological tests and equilibrium dialysis can be used to assist in characterisation of new and potential proteomic markers (Ohlendieck, 2011B).

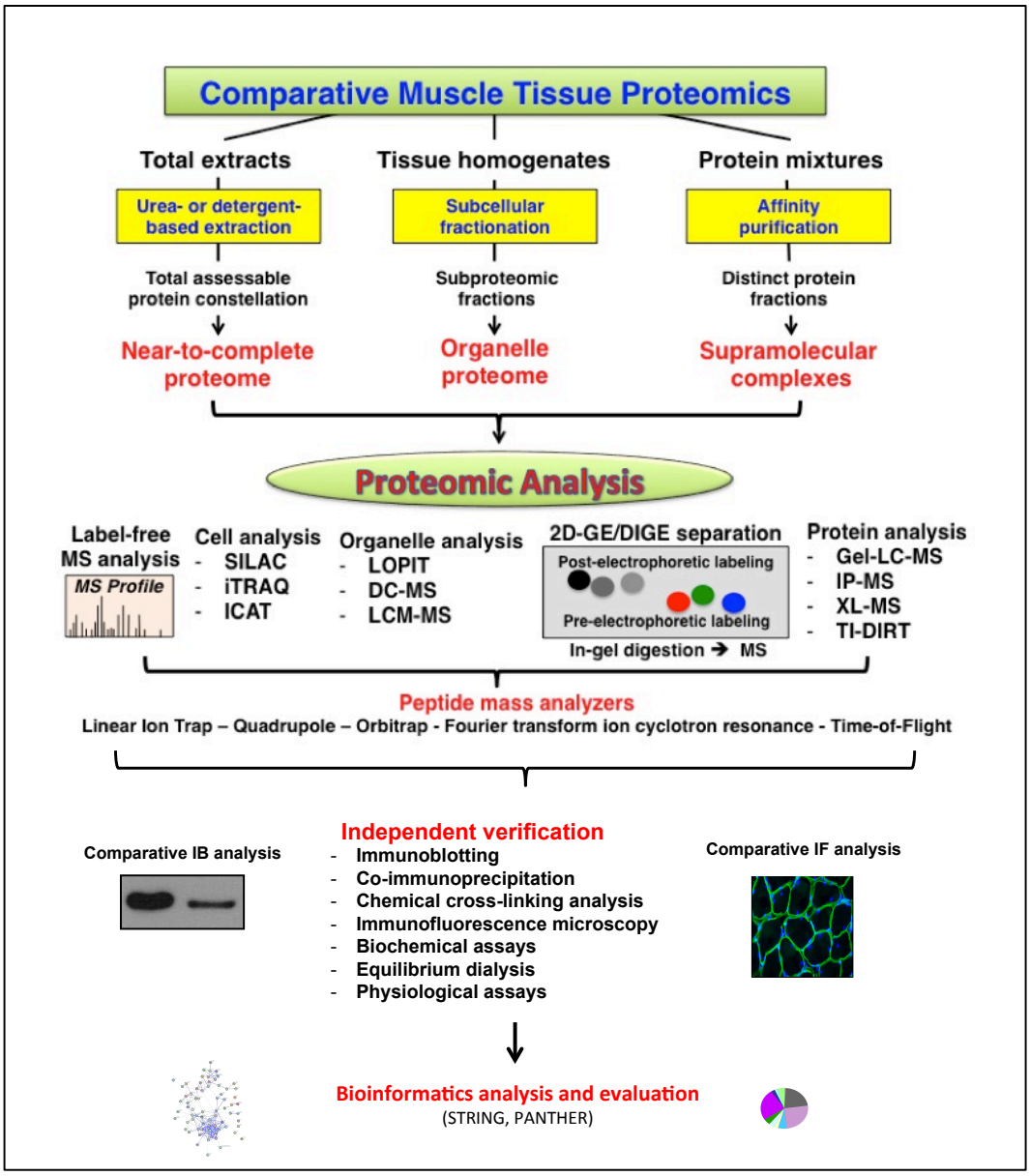

Figure 1.15 Flowchart of the various bioanalytical strategies used in comparative muscle tissue proteomics.

Cellular analyses are often carried out by relative quantitation methods such as SILAC (stable isotope labelling with amino acids in cell culture), iTRAQ (isobaric tags for relative and absolute quantitation) or ICAT (isotope-code affinity tag). Organelle proteomics encompasses LOPIT (localisation of organelle proteins by isotope tagging), LCM (laser capture microscopy) and DC (differential centrifugation) approaches. The most powerful two-dimensional gel electrophoresis (2D-GE) technique used in comparative muscle proteomics is represented by DIGE (difference in-gel electrophoresis). Protein affinity purification methods include IP (immunoprecipitation), XL (chemical crosslinking) and the TI-DIRT method (transient isotopic differentiation of interactions as random or targeted). Distinct protein populations can also be conveniently analysed by a combination of one-dimensional gel electrophoresis and liquid chromatography (LC), followed by MS (mass spectrometry). *Image adapted from Holland and Ohlendieck, 2014E

1.5.1 Gel electrophoresis

Routine protein separation can be accomplished with different gel electrophoretic methods, including one-dimensional gels, two-dimensional gels, and/or advanced liquid chromatography. These gel-based approaches are compatible with both pre- and post-labelling methods. One-dimensional gel electrophoresis, 1D-GE, separates proteins based on their molecular mass, while two-dimensional gel electrophoresis, 2D-GE, involves separation of proteins in two dimensions (O'Farrell, 1975). During 2D-GE proteins are separated in the first dimension on thin strips of polyacrylamide gel containing an immobilised pH gradient, IPG. Proteins can be passively loaded onto IPG strips during strip rehydration. Once rehydrated, an electric current is applied to the IPG strips during isoelectric focusing, IEF, a process in which proteins move through the gel until they reach their *p*I, a pH at which the protein has a net charge of 0. Following this focused strips are equilibrated, through reduction and alkylation, and loaded onto a polyacrylamide slab gel for separation in the second dimension. An electric current is passed through the gel and causes the proteins to migrate through the gel in a process known as polyacrylamide gel electrophoresis, PAGE. Small molecular mass proteins migrate faster down the gel than larger proteins (Ohlendieck, 2011B). Both forms of gel electrophoresis require a staining process to visualise the separated proteins, which can be done pre- or post-electrophoresis. The method of staining is dependent on the protein concentration initially loaded on the gel, the sensitivity of detection level required, and the compatibility with subsequent detection and identification methods (Ohlendieck, 2011B).

One of the most reputable and powerful comparative techniques in protein biochemistry is fluorescence difference in-gel electrophoresis (DIGE) (Minden *et al.,* 2009). DIGE is based on a pre-electrophoresis protein tagging method with CyDyes to swiftly analyse thousands of proteins (Lewis *et al.,* 2012). The DIGE technique can be employed to comparatively analyse 2 or 3 protein sample sets on the one high resolution analytical gel, by a 2-dye or a 3-dye labelling system and a pooled internal standard (Figure 1.16). DIGE can circumvent the inherent variability of 2D-GE (Minden *et al.,* 2009).

Routine 2D-GE can under represents certain classes of proteins, including low copy number proteins, highly hydrophobic membrane proteins and high-molecular mass proteins, alternative and complementary techniques have been used in muscle proteomics (Altelaar and Heck, 2012).

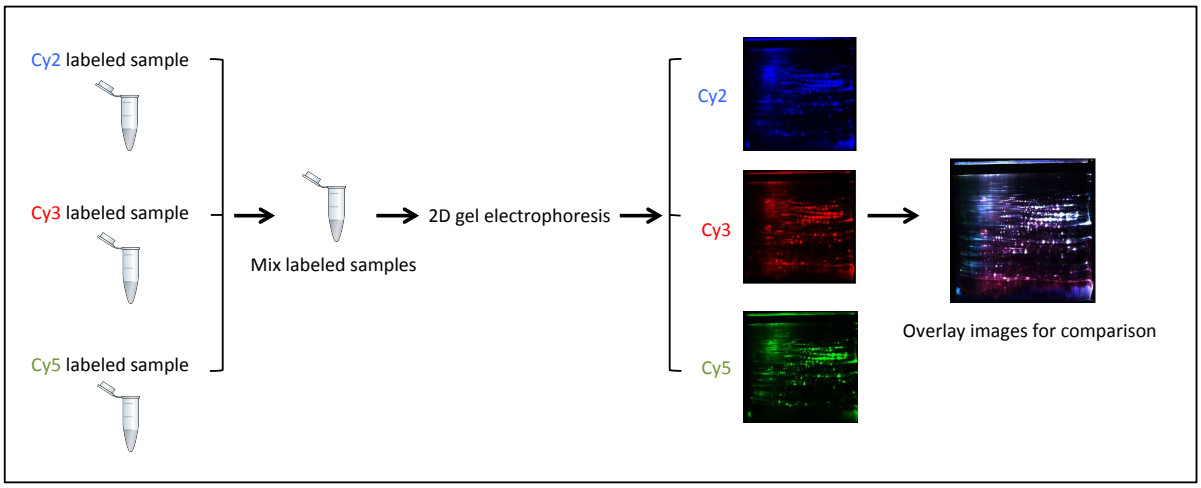

Figure 1.16 Overview of the main approach used in fluorescence difference in-gel electrophoresis (DIGE) proteomics.
Shown is a 3 CyDye system application method of protein labelling used for studying global changes in complex protein samples. Samples are labelled with Cy2, Cy3 and Cy5 CyDyes prior to electrophoresis, label samples are combined and subjected to 2D-GE separation based on their isoelectric point and molecular mass. Gels are then scanned and computational image analysis of the differential expression patterns of fluorescently labelled proteins is carried out (Minden *et al.,* 2009).
*Image modified from www.cgs.hku.hk

1.5.2 Label-free mass spectrometry

Advances in mass spectrometry, MS, technologies and bioinformatic capabilities have increased the reliability, reproducibility and efficiency of label-free MS proteomic studies (Walther and Mann, 2010; Ramasamy *et al.,* 2014). In contrast to gel-based methods, liquid chromatography in combination with advanced mass spectrometry can identify a broader range of proteins including low copy number proteins, integral membrane proteins, high molecular mass proteins and components with extreme isoelectric points, *p*I, and/or post-translational modifications (Holland and Ohlendieck, 2014E; Dowling *et al.,* 2014). It is for these reasons that in recent years label free MS has replaced gel-based approaches in many areas of proteomics. Label-free MS has been shown to provide increased proteome coverage in comparison to gel-based methods as it can identify a considerably larger cohort of proteins (Holland and Ohlendieck, 2014E; Dowling *et al.,* 2014). However label-free MS is a complementary proteomic method to use as certain proteins resolve better in a gel-based matrix.

Label-free MS can analyse complex proteomic samples, where an entire proteome is digested without prior protein separation and provide a profile of what proteins are present within a system at a given time (Patel *et al.,* 2009). Technical advances in the field of MS have allowed for comparative and relative quantitation.

Sample bias is minimised in label-free MS due to the absence of artificially labelling analytes, reduced sample handling and reduction in potential contaminants. This in turn increases sample throughput (Ramasamy *et al.,* 2014). The underlying principle of this technology is based on direct comparison of MS signal intensities between different analytes. Bioinformatic technologies

are employed to interpret MS data for quantification of peptide ion intensities to produce relative quantification (Ramasamy *et al.,* 2014). Liquid chromatography, LC, alignment software can be used to optimise the chromatographic profiles of peptides and to account for a drift in peptide retention time, further increasing reproducibility (Mallick and Kuster, 2010). Sequence coverage can be improved when peptide ions (first MS) are subject to tandem MS (MS/MS) to generate sequence specific information for database searching and identification (Ramasamy *et al.,* 2014).

Combinations of label-free MS and highly sensitive 2D-DIGE analysis are of considerable importance in the field of muscle pathology and are crucial for furthering the discovery of specific protein biomarkers of neuromuscular disorders (Dowling *et al.,* 2014).

1.6 Proteomic biomarker discovery

Magnetic resonance imaging, MRI, and spectroscopy are increasingly being used to confirm the diagnosis of certain neuromuscular pathologies by non-invasive means (Forbes *et al.,* 2013). However, this advanced approach for diagnostics or prognostics is not yet a suitable means for screening in muscle pathology as it requires specialized facilities and comes with a relatively high-cost. Thus, the histological, histochemical and immunohistochemical assessment of muscle biopsies are still crucially important in conventional diagnosis of muscular diseases (Dubowitz *et al.,* 2013).

Biochemical analysis is routinely employed though enzyme assays for the detection of tissue damage markers, such as muscle enzyme related serum activity (Mendell *et al.,* 2012; Ohlendieck, 2013). These muscle-specific biomarkers are generally non-specific and/or have consistent concentration changes in the acute or chronic disease stage restricting their usefulness for accurate diagnosis, proper monitoring of disease progression and clinical outcome measures (Brancaccio *et al.,* 2010). This has caused a major research drive to identify novel disease-specific protein indicators that can potentially be employed for the improved diagnosis, prognosis and/or therapy monitoring of frequent muscle diseases (Dowling *et al.,* 2014). High throughput biochemical screening techniques can combine the use of large-scale separation methods, e.g. gel electrophoresis and/or liquid chromatography, with extremely sensitive mass spectrometry giving muscle biopsies a superior investigative value (Ohlendieck, 2011B). In order to develop dependable, minimally invasive and non-invasive tests, large-scale mass spectrometric screens are imperative for biomarker discovery of neuromuscular diseases. Relatively small amounts of

muscle tissue can be used in routine proteomic screenings in order to generate significant insights in the global alterations in the proteome of pathological muscle samples (Ohlendieck, 2010A; Gelfi *et al.,* 2011). The systematic screening of the assessable muscle proteome can be employed for the swift identification of a new proteomic biomarker signature and the global pathobiochemical analysis of cellular dysregulation, as outlined in the flowchart in Figure 1.17.

In general an ideal protein biomarker should be (i) easily assessable, (ii) highly sensitive, (iii) diagnostically conclusive, (iv) very specific for subtypes of distinct disorders, (v) informative in relation to individual stages of disease progression and finally (vi) exhibit physicochemical properties that make a particular protein species suitable for the establishment of a meaningful and cost-effective test system (Ohlendieck, 2013).

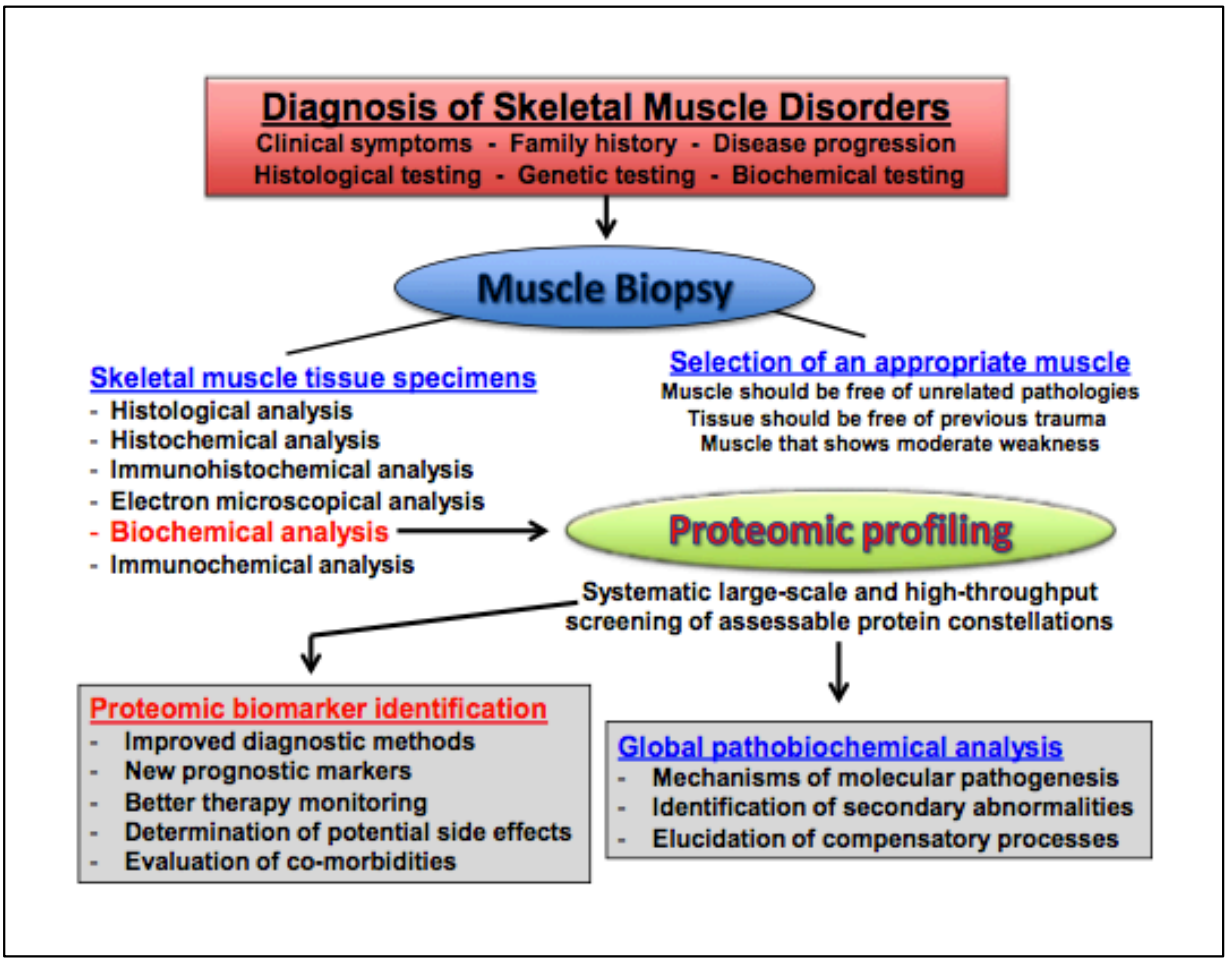

Figure 1.17 Diagnosis of skeletal muscle disorders.
Shown is a flowchart summarising routine analyses performed with muscle biopsy specimens and the new bioanalytical value of skeletal muscle samples for the proteomic profiling of neuromuscular diseases.
*Image from Holland and Ohlendieck, 2014E

1.6.1 Complexity of the muscle proteome

A common difficulty in muscle proteomics is accurately delineating the exact protein constellation that defines the muscle proteome. Muscle tissue has a remarkably heterogeneous composition and is extremely plastic as it can quickly adapt to changed functional and metabolic demands (Matsakas and Patel, 2009). The genome is relatively stable, while the muscle tissue proteome is continuously fluctuating to adjust its protein repertoire in response to physiological challenges (Altelaar and Heck, 2012).

Separation of the assessable protein constellation from total muscle extracts has been attempted with the aim of establishing the almost complete proteome of distinct skeletal muscle (Højlund *et al.,* 2008; Raddatz *et al.,* 2008; Parker *et al.,* 2009; Burniston *et al.,* 2014; Murgia *et al.,* 2015; Deshmukh *et al.,* 2015). Two-dimensional gel electrophoresis and liquid chromatography have previously been employed for the large-scale protein separation from human muscle specimens and several animal muscle preparations of biomedical or agricultural importance. The systematic application of tissue proteomics has so far resulted in the identification of more than 2,000 muscle-associated proteins (Parker *et al.,* 2009).

1.6.2 Tissue complexity and heterogeneity in skeletal muscle

Crude muscle samples have a high degree of cellular complexity. This complexity needs to be considered when interpreting results from biochemical analysis of human biopsies. In addition to the complex combination of fibre types within a single muscle, capillaries, the epimysium, the perimysium, the

endomysium and the motor neuron system represent other tissue groups found in muscles (Schiaffino and Reggiani, 2011). Therefore, it is crucially important to use independent bioanalytical methods, such as immunofluorescence microscopy, immunoblotting surveys or functional assay, to verify all proteomic and biochemical findings of routine screening studies (Ohlendieck, 2011B; Dowling *et al.,* 2014). Technical problems, such as tissue perfusion prior to proteomic analysis, and biological matters can sometimes genuinely complicate the proper interpretation of findings from comparative muscle tissue proteomics. This can cause difficulties in distinguishing between protein changes as a consequence of general tissue damage, adaptive process during regeneration cycles and highly disease-specific alterations downstream from the initial genetic insult (Dubowitz *et al.,* 2013).

As mentioned previously, Section 1.4, genetic animal models of human muscle diseases are routinely used for biomedical purposes. It is important to take the differing fine structure of the neuromuscular system and the dissimilarities of the immune system, physiological adaptions and metabolic regulation into account when attempting to properly deduce the finding from animal testing to human pathology (Doran *et al.,* 2007A).

1.6.3 Technical limitations and bioanalytical challenges in comparative tissue proteomics

The most significant technical obstacle creating a major limiting factor in the majority of comparative proteomic studies is that no individual set of protein biochemical methods has the ability to separate and analyse the entire spectrum

of proteins contained in a complex tissue proteome (Altelaar and Heck, 2012). Global biochemical analyses are technically challenging due to the huge dynamic range of concentration levels of individual protein species and the greatly differing physicochemical properties of proteins with respect to hydrophobicity (Dowling *et al.,* 2014). The extremely broad dynamic range of protein concentrations in muscle tissue is a major problem. Low abundance proteins, e.g. cytokines are present at a concentration in the *ρ*g/ml range, in contrast albumin is present in the 30-45 mg/ml concentration range (Pieper *et al.,* 2003). The large difference in concentrations represent at least twelve orders of magnitude and has the potential to be even greater as many biomolecules are present at lower concentrations than cytokines (Hortin and Sviridov, 2010). Furthermore, numerous low-abundance components bind to proteins like albumin that are in high abundance and mask their presence. This furthers the complexity for detection and quantification of certain proteins and is a prime reason for using pre-fractionation approaches, like immune-depletion (Zolotarjova *et al.,* 2008; Pernemalm *et al.,* 2009).

Urea or detergent based extraction of total muscle tissue specimens are usually employed for the analysis of the near-to-complete proteome. These fractionation methods can be combined with different label-free or label-based strategies for protein identification. Reduction of sample complexity can be achieved through (i) the use of subcellular fractionation, as regularly used is organelle proteomics (Lee *et al.,* 2010) and (ii) affinity purification methods to enrich for supramolecular protein complexes pre mass spectrometric analysis (Rappsilber, 2011).

1.7 Hypothesis of the project

Proteomic profiling methodologies are large-scale high throughput approaches used to deliver unbiased scientific discoveries. This form of research does not follow the conventional hypothesis driven approach, however the results generated from both gel-based and label-free mass spectrometry proteomic analysis can be hypothesis generating.

The studies presented in this thesis explore the consequences and knock on effects due to the absence of key proteins in muscle tissue as seen with the decreased concentration of VPS54 and Dp427 in wobbler and *mdx*/*mdx-4cv* mice respectively. It can be hypothesized that the dysregulated protein expression patterns of both VPS54 and Dp427 in their respective animal models can cause a systematic disruption to other major protein families.

These protein families, or in fact individual proteins species, could potentially represent valuable targets in their relevant diseases. The identification of such could lead to an increased understanding of the mechanisms that underlie their expression and may provide important clues to use to develop new therapeutic applications or potential biomarker signatures of the diseases. Therefore large-scale systematic analysis of muscle protein groups from animal models of neuromuscular disorders would be highly beneficial to appreciate their roles in health and disease.

1.8 Aims of the project

The primary aim of this project was to carry out investigative proteomic profiling studies on animal models of motor neuron disease and muscular dystrophy in an attempt to potentially identify a biomarker signature and further the general understanding of the dysregulation that underlies these complex muscle diseases. An additional aim of this research was to investigate the secondary feature of impaired spermiogenesis in the wobbler mouse. The objective of this section of research was to gain a proteomic insight into the pathophysiological mechanisms of globozoospermia, a testis-associated disease linked with male infertility.

Amyotrophic lateral sclerosis is the most prevalent form of motor neuron disease. Part of this research employed label-free mass spectrometry-based proteomic techniques on skeletal muscle from the wobbler mouse model of ALS to look at the muscle specific affects denervation has on skeletal muscle tissue.

The wobbler mouse has a secondary feature of impaired spermiogenesis. In order to determine proteome-wide changes, affected testes were analyzed by fluorescence 2D-DIGE coupled with mass spectrometry to reveal alterations in testis-associated proteins in the wobbler mouse.

Duchenne muscular dystrophy is the most frequent neuromuscular disorder in humans and is characterized by deficiency in the cytoskeletal protein dystrophin. As the majority of patients affected with DMD develop cardiomyopathic complications, we carried out a large-scale label-free mass spectrometry-based proteomic study of global cardiac changes for the potential identification of new biomarkers of dystrophinopathy. This study focused on age related alterations in the proteome of dystrophin-deficient cardiomyopathic

tissue from young versus aged *mdx* mice.

Following this we completed a further proteomic investigation on the more advanced *mdx-4cv* mouse model of muscular dystrophy. This study primarily looked at the *mdx-4cv* mouse diaphragm proteome, compared and contrasted it to the *mdx* diaphragm proteome and then looked at the trend of key diaphragm proteins during senescence in the *mdx-4cv* model. The purpose of this section of the research was to establish a more detailed proteomic profile on differently affected dystrophin deficient muscle groups from animal models of muscular dystrophy.

The last decade has seen mass spectrometry-based proteomics being instrumental for the detailed elucidation of pathobiochemical mechanisms involved in major neuromuscular diseases such as ALS and DMD. As there is an urgent need for superior biomarkers, large-scale proteomic studies like these are ideal for looking at global muscle proteome changes for the identification of new potential protein biomarkers of motor neuron disease, globozoospermia and dystrophinopathy. These biomarkers can potentially be utilized to better monitor the therapeutic success of experimental treatments and evaluate potential side effects, as well as generally improve diagnostic procedures.

Chapter 2

Materials and Methods

2.1 Materials

2.1.1 General chemicals and reagents

Distilled H_2O, dH_2O, was purified using a Millipore Milli-Q apparatus to obtain milli-Q water 18MΩ. Complete mini tablets containing protease inhibitors were from Roche Diagnostics (Mannheim, Germany). Bradford reagent for protein quantification and PrepReady™ 2D cleanup kit were purchased from Biorad Laboratories (Hemel-Hempstead, Hertfordshire, UK). All other general reagents and chemicals were purchased from Sigma Chemical Company (Dorset, UK) and were of analytical/electrophoretic/proteomic grade, unless stated otherwise.

2.1.2 1D and 2D electrophoresis

Ultrapure Protogel acrylamide stock and 4X Protogel Resolving Buffer stock solutions were obtained from National Diagnostics (Atlanta, GA, USA). Isoelectric focusing immobilized pH gradient, IPG, drystrips for 2D electrophoresis, ampholytes and cover fluid were purchased from Amersham Bioscience/GE Healthcare (Little Chalfont, Buckinghamshire, UK). Protein molecular weight ladder (Figure 2.1) and laemmli-type buffer were purchased from Biorad Laboratories (Hemel-Hempstead, Hertfordshire, UK).

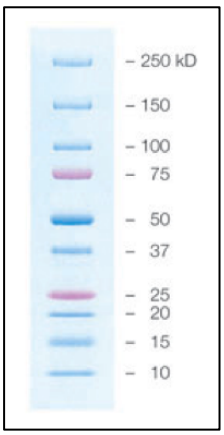

Figure 2.1 Molecular weight ladder.
Bio-Rad Precision Plus Protein™ Dual Color Standards containing a mixture of 8 blue-stained recombinant proteins (10–250 kDa) with two pink reference bands (25 and 75 kDa).

2.1.3 Protein staining

CyDye DIGE fluor minimal dyes Cy2, Cy3 and Cy5 and Coomassie Blue G-250 tablets were purchased from Amersham Biosciences/GE Healthcare (Little Chalfont, Buckinghamshire, UK). Ultrapure lysine for quenching the DIGE labeling was obtained from Sigma Chemical Company (Dorset, UK). Bathophenanthroline disulfonic acid and disodium salt hydrate for RuBPs dye were purchased from Reagecon Diagnostic Limited (Shannon, Ireland). Sodium ascorbate and potassium pentachoro aquo ruthenate for RuBPs and silver nitrate for silver staining was purchased from Sigma Chemical Company (Dorset, UK).

2.1.4 Mass spectrometry

Sequence grade-modified trypsin and Lys-C were purchased from Promega (Madison, WI, USA). Ultra-clean LC-MS Chromaslv water and formic acid were from Fluka (Dorset, UK). Acetonitrile was obtained from Amersham Biosciences/GE Healthcare (Little Chalfont, Buckinghamshire, UK). Spin filters were obtained from Fisher Scientific (UK). Model 6340 Ion Trap LC/MS, LC/MS vials, LC/MS vial caps and ProtID-Chip-150 II 300A C18 150 nm column were obtained from Agilent Technologies Ltd. (Santa Clara, CA, USA). All other analytical grade chemicals and materials used for the MS-based proteomic profiling and analysis were obtained from Amersham Biosciences/GE Healthcare (Little Chalfont, Buckinghamshire, UK), Sigma Chemical Company (Dorset, UK) and BioRad Laboratories (Hemel-Hempstead, Hertfordshire, UK).

2.1.5 Immunoblotting

Whatman nitrocellulose transfer membrane was obtained from Invitrogen (Carlsbad, CA, USA). Chemiluminescence substrate was purchased from Roche Diagnostics (Mannheim, Germany). X-ray film was purchased from Santa Cruz Biotechnology (Santa Cruz, CA, USA). GBX Developer/Replenisher, GBX Fixer/Replenisher and Ponceau S-Red Staining Solution were obtained from Sigma Chemical Company (Dorset, UK). Memcode reversible stain was purchased from Thermo Scientific (MA, USA). All commercially available primary antibodies used in this research were purchased from companies outlined in Table 2.1. Peroxidase-conjugated secondary antibodies used were obtained from Chemicon International (Temecula, CA, USA). For antibodies and dilutions used see Table 2.2.

2.1.6 Immunofluorescence microscopy

OCT™ (optimum cutting temperature) compound was purchased from Sakura Finetek Europe B.V (Zoeterwoude, Netherlands). The DNA binding dye DAPI (diamidino-phenyindole), Liquid Blocker Super PAP Pen and Dako Faramount Aqueous Mounting Medium were obtained from Sigma Chemical Company (Dorset, UK). Superfrost Plus positively-charged microscope slides were purchased from Menzel Gläser (Braunschweig, Germany). All commercially available primary antibodies used in this research were purchased from the companies detailed in Table 2.1 and Table 2.2. Fluorescent secondary antibodies Alexa fluor 488 goat anti-rabbit IgG, Alexa fluor 488 goat anti-mouse IgG and were from Molecular Probes (Eugene, Oregon, USA).

Table 2.1 Antibody Suppliers

Company	Address
Abcam	Abcam Plc (Cambridge, UK)
Chemicon	Chemicon International (Temecula, CA, USA)
Molecular Probes	Molecular Probes (Eugene, Oregon, USA)
Novo Castra	Novo Castra Laboratories Ltd. (Newcastle upon Tyne, UK)
Novus	Novus Biologicals (Cambridge, UK)
Santa Cruz	Santa Cruz Biotechnology (Santa Cruz, CA, USA)
Sigma	Sigma Chemical Company (Poole, Dorset, UK)

Table 2.2 Antibodies

List of all commercially available antibodies used including the dilutions used for each primary (1° Ab) and secondary antibody (2° Ab), host species (species), antibody specificity, molecular weight (MW), ordering information (company and catalogue number) and antibody use (use).

Antibody	1°Ab dilution	2°Ab dilution	Species	Antibody specificity	MW (kDa)	Company	Catalogue number	Use
Aconitase	1:500	1:500	Rb	pAb	85	Abcam	ab71440	WB
Actin	1:500	1:1000	Rb	pAb	42	Abcam	ab1801	WB
Annexin A2	1:1000	1:1000	Rb	pAb	38	Abcam	ab41803	WB
ATP-synthase β	1:2000	1:3000	Chk	pAb	59	Abcam	ab43176	WB
BHD-1	1:500	1:1000	Ms	mAb	38	Abcam	ab93931	WB
CA-3	1:500	1:1000	Rb	pAb	30	Abcam	ab85366	WB
Calsequestrin	1:1000	1:2000	Rb	pAb	55	Abcam	ab3516	WB
Catalase	1:500	1:1000	Rb	pAb	60	Abcam	ab16731	WB
Collagen-VI	1:500	1:1000	Rb	pAb	100	Abcam	ab6588	WB
Creatine-kinase M	1:500	1:1000	Rb	pAb	43	Abcam	ab38178	WB
Desmin	1:1000	1:1000	Rb	pAb	53	Abcam	ab8592	WB
Dp427	1.100	1:200	Rb	pAb	-	Abcam	ab15277	IF
FABP-3	1:500	1:1000	Ms	mAb	15	Abcam	ab16916	WB
GAPDH	1:1000	1:1000	Gt	pAb	37	Abcam	ab34492	WB
HSP-27	1:500	1:1000	Rb	pAb	27	Abcam	ab5579	WB
HSP-70	1:500	1:1000	Ms	mAb	70	Abcam	ab2787	WB
HSP-90	1:500	1:1000	Ms	mAb	90	Abcam	ab13492	WB
Isocitrate Dehydrogenase	1:500	1:1000	Rb	pAb	40	Abcam	ab36329	WB
Lamin A/C	1:1000	1:1000	Rb	pAb	76	Abcam	ab26300	WB
Lamin A/C	1:1000	1:1000	Rb	pAb	76	Abcam	ab8984	WB
Lamin-B	1:500	1:1000	Rb	pAb	68	Abcam	ab16048	WB
Laminin	1:1000	1:1000	Rb	pAb	337	Sigma	L-9393	WB
Laminin	1:100	1:200	Rb	pAb	-	Sigma	L-9393	IF
Malate dehydrogenase	1:500	1:1000	Shp	pAb	36	Abcam	ab34830	WB
MBP-C	1:1000	1:1000	Ms	mAb	37	Abcam	ab55559	WB
MLC-2	1:1000	1:1000	Rb	pAb	19	Abcam	ab48003	WB
MLC-2	1:1000	1:1000	Rb	mAb	19	Abcam	ab92721	WB
Myoglobin	1:1000	1:1000	Rb	mAb	17	Abcam	ab77232	WB
Nidogen	1:500	1:500	Rb	pAb	137	Abcam	ab14511	WB
Parvalbumin	1:1000	1:1000	Rb	pAb	12	Abcam	ab11427	WB

Periostin	1:200	1:200	Rb	pAb	-	Novus	NBP-1-30042	IF
Periostin	1:500	1:500	Rb	pAb	94	Novus	NBP-1-30042	WB
Periostin	1:500	1:500	Rb	pAb	94	Abcam	ab92460	WB
Prohibitin	1:500	1:1000	Rb	pAb	30	Abcam	ab28172	WB
Pyruvate dehydrogenase	1:1000	1:2000	Ms	mAb	43	Abcam	ab110330	WB
Sarcalumenin	1:200	1:500	Ms	mAb	150	Santa-Cruz	sc58845	WB
SERCA-1	1:500	1:1000	Ms	mAb	99	Abcam	ab2818	WB
SERCA-2	1:500	1:500	Ms	mAb	110	Abcam	ab2861	WB
SOD-1	1:500	1:1000	Rb	pAb	18	Abcam	ab13498	WB
SOD-2	1:1000	1:1000	Rb	pAb	25	Abcam	ab13533	WB
Transferrin	1:500	1:500	Shp	pAb	80	Abcam	ab9033	WB
Tropomyosin	1:3000	1:3000	Ms	mAb	33	Abcam	ab7785	WB
Troponin I	1:500	1:1000	Rb	pAb	21	Abcam	ab103636	WB
Troponin T	1:500	1:1000	Ms	mAb	32	Abcam	ab97708	WB
VDAC-1	1:1000	1:1000	Ms	mAb	39	Abcam	ab14734	WB
Vimentin	1:1000	1:2000	Ms	mAb	57	Abcam	ab20346	WB
VPS-54	1:50	1:100	Rb	pAb	111	Abcam	ab171407	WB
α-Actinin-2	1:250	1:500	Ms	mAb	103	Abcam	ab9465	WB
α-Actinin-3	1:150	1:250	Rb	pAb	103	Abcam	ab108196	WB
αB Crystallin	1:1000	1:1000	Ms	mAb	21	Abcam	ab13496	WB
β-dystroglycan	1:500	1:1000	Ms	mAb	43	Santa-Cruz	Sc-33701	WB
β-dystroglycan	1:500	1:1000	Ms	mAb	-	Nova Castra	NCL-b-DG	IF

*Chk= Chicken
Gt= Goat
Ms= Mouse
Rb= Rabbit
Shp= Sheep
mAb = Monoclonal Antibody
pAb= Polyclonal Antibody
IF= Immunofluorescence microscopy
WB= Western Blotting, immunoblotting

2.2 Methods

2.2.1 Animals and dissections

The stock carrying the wobbler (*wr*) mutation on a C57/bl6 background was obtained in 1979 from Harvard Medical School to our collaborators in Prof. Harald Jockusch's lab in the University of Bielefed, Germany. Both the wobbler mouse and control wild-type counter parts used in experimental procedures presented here were on a C57/bl6 background (Kaupmann *et al.,* 1992). The *wr* mutation maps to chromosome 11 and has been identified as a missense mutation in the ubiquitously expressed gene *Vps54* (Kaupmann *et al.,* 1992; Schmitt-John *et al.,* 2005). Breeding of WR mice has been carried out in the animal house of Bielefeld University, Germany, and Århus University, Denmark, in accordance with German and Danish laws on the protection of laboratory animals and approved by the local authorities, respectively. The hind limb muscles (HLM); *gastrocnemius*, *tibialis anterior* and *vastus lateralis,* were dissected from 9-week old WR and control mice (Chapter 3). Similarly testes, without epididymis, were prepared from 9-week old wobbler mice and age-matched normal C57/bl6 mice (Chapter 4). WR and WT mice, used in both studies, had an average body weight of 9.6±1.6 g (n = 9) and 23.2±3.0 g (n = 5), respectively (Staunton *et al.,* 2011; Jockusch *et al.,* 2013; Holland *et al.,* 2014A).

The *mdx* mouse is an established animal model missing the full-length dystrophin isoform Dp427 due to a point mutation in exon 23 (Sicinski *et al.,* 1989). Both the *mdx* mouse and control wild-type counter parts used in experimental procedures presented here were on a C57/bl10 background (Irintchev *et al.,* 1997). Cardiac muscle tissue from 7-week-old (n = 4) and 20-

month-old (*n* = 4) *mdx* mice and aged matched control C57/bl10 mice (*n* = 4; for both age groups) were employed for the aging cardiac study in Chapter 5 (Holland *et al.,* 2013B).

The *mdx-4cv* mouse is an alternative established DMD animal model that exhibits less revertant fibres as compared to the conventional *mdx* mouse (Danko *et al.,* 1992). The full-length dystrophin Dp427 isoform is absent in the *mdx-4cv* mouse due to a mutation in exon 53 (Banks *et al.,* 2010). Both the *mdx-4cv* mouse and control wild-type counter parts used in experimental procedures presented here were on a C57/bl6 background. Wet weight of primarily analyzed 3-month old diaphragm muscle of *mdx-4cv* and control mice used in Chapter 6 were 30 ± 12.25 mg (*n* = 4) and 17.5 ± 8.29 mg (*n* = 4), respectively. 2, 3, 8, 12 and 15-month old diaphragm muscle from *mdx-4cv* mouse and age matched controls were further employed for minor comparative analysis for an aging experiment in the study, also outlined in Chapter 6 (Holland *et al.,* 2015). *Mdx-4cv* mice and wild type controls, as well as conventional *mdx* mice, and their control counterparts, used in the cardiac (Chapter 5) and diaphragm (Chapter 6) study respectively, were obtained from the Animal Facility of the University of Bonn, Germany (Carberry *et al.,* 2012A; Holland *et al.,* 2013B; Holland *et al.,* 2015).

All mice (WR, *mdx* and *mdx-4cv* and their appropriate controls) were kept under standard conditions and all procedures were carried out in accordance with Danish, German and Irish guidelines on the use of animals for scientific experiments. Animals were sacrificed by cervical dislocation and tissue immediately quick-frozen in liquid nitrogen. Muscle samples were transported to

Maynooth University, Ireland, on dry ice and stored at -80°C prior to proteomic analyses.

2.2.2 Extraction of total muscle protein complement

All muscle protein extracts used in each study were prepared separately. Crude tissue (cardiac muscle, skeletal muscle from various sub-groups and testis tissue) was washed in dH_2O to assist in removal of remaining hair, skin, bone and blood. Equal amounts (100 mg wet weight) of diseased (*mdx, mdx-4cv* or WR) and WT tissue samples were resuspended in 1 ml (1:10 dilution) of homogenization or lysis buffer appropriate to the proteomic study, as outlined in Table 2.3. To prevent proteolytic degradation of sensitive muscle proteins, all buffers were supplemented with a protease inhibitor cocktail (PIC mixture; pronase, thermolysin, chymotrypsin, trypsin, papain, pancrease-extract) (Doran *et al.,* 2006A). Samples were initially finely chopped with a blade and (i) deep frozen in liquid nitrogen and ground into a fine powder using a pestle and mortar continually in the presence of liquid nitrogen or (ii) carefully homogenized with a hand-held IKA T10 Basic Homogenizer from Fisher Scientific (Dublin, Ireland). All freshly prepared muscle extracts were then gently shaken at 4°C for 2.5 h using a Thermomixer from Eppendorf Hamburg, Germany, followed by centrifugation at 4°C for 20 min at 14 000 *g* using Eppendorf 5417 R centrifuge (Eppendorf, Hamburg, Germany). The resulting pellet and top layer were discarded and the middle layer containing urea-soluble proteins was extracted and retained for proteomic analysis and stored, until required, at -80°C.

Table 2.3 Sample preparation buffers
List of studies undertaken with the appropriate sample buffers used and the composition of the buffer.

Study (Chapter)	Buffer	Buffer composition
WR label-free MS leg muscle study (Chapter 3)	Lysis buffer	7 M urea, 2 M thiourea, 65 mM CHAPS, 100 mM DTT, PICS
WR DIGE testis study (Chapter 4)	DIGE lysis buffer	9.5 M urea, 2% (w/v) CHAPS, 20 mM Tris
mdx label-free MS cardiac study (Chapter 5)	Homogenization buffer	0.5 M HEPES, pH 7.4, 200 mM EGTA, 10% (w/v) sucrose, 3 mM magnesium chloride, 0.1% (w/v) sodium azide, PICS
mdx-4cv label-free MS diaphragm study (Chapter 6)	Lysis buffer	7 M urea, 2 M thiourea, 65 mM CHAPS, 100 mM DTT, PICS

2.2.3 Acetone precipitation

Protein samples were initially precipitated with 100% ice-cold acetone at a dilution of 1:4. The mixture was vortexed for 20 s and incubated at -20°C for 1 h. Samples were centrifuged at 12,000 *g* in an Eppendorf 5417 R centrifuge (Eppendorf, Hamburg, Germany) for 10 min, the supernatant was discarded and the pellet retained. The pellet was then resuspended in 80% acetone at a dilution of 1:4 (of original sample volume). The mixture was vortexed and incubated as before. Samples were spun at 12,000 *g* for 5 min. Again the supernatant was discarded and pellet retained. The pellet was resuspended in an appropriate volume of lysis buffer (same as original starting volume of sample). Resuspension of protein sample was aided by vortexing or sonication with a Sonoplus HD 2200, Bandelin (Berlin, Germany).

2.2.4 2D Cleanup Kit (BioRad)

As an alternative to acetone precipitation, Section 2.2.3, ReadyPrep™ 2D Cleanup Kit from BioRad Laboratories, Inc. (Hemel-Hempstead, Hertfordshire, U.K.) was employed and carried out as per manufacturer's manual recommendations and guidelines.

2.2.5 Protein quantification via Bradford assay

Quantification of protein sample concentration was determined using the Bradford assay system (Bradford, 1976). A standard curve was prepared by diluting a stock solution of 5 mg/ml BSA with dH_2O generating a concentration range of 0-5 mg BSA. Standards were prepared in duplicate and samples in

triplicate. The assay was run on a 96-well plate, with 5 µl standard or sample added to a well plus 250 µl Bradord reagent (diluted 1:3). The 96-well plate was incubated at room temperature for 10 min in the dark prior to analysis, allowing for complete binding to occur. Absorbance of standards and samples was read at λ=595nm using a Synergy HT BIO-TEK unit and KC4 software from Mason Technology Ltd. (Dublin, Ireland). Protein concentration was determined by comparing the unknown BSA samples to the standard curve (Bradford, 1976).

2.2.6 1D gel electrophoresis

One-dimensional, 1D, sodium dodecyl sulphate polyacrylamide gel electrophoresis, SDS-PAGE, separation of proteins was carried out under reducing conditions in accordance with Laemmli *et al.,* (1970). 1D SDS-PAGE was performed using a Bio-Rad Mini-Protean III gel system (Biorad Laboratories, Hemel-Hempstead, Hertfordshire, UK). Separation of proteins was achieved by varying the acrylamide gel concentration, dictated by the molecular weight of the proteins under investigation. Resolving gel was made of 10% (w/v) acrylamide from protogel acrylamide stock, 4X Protogel resolving buffer, 0.69 M ammonium persulphate, APS, and 0.1% (v/v) N, N, N', N'-tetramethylethylenendiamine, TEMED. Stacking gel was made of 5% (w/v) acrylamide, 0.5 M tris pH 6.8, 0.438 M SDS, 0.69 M APS and 0.1% (v/v) TEMED. Resolving gel was poured into 1.0 mm plates, over laid with methanol and allowed to polymerize. Once polymerized, methanol was removed and top of gel washed with dH_2O. Stacking gel was layered over resolving gel and 10 well combs inserted prior to polymerization. Samples for 1D electrophoresis were diluted 1:1 (v/v) with Laemmli buffer supplemented with 350 mM DTT, and mixture boiled at 97°C for

10 min. Protein sample (5-20 µg) was loaded on the gel. Electrophoresis was carried out in the presence of SDS running buffer (25 mM tris base, 192 mM glycine, 0.1% (w/v) SDS) and initially run at 60 V, and later increased to 120 V, until the bromophenol blue tracking dye migrated to the end of gel. Molecular weight standards (Biorad Laboratories; Hemel-Hempstead, Hertfordshire, UK) ranging in sizes from 10 kDa to 250 kDa were run on all 1D gels in tandem with samples under investigation. Following electrophoresis gels were either fixed in fixing solution (Section 2.2.8) or transferred onto nitrocellulose membrane for immunoblotting (Section 2.2.11).

2.2.7 2D gel electrophoresis

2D electrophoresis initially separates proteins by their iso-electric point; *pI*. The *pI* value of a protein is the pH at which the overall net charge of the protein is neutral or at 0. Separation based on *pI* is achieved by isoelectric focusing, IEF. Focused proteins are subsequently separated in the second dimension on a SDS polyacrylamide slab gel. This separation is based on the molecular weight of the protein, the smaller the protein the further down the gel it will migrate, i.e. the heavier molecular weight proteins will be closer to the top of the gel.

2.2.7.1 DIGE labeling

To minimize non-specific labeling high-grade fresh DIGE compatible reagents were used. Cy3 and Cy5 DIGE dyes were reconstituted as a stock solution of 1mM in fresh anhydrous dimethylformamide (DMF). This stock solution was diluted to a working solution of 0.2 mM (200 ρmol) prior to

labeling, and was used within two weeks. Proteins samples were in a DIGE compatible lysis buffer (Table 2.3). Prior to labeling all samples were adjusted to pH 8.5 using DIGE lysis buffer. CyDye protein minimal labeling was performed with 200 ρmols of Cy3 working solution per 50 µg protein sample being studied; normal and diseased extracts. The pooled sample contained equal concentrations of protein from all replicates being used in the experiment and 50 µg protein was labeled with 200 ρmols of Cy5 working solution. The pooled sample was used as an internal standard. The labeling reaction was carried out with the appropriate amount of dye and after brief vortex incubated for 30 min on ice in the dark. To quench the labeling reaction an equal volume of 10 mM lysine was added to the samples and incubated on ice for a further 10 min in the dark. The labeled protein samples were pooled and immediately used for 2D electrophoresis. An equal volume of 2X buffer (9.5 M urea, 2% CHAPS, 2% IPG buffer pH3-10 and 2% DTT) was added to the mixture, vortexed and left on ice for 10 min before 2D electrophoretic separation, Section 2.2.7.2 and 2.2.7.3, (Minden, 2012).

2.2.7.2 Separation in the first dimension, IEF

Separation of proteins in the first dimension was achieved through IEF. Immobilised pH gradient, IPG, strips were passively rehydrated for 12 h with rehydration buffer (8 M urea, 0.5% CHAPS, 0.2% DTT, 0.2% ampholytes; pH 3-10 and 0.001% bromophenol blue as a tracking dye) and sample in a re-swelling tray from Amersham Biosciences/GE Healthcare (Little Chalfont, Buckinghamshire, UK). Different volumes (protein sample and rehydration buffer) were used according to the IPG strip length (Table 2.4) and different

concentrations of protein sample required depending on staining technique (Table 2.5). After strip rehydration, the IPG strips were loaded gel side up in an Amersham Ettan IPGphor manifold, wicks resting on top dampened with 100 mM DTT, manifold covered with 108 ml of cover-fluid and finally clamped in place with electrodes. The strips were run for a total of approximately 70,000 Vh, as per IEF running protocols outlined in Table 2.6. Focused strips were used immediately for separation on the second dimension or stored at -80°C until required.

Table 2.4 Volume of rehydration buffer required based on strip length for isoelectric focusing

Strip length (cm)	Total volume (µl)
7	125
11	200
13	250
18	350
24	450

Table 2.5 Protein concentrations required for 2D gel staining

Staining technique	Protein concentration (µg)
DIGE	25-75
Silver Stain	50-100
Colloidal Coomassie Blue (CCB)	400-800
RuBPs	400-800

Table 2.6 IEF running protocols
(24cm strips pH 3-10, linear)

WR
120min - 100V
90min - 500V
60min - 1000V
60min - 2000V
60min - 4000V
120min - 6000V
240min - 8000V
180min - 500V
240min - 8000V

2.2.7.3 Separation in the second dimension, SDS-PAGE

Following separation in the first-dimension gel strips were equilibrated. Focused strips were incubated in equilibration buffer (6 M urea, 30% (v/v) glycerol, 2% (w/v) SDS, 100 mM tris; adjusted to pH 8.8) with 100 mM DTT for 20 min with gentle agitation followed by incubated in equilibration buffer supplemented with 250 mM iodoacetamide for 20 min with gentle agitation in the dark. The equilibrated strips were briefly washed in SDS running buffer (25 mM tris base, 192 mM glycine, 0.1% (w/v) SDS) and placed on top of a 12.5% (w/v) resolving gel made in the lab. The strips were inserted on top of the gel and set in place using a 1% (w/v) agarose sealing gel. An Ettan Dalt-Tweleve system from GE Healthcare (Little Chalfont, Buckinghamshire, UK) was used for standard SDS-PAGE separation of proteins in the second dimension (Doran *et al.,* 2006A). Gels were run in parallel at 0.5 W/gel for 60 min and increased to 15 W/ gel (or 1 W/ gel if being run overnight) until the bromophenol blue tracking dye had migrated to the end of the gel.

2.2.8 Protein staining

Protein staining allows for the visualization of separated proteins post-electrophoresis. Bio-chemical staining methods, as outlined below, have varying degrees of sensitivity. The initial concentration of protein required for gel loading is dependent on the type of stain being employed, see Table 2.5, and must be determined prior to electrophoretic separation.

2.2.8.1 Silver staining

Silver staining was carried out according to Chevallet and colleagues (2006). Following electrophoresis, gels were fixed in 30% ethanol, 10% acetic acid for a minimum of 30 min to fix proteins in the gel. The gels were rinsed twice in 20% ethanol for 10 min, followed by a further two rinses in 100% dH_2O for 10 min. Gels were incubated in sensitising solution (0.8 mM sodium thiosulphate) for 1 min and rinsed twice for 10 min in 100% dH_2O. The gels were incubated in staining solution (12 mM silver nitrate) for 20 min to 2 h. Gels were then briefly washed in 100% dH_2O and developed (15 g (w/v) sodium carbonate, 125 µl formaldehyde, 62.5 µL 10% sodium thiosulphate, brought up to 500 ml with dH_2O) until the protein pattern on the gel became visible and stopped by adding stopping solution (20 g tris, 10 ml acetic acid in 500 ml dH_2O). Gels were scanned in a G-Box Chemi-XT4 GeneSys from Mason Technology Ltd., (Dublin, Ireland) and stored in 5% acetic acid following staining and scanning.

2.2.8.2 RuBPs stain preparation

Ruthenium II Bathophenathroline Disulfonate (RuBPs) Chelate 20 mM stock solution was prepared according to Rabilloud *et al.,* (2001). Under constant reflux 0.2 g potassium pentachloro aquo ruthenate was dissolved in 20 ml boiling dH_2O until solution turned a deep red-brown colour. Under reflux 3 M (0.9 g) bathophenanthroline disulfonate was added and after 20 min a greenish-brown colour is achieved. A 500 mM sodium ascorbate solution was prepared and 5 ml was added to the mixture and reflux was continued for a further 20 min until solution turned deep orange-brown. The chelate was allowed to cool and pH was adjusted to pH 7.0 with sodium hydroxide. The final volume was brought

up to 26 ml with dH_2O. Chelate stain was stored at 4°C in a light eliminating container, as it is photosensitive, for several months.

2.2.8.3 RuBPs staining

Following electrophoresis, gels were fixed in 30% ethanol, 10% acetic acid overnight to fix proteins in gel. Gels were rinsed in 20% ethanol for 30 min and repeated twice. Gels were stained for 6 h in 20% ethanol containing 200 mM ruthenium chelate (Section 2.2.8.2). Gels were de-stained (40% ethanol, 10% acetic acid) for 15 h and re-equilibrated in 100% dH_2O for 10 min prior to scanning using a Typhoon Trio Variable Mode Imager from Amersham Biosciences/GE Healthcare (Little Chalfont, Buckinghamshire, UK).

2.2.8.4 Colloidal Coomassie blue staining

Colloidal Coomassie blue, CCB, staining was carried out according to the procedure of Neuhoff (*et al.,* 1988). Following electrophoresis gels were washed twice for 10 min in dH_2O and stained overnight in colloidal Coomassie staining solution (1 part stock staining solution A (5% Coomassie brilliant blue G-250), 40 parts stock staining solution B (10% ammonium sulphate, 2% phosphoric acid), 10 parts methanol). Gels were incubated in neutralization buffer (0.1 M tris, pH 6.5) for 3 min. Following this, gels were washed in 25% methanol for 1 min to reduce background and transferred to fixation solution (20% ammonium sulphate). This staining procedure was repeated 3-4 times or until sufficient visualization of protein pattern was achieved. Colloidal Coomassie gels were scanned using Image-scanner II (GE Healthcare).

2.2.8.5 2D gel image acquisition and analysis

Typhoon scanning uses fluorescence imaging to identify fluorescently labeled proteins contained within a gel matrix. Visualization of RuBPs post-stained proteins and DIGE minimally pre-labeled proteins after 2D electrophoresis was carried out using a Typhoon Trio Variable Mode Imager from Amersham Biosciences/GE Healthcare (Little Chalfont, Buckinghamshire, UK). Scanned gels were imported and stored in Image Quant for further analysis. Images were scanned at wavelengths as outlined in Table 2.7. All images for analysis were scanned at a resolution of 100 microns (RuBPs) or 50 microns (DIGE) with adjusted photomultiplier tube, PMT, values (ranging from 500 V to 700 V) so the maximum pixel volume of the most abundant protein was in the range of 85,000 to 98,000 pixels, ensuring images were not saturated so images were compatible for statistical analysis. When a laser is used each one pixel of a fluorescent sample emits a light with a characteristic spectrum. PMT converts the signal from the emission filter into digital information. If gels were assembled in plates (low fluorescent plates were used for DIGE gels) the press sample and +3mm options were selected.

Gel images were analysed using Progenesis Same Spots software version 3.2.3 from NonLinear Dynamics (Newcastle Upon Tyne, UK). All gels in an experiment were aligned to one master reference gel. Protein spots on the gels were detected and filtered. Following filtering, the images were segregated into two groups (control versus disease) and spots then went forward for analysis to detect relative changes in abundance. All proteins underwent strict statistical analysis and only proteins that fit strict criteria were brought forward for further analysis; Power Score ≥ 0.8, P-value ≤ 0.5, ANOVA ≤ 0.5. An ANOVA score was

determined though the use of a one-way ANOVA test. Protein spots that met all the above criteria were subsequently identified by liquid chromatography-mass spectrometry (LC-MS), see Section 2.2.9.

Table 2.7 Fluorescence acquisition mode settings

Protein Stain (Dye)	Emission Filter (nm)	Laser (λ)
Cy2	520 BP 40	Blue2 (488nm)
Cy3	580 BP 30	Green (532nm)
Cy5	670 BP 30	Red (633 nm)
RuBPs	580 BP 30	Green (532nm)

2.2.9 ESI-ion trap liquid chromatography mass spectrometry

2.2.9.1 Sample preparation for ESI-ion trap LC/MS

The Shevchenko method for in-gel digestion was employed for sample preparation for LC-MS analysis (Shevchenko *et al.,* 2006). Excision, washing, destaining and treatment with trypsin were all performed by an optimized method (Doran *et al.,* 2004); Coomassie stained 2D gels were washed twice for 10 min in dH_2O. Gels spots of interest were excised from gels and plugs were transferred into individual eppindorf tubes. Individual Coomassie stained gel plugs were destained by addition of 100 µL of 50 mM ammonium bicarbonate: neat acetonitrile (1:1) solution for 30 min at 22°C on thermoshaker with agitation. The solution was removed and 300 µL neat acetonitrile was added to each plug and incubated at room temperature until gel plugs became opaque. Samples then under-went in-gel trypsin digestion; 50 µL resuspended trypsin was added to each gel plug and incubated at 4°C for 30 min to allow slow diffusion of solution into the plugs. A further 50 µL of trypsin buffer was added to plugs and incubated for 90 min. A 100 mM ammonium bicarbonate was made and 20 µL of it was added to plugs and left to incubate at 37°C overnight. 100 µL extraction buffer (1:2 (v/v) formic acid: acetonitrile) was added to gel plugs and incubated at 37°C for 15 min. All supernatant-containing peptides were removed; gel plugs kept in original tube, and supernatant put into fresh eppendorf tubes. Peptides were subsequently dried down using a vacuum centrifuge. Peptides were resuspended in 12 µL 0.1% formic acid, sonicated for 5 min to aid resuspension and centrifuged briefly. Peptides were transferred to spin filter tubes and centrifuged at 4°C for 5 min to remove any remaining gel pieces. A further 8 µL 0.1% formic acid was added to the spin filter and

centrifuged as before. Peptides were then transferred to MS vials and ready to undergo identification by ion trap LC/MS (liquid chromatography/ mass spectrometry) analysis.

2.2.9.2 Ion trap mass spectrometry

In order to generate representative peptide populations from proteins of interest, gel spots of proteins for identification were excised, washed, destained and then treated with trypsin as outlined in Section 2.2.9.1. The mass spectrometric analysis of peptides was carried out in the Proteomics Suite of Maynooth University with a Model 6340 Ion Trap LC/MS apparatus from Agilent Technologies (Santa Clara, California, USA). Separation of peptides was performed with a nanoflow Agilent 1200 series system (Agilent Technologies), equipped with a Zorbax 300SB C18 5mm, 4mm, 40 nL pre-column and a Zorbax 300SB C18 5 mm, 43mm x 75mm analytical reversed phase column using HPLC-Chip technology (Staples *et al.,* 2009). The mobile phases used were A: 0.1% formic acid, B: 50% acetonitrile and 0.1% formic acid. A total volume of 5 µL of sample was loaded into the enrichment at a capillary flow rate set to 2 µL /min with a mix of A and B (0.1% formic acid and 50% acetonitrile and formic acid) at a ratio of 19:1. The capillary voltage was set to 1700 V, the flow rate was 4 µL/min and the temperature of the drying gas was 300°C, respectively. Tryptic peptides were eluted with a linear gradient of 10-90% solvent B over 15 min with a constant nano pump flow rate of 0.60 mL/min. A 1-5 min post time of solvent A was used to remove any sample carryover. For protein identification, database searches were carried out with MASCOT MS/MS Ion search (Matrix Science, London, UK) and the NCBI database, release 20100212. All searches

used *"Mus musculus"* as taxonomic category along with the following parameters: (i) two missed cleavages by trypsin, (ii) mass tolerance of precursor ions ± 2.5 Da and product ions ± 0.7 Da, (iii) carboxymethylated cysteins fixed modification, (iv) oxidation of methionine as variable modification, and (v) at least 2 matched distinct peptides. Identification of protein of interest was accepted if a MASCOT score > 49 was obtained. By choosing a score of greater than 49 we are 95% confident our match is correct. The percentage of sequence coverage was acceptable over 10%. All *pI*-values and molecular masses of identified proteins were compared to the relative position of their corresponding two-dimensional spots on analytical slab gels.

2.2.10 Orbitrap mass spectrometry

2.2.10.1 Sample preparation for label-free LC-MS/MS analysis

Crude muscle samples were pre-treated with the Ready Prep 2D clean up kit from BioRad Laboratories. The resulting protein pellets were re-suspended in label-free solubilisation buffer (6 M urea, 2 M thiourea and 10 mM tris, pH 8.0 in LC-MS grade water) (Meleady *et al.,* 2012). Protein suspensions were vortexed, sonicated and centrifuged to ensure pellets were fully re-suspended and subsequent protein concentration was determined, see Section 2.2.5. For label-free MS analysis, volumes were kept to a minimum and initially equalised using label-free solubilisation buffer. Samples were reduced for 30 min with 10 mM DTT and alkylated for 20 min in the dark with 25 mM iodoacetamide in 50 mM ammonium bicarbonate. The initial proteolytic digestion was carried out with sequencing grade Lys-C at a ratio of 1:100 (protease/protein) for 4 h at 37°C. The samples were subsequently diluted with four times the initial sample volume in

50 mM ammonium bicarbonate. A second digestion step was performed with sequencing grade trypsin at a ratio of 1:25 (protease/protein) overnight at 37°C. Prior to MS analysis, the digested protein preparations were diluted 3:1 (v/v) with 2% TFA in 20% acetonitrile, vortexed and sonicated to ensure an even suspension.

2.2.10.2 Label-free LC-MS/MS analysis

An Ultimate 3000 nanoLC system (Dionex) coupled to a an LTQ Orbitrap XL mass spectrometrer from Thermo Fisher Scientific (Dublin, Ireland) was employed for nano LC– MS/MS analysis in the Proteomics Facility of the NICB, Dublin City University, as previously described by Meleady *et al.,* (2012). Digested peptide mixtures (5 µL volume) were loaded onto a C18 trap column (C18 PepMap, 300 µm id × 5 mm, 5 µm particle size, 100 Å pore size; Dionex). Desalting was carried out at a flow rate of 25 µL/min in 0.1% TFA for 10 min. The trap column was switched on-line with an analytical PepMap C18 column (75 µm id × 250 mm, 3 µm particle and 100 Å pore size; Dionex). Peptides generated from muscle proteins were eluted with the following binary gradients: solvent A (2% acetonitrile and 0.1% formic acid in LC-MS grade water) and 0–25% solvent B (80% acetonitrile and 0.08% formic acid in LC-MS grade water) for 240 min and 25–50% solvent B for a further 60 min. The column flow rate was set to 350 nL/min (Meleady *et al.,* 2012). Data were acquired with Xcalibur software, version 2.0.7 (Thermo Fisher Scientific). The MS apparatus was operated in data-dependent mode and externally calibrated. Survey MS scans were acquired in the Orbitrap in the 400–1800 *m/z* range with the resolution set to a value of 30 000 at *m/z* 400 and lock mass set to 445.120025 u. CID

fragmentation was carried out in the linear ion trap with up to seven of the most intense ions (1+, 2+ and 3+) per scan. Within 40 s, a dynamic exclusion window was applied. A normalised collision energy of 35%, an isolation window of 3 *m/z* and one microscan were used to collect suitable tandem mass spectra (Meleady *et al.,* 2012).

2.2.10.3 Quantitative profiling by label-free LC-MS/MS analysis

Progenesis label-free LC-MS software version 3.1 from Non-Linear Dynamics (Newcastle Upon Tyne, UK) was used to process the raw data generated from LC-MS/MS analysis. Data alignment was based on the LC retention time of each sample, allowing for any drift in retention time given and adjusted retention time for all runs in the analysis (Meleady *et al.,* 2012). A reference run was established with the sample run that yielded most features (i.e. peptide ions). The retention times of all of the other runs were aligned to this reference run and peak intensities were then normalized. Prior to exporting the MS/MS output files to MASCOT (www.matrixscience.com) for protein identification, a number of criteria were employed to filter the data. These data included (i) peptide features with ANOVA < 0.05 between experimental groups, (ii) mass peaks (features) with charge states from +1, +2, +3, and (iii) greater than one isotope per peptide. A MASCOT generic file was generated from all exported MS/MS spectra from Progenesis software. The MASCOT generic file was used for peptide identification with MASCOT (version 2.2) and searched against the UniProtKB-SwissProt database (downloaded in April 2012) with 16,638 proteins (taxonomy: *Mus musculus*). The following search parameters were used for protein identification: (i) MS/MS mass tolerance set at 0.5 Da, (ii)

peptide mass tolerance set to 10 ppm, (iii) carbamidomethylation set as a fixed modification, (iv) up to two missed cleavages were allowed and (v) methionine oxidation set as a variable modification. For further consideration and re-importation back into Progenesis LC–MS software for further analysis, only peptides with ion scores of 40 and above were chosen. Importantly, the following criteria were applied to assign a muscle-associated protein as properly identified: (i) an ANOVA score between experimental groups of ≤0.05, (ii) proteins with ≥2 peptides matched and (iii) a MASCOT score >40 (Meleady *et al.,* 2012).

2.2.11 Immunoblotting

In order to confirm altered concentration levels of distinct proteins revealed by MS analysis, immunoblotting was employed. 1D gel electrophoresis (Section 2.2.6) and subsequent wet transfer were carried out with a Mini-Protean II electrophoresis and transfer system from Bio-Rad Laboratories Inc. (Hemel-Hempstead, Hertfordshire, UK). Electrophoretic transfer of proteins from 1D gel to Whatman Protan NC nitrocellulose membrane was carried out by standard protocol (Towbin *et al.,* 1979). Proteins were transferred at 100 V for 70 min at 4°C in transfer buffer (28.28g glycine, 6.56g tris, 400 ml methanol, brought up to 2 L with dH_2O). Effectiveness of protein transfer to membrane was evaluated by reversible Ponceau-S Red staining (0.1% PonceauS in 5% acetic acid). Membranes were de-stained with phosphate buffered saline (PBS) (50mM sodium phosphate, 0.9% (w/v) NaCl, pH 7.4) and blocked in blocking solution (5% (w/v) fat-free milk powder in PBS) for 1 h at room temperature to prevent non-specific antibody binding. Membranes were incubated with primary

antibody suitably diluted in blocking solution, as per Table 2.2, and incubated at room temperature for 3 h or at 4°C overnight with gentle agitation. Membranes were washed three times in PBS for 5 min. Following this, membranes were incubated in a compatible peroxidase-conjugated secondary antibody diluted in blocking solution, as per Table 2.2, for 1-2 h at room temperature with gentle agitation. Membranes were washed three times in PBS for 5 min. Immuno-decorated protein bands were then visualized on membrane using the enhanced chemiluminescence (ECL) method with chemiluminescence substrate from Roche Diagnostics (Mannheim, Germany) and exposed to X-ray film (Santa Cruz Biotechnology, California, USA) that was subsequently developed and fixed as appropriate.

2.2.12 Statistical analysis

Densitometric scanning of immunoblots was performed with a HP PSC-2355 scanner and ImageJ software (NIH, Bethesda, Maryland, USA). Statistical analyses of densitometry results from immunoblots were carried out through Graph-Pad Prism statistical software (Graph-Pad software Inc., San Diego, California, USA). Results were given in the form of mean ± standard error of the mean (SEM). Between group difference was statistically evaluated using a Student's *t-test* ($n > 3$; $*p < 0.05$; $**p < 0.01$, $***p < 0.001$), meaning our data is statically significant with 95% confidence.

In order to analyze the differences among group means analysis of variance, ANOVA, was performed on mass spectrometric data using Progenesis software. A p-value of < 0.05 was considered significant.

2.2.13 Cryosectioning

Samples for cryosectioning were mounted in cryomolds with OCT compound and snap frozen in liquid nitrogen. Once embedded in OCT, transverse cryosections of 10 μm thickness were prepared with the help of a Shandon Cryotome, Life Sciences International (Cheshire, UK) at -20°C. Tissue sections were mounted on Superfrost Plus positively charged microscope slides and used for indirect immunofluorescence labeling experiments.

2.2.14 Immunofluorescence microscopy

Indirect immunofluorescence microscopy was employed for localization of select marker proteins and nuclei (Doran *et al.,* 2006A). Sections mounted on Superfrost Plus positively charged microscope slides were incubated in ice-cold acetone for 5 min to fix tissue sections. Tissue sections were left to dry at room temperature before being washed briefly in ice-cold PBS. After removal of excess PBS, a hydrophobic layer of wax was drawn around individual sections with a Liquid Blocker Super PAP pen. For immuno-decoration, sections were initially blocked in 0.2% (w/v) bovine serum albumin (BSA), 0.2% (v/v) triton X-100 and 2.5% goat serum in PBS for 30 min and subsequently incubated in appropriately diluted primary antibodies (see Table 2.2) overnight at 4°C. Samples were carefully washed three times for 5 min in 0.2% (w/v) BSA and 0.2% (v/v) triton X-100 in PBS. Samples were incubated for 1 h at room temperature with Alexa Flour dye-conjugated secondary antibodies and washed again prior to counterstaining (Doran *et al.,* 2008). For nuclei labeling, sections were incubated with 1 μg/ml DAPI for 10 min, washed briefly in PBS and immuno-decorated

tissue sections covered with one drop of Dako Faramount Aqueous Mounting Medium and a coverslip. Image acquisition and fluorescent scanning was carried out with a Nikon Eclipse E600 laser-scanning microscope using NIS Elements F-Package imaging software.

2.2.15 Electron microscopy

Samples of tissue for transmission electron microscopy (TEM) were prepared as previously described in detail (Heimann *et al.,* 1991). Spermatozoa for scanning electron microscopy (SEM) were obtained from the epididymis, fixed by standard procedures, and critical point dried, Au-sputtered and examined in a Hitachi scanning electron microscope. Collaborator, Dr. Peter Heimann, from the Department of Cell Biology, University of Bielefeld, Germany carried out all sample preparation for TEM and SEM and electron microscopy work.

2.2.16 Bioinformatics analysis of protein interactions

To identify and visualize potential protein interactions and the clustering of molecular functions of the mass spectrometrically identified proteins with a changed abundance bioinformatic software was applied. Analyses were performed with (i) the STRING (http://string-db.org/, version 9.1) database of known and predicted protein interactions that include direct physical and indirect functional protein associations (Franceschini *et al.,* 2013), (ii) the IntAct (http://www.ebi.ac.uk/intact, version 4.1) molecular interaction database that is populated by data either curated from the literature or from direct data depositions (Kerrien *et al.,* 2012) and (iii) the PANTHER (http://pantherdb.org,

version 8.1) comprehensive database of protein families for the cataloguing of molecular functions (Mi *et al.,* 2013).

Chapter 3

Label-Free Mass Spectrometry Analysis of Wobbler Hind Limb Muscle

3.1 Introduction

Motor neuron disease is a major group of fatal neurological disorders that can be genetically inherited or spontaneous in nature. Amyotrophic lateral sclerosis, ALS, is the most progressive and frequent form of adult onset motor neuron disease (Wijesekera and Leigh, 2009). Progressive paralysis is a hallmark symptom of ALS, which occurs due to loss of upper and lower motor neurons. This in turn causes disease-related muscular atrophy and leads to limb and bulbar muscle weakness and respiratory insufficiency (Musarò, 2013). Various genes have been shown to be involved in inherited forms of ALS (fALS), including *SOD1*, *TARDBP*, *FUS, ALS2*, *PFN1*, *VAPB*, *UBQLN2* and *ANG* (Kudo *et al.,* 2010; Da Cruz and Cleveland, 2011; Paratore *et al.,* 2012; Pratt *et al.,* 2012).

Animal models of ALS, including the wobbler mouse (genotype *wr/wr*, phenotype WR), play a pivotal role in ALS research (Duchen and Strich, 1968; Moser *et al.,* 2013). The wobbler, WR, mouse is an established ALS model used for research of this form of motor neuron disease as it exhibits progressive neurodegeneration and neuroinflammation similar to that of the human form (Laage *et al.,* 1988; Karlsson *et al.,* 2013; Broch-Lips *et al.,* 2013). A missense mutation in the WR genotype was identified in the *Vps54* gene, leading to a change in the primary amino acid sequence in the polypeptide chain of the VPS-54 protein. The leucine to glutamine, hydrophobic-to-hydrophilic, replacement (L967Q) occurs near the C-terminus of the complete 977 amino acid sequence of VPS-54 (Schmitt-John *et al.,* 2005). The vesicular protein sorting factor VPS-54 protein is an essential component of the hetero-trimeric Golgi-associated retrograde protein (GARP) complex. The mutation in the primary amino acid sequence creates a destabilization affect in the tertiary protein structure, leading

to a reduction in the concentration levels of VPS-54 (Perez-Victoria *et al.,* 2010).

The continuum of mammalian skeletal muscles is characterized by distinct fibre type-specific differences in physiological, biochemical and cellular properties (Pette and Staron, 2000; Spangenburg and Booth, 2003; Schiaffino and Reggiani, 2011). On the molecular level, this is reflected by highly complex and differential protein expression patterns (Okumura *et al.,* 2005; Gelfi *et al.,* 2006; Galpin *et al.,* 2012). Mature skeletal muscles exhibit an astonishing potential to adapt to changed functional demands, which is illustrated by swift transitions of muscle phenotypic profiles in response to altered neuromuscular activity levels (Pette and Staron, 2001; Matsakas and Patel, 2009; Canepari *et al.,* 2010). Enhanced neuromuscular activity or chronic low-frequency electro-stimulation causes a stepwise fast-to-slow transformation processes in skeletal muscle, disuse-related muscular atrophy or complete denervation is typically associated with slow-to-fast transitions (Trappe *et al.,* 2006; Gallagher *et al.,* 2005; Nuhr *et al.,* 2003; Schiaffino *et al.,* 2013; Wang and Pessin, 2013). The detailed biochemical analysis of the sarcomeric myosin heavy chains (MHC's) has identified hyper-excitability, denervation or muscular dystrophy as causing very different changes in the isoform expression patterns of this essential contractile protein in skeletal muscles (Agbulut *et al.,* 2014). The biochemical consequences outlined above of fibre type shifting are also evident by proteome-wide alterations in the abundance and isoform expression pattern of contractile proteins and metabolic enzymes (Ohlendieck, 2010A; Gelfi *et al.,* 2011; Ohlendieck, 2012). During motor neuron disease associated paralysis, the pathophysiology of preferential alterations in fibre innervation, appears to be linked with less unilateral changes in muscle fibres (Pansaeasa *et al.,* 2014). The

denervation-reinnervation patterns found in neurogenic atrophy are also associated with the presence of small fibres and the expression of immature isoforms of myosin heavy chains (Doppler *et al.,* 2008). The comprehensive analysis of progressive neurodegeneration and its down-stream effects on contractile fibres within affected motor units requires systematic approaches to understand the complexity of molecular changes (Pal *et al.,* 2014).

Previous proteomic profiling studies of the effects of progressive neurodegeneration has included cerebrospinal fluid, cervical spinal cord specimens, lumbar spinal cord preparations and skeletal muscles (Ranganathan *et al.,* 2005; Staunton *et al.,* 2011; Capitanio *et al.,* 2012). Earlier gel-based surveys of the WR and SOD mouse models of ALS, have used fluorescence two-dimensional difference in-gel electrophoresis, DIGE, proteomic techniques (Staunton *et al.,* 2011; Capitanio *et al.,* 2012). This electrophoretic method is the most reproducible of all staining techniques and is highly sensitive (Minden, 2012). Here, this study has employed a complementary gel-free method of label-free mass spectrometry, to determine secondary changes in WR skeletal muscle tissue due to abnormal expression of the GARP component VPS-54. In contrast to gel-based methods, label-free mass spectrometry can routinely identify low copy numbers of integral membrane proteins, high molecular weight proteins and components with extreme isoelectric points, p*I*, and/or post-translational modifications, PTMs, (Holland and Ohlendieck, 2014C).

Over the past decade, mass-spectrometry based proteomics has played an instrumental role in performing global surveys and altered protein expression patterns when comparing diseased versus normal muscle tissue and for biomarker discovery (Ohlendieck, 2010A; Calligaris *et al.,* 2011). Reliable

disease-specific biomarkers are crucially important for a broad range of reasons including; improved diagnostics, creating new therapeutic targets, enhanced monitoring of disease progression and to determine benefits of experimental drug therapies (Bowser *et al.,* 2006).

3.1.1 Experimental design

In order to evaluate the intricate effects of primary motor neuronopathy on the skeletal muscle proteome, label-free MS was employed to the study global alterations in the wobbler, WR, mouse model of progressive neurodegeneration. The urea soluble protein complement was prepared from the hind limb muscle of WR (n = 4) and age matched WT (n = 4) control counterparts. Label-free MS was used to study the global alterations of this specific muscle group at 9-weeks old. Skeletal muscle protein samples were analysed by label-free mass spectrometry, relatively quantified by label-free Progenesis software, identified with MASCOT and searched against the UniProtKB-SwissProt database. Bioinformatics software was applied to identify the clustering of molecular functions and potential protein interactions of the MS-identified muscle proteins with a changed abundance in the WR mouse. This analysis was performed with (i) the comprehensive PANTHER database of protein families for the cataloguing of molecular functions and (ii) STRING software to visualise the known and predicted proteins interactions of direct physical and indirect functional protein associations. Key proteomic findings were independently verified by immunoblot analysis to confirm changed concentration levels of distinct muscle associated proteins as revealed by label-free LC-MS/MS analysis.

3.2 Results

The label-free mass spectrometry-based proteomic analysis of 9-week old WR hind limb muscle, HLM, versus age-matched control WT muscle was performed with the aim of establishing the extent of altered protein concentrations in an established mouse model of motor neuron disease. Protein changes were determined by label-free LC-MS/MS analysis and alterations in proteomic hits of interest were confirmed by comparative immunoblotting analysis.

3.2.1 Label-free LC-MS/MS analysis of WR versus WT hind limb muscle

Proteomic profiling of WR HLM muscle showed significant alterations (ANOVA score of $p \leq 0.05$) in the abundance of 72 proteins species with a fold change ≥ ±1.2. Table 3.1 lists the significantly altered proteins, of which 9 proteins were found to be decreased and an increased concentration was discovered in the case of 63 proteins. Changes of 2-fold or higher were observed for 20 increased proteins and 2 decreased proteins. Moderate expression level alterations, less than 2 fold, occurred in 50 other muscle-associated proteins presented here. Proteins that exhibited a considerable increase in concentration were identified with a broad range in function, varying from contractile elements, including myosin light chains, troponin subunits TnI, TnC and TnT, to tropomyosin. In addition, the nuclear envelope protein lamin, the mitochondrial enzyme aldehyde dehydrogenase, histone protein H4, the molecular chaperone αB-crystallin, fatty acid binding protein, fructose-1,6-bisphosphatase, four and a half LIM domains protein 1, carbonic anhydrase CA3, heat shock protein β-1,

annexin and peptidyl-prolyl cis-trans isomerase A were drastically increased in WR muscle. The haemoglobin subunits α and β were both shown to be approximately 2-fold increased, suggesting that the WR and WT muscle fibres of hind limbs are possibly not equally well vascularized. The apparent increased levels of haemoglobin may be due to higher levels of blood supply to WR muscles. The animals had not been perfused prior to sacrificing, meaning this finding could be an artifact of the isolation procedure and therefore both the WR and WT tissues may be equally well vascularized.

Table 3.1 List of proteins with a changed concentration in WR leg muscle as revealed by label-free mass spectrometry

Accession number	Protein name	Peptides	Score	ANOVA	Fold change
P05977	Myosin light chain 1/3, skeletal muscle isoform	2	126.35	0.0187	179.27
Q9WUZ5	Troponin I, slow skeletal muscle	3	180.85	0.0047	7.91
P19123	Troponin C, slow skeletal and cardiac muscles	4	296.17	0.0016	6.25
O88346	Troponin T, slow skeletal muscle	3	181.30	0.0050	6.09
P21107	Tropomyosin alpha-3 chain	4	438.44	0.0020	4.69
Q91Z83	Myosin-7	33	3080.77	0.0012	4.30
P51667	Myosin regulatory light chain 2, ventricular/cardiac muscle isoform	5	270.34	0.0086	3.90
P48678	Prelamin-A/C	9	592.98	0.0034	2.93
P47738	Aldehyde dehydrogenase, mitochondrial	4	236.63	0.0020	2.93
P09542	Myosin light chain 3	4	365.98	0.0143	2.75
P62806	Histone H4	3	228.77	0.0010	2.59
P23927	Alpha-crystallin B chain	3	170.51	0.0088	2.57
P04117	Fatty acid-binding protein, adipocyte	3	261.47	0.0007	2.48
P70695	Fructose-1,6-bisphosphatase isozyme 2	2	109.38	0.0013	2.34
P97447	Four and a half LIM domains protein 1	3	187.59	0.0030	2.34
P02088	Hemoglobin subunit beta-1	5	480.94	0.0103	2.30
P16015	Carbonic anhydrase 3	6	521.62	0.0152	2.23
P14602	Heat shock protein beta-1	3	153.41	0.0004	2.22
P07356	Annexin A2	3	159.34	0.0196	2.04
P17742	Peptidyl-prolyl cis-trans isomerase A	3	171.81	0.0231	1.99
Q8VHX6	Filamin-C	20	1399.68	0.0003	1.95
P60710	Actin, cytoplasmic 1	4	393.11	0.0327	1.89
P01942	Hemoglobin subunit alpha	4	388.07	0.0192	1.89
P67778	Prohibitin	2	114.26	0.0210	1.83
P54071	Isocitrate dehydrogenase [NADP], mitochondrial	3	248.98	0.0024	1.72
P20152	Vimentin	6	347.23	0.0105	1.68
Q9JI91	Alpha-actinin-2	16	1373.39	0.0008	1.64
Q9D0K2	Succinyl-CoA:3-ketoacid coenzyme A transferase 1, mitochondrial	2	89.70	0.0041	1.63
Q9JKB3	DNA-binding protein A	2	167.62	0.0021	1.63
O08539	Myc box-dependent-interacting protein 1	4	215.92	0.0067	1.60
P07724	Serum albumin	11	792.98	0.0006	1.56
P20029	78 kDa glucose-regulated protein	2	225.91	0.0033	1.55
P62259	14-3-3 protein epsilon	3	188.90	0.0091	1.55
P31001	Desmin	9	705.13	0.0041	1.54
Q04857	Collagen alpha-1(VI) chain	4	267.81	0.0146	1.52
P10126	Elongation factor 1-alpha 1	3	171.89	0.0294	1.50
Q02788	Collagen alpha-2(VI) chain	5	317.30	0.0306	1.49
Q99JY0	Trifunctional enzyme subunit beta, mitochondrial	7	497.11	0.0060	1.49
P51885	Lumican	2	126.04	0.0145	1.49
P11499	Heat shock protein HSP 90-beta	5	375.59	0.0060	1.47
Q7TQ48	Sarcalumenin	6	381.25	0.0039	1.47
P51174	Long-chain specific acyl-CoA dehydrogenase, mitochondrial	3	165.65	0.0004	1.44
Q9JIF9	Myotilin	4	296.40	0.0063	1.43
Q61171	Peroxiredoxin-2	2	119.91	0.0228	1.40
P63038	60 kDa heat shock protein, mitochondrial	2	135.87	0.0034	1.39
P58252	Elongation factor 2	3	194.77	0.0121	1.39
Q8QZT1	Acetyl-CoA acetyltransferase, mitochondrial	2	134.75	0.0020	1.38
P68372	Tubulin beta-4B chain	2	548.87	0.0045	1.36
Q8BMS1	Trifunctional enzyme subunit alpha, mitochondrial	6	360.96	0.0166	1.36

Table 3.1 Continued

Accession number	Protein name	Peptides	Score	ANOVA	Fold change
Q99LC5	Electron transfer flavoprotein subunit alpha, mitochondrial	2	210.91	0.0181	1.35
P05202	Aspartate aminotransferase, mitochondrial	2	109.34	0.0083	1.32
Q91ZJ5	UTP--glucose-1-phosphate uridylyltransferase	2	117.55	0.0095	1.31
P56480	ATP synthase subunit beta, mitochondrial	6	463.83	0.0263	1.31
Q9JKS4	LIM domain-binding protein 3	2	163.43	0.0020	1.29
P50544	Very long-chain specific acyl-CoA dehydrogenase, mitochondrial	4	261.63	0.0019	1.29
P38647	Stress-70 protein, mitochondrial	2	108.01	0.0009	1.27
Q9D2G2	Dihydrolipoyllysine-residue succinyltransferase component of 2-oxoglutarate dehydrogenase complex, mitochondrial	2	98.57	0.0163	1.26
Q99KI0	Aconitate hydratase, mitochondrial	5	304.47	0.0168	1.26
Q9DB20	ATP synthase subunit O, mitochondrial	2	117.63	0.0425	1.25
P63017	Heat shock cognate 71 kDa protein	4	407.65	0.0170	1.24
Q9DCW4	Electron transfer flavoprotein subunit beta	3	201.29	0.0171	1.24
Q03265	ATP synthase subunit alpha, mitochondrial	4	365.70	0.0168	1.23
Q62234	Myomesin-1	3	176.76	0.0467	1.22
O88990	Alpha-actinin-3	4	431.15	0.0131	-1.21
Q9WUB3	Glycogen phosphorylase, muscle form	5	343.10	0.0130	-1.26
A2ASS6	Titin	42	2579.98	0.0005	-1.26
Q9D0F9	Phosphoglucomutase-1	6	438.29	0.0105	-1.33
Q3V1D3	AMP deaminase 1	3	218.71	0.0271	-1.38
Q8R429	Sarcoplasmic/endoplasmic reticulum calcium ATPase 1	5	398.20	0.0042	-1.63
Q5SX39	Myosin-4	4	990.28	0.0179	-1.83
Q5XKE0	Myosin-binding protein C, fast-type	4	268.17	0.0291	-1.98
P07759	Serine protease inhibitor A3K	2	154.17	0.0086	-3.59

* Wobbler versus normal muscle tissue

** UniProtKB-SwissProt database (downloaded January 2013) with 16,638 proteins *(Mus musculus*)

3.2.2 Summary of protein functions with a changed concentration in WR skeletal muscle and protein interaction analysis

The newly identified WR muscle proteins with an altered concentration, Table 3.1, were put through the bioinformatics PANTHER database of protein families to reveal a list of molecular functions (Mi *et al.,* 2013). Figure 3.1 illustrates the cataloging of the proposed protein functions in a pie chart: transporter activity (4.8%), antioxidant activity (1%), binding activity (21.8%), catalytic activity (25.6%), enzyme regulator activity (5.7%), ion channel activity (2.9%), motor activity (3.8%), receptor activity (4.8%), structural molecule activity (24.8%), transcription regulator activity (2.9%) and translation regulator activity (1.9%).

In order to determine potential protein-protein interactions of the MS-identified proteins with an altered concentration in atrophying WR muscle, the publically available STRING (http://string-db.org/; version 9.1) database was used. STRING contains known and predicted protein interactions including direct physical and indirect functional protein associations (Franceschini *et al.,* 2013). Figure 3.2 illustrates the findings from the bioinformatics analysis.

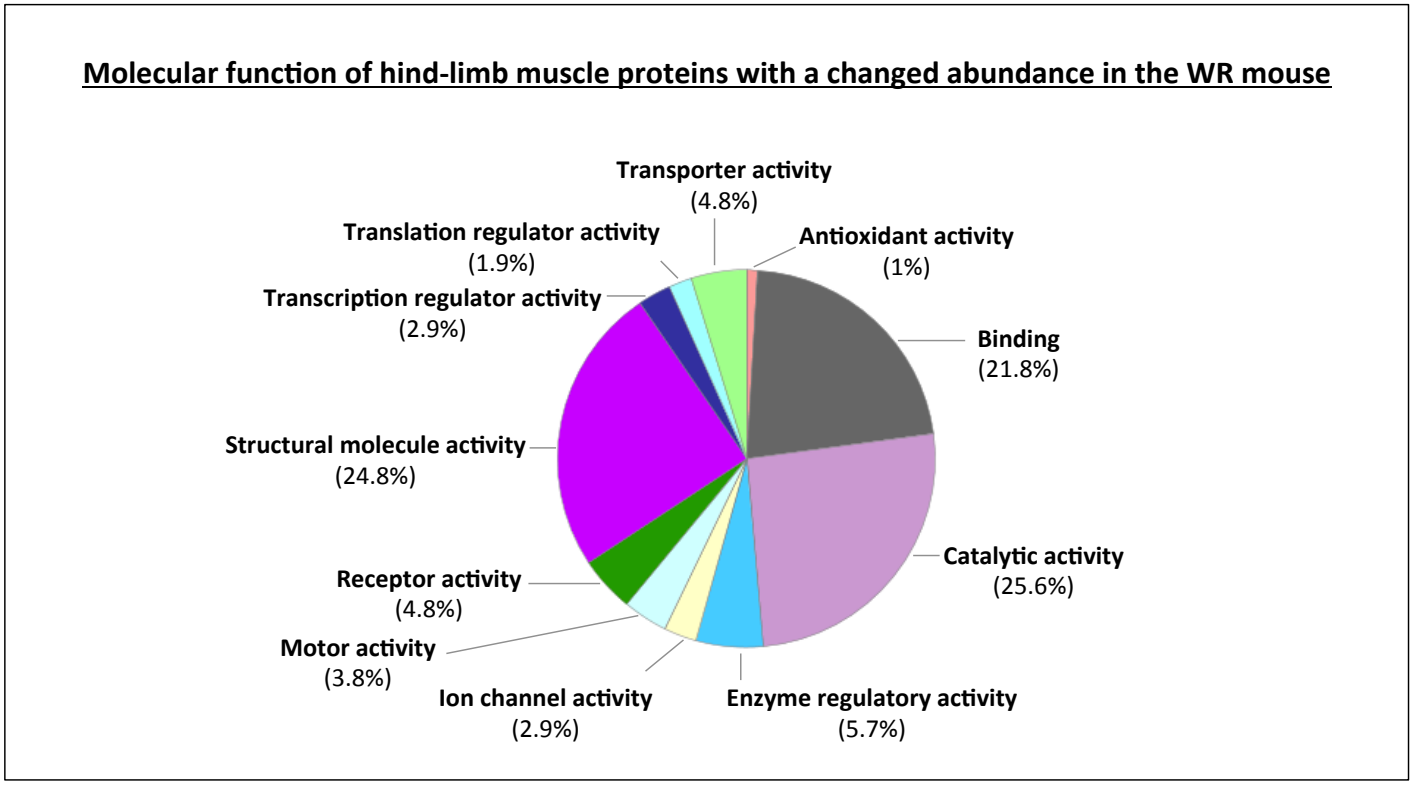

Figure 3.1 Molecular functions of WR muscle proteins with an altered abundance. The publically available bioinformatics software PANTHER was employed to identify the clustering of molecular functions of MS-identified muscle proteins with an altered abundance in the WR mouse (Table 3.1). The analysis was performed with the PANTHER database, version 8.1 (Mi *et al.,* 2013).

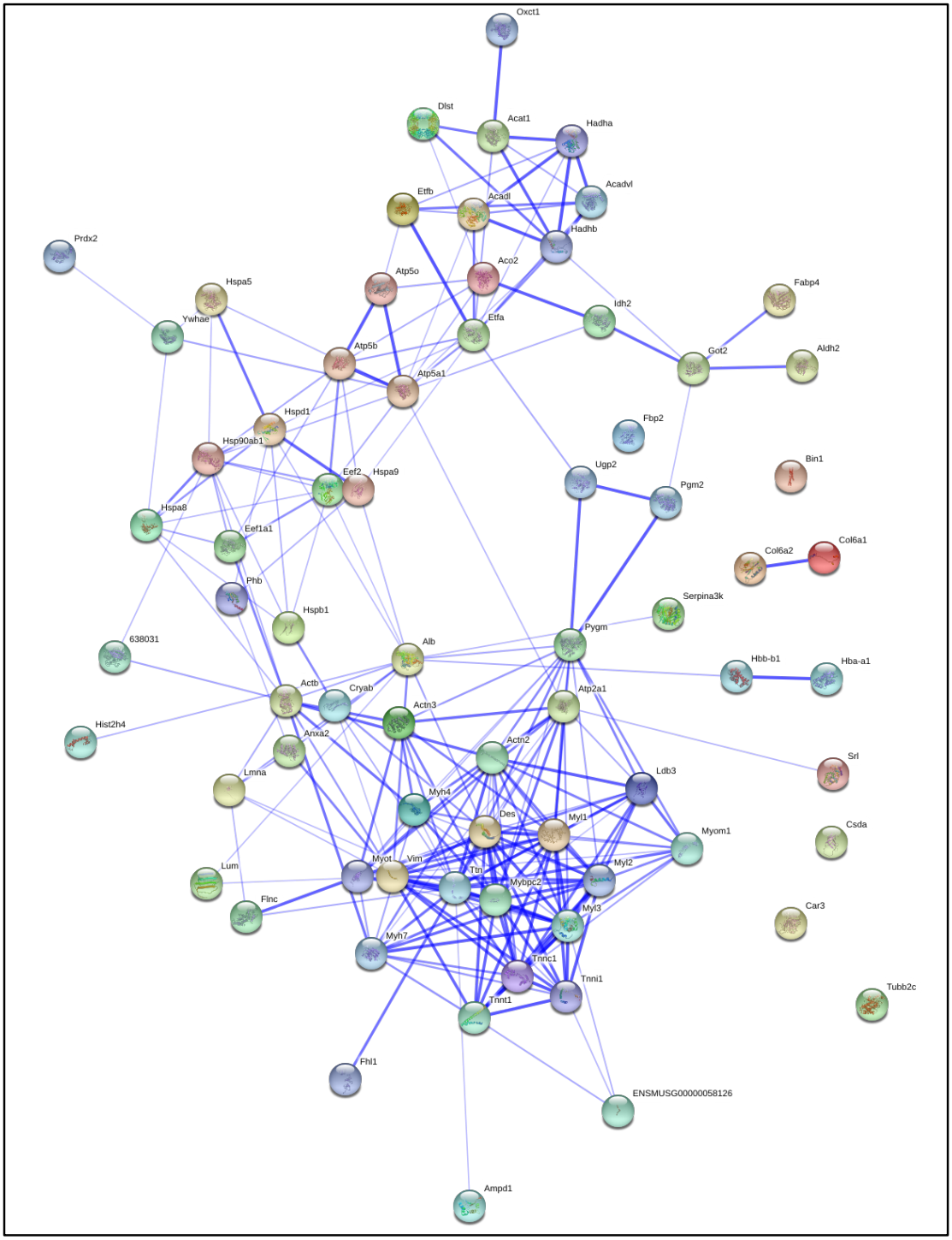

Figure 3.2 Protein interaction map of WR hind limb muscle proteins with an altered expression level.
Shown is a protein interaction map of MS-identified muscle proteins with an altered abundance in the WR mouse (Table 3.1) generated with the STRING database, version 9.1 (Franceschini *et al.,* 2013). The interaction map illustrates the potential complexity of protein interactions between affected proteins in WR muscle.

3.2.3 Verification of proteomic findings by comparative immunoblotting of WR versus WT hind limb muscle

Following the mass spectrometric identification of protein changes in WR hind leg muscle, a variety of proteomic hits were verified by immunoblot analysis (Figures 3.5-3.9). The immunoblots included marker proteins of the contractile apparatus, the cytoskeleton, the nuclear envelope, the extracellular matrix, the cellular stress response, muscle metabolism, mitochondrial bioenergetics and mitochondrial regulation. Figure 3.3 shows a 1D silver-stained gel of 4 biological repeats of preparations from WR versus WT muscle, illustrating equal protein loading and a relatively comparable protein binding pattern between the two different muscle specimens. Immunoblotting with a commercially available antibody to the major extracellular matrix protein laminin demonstrated comparable levels of this protein in atrophying WR and normal WT muscle samples (Figure 3.4).

In contrast, significant concentration changes were confirmed by immunoblotting for a range of muscle-associated proteins. While myosin binding protein MBP-C was decreased in WR muscle (Figure 3.5 A, B), the contractile proteins troponin TnT and myosin light chain MLC2 exhibited increased levels (Figure 3.5 C-D and E-F, respectively). The cytoskeletal element desmin (Figure 3.5 G, H), the matrix-cell interaction protein annexin-A2 (Figure 3.6 A, B) and the nuclear envelope protein lamin A/C (Figure 3.6 C, D) showed an increased concentration in WR skeletal muscle. The traditional banding pattern for Lamin A/C exhibits two bands at approximately 60-75kDa, however the banding pattern illustrated in Figure 3.6 C shows a single band. This could be a result of the lack of specificity to the commercial antibody employed or that one of the

bands had been at too low a concentration to be detected by immunoblotting methods. In contrast to the unchanged levels of the basal lamina component laminin (Figure 3.4 A-B) used to demonstrate equal loading in immunoblotting, collagen-VI was found to be increased in WR muscle (Figure 3.6 E, F). Agreeing with cellular stress and modifications of the contractile apparatus, a drastically increased concentration of αB-crystallin was confirmed by antibody decoration (Figure 3.6 G, H). In addition, the enzymes carbonic anhydrase CA3, mitochondrial ATP synthase and isocitrate dehydrogenase, as well as the regulatory protein prohibitin exhibited changes in their expression levels (Figure 3.7 A-H), in agreement with the proteomic results listed in Table 3.1. Figure 3.8 summarizes the immunoblot analysis of three crucial Ca^{2+}-binding proteins, i.e. the cytosolic protein parvalbumin, the luminal Ca^{2+}-shuttle protein sarcalumenin and the abundant Ca^{2+}-buffering protein calsequestrin of the terminal cisternae region of the sarcoplasmic reticulum. While parvalbumin was shown to be greatly reduced in WR muscle (Figure 3.8 A, B), the luminal Ca^{2+}-binding proteins exhibited increased levels in atrophying muscle preparations as seen in Figure 3.8 C-F). Immunoblot analysis of superoxide dismutase isoforms SOD-1 (Figure 3.9 A, B), and SOD-2 (Figure 3.9 C, D), found an apparent decrease and increase in abundance in WR samples respectively. MS identified proteins fatty acid binding protein, FABP-3 (Figure 3.9 E, F), and TnI (Figure 3.9 G, H), were validated by immunoblotting. Significant increases were found in both proteins.

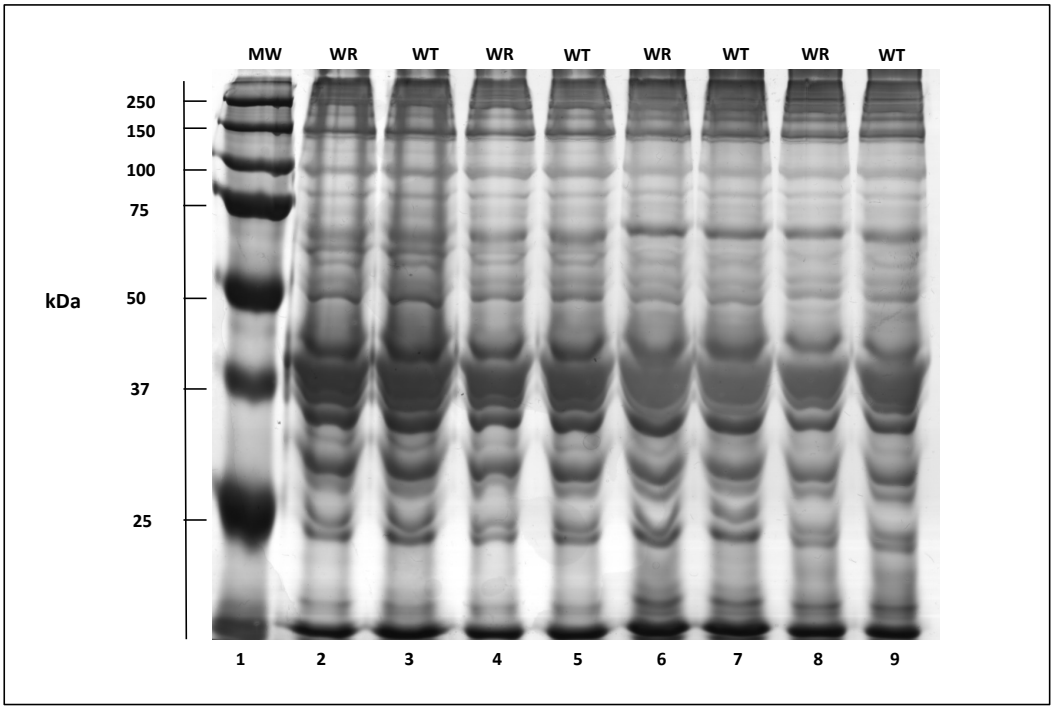

Figure 3.3 Electrophoretic analysis of WR and WT muscle preparations used for LC-MS/MS analysis.
Shown is a silver-stained 1D gel. Lane 1 shows molecular mass (MW) standards with their values in kDa on the left side of the panel. Lanes 2 to 9 represent 4 biological repeats of WR versus normal WT muscle preparations, respectively (i.e. *n* = 4).

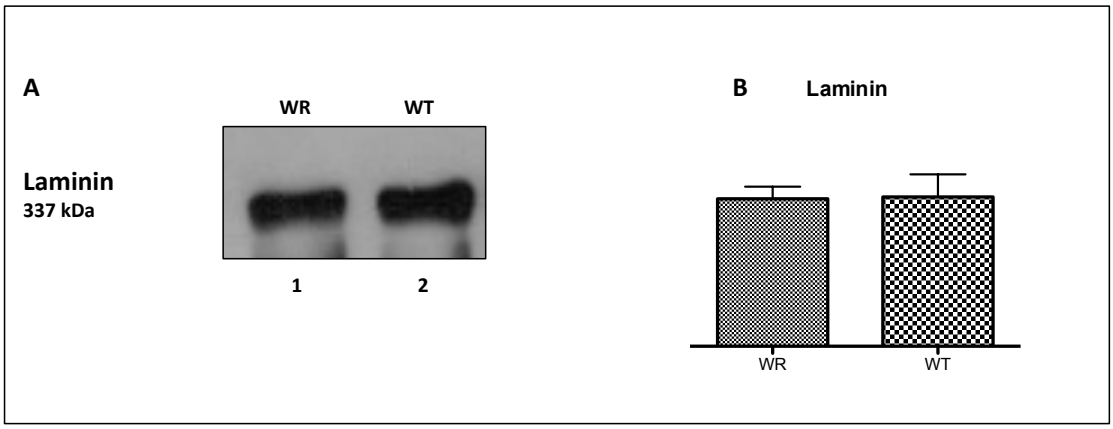

Figure 3.4 Equal loading immunoblot for WR hind limb muscle.
Shown is a representative immunoblot with an expanded view of immuno-decorated bands labeled with an antibody to laminin (A). The extracellular matrix protein laminin did not show significant changes in its concentration between WR and WT muscle extracts (B) (unpaired Student's *t*-test; $n \geq 4$; NS).

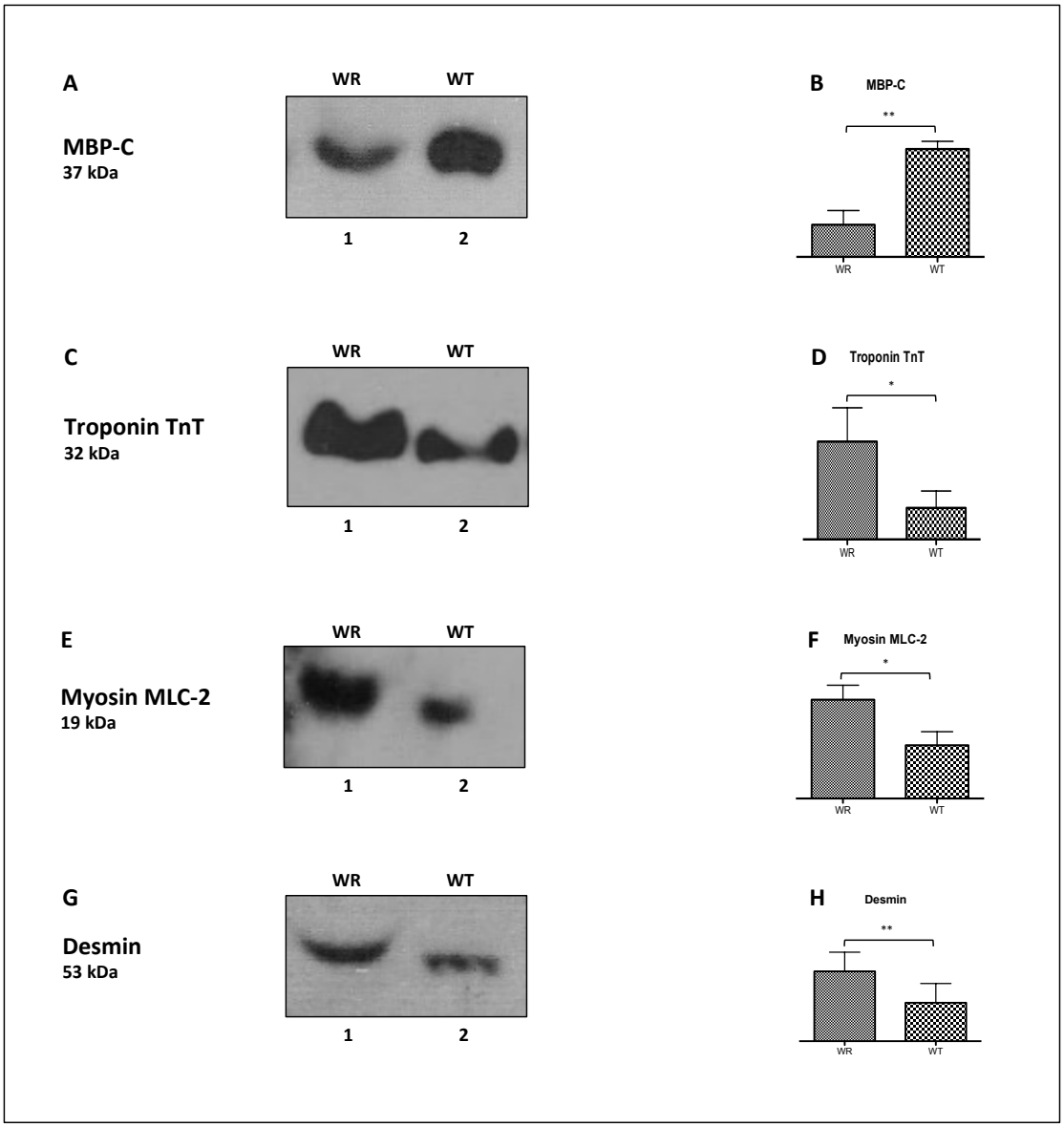

Figure 3.5 Immunoblot and quantitative analysis of proteins with an altered abundance in WR muscle.

Shown are representative immunoblots with expanded views of immuno-decorated bands labeled with antibodies to myosin binding protein MBP-C (A, B), troponin subunit TnT (C, D), myosin light chain MLC-2 (E, F) and desmin (G, H). Lanes 1 and 2 represent WR versus WT muscle preparations, respectively. Densitometric analysis of the immunoblot survey of proteins with a changed abundance in WR muscle was carried out and the comparative immunoblot analysis was statistically evaluated using an unpaired Student's *t*-test ($n \geq 4$; *$p < 0.05$; **$p < 0.01$).

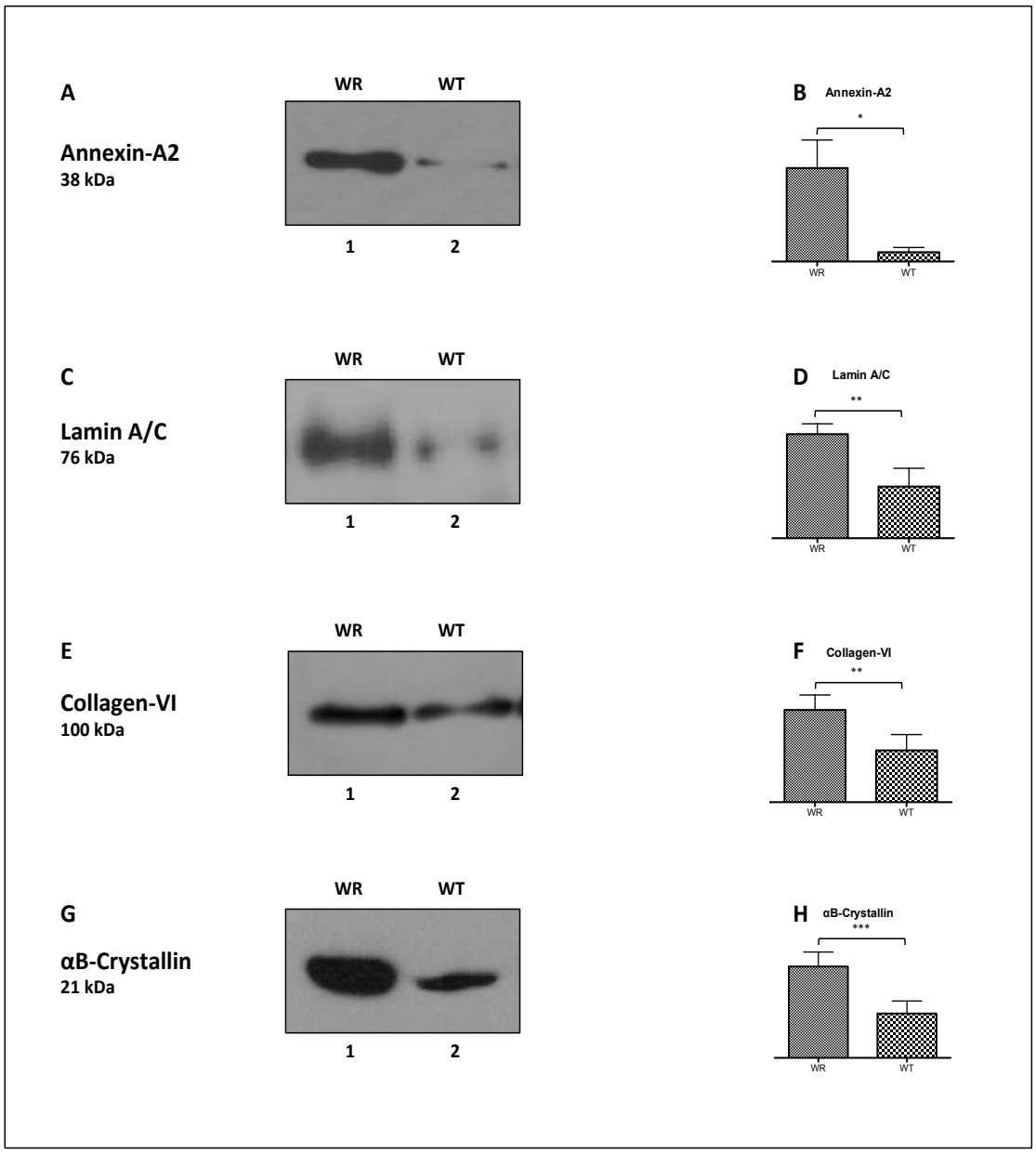

Figure 3.6 Immunoblot and quantitative analysis of proteins with an altered abundance in WR muscle.

Shown are representative immunoblots with expanded views of immuno-decorated bands labeled with antibodies to annexin-A2 (A, B), lamin A/C (C, D), collagen-VI (E, F) and αB-crystallin (HSPB5) (G, H). Lanes 1 and 2 represent WR versus WT muscle preparations, respectively. Densitometric analysis of the immunoblot survey of proteins with a changed abundance in WR muscle was carried out and the comparative immunoblot analysis was statistically evaluated using an unpaired Student's *t*-test ($n \geq 4$; *$p < 0.05$; **$p < 0.01$; ***$p < 0.001$).

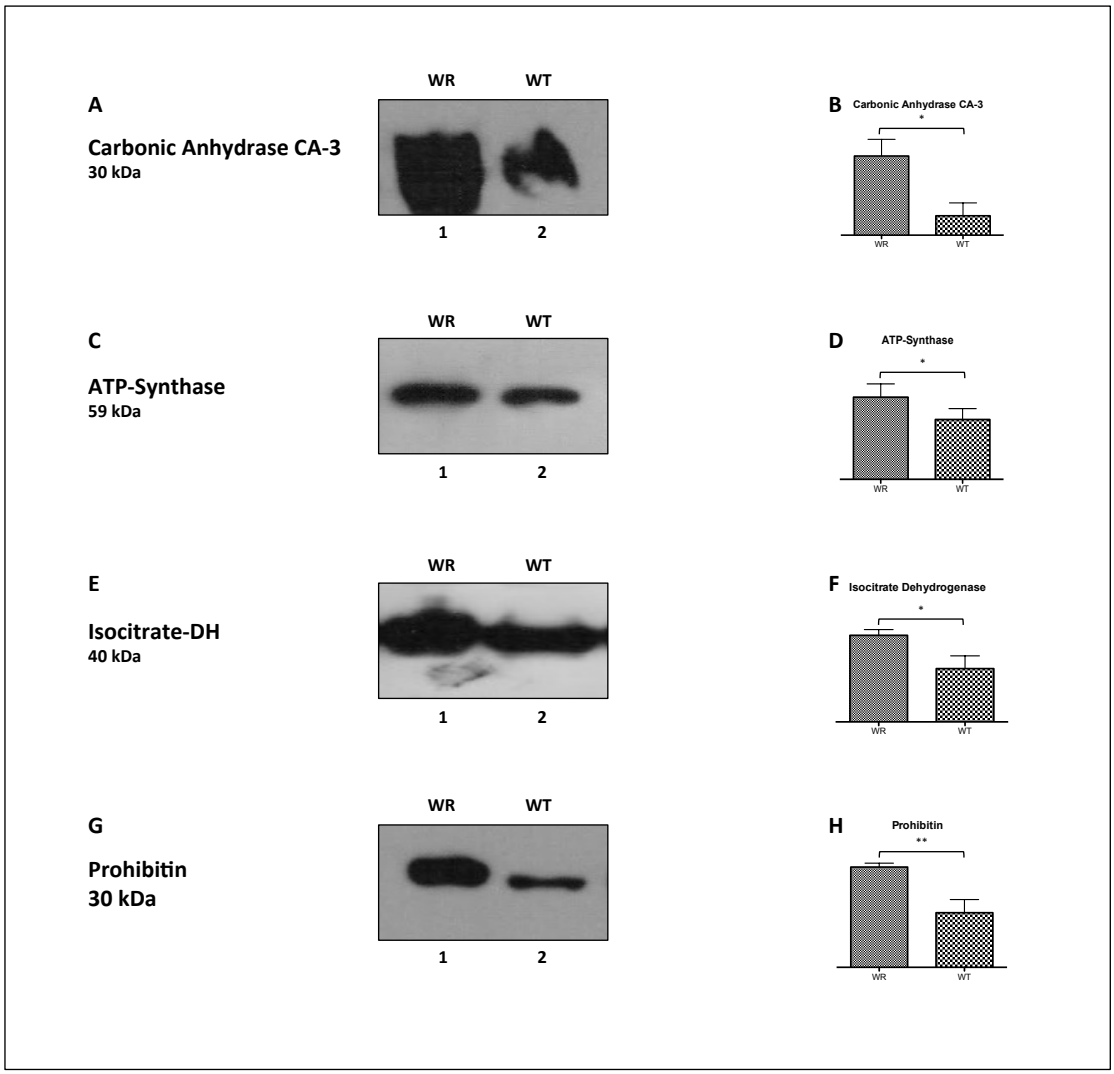

Figure 3.7 Immunoblot and quantitative analysis of proteins with an altered abundance in WR muscle.

Shown are representative immunoblots with expanded views of immuno-decorated bands labeled with antibodies to carbonic anhydrase isoform CA-3 (A, B), mitochondrial ATP-synthase (C, D), isocitrate dehydrogenase (E, F) and prohibitin (G, H). Lanes 1 and 2 represent WR versus WT muscle preparations, respectively. Densitometric analysis of the immunoblot survey of proteins with a changed abundance in WR muscle was carried out and the comparative immunoblot analysis was statistically evaluated using an unpaired Student's *t*-test ($n \geq 4$; *$p < 0.05$; **$p < 0.01$).

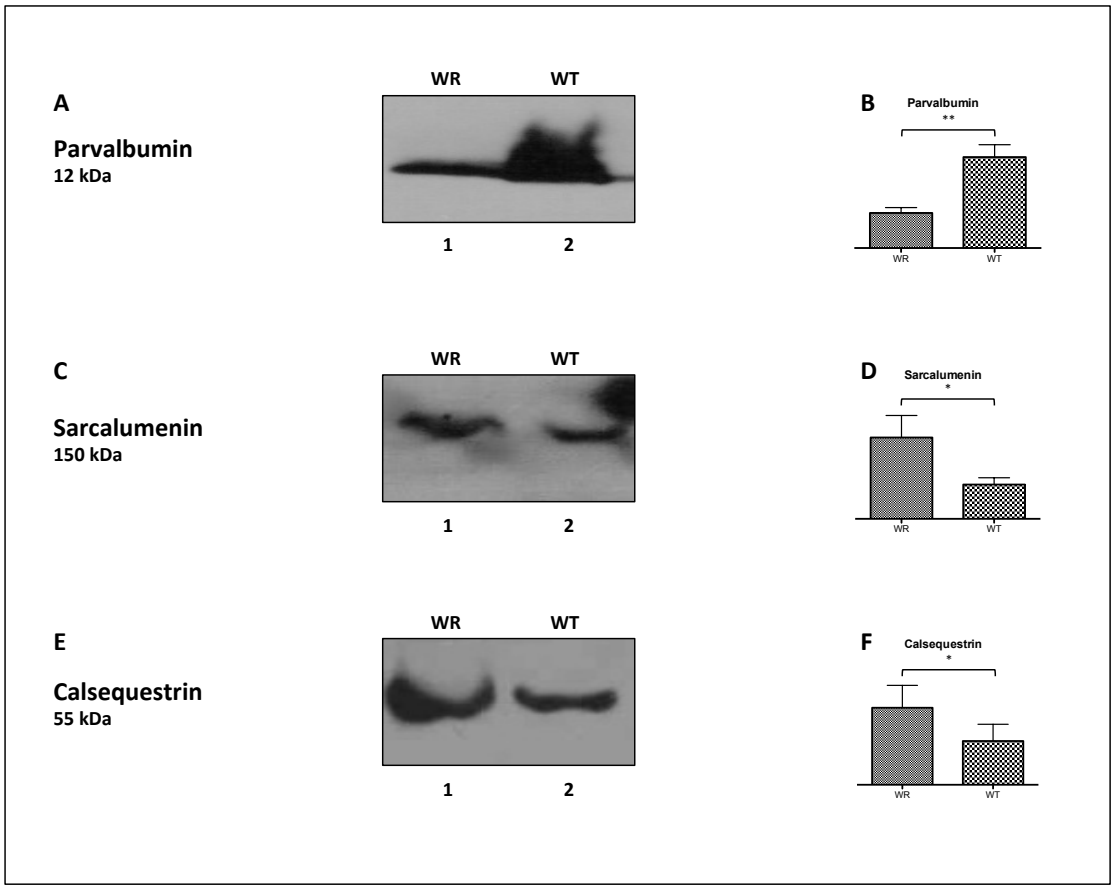

Figure 3.8 Immunoblot and quantitative analysis of Ca^{2+}-binding proteins with a changed abundance in WR hind limb muscle.

Shown are representative immunoblots with expanded views of immuno-decorated bands labelled with antibodies to the cytosolic Ca^{2+}-binding protein parvalbumin (A, B), the luminal Ca^{2+}-shuttle protein sarcalumenin of the sarcoplasmic reticulum (SR) (C, D) and the luminal Ca^{2+}-binding protein calsequestrin of the terminal cisternae region of the sarcoplasmic reticulum (E, F). Lanes 1 and 2 represent WR versus WT muscle preparations, respectively. Densitometric analysis of the immunoblot survey of proteins with a changed abundance in WR muscle was carried out and the comparative immunoblot analysis was statistically evaluated using an unpaired Student's *t*-test ($n \geq 4$; $^{*}p < 0.05$; $^{**}p < 0.01$).

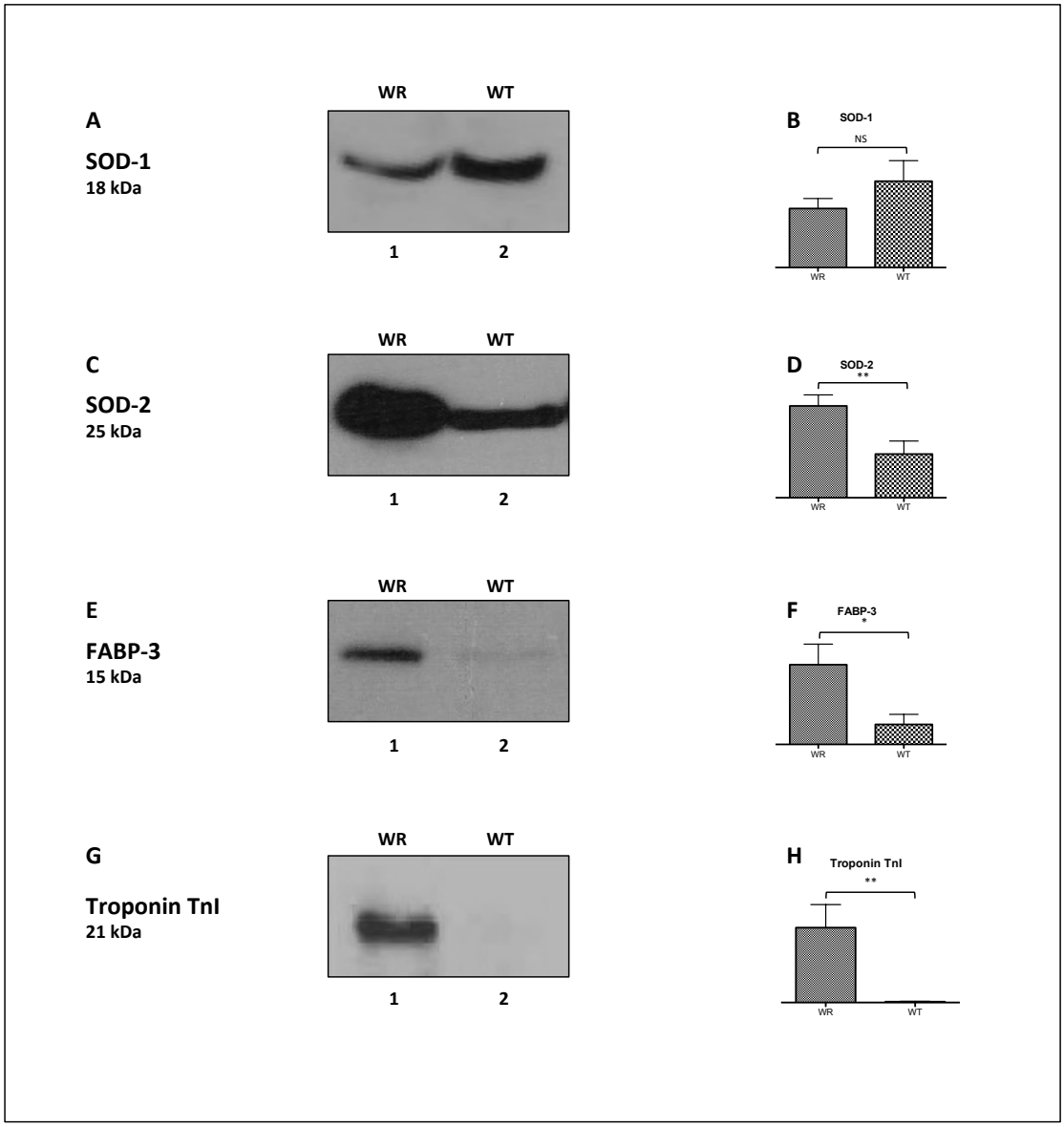

Figure 3.9 Immunoblot and quantitative analysis of proteins with an altered abundance in WR muscle.

Shown are representative immunoblots with expanded views of immuno-decorated bands labeled with antibodies to SOD-1 (A, B), SOD-2 (C, D), FABP-3 (E, F) and troponin TnI (G, H). Lanes 1 and 2 represent WR versus WT muscle preparations, respectively. Densitometric analysis of the immunoblot survey of proteins with a changed abundance in WR muscle was carried out and the comparative immunoblot analysis was statistically evaluated using an unpaired Student's *t*-test ($n \geq 4$; NS = not significant, $^{*}p < 0.05$; $^{**}p < 0.01$).

3.3 Discussion

Distinct changes in innervation patterns have a profound influence on skeletal muscle differentiation, fibre regeneration and the reprogramming of motor units during physiological adaptations to changed functional demands. The proteomic profiling of muscle plasticity has established discrete changes in the abundance and expression pattern of contractile proteins and metabolic enzymes during myogenesis and fibre maturation, as well as in response to enhanced neuromuscular activity, disuse-associated atrophy or chronic electro-stimulation (Ohlendieck, 2012). Here, we have used the WR mouse model of primary neuronopathy (Moser *et al.,* 2013; Schmitt-John *et al.,* 2005) to evaluate the complexity of proteome-wide changes in response to disease-induced alterations in fibre innervation. The label-free MS analysis of proteome-wide changes in neurogenic muscular atrophy has noticeably shown that distinct differences exist between the effects of nerve crush or complete denervation of skeletal muscles versus the influences of progressive degeneration of discrete motor neuron populations. The downstream biochemical effects of altered innervation patterns on neuromuscular modulation are clearly reflected by drastic changes in the concentration levels of muscle proteins.

Importantly, this study has established that a more complex pattern of proteome-wide changes occurs in disease-associated muscular atrophy as compared to muscular disuse or denervation (Ohlendieck, 2012).

3.3.1 Fibre transformation in WR hind limb muscle

The proteomic analysis of WR hind limb muscle agrees with the idea that fibre type specification and the metabolic weighting of bioenergetic pathways is clearly influenced by both a differing degree of a subtype-specific vulnerability of neuromuscular synapses and compensatory mechanisms of fibre type shifting in motor neuron disease. Typically, experimental denervation, traumatic nerve injury or prolonged neuromuscular disuse results in relatively unilateral skeletal muscle transitions. While enhanced neuromuscular activity triggers a clear fast-to-slow transition in skeletal muscle, disuse-related muscular atrophy or complete denervation is mostly associated with a slow-to-fast transformation. In contrast, the new label-free proteomic data presented here (Table 3.1) demonstrates that protein changes in motor neuron disease are more complex and that this disease is not associated with a straightforward slow-to-fast transformation process. Motor neuron disease appears to be connected with complex differential expression patterns of both fast and slow muscle protein isoforms.

3.3.2 Glucose metabolism and glycolytic enzymes

The lower concentration of glycogen phosphorylase and phosphoglucomutase agrees with the idea of a disturbed glucose metabolism in WR muscle. However, the glycolytic enzyme fructose-1,6-bisphosphatase was found to be increased in WR preparations, which was also shown in a previous gel-based study of WR muscle (Staunton *et al.,* 2011). Since some glycolytic enzymes are multi-functional and are also potentially involved in cellular

signaling (Ohlendieck, 2010B), the differential expression levels of individual glycolysis-related proteins may reflect changes in other biochemical processes than anaerobic metabolism (Staunton *et al.,* 2011; Capitanio *et al.,* 2012). The complex alterations in glycolytic and mitochondrial muscle enzymes shown in this study indicate that the metabolic transitions in WR muscle are more complex than a unidirectional shift towards a particular bioenergetic phenotype.

3.3.3 Calcium handling

Interestingly, the SERCA1 isoform of the relaxation-inducing Ca^{2+}-ATPase of the sarcoplasmic reticulum was identified by label-free MS analysis. This finding illustrates suitably the advantages and complementary nature of gel-free separation approaches in muscle proteomics and shows that liquid chromatography-coupled MS analysis is capable of detecting changes in integral and highly hydrophobic muscle enzymes (Schreiber and Ohlendieck, 2007).

Since the Ca^{2+}-pumping ATPase is a relatively abundant protein, it is difficult to interpret whether changes in the SERCA1 isoform play a major role in the atrophy-related fibre changes or represent a minor alteration within the extensive network of the sarcoplasmic reticulum membrane system.

Immunoblotting with antibodies to the Ca^{2+}-ATPase from the sarcoplasmic reticulum resulted in excessive background staining, which prevented a proper verification of this proteomic finding. Interestingly, the concentration of the luminal Ca^{2+}-binding proteins sarcalumenin and calsequestrin is considerably increased in WR muscle, which is indicative of a greater demand for Ca^{2+}-buffering within the sarcoplasmic reticulum. These

proteomic results were validated by immunoblotting and were statistically significant, as seen in Figure 3.8 C-F. A possible reason for this is the avoidance of Ca^{2+}-dependent proteolysis and/or abnormal cellular signaling on the level of excitation-contraction coupling, as is commonly observed in muscular disorders (Hopf *et al.,* 2007). As previously shown by immunoblotting and proteomics in the WR and SOD mouse models of ALS (Staunton *et al.,* 2011; Capitanio *et al.,* 2012), respectively, the concentration of the cytosolic Ca^{2+}-binding protein parvalbumin is drastically lowered in motor neuron disease. This reduced capability of cytosolic Ca^{2+}-buffering might be related to the increased levels of luminal Ca^{2+}-binding capacity in WR muscle preparations and agrees with previously described decreased mRNA levels of parvalbumin in the same animal model of ALS (Sedehizadw *et al.,* 1997). This study did not identify parvalbumin as being significantly changed by label-free MS, however it was recognized as being significantly decreased by immunoblotting, as seen in Figure 3.8 A, B.

3.3.4 Contractile apparatus proteins

The findings of a previous DIGE-based analysis of WR muscle in 2011 (Staunton *et al.,*) are in agreement that disease-associated muscular atrophy causes a reduced concentration of the fast myosin binding protein MBP-C. Immunoblot analysis has confirmed the lower concentration of this contractile protein in WR muscle (Figure 3.5 A, B). In addition, the study presented here has established a reduction in α-actinin, titin and myosin 4, the foetal muscle isoform of MHCIIb, indicating remodelling of the cytoskeletal network and the auxiliary structure and contractile elements of the actomyosin apparatus (Holland and

Ohlendieck, 2013).

In contrast to the previously mentioned decreases in metabolic enzymes and contractile proteins, a significant number of proteins were found to be increased in WR hind limb muscle. This included proteins involved in muscle contraction, the cytoskeleton, the extracellular matrix, metabolite transportation, muscle metabolism, mitochondrial regulation, ion handling and the cellular stress response. The immunoblot survey presented in this study has confirmed these concentration changes in a variety of marker proteins of distinct subcellular regions of skeletal muscle tissue. Striking increases were observed for several slow isoforms of myosin light chains and the TnI, TnC and TnT subunits of the troponin complex (Holland and Ohlendieck, 2013). The increases in TnI and TnT were validated by immunoblotting and found to be statistically significant, as illustrated in Figures 3.9 G, H and 3.5 C, D, respectively. Thus, in divergence to unilateral slow-to-fast transitions due to chronic unloading or experimental denervation procedures, as shown by several different proteomic studies (Togio *et al.,* 2005; Sun *et al.,* 2006; Seo *et al.,* 2006; Moriggi *et al.,* 2008; Ferreira *et al.,* 2009), the increase in slow forms of essential contractile proteins possibly reflects an initial preferential loss of the fast type of neuromuscular synapses in the WR model of ALS. Increased levels of a variety of mitochondrial components such as aldehyde dehydrogenase, isocitrate dehydrogenase (Figure 3.7 E, F), prohibitin (Figure 3.7 G, H), succinyl-CoA:3-ketoacid coenzyme A transferase, long-chain specific acyl-CoA dehydrogenase, trifunctional enzyme, electron transfer flavoprotein, aspartate aminotransferase, acetyl-CoA acetyltransferase, aconitate hydratase, oxoglutarate dehydrogenase and ATP synthase (Figure 3.7 C, D) would agree with this idea. These alterations are

therefore probably not directly related to an organized or adaptive pattern of fibre type shifting, but more likely based on the initial consequence of a preferential loss of neuromuscular synapses that normally function within a fast type of innervation process.

3.3.5 Nuclear proteins

The raised levels of the nuclear envelope protein lamin-A/C (Figure 3.6 C, D) and the histone H4 protein indicate possible changes or restructuring of muscle nuclei within select fibre populations of the WR mouse muscle. Lamin A/C and lamin B of the nuclear envelope form stabilizing LINC complexes with SUN1/2 proteins and nesprins, which in turn bind to cytoskeletal filaments (Sosa *et al.,* 2013). Therefore, an indirect link might exist with respect to other changed muscle proteins, such as filamin, desmin (Figure 3.5 G, H), tubulin and vimentin. Muscle-specific filamin C acts as an actin cross-linking protein, desmin and vimentin are intermediate filament components and tubulin constitutes an essential protein of microtubules (Capetanaki *et al.,* 2007). Their increased abundance, as already previously reported (Staunton *et al.,* 2011), suggests a reorganization of the muscle cytoskeleton and interior filament network in response to neurodegeneration-related unloading. The extracellular matrix protein collagen (Figure 3.6 E, F) and the multi-functional protein annexin A2 (Figure 3.6 A, B), which binds to sarcolemmal dysferlin and is probably involved in cell-matrix interactions, were also shown to be increased, which could be a compensatory response to stabilize the weakened fibre periphery during disease-related fibre unloading. Since the surface membrane-associated

dystrophin-glycoprotein complex and the neuromuscular junction-coupled utrophin-glycoprotein complex are closely linked to the actin membrane cytoskeleton (Holland *et al.,* 2013A), which is indirectly associated with the complex cytoskeletal filaments within the muscle interior and the outside structural support of the nuclear envelope, it is possible that external stimuli affect the entire cytoskeletal network of muscle fibres simultaneously, including the lamin-associated LINC complex (Sosa *et al.,* 2013). Thus, it is reasonable to conclude that motor neuron disease appears to be associated with considerable changes in the extracellular matrix, the actin cytoskeleton, intermediate filaments, microtubules and the nuclear envelope.

3.3.6 Stress response in WR hind limb muscle

Elevated levels of the molecular chaperones αB-crystallin (HSPB5) (Figure 3.6 G, H), HSP-27 (HSPB1, beta-1), the large heat shock protein HSP-90-β (HSPC), the stress-70 protein, the mitochondrial 78 kDa glucose-regulated protein, the mitochondrial 60 kDa heat shock protein and the heat shock cognate 71 kDa protein are indicative of considerable cellular stress levels in WR muscle and the need for extensive re-folding or the swift removal of mis-folded muscle proteins (Nishimura and Sharp, 2005). Increases in a variety of heat shock proteins were also reported by Capitanio *et al.,* (2012) to occur in the SOD mouse model of ALS. Thus, the missense mutation in the *Vps54* gene that causes a L967Q replacement in the vesicular protein-sorting factor VPS-54 (Schmitt-John *et al.,* 2005) triggers substantial cellular stress in affected muscle tissues. The destabilization of the tertiary protein structure of VPS-54 and subsequent

reduction in its abundance levels seems to severely disturb the function of the GARP complex and indirectly trigger an extensive stress response as seen in Table 3.1. The predominant initial effect on fast type synapses is substantiated by the fact that increased amounts of the CA-3 isoform of carbonic anhydrase were identified in WR muscle as seen in Figure 3.7 A, B. Since immunocytochemical studies by Fremont *et al.,* (1988) have demonstrated higher levels of carbonic anhydrase in *soleus* muscle as compared to *vastus lateralis* muscle, possible changes in muscle mass and contractile function are focused initially on fast-twitching fibres populations in motor neuron disease. Alternatively, the pathophysiological changes in WR muscle may require an increased demand for efficient CO_2-removal during fibre remodeling.

3.3.7 Other proteins

Recently, early gene expression changes were studied by microarray screening of *gastrocnemius* muscle from the SOD1 mouse model of ALS (de Oliveria *et al.,* 2014). The investigation identified differential gene activation levels in the Wnt/PI3-K signaling pathways and epithelial-mesenchymal transitions in pre-symptomatic skeletal muscle. Since the PI3-K pathway is involved both in the inhibition of cell death and the promotion of cell proliferation, the maintenance and repair of affected fibre populations may be impaired. Glucose uptake and fibre differentiation may also be altered, agreeing with the general idea of motor neuron disease being a multisystem disorder with a defective muscle metabolism. The gene expression changes observed in the *gastrocnemius* muscle of SOD1-G93A transgenic mice suggest that

neuromuscular impairments precede motor neuron death at pre-symptomatic periods of motor neuron disease (de Oliveria *et al.,* 2014). The analysis of muscle biopsies from ALS patients identified interesting alterations in gene expression patterns in this form of motor neuron disease, including elevated levels of mRNA encoding myosin-8, collagen, actin and annexin (Shtilbans *et al.,* 2011). Decreased mRNA levels of actinin α-3 and the fast isoform of myosin binding protein MPB-C agree with the findings from this proteomic study. Since decreased levels of fast MBP-C were shown to occur in degenerating muscle by both label-free MS analysis and gel-based proteomics, as well as transcriptomic analysis of ALS muscle biopsies (Shtilbans *et al.,* 2011), this protein represents an excellent new candidate of an internal muscle-associated biomarker of motor neuron disease. Other transcriptomic analyses have focused on the spinal cord from animal models and ALS patients (Perrin *et al.,* 2006; Offen *et al.,* 2009; Chen *et al.,* 2010).

As illustrated with immunoblot analysis in Figure 3.9 A-D, the relative abundance of the predominantly cytosolic SOD1 isoform and the mitochondrial SOD2 isoform of superoxide dismutase is differently affected in WR skeletal muscle, as also found by Staunton *et al.,* (2011).

Altered patterns of cell adhesion, the immune response, lipid metabolism and inflammation were shown to be involved in the onset of progressive paralysis, muscular atrophy and a hyper-metabolic state in motor neuron disease (Chen *et al.,* 2010).

3.3.8 Proteomic expression changes in WR hind limb muscle and bioinformatics analysis

The pie chart in Figure 3.1 created with PANTHER catalogues the proteins identified in with an altered abundance in WR muscle based on molecular function. The chart based on the MS hit-list table (Table 3.1) outlines proteins with the most highly altered classes included binding (21.8%), catalytic activity (25.6%) and structural molecule activity (24.8%). These high percentages, along with the other less affected clusters of molecular functions, show the diverse range of areas that are affected in WR muscle due to disease-related denervation.

The protein interaction map seen in Figure 3.2, generated with STRING (version 9.1) software, illustrates the complexity of the protein interaction patterns between the affected protein species in WR hind limb muscle. This is especially striking with respect to interaction nodes containing contractile elements, cytoskeletal proteins, metabolic enzymes and molecular chaperones.

3.3.9 Comparison of gel free versus gel based WR leg muscle proteomic analysis

The label-free MS analysis presented here determined altered expression levels in a considerably larger number of proteins than previously identified before using fluorescence 2D-DIGE. The previous application of 2D-DIGE resulted in the identification of 14 changed proteins, with several proteins being recognized to be present in more than one protein spot (Staunton *et al.,* 2011), however the label-free MS analysis here determined altered expression levels in a considerably larger number of proteins. The fact that the previously identified increase in glyceraldehyde-3-phosphate dehydrogenase was not recognized by label-free MS analysis could be due the fact that this protein is better separated and resolved by 2D gel electrophoresis as compared with LC and/or that this glycolytic protein digests in an optimum way by in-gel methodology to produce large numbers of detectable peptides. Both proteomic techniques established common over-lapping findings. As illustrated in Figure 3.10 both proteomic methods identified similar findings for desmin, myosin light chain (Figure 3.5 E, F), troponin C, actin, α-actinin-3 and the fast isoform of MBP-C (Staunton *et al.,* 2011; Holland and Ohlendieck, 2014C).

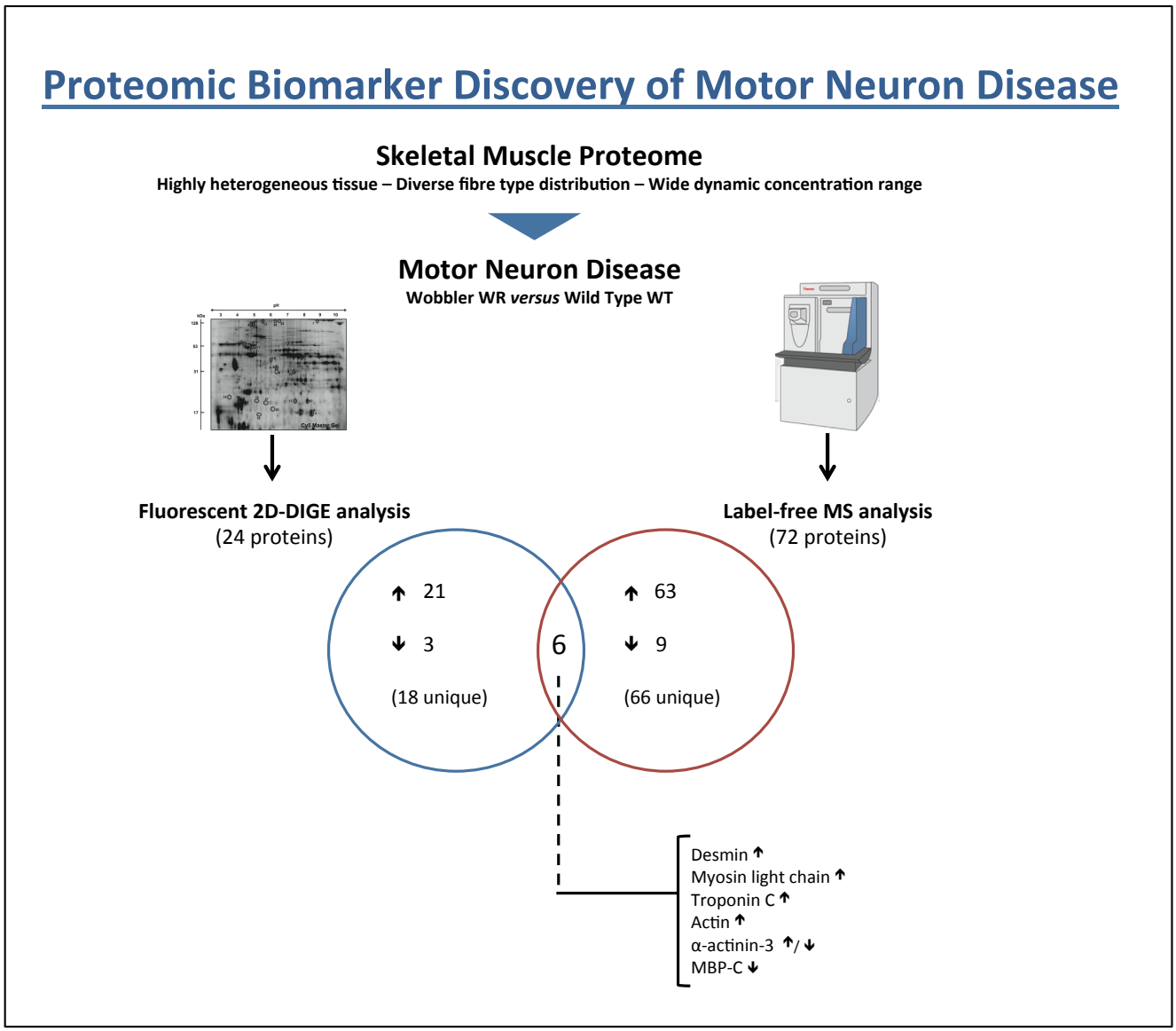

Figure 3.10 Proteomic identification of novel biomarker candidates of motor neuron disease.
Proteomic findings from 2D-DIGE and label-free LC-MS/MS analysis of hind limb muscle from the WR mouse model of ALS are contrasted.
*Image adapted from Holland and Ohlendieck, 2014C

3.3.10 Conclusion

Certain pathophysiological mechanisms involve the preferential loss of motor neurons and/or are associated with defective re-innervation patterns, as seen in muscle aging or motor neuron diseases. While primary motor neuronopathies like ALS clearly lead to muscular atrophy, the effect of progressive neurodegeneration on the contractile phenotype or bioenergetics processes is not as one sided as in the case of complete denervation. The preferential loss of certain types of motor neurons exerts a differential effect on fibre type specification and metabolic pathways.

In contrast to the characteristic slow-to-fast transitions associated with disuse-related muscular atrophy or denervation-associated fibre wasting, the label-free MS analysis presented here could show that motor neuron disease exhibits more complex protein alterations on the level of metabolic enzymes and contractile proteins. There certainly exists a distinct association between changed neuromuscular functions and complex proteome-wide alterations in skeletal muscle. The newly identified alterations in muscle proteins can now potentially be exploited as novel diagnostic, prognostic or therapeutic targets to improve the evaluation and treatment of motor neuron disease.

A potentially promising new muscle associated biomarker for motor neuron disease is the fast isoform of myosin binding protein MBP-C. This major auxiliary protein was has demonstrated decreased levels in fluorescent 2D-DIGE, label-free LC-MS/MS and in transcriptomic screening of ALS muscle biopsies (Staunton *et al.,* 2011; Shtilbans *et al.,* 2011). Making this protein isoform a good candidate to be exploited as a new marker for designing improved assay systems.

Chapter 4

DIGE Analysis of Testicular Tissue of the Wobbler Mouse Model of Globozoospermia

4.1 Introduction

The wobbler (genotype *wr/wr,* phenotype WR) mouse mutant (Duchen and Strich, 1968) represents an established animal model of progressive neurodegeneration (Moser *et al.* 2013). The WR mouse has a C57/bl6 background and the phenotype is paralleled by distinct deficiencies in spermatogenesis (Leestma and Sepsenwol, 1980; Heimann *et al.,* 1991). In the wobbler (WR) mouse a L967Q missense mutation in the vesicular protein-sorting factor VPS-54 causes motor neuron degeneration and globozoospermia. The *Vps54* gene encodes vesicular protein-sorting factor VPS-54, an essential factor of intracellular transport mechanisms in the heterotetrameric Golgi-associated retrograde protein (GARP) complex (Bonifacino and Hierro, 2011). This hydrophobic-to-hydrophilic exchange destabilizes the tertiary structure and causes a reduction in the concentration of VPS-54 (Pérez-Victoria *et al.,* 2010). At present no human neurodegenerative disease has been identified in which the gene that encodes the VPS-54 protein is affected (Meisler *et al.,* 2008). A homozygous knockout of the *Vps54* gene confers embryonic lethality (Schmitt-John *et al.,* 2005). The *wr* missense allele is relatively mild allowing homozygous animals to survive for several months, albeit with rapidly developing muscular atrophy (Moser *et al.,* 2013) and a defect in spermatogenesis (Leestma and Sepenwol, 1980; Heimann *et al.,* 1991; Paiardi *et al.,* 2011).

Abnormal density, motility or morphology of sperm cells plays a crucial role in male infertility. The WR mutant exhibits a defect in sperm assembly and is associated with a failure to form an acrosome and an elongated sperm head (Leestma and Sepenwol, 1980; Heimann *et al.,* 1991). This results in an abnormality similar to globozoospermia in humans (Dam *et al.,* 2007), whereby

sperm heads lacking an acrosome are unable to penetrate the *zona pellucida* and prevent proper interaction and fusion with the female oocyte. Human globozoospermia exhibit round-headed spermatozoa lacking an acrosome, which similarly cannot properly interact with oocytes. Even intra-cytoplasmic sperm injection often results in fertilization failure due to a deficient activation capacity in oocytes (Perrin *et al.,* 2013). In analogy, WR sperm cells show a round-headed irregular morphology reminiscent of globozoospermia (Leestma and Sepenwol, 1980; Heimann *et al.,* 1991; Paiardi *et al.,* 2011), making the testis of this WR mouse mutant an ideal model to systematically study pathobiochemical aspects of this type of impaired spermatogenesis. It was previously shown that WR spermatids exhibit increased amounts of the mouse ubiquitin-specific processing protease mUBPy and differential sorting of this deubiquitinating enzyme (Chianese *et al.,* 2010). In addition, the oocyte-activating factor phospholipase PLC-zeta has an abnormal localization in WR sperm cells with a reduced fertilizing capacity (Heytens *et al.,* 2010).

Molecular and cellular aspects of testis biology and the developmental process of spermatogenesis have been well documented and widely studied by cell biological and microscopical methods (Oatlet and Brinster, 2012). In contrast to cellular aspects of sperm development, the complexity of global changes in the protein constellation of the testis has not been well understood until the emergence of modern proteomics (Oliva *et al.,* 2010). MS-based proteomics has shown the diversity of the catalogued proteome of spermatozoa from a variety of different species (Johnston *et al.,* 2005; Martínez-Heredia *et al.,* 2006; Wang *et al.,* 2013; Baker *et al.,* 2008) and has been applied to the large-scale analysis of sperm head and flagella sub-compartments (Baker *et al.,* 2013), sperm surface

proteins (Brewis and Gadella, 2010), the epididymal maturation of mammalian spermatozoa (Dacheux *et al.,* 2012), sperm capacitation (Ficarro *et al.,* 2003; Secciani *et al.,* 2009; Baker *et al.,* 2010; Baker *et al.,* 2012), the effect of androgen manipulation during spermatogenesis (Stanton *et al.,* 2012), male gametes in relation to oxidative stress (Hamada *et al.,* 2013), sperm protein phosphorylation patterns (Ficarro *et al.,* 2003; Porambo *et al.,* 2012) and sperm–oocyte interactions (Sutovsky, 2009). Thus, testis and sperm cell proteomics has a biomedical potential to identify novel protein markers of genetic abnormalities or the effects of environmental insults and disease factors that may be involved in male infertility (Tomar *et al.,* 2010; Xu *et al.,* 2012; Parte *et al.,* 2012; Milardi *et al.,* 2013).

Here, we have employed gel electrophoresis based proteomics to investigate potential differences in protein expression levels between wild-type (WT) mouse testis and mutant WR testis. Fluorescence 2D difference in-gel electrophoresis, DIGE, analysis represents one of the most powerful comparative techniques in protein biochemistry and analytical biosciences as it enables the direct comparison of two different protein populations on the same high-resolution 2D gel system (Minden, 2012). Gel electrophoretic analyses and proteomic approaches have previously been applied to the screening of WR tissues, i.e. spinal cord (Laage *et al.,* 1988; Bastone *et al.,* 2009; Zhai *et al.,* 2009) and skeletal muscle (Staunton *et al.,* 2011), and used here for studying total extracts from normal versus affected testis tissue.

4.1.1 Experimental design

This chapter looked at the morphological features of spermatozoa from the VPS-54 deficient WR mouse compared to normal WT spermatozoa by SEM and TEM. Prior to comparative proteomics of WR versus WT testis preparations, the protein constellation of normal testis was evaluated by gel electrophoresis and major protein species identified by mass spectrometry, MS. Following this, pre-electrophoretic fluorescent tagging and subsequent comparative high-resolution 2DE was carried out to analyze the urea soluble protein content through the highly sensitive and reproducible technique of 2D-DIGE, using a 2-dye systematic approach with a pooled internal standard. Each protein sample under investigation had 50 µg protein fluorescently labeled prior to electrophoresis. WR (n = 4) and WT (n = 4) testis tissue extracts were labeled with Cy3 DIGE flour. The pooled samples were labeled with Cy5 DIGE flour. Gel electrophoretic separation was carried out with a total of 100 µg protein per analytical gel and were separated on a 24 cm strip over a linear pH range of 3-10. Key proteomic finding identified from MS were verified by immunoblotting. Bioinformatics analysis was also carried out to cluster proteins by molecular function and identify potential protein-protein interactions.

4.2 Results

4.2.1 Ultra-structural analysis of WR testicular tissue

Fluorescence and electron microscopy has revealed that the most prominent feature in WR spermatogenesis is the failure to form an intact acrosome by fusion of pro-acrosomal Golgi-derived vesicles, the association of an acrosome with the nucleus and the flattening into an eagle-beak-like structure (Heimann *et al.,* 1991), as confirmed by Paiardi *et al.,* (2011). The development and formation of WR spermatozoa within the testis has previously been described in detail (Heimann *et al.,* 1991). Mature spermatozoa from the epididymis are shown in Figure 4.1 and 4.2. Intact WT spermatozoa show the typical zoning into a head structure (with highly condensed nucleus and acrosome) and sperm tail with a mid piece (characterized by tightly packed mitochondria), a principal and an end piece (Figure 4.2 A). In contrast, the hallmark of WR spermatozoa is an irregularly rounded head containing a strongly deformed (often bizarre and fragmented) nucleus of usually heterogeneous density and lacking an acrosome (Figure 4.1 and 4.2 B, C). Often the zoning into head and mid piece is incomplete, and head and mid piece are combined either into one globular region (Figure 4.2 B) or the elongation and allocation process is faulty and all mitochondria remain in the head region, though a shortened mid piece is developed (Figure 4.2 C). Despite some spermatozoa displaying an intact morphology within the principal piece, most spermatozoa show aberrations in the 9 × 2 + 2 axoneme structure (Leestma and Sepsenwol, 1980), as well as in presence, number and size of the outer dense fibres (Figure 4.2 D). While the cell membrane is missing to a large extent, the

fibrous sheath of the principal piece, as the sole component, seems not to be altered in the WR mouse (Figure 4.2 D). In view of these detailed morphological findings, more information on the pathogenesis in WR testis could be expected from execution of complementary biochemical analyses of global protein changes.

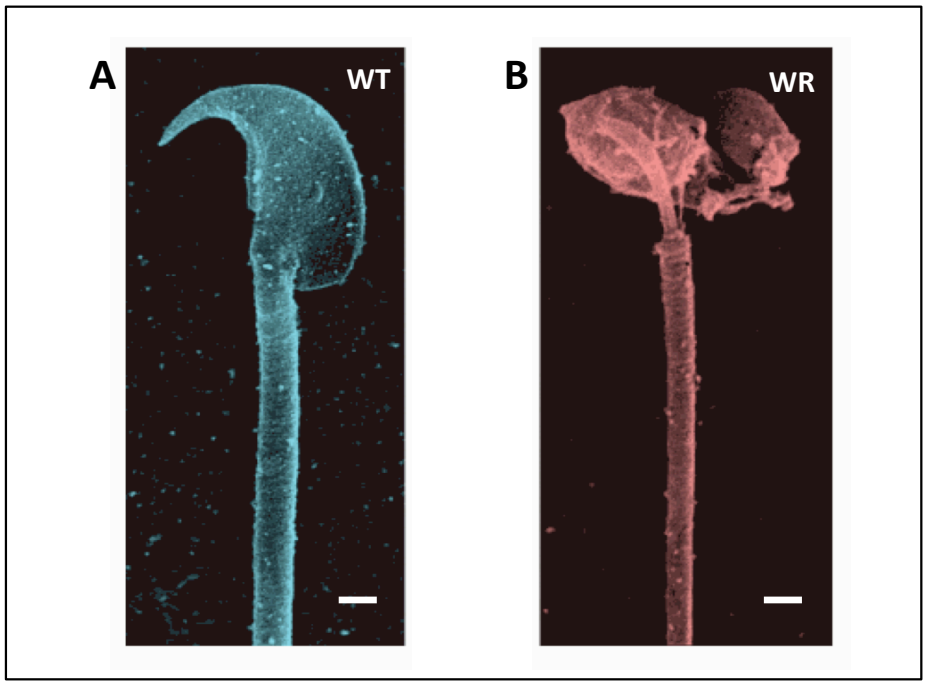

Figure 4.1 Impaired spermatozoa from the WR mouse.
Shown are scanning electron microscopical, SEM, images of mature isolated spermatozoa from normal wild-type WT (A) and diseased WR (B) mice. Panel B illustrates the abnormally round-headed spermatozoa from the WR mouse due the lack of a proper acrosome. Bars equal 1µm.
*Image kindly provided by collaborator Dr. Peter Heimann in the Department of Cell Biology, University of Bielefeld, Germany.

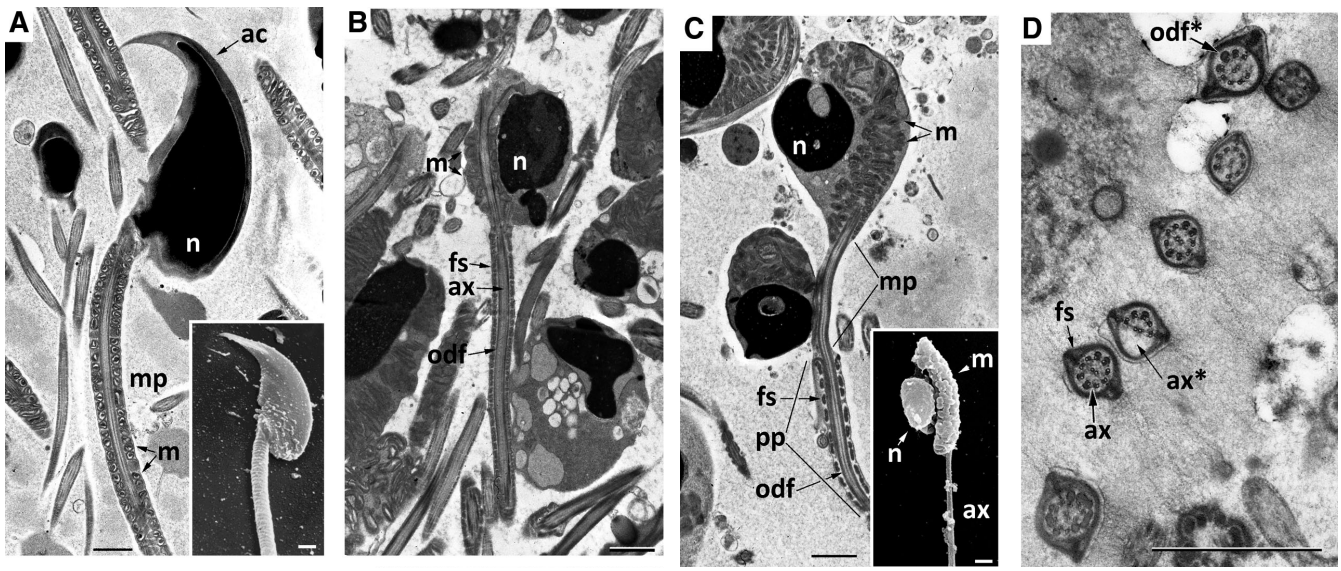

Figure 4.2 Defective spermatogenesis in the WR mouse: fine structure of spermatozoa.

Main panels contain transmission electron microscopy, TEM, of ultra-thin sections through epididymis of WT (A) and WR (B, C, D) preparations. Insets of panel A and C are scanning electron microscopy, SEM, images of isolated individual spermatozoa. Mature WT spermatozoon (A) shows typical zoning into head (with highly condensed nucleus and acrosome) and tail with mid piece (characterized by tightly packed mitochondria) and (not shown) principal and end piece (sagittal section). Inset in panel (A) are a spermatozoon head and mid piece region. WR spermatozoa (B, C) display an irregularly rounded shape of head with a strongly deformed and fragmented nucleus. There is no acrosome. Often the zoning into head and mid piece is incomplete and head and mid-piece are combined either into one globular region (B) or the elongation and allocation process is faulty and all mitochondria remain in the head region, though a shortened mid-piece lacking mitochondria (C). Inset in panel C are isolated spermatozoon with mid-piece region (with mitochondria) attached to the head (with nucleus). Although some WR spermatozoa (D) display an intact morphology within the principal piece, most WR spermatozoa show aberrations in the 9 × 2 + 2 axoneme structure (ax*), as well as in presence, numbers and size of the outer dense fibres (odf*). The fibrous sheath of the principal piece seems not to be altered. ac, acrosome; ax, axoneme; fs, fibrous sheath; m, mitochondria; mp, mid-piece; n, nucleus; odf, outer dense fibber; pp, principal piece. All scale bars are 1µm.

*Image kindly provided by collaborator Dr. Peter Heimann in the Department of Cell Biology, University of Bielefeld, Germany.

4.2.2 Proteomic profiling of normal mouse testis

The fluorescence 2D-DIGE technique is capable of detecting changes in a wide range of protein concentrations (Minden, 2012), making this comparative method an ideal analytical tool to study proteome-wide alterations in the WR mutant. Prior to the DIGE based proteomic profiling of WT versus WR testis preparations, the protein constellation of normal (WT) mouse testis was evaluated by gel electrophoresis and major protein species identified by MS. Since fluorescence DIGE-based investigations can swiftly assess potential concentration changes in thousands of protein spots, it was advantageous to establish a select number of reliable and unchanged 2D landmark protein spots for control purposes. Gel electrophoretic approaches using isoelectric focusing, IEF, in the first dimension and polyacrylamide slab gel electrophoresis in the second dimension very efficiently separate the urea-soluble sub-proteome from crude tissue extracts. A representative proteomic map is shown in Figure 4.3 to illustrate the general distribution pattern of testis-associated proteins, based on their unique combinations of isoelectric point, p*I,* and molecular mass.

Abundant constituents were picked from gels, digested with trypsin and subsequently identified by MS. The identified marker proteins covered a p*I* range from p*I* 4.74 to 7.96 (Figure 4.2, spot 1, endoplasmin; spot 9, haemoglobin) and ranged in molecular mass from apparent 15.1 to 92.7 kDa (Figure 4.2, spot 1, endoplasmin; spot 9, haemoglobin). Table 4.1 lists identified spot numbers (corresponding to Figure 4.3), testis marker proteins, their protein accession number, number of matched peptide sequences, MASCOT score, percentage sequence coverage, isoelectric point (p*I*) and molecular mass. Spots 1 to 9 represent major testis proteins with isoelectric point to molecular mass

combinations of approximately p*I* 4.74/92.7 kDa, p*I* 4.93/85.1 kDa, p*I* 5.07/72.5 kDa, p*I* 5.51/69.9 kDa, p*I* 4.82/50.9 kDa, p*I* 5.56/41.3 kDa, p*I* 4.09/16.7 kDa, p*I* 7.14/15.8 kDa and p*I* 7.96/15.1 kDa, respectively. The mass spectrometric analysis of their respective peptide populations revealed the presence of specific isoforms of endoplasmin, HSP-90, 78-kDa glucose-regulated protein, tubulin, actin, calmodulin, β-globin and α-globin, respectively, in these major unchanged 2D protein spots (Table 4.1). The presence of haemoglobin reflects the fact that the animals had not been perfused prior to sacrificing, and that the WR and WT tissues were equally well vascularized.

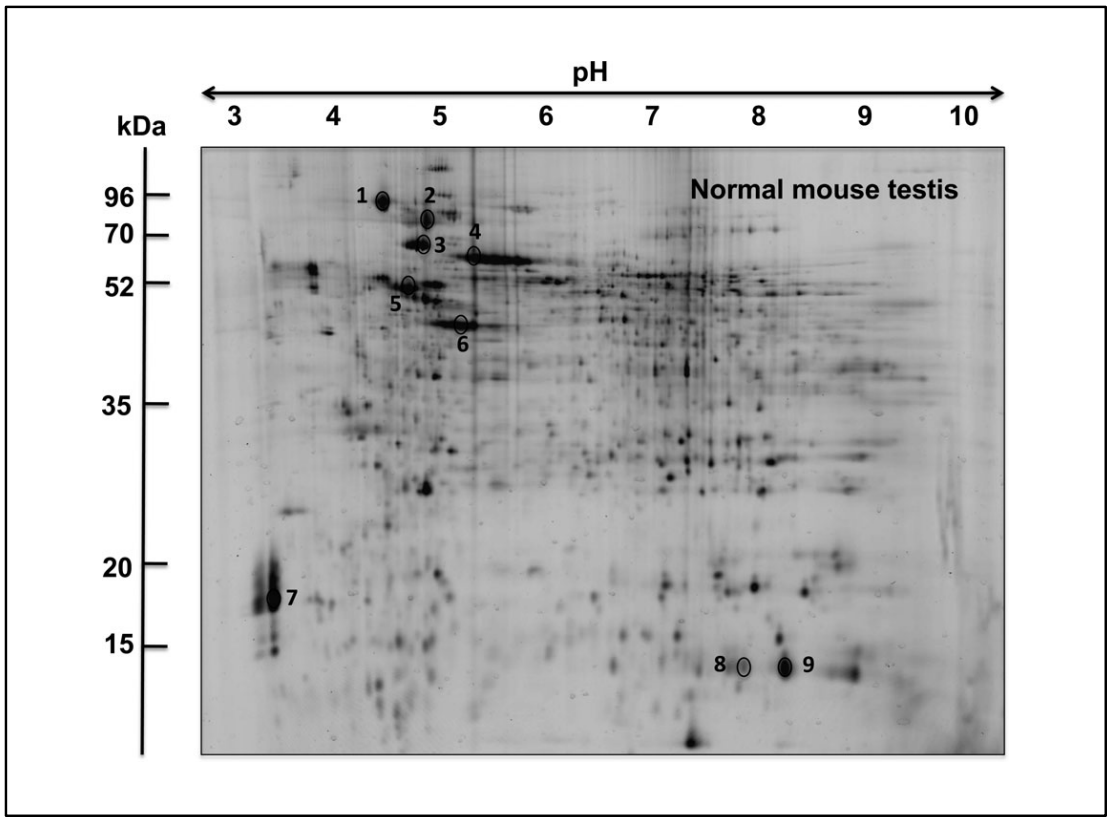

Figure 4.3 2D gel electrophoretic analysis of WT testis.
Shown is a 2D gel of total extracts from 9-week-old mouse testis. Major protein spots are marked by circles and are numbered 1 to 9. See Table 4.1 for the mass spectrometric identification of 2D landmark proteins that are not changed in the WR model of globozoospermia. The pH values of the first dimension gel system and molecular mass standards (in kDa) of the second dimension are indicated on the top and on the left of the panel, respectively.

Table 4.1 MS-identified 2D landmark proteins from WT mouse testis tissue

Spot number	Protein name	Accession number	Peptides	Score	Coverage (%)	p*I*	Molecular mass (kDa)
1	Endoplasmin GRP94	gi|6755863	37	986	44	4.74	92 708
2	Hsp 90-alpha	gi|6754254	27	377	35	4.93	85 141
3	78-kDa glucose-regulated protein	gi|254540166	29	778	48	5.07	72 493
4	Heat shock related 70-kDa protein 2	gi|31560686	23	390	42	5.51	69 889
5	Tubulin, beta-3 chain	gi|12963615	14	295	34	4.82	50 850
6	Actin, gamma	gi|809561	16	243	52	5.56	41 340
7	Calmodulin	gi|71664	10	219	52	4.09	16 696
8	Haemoglobin subunit beta	gi|156257625	7	467	56	7.14	15 769
9	Haemoglobin subunit alpha	gi|122441	7	163	50	7.96	15 134

* The table lists major landmark 2D protein spots from WT testicular tissue preparations. The haemoglobin spots 8 and 9 are due to the fact that testis preparations were not perfused prior to snap freezing in liquid nitrogen

** NCBI Database, release 20100212 *(Mus musculus*)

4.2.3 Comparative proteomic analysis of WR versus WT testis

Following the initial mass spectrometric identification of testis marker proteins from normal WT control mice, pre-electrophoretic fluorescent tagging and subsequent comparative high-resolution 2D-GE was carried out. Figure 4.4 gives an overview of the DIGE gels used in this study and illustrates the images generated with CyDye Cy3 labeling of mutant WR testis and WT testis, as well as CyDye Cy5 labeling of internal pooled standards. For image analysis and densitometric scanning, four biological repeats were used, which resulted in mutant samples Cy3 WR1 to WR4 and pooled controls Cy5 WR1 to WR4, as well as WT samples Cy3 WT1 to WT4 and pooled controls Cy5 WT1 to WT4. Densitometric scanning revealed significant changes in 43 testis-associated proteins. Figure 4.5 shows a DIGE master gel of testis extracts from the WR mouse. The 43 testis associated protein spots with a changed concentration in WR testis are indicated by circles and numbered 1-43 corresponding with Table 4.2.

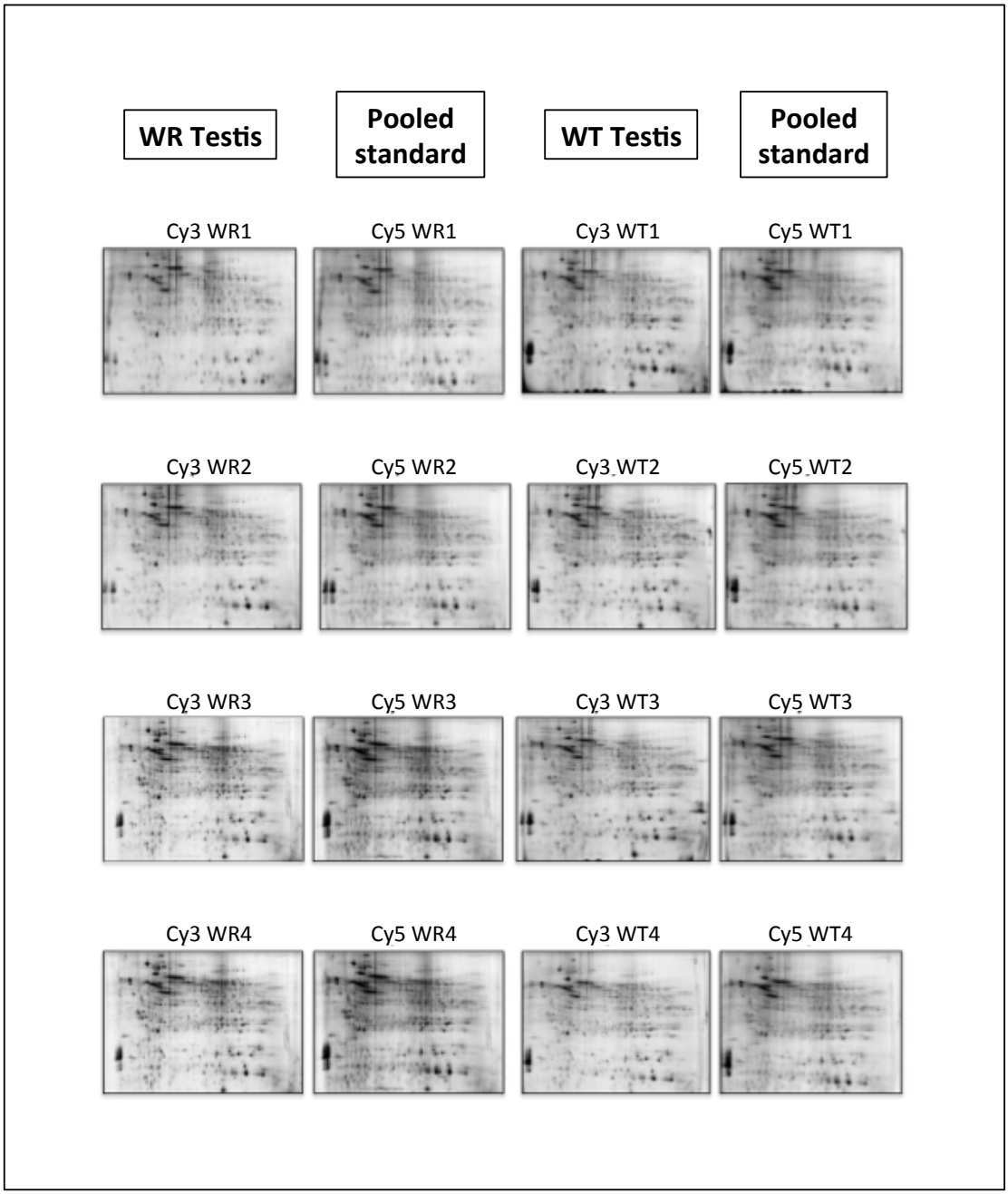

Figure 4.4 2D-DIGE analysis of WR versus normal WT testis tissue.
Shown are Cy3-labelled gels of total testis extracts from WR (WR1 to WR4) versus normal WT (WT1 to WT4) mice, as well as Cy5-labelled gels containing pooled internal standards. DIGE images shown were carried out over a pH 3–10 range.

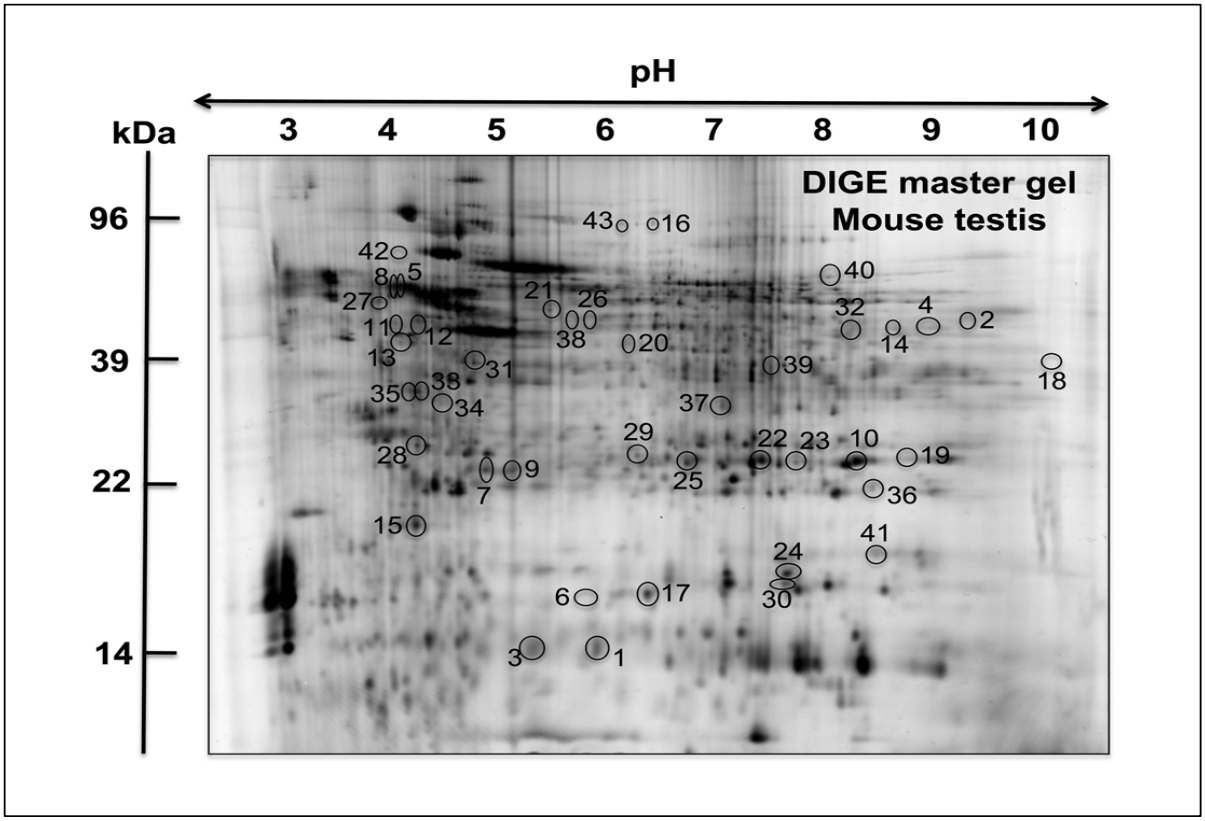

Figure 4.5 Fluorescence DIGE analysis of WR testis tissue.
Shown is a CyDye-labeled master gel of testis extracts from the WR mouse model of globozoospermia, covering the pH 3–10 range. Protein spots with a changed concentration in WR testis preparations are marked by circles and are numbered 1 to 43. See Table 4.2 for a detailed listing of protein species with a changed abundance in WR testis. The pH values of the first dimension gel system and molecular mass standards (in kDa) of the second dimension are indicated on the top and on the left of the panels, respectively.

4.2.4 Mass spectrometric identification of changed proteins in WR testis

A CyDye-labelled 2D master gel of WR testis covers a pH 3-10 range as shown in Figure 4.5. An altered concentration of significant proteins (with an ANOVA score of $p \leq 0.05$ and fold change $\geq \pm 1.1$) in WR testis included components in 2D spots that ranged in molecular mass from approximately 14.8 kDa (fatty acid binding protein FABP3, spot 1) to 85.1 kDa (HSP-90, spot 43) and covered a p*I* range from approximately 4.79 (tubulin, spot 5) to 10.36 (spermatid-specific protein, spot 6). The proteomic identification of the 43 altered protein spots is shown in Table 4.2 and lists spot number, protein name, international accession number, number of matched peptide sequences, MASCOT score, percentage sequence coverage, p*I* value, molecular mass, ANOVA score and fold change. The concentration of 35 proteins (spots 1–35) was reduced and 8 proteins (spots 36–43) were increased in WR testis relative to WT testis. Changes were relatively moderate, whereby a two-fold or higher alteration in abundance was evident for only four testis-associated proteins (spots 1-4).

The highest increase of 1.8-fold was shown for two HSP's of apparent 70 and 90 kDa (spots 42 and 43). The other proteins with an elevated concentration were identified as phospholipid hydroxide GSH peroxidase (spot 41), alpha-actin (spots 38, 40), aldolase reductase (spot 39), VDAC-2 (spot 37) and peroxiredoxin (spot 36). In contrast, the largest decrease of 2.4-fold was found for fatty acid binding protein FABP-3 (spot 1). A reduced concentration was also shown for acetyl-CoA acetyl- transferase (spots 2 and 4), beta-galactoside binding protein (spot 3), tubulin (spots 5, 8), spermatid-specific protein (spot 6), huntingtin-interacting protein-2 (spot 7), PKCq-interacting protein PICOT (spot 9), GST (spots 10, 19, 23, 25), vimentin (spots 11, 27), protein phosphatase (spot 12), the

40-kDa protein (spot 13), ATP-synthase (spot 14), urinary protein types 2 and 8 (spot 15), Alix protein (spot 16), Cu/Zn SOD (spot 17), heterogenous nuclear ribonucleo-protein A2/B1 (spot 18), DnaJ protein (spots 20 and 29), selenide water dikinase (spot 21), flavin reductase (spot 22), nucleoside diphosphate kinase (spot 24), ornithine amino-transferase (spot 26), ubiquitin C-terminal hydrolase (spot 28), cofilin (spot 30), SUMO-activating enzyme (spot 31), isocitrate dehydrogenase (spot 32), annexin (spots 33 and 35) and coatomer (spot 34). The identification of specific protein isoforms being present in more than one 2D spot is probably due to differences in PTM's, such as varying degrees of phosphorylation.

Table 4.2 2D-DIGE identified proteins with a changed abundance in WR versus WT testis tissue

Spot number	Protein name	Accession number	Peptides	Score	Coverage (%)	p*I*	Molecular mass (kDa)	ANOVA	Fold change
1	Fatty acid-binding protein FABP3, testis	gi|6753810	7	344	60	6.11	14810	0.0040	-2.4
2	Acetyl-Coenzyme A acyltransferase 2	gi|148677571	3	152	24	8.48	25618	0.0030	-2.2
3	Beta-galactoside binding protein	gi|193442	4	158	37	5.32	15144	0.0001	-2.1
4	Acetyl-CoA acetyltransferase	gi|21450129	7	292	22	8.71	45135	0.0040	-2.0
5	Tubulin, beta 2C	gi|1354268	12	258	35	4.79	50247	0.0008	-1.8
6	Spermatid-specific protein	gi|556310	5	94	33	10.36	15099	0.0110	-1.8
7	Huntingtin interacting protein-2	gi|2897818	8	221	47	5.33	22505	0.0010	-1.7
8	Tubulin alpha-3 chain	gi|6678465	6	324	18	4.97	50624	0.0020	-1.7
9	PKCq-interacting protein PICOT	gi|6840949	14	104	104	5.42	38048	0.0060	-1.7
10	GST Mu 2	gi|6680121	16	267	66	6.90	25874	0.0090	-1.7
11	Vimentin	gi|2078001	15	117	36	4.96	51591	0.0060	-1.6
12	Protein phosphatase 1 regulatory subunit 7	gi|12963569	6	136	26	4.85	41382	0.0110	-1.6
13	Protein 40kDa	gi|226005	10	156	41	4.80	32848	0.0140	-1.6
14	ATP synthase subunit alpha	gi|6680748	5	107	13	9.22	59832	0.0004	-1.5
15	Major urinary proteins 11 and 8	gi|127531	3	113	23	4.85	17723	0.0010	-1.5
16	Alix protein	gi|3550456	6	82	9	6.15	96530	0.0030	-1.5
17	Cu/Zn SOD	gi|226471	4	171	45	6.03	15926	0.0070	-1.5
18	Heterogenous nuclear ribonucleoprotein A2/B1	gi|3329498	15	321	46	8.67	36029	0.0090	-1.5
19	GST Mu 1	gi|6754084	13	163	47	7.71	26069	0.0100	-1.5
20	DnaJ homolog subfamily B member 11 precursor	gi|110625998	8	430	26	5.92	40820	0.0110	-1.4
21	Selenide, water dikinase 2	gi|15011843	4	119	21	5.75	48210	0.0120	-1.4
22	Flavin reductase (NADPH)	gi|21450325	3	71	18	6.49	22299	0.0120	-1.4
23	GST Mu 2	gi|6680121	2	81	32	6.90	25700	0.0004	-1.3
24	Nucleoside diphosphate kinase B	gi|6679078	7	287	50	6.97	17468	0.0010	-1.3
25	GST Mu 1	gi|6754084	7	409	37	7.71	26069	0.0080	-1.3
26	Ornithine aminotransferase, mitochondrial precursor	gi|8393866	4	234	22	6.19	48324	0.0090	-1.3
27	Vimentin	gi|2078001	8	66	19	4.96	51591	0.0100	-1.3
28	Ubiquitin C-terminal hydrolase L3	gi|7578956	6	113	32	5.08	26336	0.0130	-1.3
29	DnaJ protein homolog 3	gi|6831566	2	87	13	5.91	26662	0.0010	-1.2
30	Cofilin-1	gi|6680924	2	120	15	8.22	18780	0.0020	-1.2
31	SUMO-activating enzyme subunit 1	gi|9790247	12	162	41	5.24	39060	0.0090	-1.2
32	NADP-dependent isocitrate dehydrogenase	gi|3641400	10	157	28	6.48	47036	0.0130	-1.2
33	Annexin A5	gi|6753060	10	206	36	4.83	35788	0.0140	-1.2
34	Coatomer subunit epsilon	gi|10946972	4	127	19	4.94	34777	0.0150	-1.2
35	Annexin A5	gi|6753060	3	215	36	4.83	35730	0.0150	-1.1
36	Peroxiredoxin-1	gi|6754976	5	163	28	8.26	22394	0.0080	1.2
37	VDAC2	gi|6755965	6	263	24	7.44	32351	0.0120	1.3
38	Actin, alpha	gi|387090	4	86	18	5.23	41758	0.0030	1.3
39	Aldose reductase	gi|3046247	13	225	40	6.71	36043	0.0090	1.4
40	Actin, alpha	gi|387090	4	49	20	5.23	42048	0.0020	1.4
41	Phospholipid hydroperoxide glutathione peroxidase	gi|3114602	5	161	31	8.34	20032	0.0010	1.5
42	Heat shock-related 70 kDa protein 2	gi|31560686	13	140	26	5.51	69889	0.0140	1.8
43	Heat shock protein HSP 90-alpha	gi|6754254	2	72	3	4.93	85141	0.0060	1.8

* Wobbler versus normal testis tissue

** NCBI Database, release 20100212 *(Mus musculus*)

4.2.5 Confirmation of changed protein concentrations by immunoblotting

Immunoblotting was used to verify key findings from the proteomic screening of WR versus WT testis (Figures 4.7-4.9). A silver stained 1D gel, Figure 4.6, was used to visualize the 1D-banding pattern between the two samples under investigation, and showed comparable patterns in both WR and WT testis tissue preparations. Although the overall protein band pattern in silver-stained 1D gels was comparable between mutant and normal preparations, the decoration of blotted proteins with specific antibodies to testis-associated components revealed distinct changes in their concentration (Figures 4.8 and 4.9). The 337 kDa extracellular matrix protein laminin was used to confirm equal loading of apparent protein levels between WR and WT testis sample preparations, shown in Figure 4.7. The reduced concentration of the FABP-3 isoform of the protein family of fatty acid binding proteins (Figure 4.8 A, B), the mitochondrial enzyme ATP-synthase (Figure 4.8 C, D) and SOD-2 (Figure 4.8 E, F) in WR testis was confirmed by immunoblotting. Potential changes in VDAC and annexin were not found to be significant (not shown). In contrast, the elevated concentration of the molecular chaperones HSP-70 and HSP-90 in WR testis was demonstrated by immunoblot analysis (Figure 4.9 A-B and C-D, respectively). Reductions in WR testis tissue of VPS-54 were illustrated in Figure 4.9 E, F.

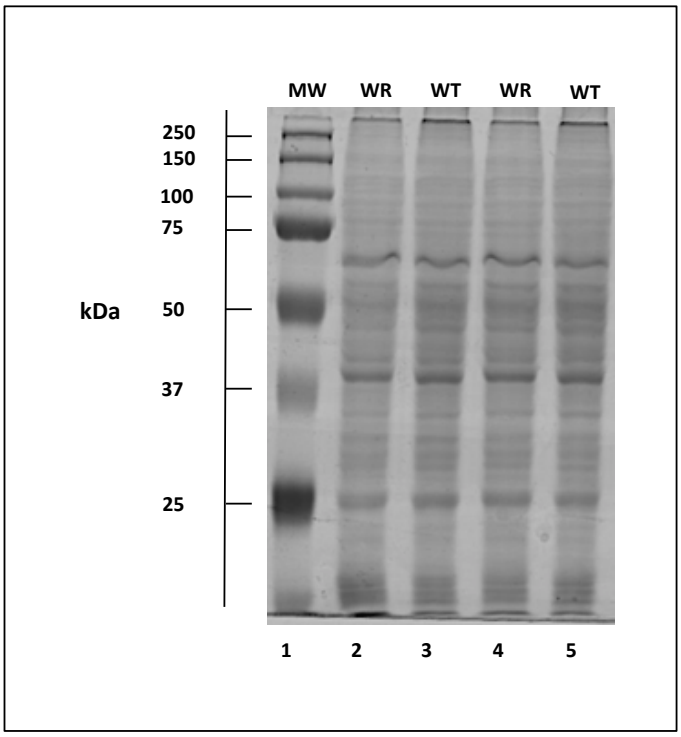

Figure 4.6 Electrophoretic analysis of WR and WT testis tissue preparations used for LC-MS/MS analysis.
Shown is a silver-stained 1D gel of preparations from WR (lanes 2 and 4) and WT (lanes 3 and 5) testis. Lane 1 shows molecular weight (MW) standards with their values in kDa represented on the left hand side.

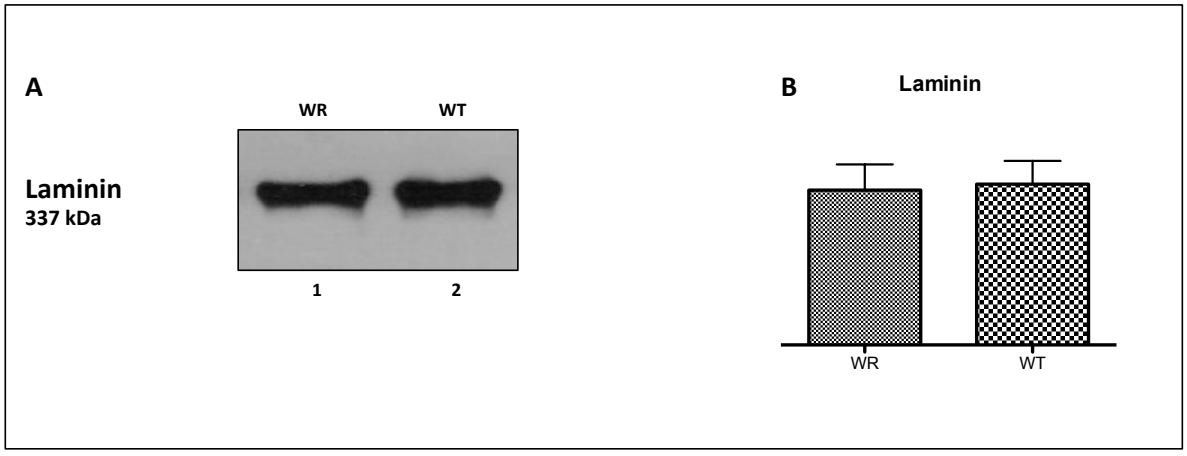

Figure 4.7 Equal loading immunoblot for WR and WT testis tissue.
Shown is a representative immunoblot with an expanded view of immuno-decorated bands labeled with an antibody to laminin (A). The extracellular matrix protein laminin did not show significant changes in concentration between WR and WT testis tissue extracts (B) (unpaired Student's *t*-test; $n \geq 4$; NS).

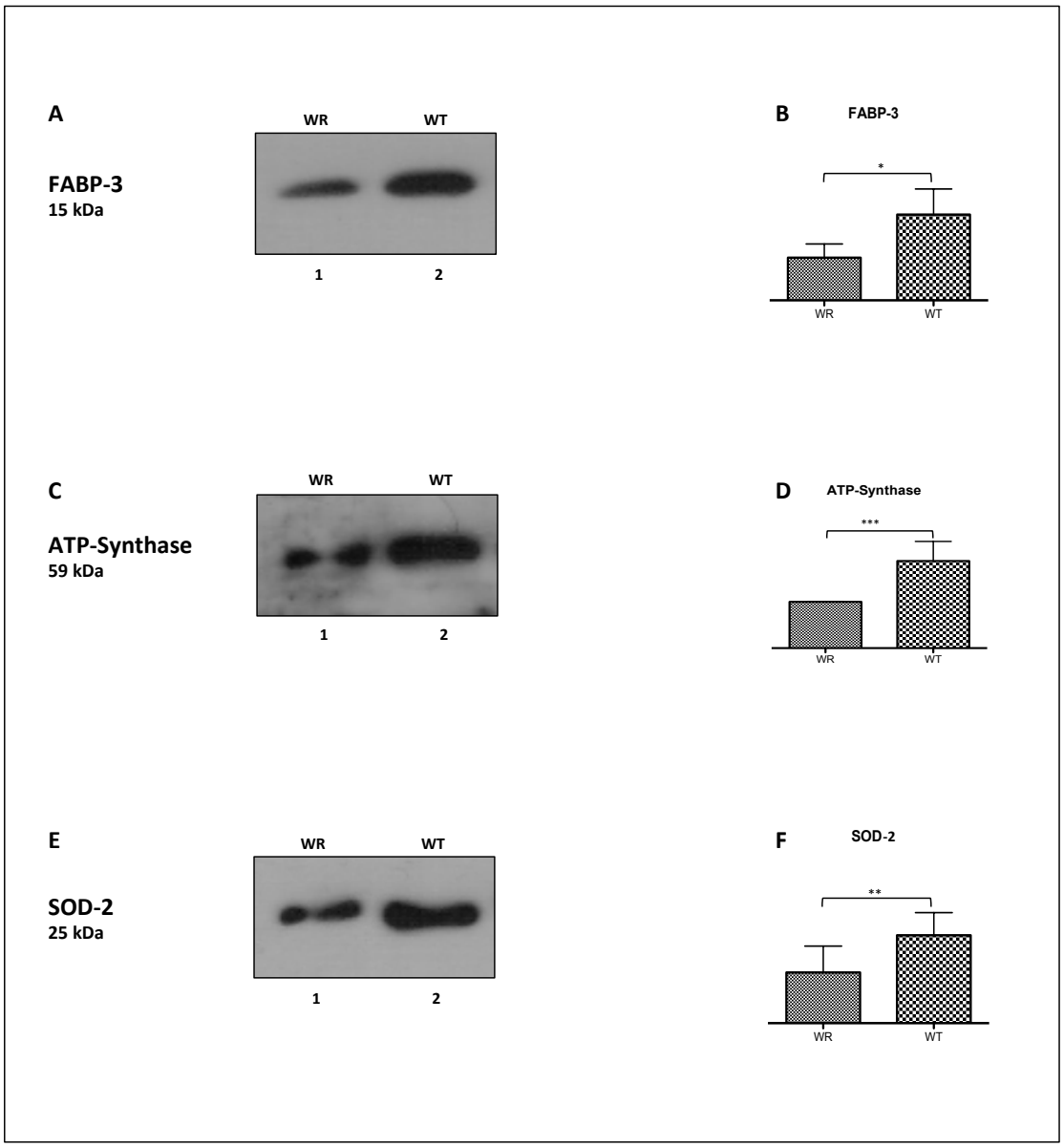

Figure 4.8 Immunoblot and quantitative analysis of select WR versus WT testis proteins.

Representative immunoblots with an expanded view of immuno-decorated bands are shown in panels A, C and E, and are labeled with antibodies to the FABP-3 testis isoform of fatty acid binding protein, ATP synthase and SOD-2 respectively. Lanes 1 and 2 represent mutant WR testis versus normal WT preparations, respectively. The graphical presentation of the statistical analysis of corresponding immunoblotting of FABP-3 (B), ATP synthase (D) and SOD (F) are shown above. (Student's *t*-test, unpaired; $n \geq 4$; *$p < 0.05$; **$p < 0.01$; ***$p < 0.001$).

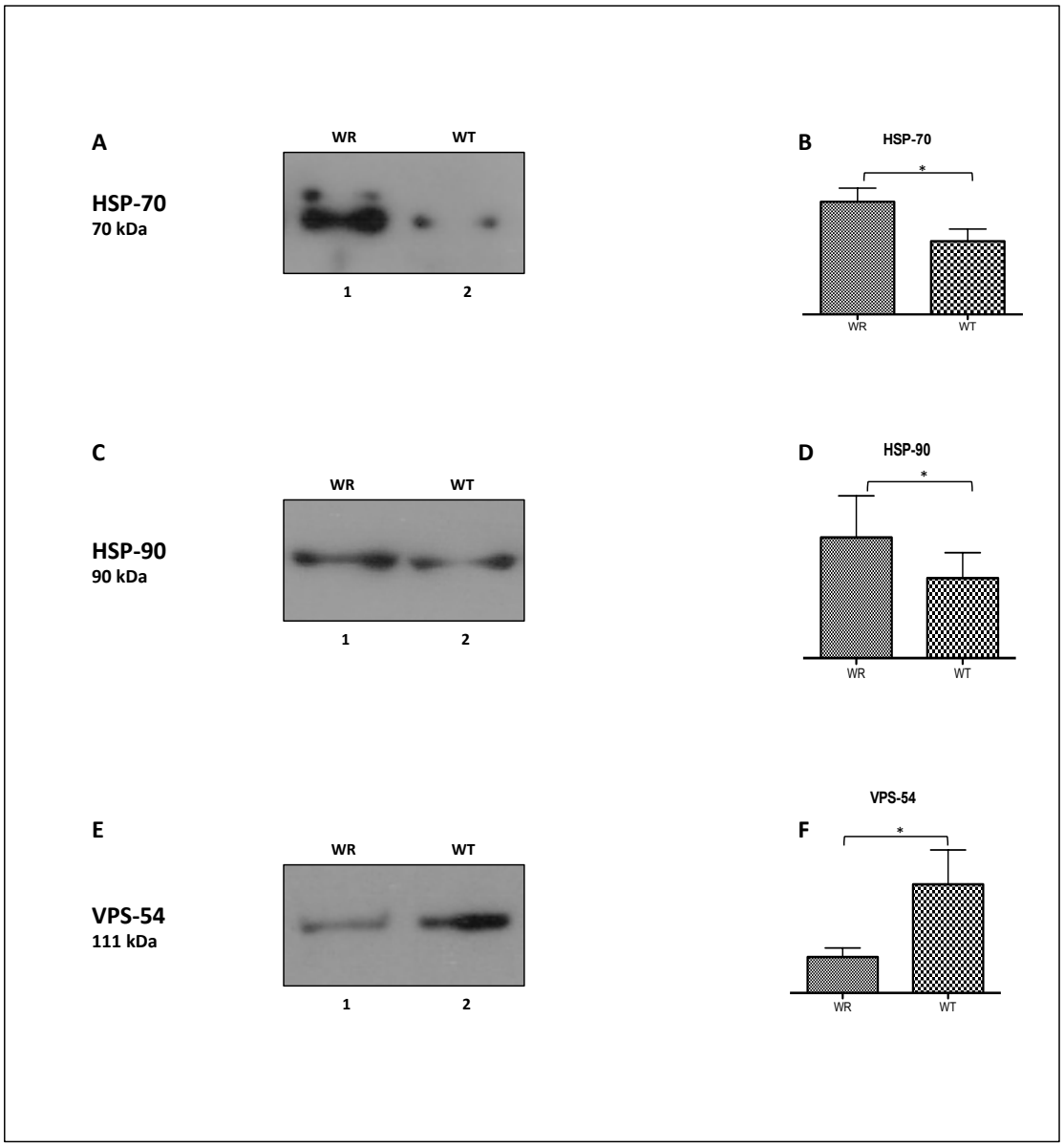

Figure 4.9 Immunoblot and quantitative analysis of select WR versus WT testis proteins.

Representative immunoblots with an expanded view of immuno-decorated bands are shown in panels A, C and E, and are labeled with antibodies to molecular chaperones HSP-70 and HSP-90 and the vesicular transport protein VPS-54 respectively. Lanes 1 and 2 represent mutant WR testis versus normal WT preparations, respectively. The graphical presentation of the statistical analysis of corresponding immunoblotting of HSP-70 (B) and HSP-90 (D) and VPS-54 (F) are shown above. (Student's *t*-test, unpaired; $n \geq 4$; $^*p < 0.05$).

4.2.6 Summary of protein classes with a changed concentration in WR testis and protein interaction analysis

An overview of changes in distinct classes of proteins, as revealed by MS-based proteomics, is given in the graphical presentation of Figure 4.10. Proteins associated with the cytoskeleton (green), metabolism (red), stress response (blue) and other enzymatic activities (black) of testis tissue are represented. The graph summarizes the relative concentrations WR/WT of identified testicular proteins. Increased proteins and decreased proteins are shown in the upper and lower part of the graph, respectively. Two-dimensional landmark protein spots with an unchanged concentration are listed on the 0/1.0 horizontal line. Solid circles mark protein species that have been identified by MS analysis and a rhombus marks proteins of which concentration changes have been additionally verified by immunoblotting. The presentation of specific protein isoforms by multiple 2D spots is probably due to differences in PTMs, such as varying degrees of phosphorylation. Abbreviations for Figure 4.10 for are as follows; ACA, acetyl-CoA acyltransferase; ACT, actin; ALDR, aldose reductase; ALX, Alix protein; ANX, annexin; AS, ATP synthase; CAM, calmodulin; COAT, coatomer; COF, cofilin; DnaJ, DnaJ homolog protein; FABP3, fatty acid binding protein isoform 3; FR, flavin reductase; GBP, galactoside-binding protein; GRP, endoplasmin GRP94; HGB, haemoglobin; HIP, huntingtin-interacting protein; HSP-70, heat shock related 70-kDa protein 2; HSP-78, 78-kDa glucose-regulated protein; HSP-90, HSP-90-alpha; ICDH, isocitrate dehydrogenase; MUP, major urinary proteins; SOD, superoxide dismutase; NDK, nucleoside diphosphate kinase; NRP, nuclear ribonucleoprotein; OAT, ornithine aminotransferase; P40, protein 40 kDa; PHGP, phospholipid hydroperoxide glutathione peroxidase;

PICOT, PKCq-interacting protein; PRXS, peroxiredoxin; PP, protein phosphatase; SAE1, SUMO-activating enzyme subunit 1; SDK, selenide, water dikinase; SSP, spermatid-specific protein; TUB, tubulin; UH, ubiquitin hydrolase; VDAC2, voltage-dependent anion-selective channel protein 2; VIM, vimentin.

Application of the PANTHER database of protein families (Mi *et al.,* 2013) resulted in the cataloguing of molecular functions of the identified WR proteins with a changed abundance as follows: transporter activity (4.5%), antioxidant activity (4.5%), binding activity (18.2%), catalytic activity (45.5%), enzyme regulator activity (4.5%), ion channel activity (9.1%), receptor activity (4.5%) and structural molecule activity (9.1%), outlined in Figure 4.11.

Following the identification of proteins with a changed abundance in WR testis, the existence of potential protein interactions was evaluated with the help of the IntAct molecular interaction database (Kerrien *et al.,* 2012) and the STRING database of direct physical and indirect functional protein interactions (Franceschini *et al.,* 2013). According to the comparison of the proteins listed in Table 4.2 and published protein interactions stored in the IntAct database, the only major interaction pattern was predicted to exist between huntingtin-interacting protein-2 (UBE2K) and nucleoside diphosphate kinase B (NME2). Application of the STRING database of direct physical and indirect functional protein interactions (Franceschini *et al.,* 2013) resulted in a more complex interaction map, shown in Figure 4.12. Strong interactions were predicted to exist between the mitochondrial proteins VDAC-2, ATP-synthase and acetyl-CoA acyltransferase. Additional interactions through the ATP-synthase hub were shown to occur with ornithine aminotransferase, heterogeneous nuclear ribonucleoprotein and coatomer protein. The bioinformatics analysis also

demonstrated a clear association between the molecular chaperones HSP-70 and HSP-90, as well as the DnaJ protein, confirming their related roles in the cellular stress response. Potential connections were highlighted between SOD, GST and peroxiredoxin and their role in antioxidant defense, biotransformation and redox regulation of testis tissue. Weak interactions are predicted to exist between the intermediate filament component vimentin and annexin.

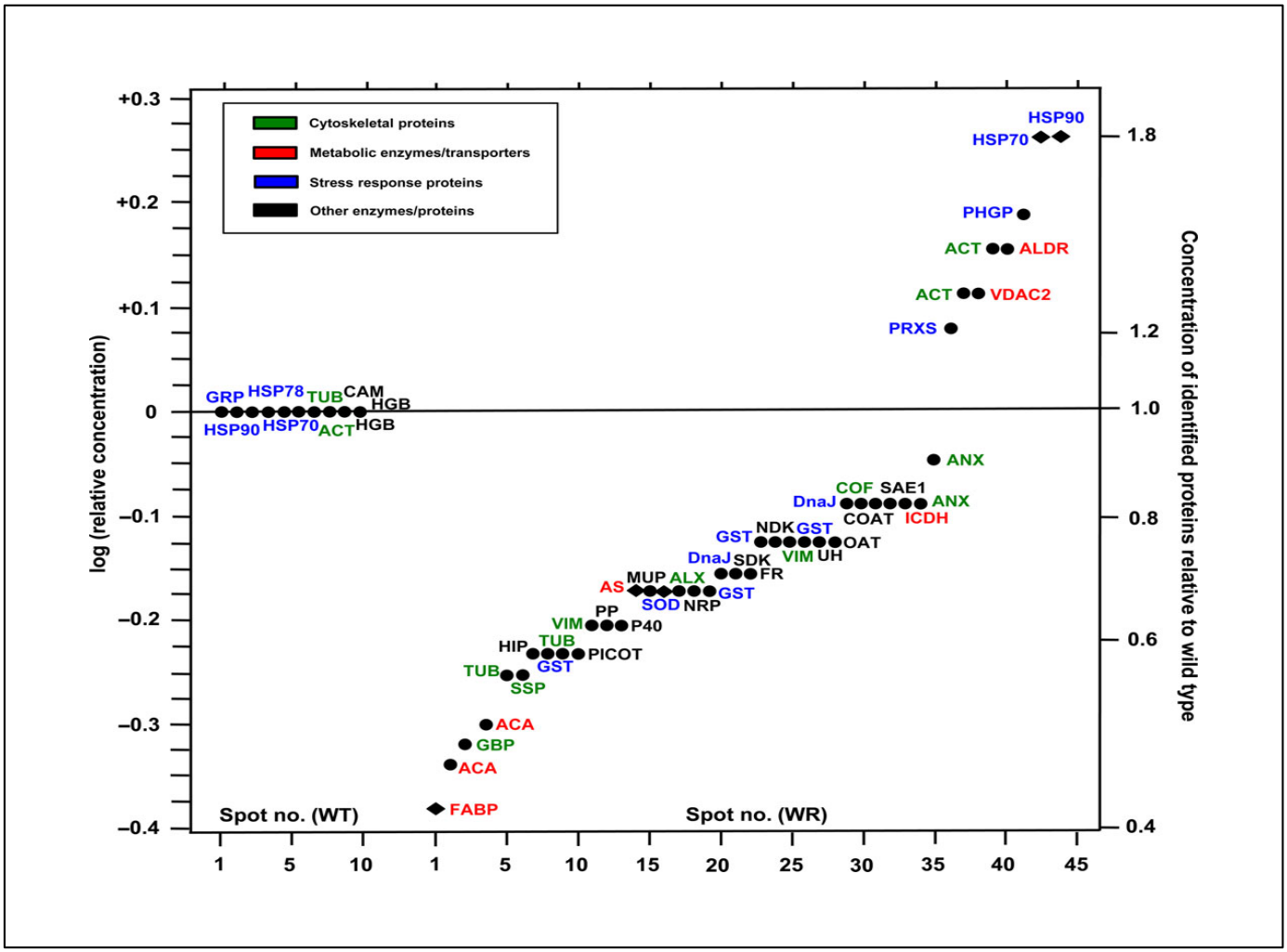

Figure 4.10 Overview of alterations in WR testicular tissue versus WT control.
The graph shows the relative concentrations WR/WT of testicular proteins as revealed by MS-based proteomics. Increased versus decreased proteins are shown in the upper and lower part of the graph, respectively, and unchanged proteins are listed on the 0/1.0 horizontal line. Proteins belonging to the cytoskeleton, metabolism, stress response and other enzymatic activities are marked by green, red, blue and black symbols, respectively. Protein species that have been identified by MS analysis, Table 4.2, are marked by a solid circle and proteins of which concentration changes have been additionally verified by immunoblotting, Figures 4.7 and 4.8, are marked by a rhombus. See section 4.2.6 for abbreviations.

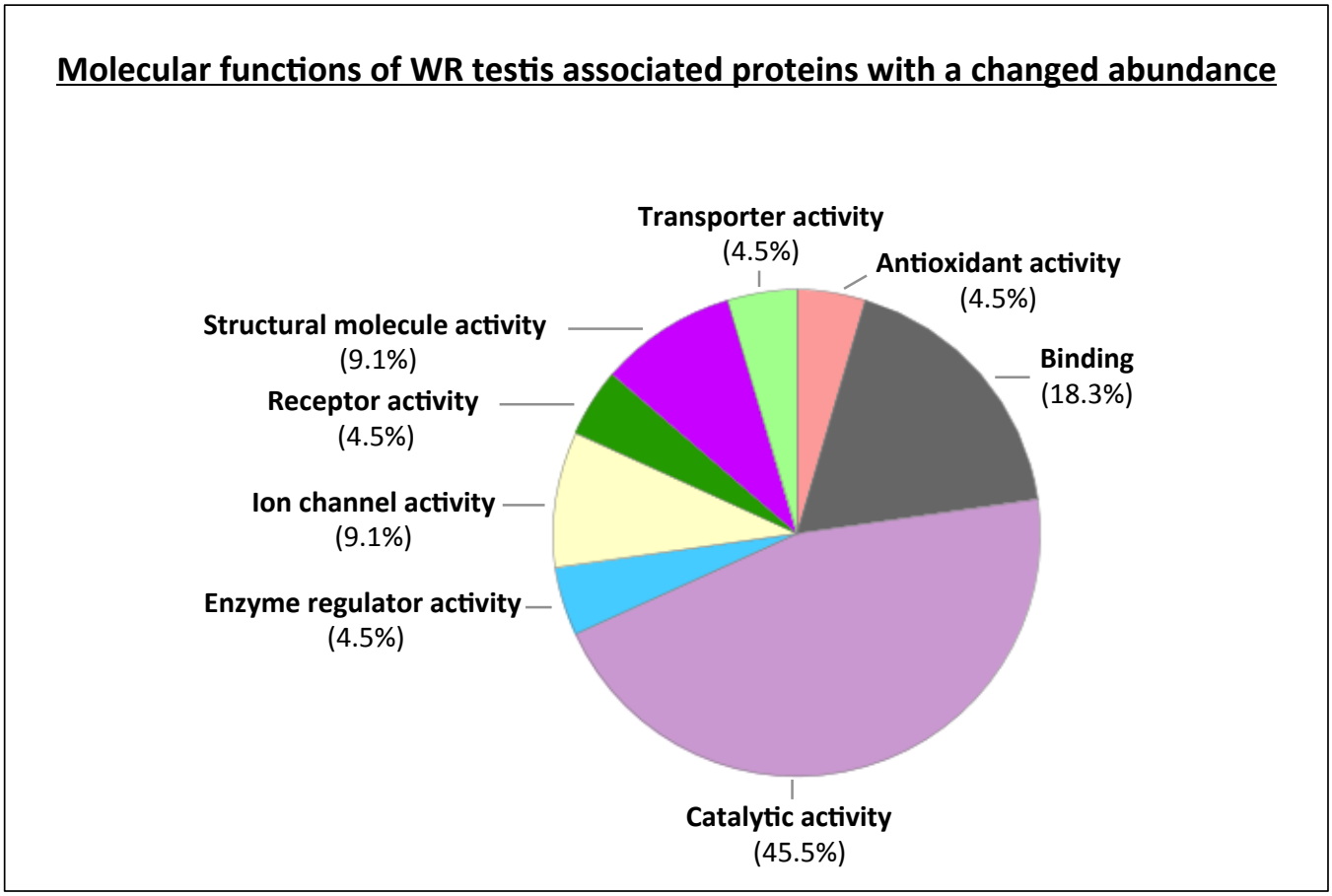

Figure 4.11 Molecular functions of WR testis associated proteins with a changed abundance.

The publically available bioinformatics software PANTHER was used to identify the clustering of molecular functions of MS-identified testis tissue proteins with an altered abundance in the WR mouse (Table 4.2). The analysis was performed with the PANTHER database (version 8.1) (Mi *et al.,* 2013).

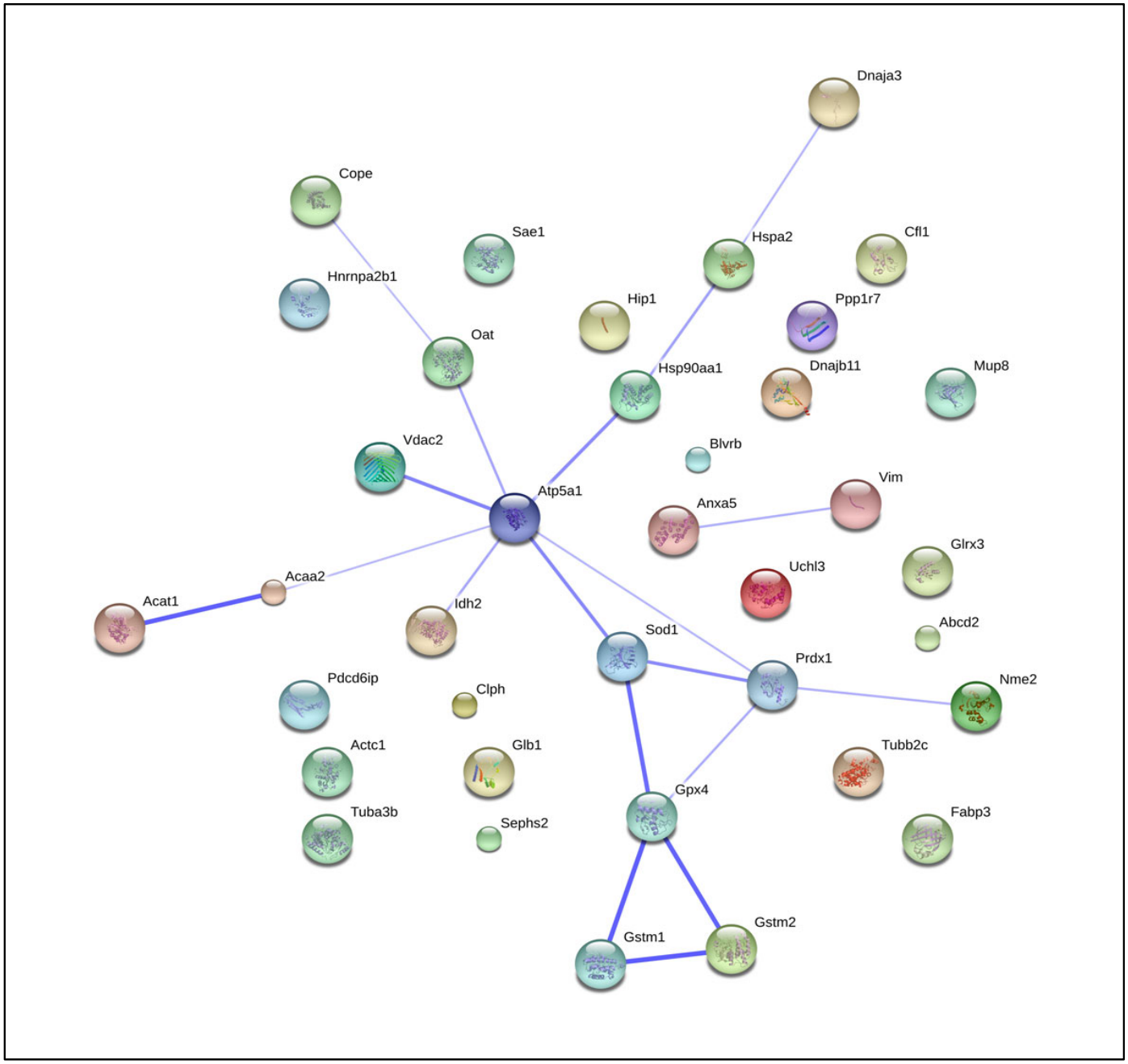

Figure 4.12 Protein interaction map of WR testis proteins.
Shown is a protein interaction map generated with the STRING database (version 9.1) of known and predicted protein associations that include direct physical and indirect functional protein linkages. The analysis was carried out with proteins that exhibited a changed abundance in WR testis (Table 4.2). The prediction of protein interactions is based on published data with respect to neighbourhood, gene fusion, co-occurrence, co-expression, experiments, databases, text-mining and homology data (Franceschini *et al.,* 2013).

4.3 Discussion

Functional VPS-54 is indispensable for the prenatal development of the mouse, as shown by knockout experiments (Schmitt-John *et al.,* 2005). Thus, the *wr* missense mutation appears to be a relatively mild allele creating both the neurological and the testis phenotype of the WR mouse. This has previously been shown by transgenic rescue (Schmitt-John *et al.,* 2005). Using X-ray and biochemical analysis, Pérez-Victoria *et al.,* (2010) elucidated the effect of the VPS-54 L967Q hydrophobic-to-hydrophilic amino acid replacement, which destabilizes the conformation of VPS-54 and renders it temperature-sensitive. This in turn leads to a partial proteolytic degradation of the miss-folded VPS-54 polypeptide at body temperature of the mouse. Thus, VPS-54 might have been expected among the proteins with a lowered concentration in WR tissue. However, VPS-54 was not identified in any spots on the analytical 2D gels (Figure 4.5 and Table 4.2) used in this study, however reduced levels were recognized by immunoblot analysis seen in Figure 4.9 E-F. 2D gel electrophoretic approaches may underestimate certain categories of sperm proteins due to technical limitations. Proteins that are most likely to experience technical drawbacks include proteins with highly hydrophobic domains, such as integral membrane proteins, along with high molecular mass proteins and low-abundance proteins. Irrespective of these technical issues this method of high-resolution gel based separation covers a large cohort of the urea-soluble proteome (Holland and Ohlendieck, 2014C). The thermal denaturation and proteolytic degradation may be less pronounced in the testis due to a lower temperature than in the trunk. This might explain why the testis phenotype of WR mice is suppressed in certain mouse strains whereas the neurological

phenotype is not (T. Schmitt-John and A. Mussmann, unpublished observation). Indeed, Paiardi *et al.,* (2011) were able to stain WR testis with an unspecified antibody directed against VPS-54, showing an intensity comparable to labeling of the WT, whereas Pérez-Victoria *et al.,* (2010) found a strongly reduced signal in central nervous system and liver extracts from WR mice, as compared to WT using immunoblotting. In the light of these findings, together with the results of a detailed electron microscopic analysis shown here in Figure 4.1 and 4.2, one would expect rather moderate changes in the protein pattern of WR testis.

4.3.1 Comparative 2D-DIGE analysis

The main findings from the proteomic profiling of WR testis (Table 4.2) revealed altered concentrations of proteins associated with metabolite transport, fatty acid metabolism, cellular interactions, microtubule assembly and the cellular stress response, Figure 4.10. In addition, minor changes were observed for proteins involved in various cellular activities, including cell redox homeostasis, biotransformation, cytoskeleton formation, PTM's, detoxification, and metabolism.

4.3.2 Stress response in WR testis tissue

The proteomic analysis of WR testis revealed an increase in two critical HSP's, i.e. HSP-70-2 (Figure 4.5, spot 42) and HSP-90α (Figure 4.5, spot 43) (Neuer *et al.,* 1999). The main functions of the HSP-70 and HSP-90 class of molecular chaperones involve the facilitation of protein folding, the maintenance of proteome integrity and the regulation of protein homeostasis (Kim *et al.,* 2013). The bioinformatics analysis using the STRING database (Franceschini *et al.,* 2013) seen in Figure 4.12 suggests close interactions between the two stress proteins and essential cooperation during chaperone-mediated protein folding processes in order to maintain cellular proteostasis. HSP-70 and HSP-90 were individually validated by immunoblotting, as seen in Figure 4.9 A-B and C-D respectively, and show significant increases. Both HSP's are believed to play major roles during spermatogenesis (Zakeri and Wolgemuth, 1987; Gruppi *et al.,* 1991; Dix, 1997). HSP-70-2 was shown to represent a protein factor that is crucial for the successful completion of meiosis in mouse spermatocytes (Eddy, 1999). Disruption of the HSP-70-2 gene results in male infertility due to failed meiosis and germ cell apoptosis (Dix *et al.,* 1996A and B). Thus, the testis-specific HSP HSP-70-2 appears to have an essential chaperone function during the meiotic phase of spermatogenesis (Eddy, 1999). A proteomic and immuno-histochemical survey of developmental changes in HSP's from porcine testis has demonstrated a differential effect on molecular chaperones, whereby the HSP-90α isoform was shown to increase after sexual maturation (Huang *et al.,* 2005). Hence, the increased abundance of HSP-70-2 and HSP-90α in WR testis suggests that these essential molecular chaperones are up regulated to counteract detrimental protein aggregation in VPS-54 deficient tissues.

4.3.3 Proteins significantly decreased in WR testis tissue

The most significant decrease in a specific protein was shown to be the approximately two-fold reduction of the fatty acid binding protein isoform FABP-3. Both, methods of densitometric scanning of fluorescent 2D gels (Figure 4.5, spot 1) and immunoblotting (Figure 4.8 A-B) agreed that this metabolite transporter is severely affected in WR testis tissue. Fatty acid binding proteins belong to the superfamily of lipid-binding proteins and are widely distributed throughout the body (Chmurzyńska, 2006). Their primary function is the regulation of fatty acid uptake and intracellular transportation of this essential energy-rich biomolecule. Various types of fatty acid binding proteins have been shown to play a role during spermatogenesis (Kido and Namiki, 2000; Kido *et al.,* 2005; Liu *et al.,* 2008). The major isoform FABP-3 exists in heart, muscle, kidney and testis (Smathers and Petersen, 2011). The reduction of FABP-3 in WR testes suggests that the reduction of VPS-54 results in downstream effects on key metabolic pathways and causes abnormal fatty acid utilization. Since the enzyme acetyl-CoA acetyltransferase (Figure 4.5, spot 4) was also shown to be reduced, the fatty acid oxidation pathway appears to be impaired in WR testes. Interestingly, the bioinformatics analysis seen in Figure 4.12 using the STRING database (Franceschini *et al.,* 2013) suggests ATP-synthase as a major hub and close associations with other metabolic enzymes and mitochondrial proteins. ATP-synthase was identified as spot 14 (Figure 4.5) and independently validated by immunoblotting, illustrating it's reduced levels in WR testis tissue, seen in Figure 4.8 C-D. This agrees with the idea that bioenergetic abnormalities affecting oxidative metabolism might be involved in impaired spermatogenesis.

4.3.4 Microtubule and intermediate filament assembly

Microtubules and intermediate filaments play an important role during spermatogenesis (Amlani and Volg, 1988). The proteomic screening of WR testis preparations carried out in this study revealed reduced levels of α-tubulin (Figure 4.5, spot 8), β-tubulin (Figure 4.5, spot 5), β-galactosied binding protein (Figure 4.5, spot 3) and vimentin (Figure 4.5, spot 11). These changes could potentially be due to variations in cytoskeletal protein levels. This could potentially reflect an abnormal cytoskeletal organization in WR testis or these altered cell composition of the WR testis as compared to WT.

4.3.5 Other proteins

The DIGE and MS analysis presented here identified concentration changes in other potentially interesting novel marker candidates that were relatively minor and their pathobiochemical relevance therefore difficult to judge. Proteins included the spermatid-specific histone H2b protein (Figure 4.5, spot 6) (Moss *et al.,* 1989), an ubiquitin-conjugating enzyme named huntingtin-interacting protein-2 (Figure 4.5, spot 7) (Wilson *et al.,* 2009), the sperm-specific HSP DnaJ (Figure 4.5, spot 29) (Boillée *et al.,* 2002; Meccariello *et al.,* 2002), and a variety of enzymes involved in metabolism, detoxification and biotransformation. The proteomic analysis of the WR testis presented here supports the general idea that global changes in protein concentrations are moderate despite the dramatic morphological abnormalities in spermatogenesis.

4.3.6 Conclusion

In conjunction with the results from the analysis of inter-strain crosses, the novel proteomic findings presented here indicate the testis phenotype of the VPS-54 L967Q missense mutation is less penetrant than the neurological phenotype. However, it has been shown impaired spermatogenesis in the WR mouse is associated with a generally perturbed protein expression pattern. Several interesting new marker proteins with an altered concentration were identified, including the FABP-3 isoform of fatty acid binding protein, the molecular chaperones HSP-70-2 and HSP-90α, and various proteins associated with cell–cell interactions, microtubule assembly, cellular homeostasis, bio-transformation, cytoskeleton formation, detoxification and bioenergetics. In the long-term, the newly identified proteins from the testis proteome may be useful candidates for advancing the molecular analysis of globozoospermia. In conclusion, the missense mutation in VPS-54, not only prevents the formation of an acrosome but also initiates a cascade of metabolic abnormalities and a stress reaction.

Chapter 5

Proteomic Profiling of Cardiomyopathic Tissue from the Aged *mdx* Model of Duchenne Muscular Dystrophy

5.1 Introduction

Duchenne muscular dystrophy, DMD, is the most frequent neuromuscular disorder in humans and is characterised by the primary deficiency in the membrane cytoskeletal protein dystrophin (Dalkilic and Kunkel, 2003). Absence of the Dp427 isoform of dystrophin triggers a significant reduction in a number of sarcolemmal glycoproteins and causes a variety of downstream abnormalities in cell signaling, excitation-contraction coupling and ion homeostasis, as well as enhanced proteolytic destruction of muscle-associated proteins (Lewis *et al.,* 2009). Disintegration of sarcolemmal integrity renders dystrophin-deficient fibres more susceptible to necrosis and eventually causes severe muscle wasting (Morrison, 2011). Importantly, cardiac dysfunction is a common clinical manifestation in neuromuscular disorders (Hermans *et al.,* 2010), particularly in hereditary muscular dystrophies (Verhaert *et al.,* 2011). During the second decade of life, the majority of patients afflicted with X-linked muscular dystrophy show serious cardiac abnormalities (Judge *et al.,* 2011), including cardiomyopathy, regional wall abnormalities and cardiac dysrhythmia (Romfh and McNally, 2010).

Since the age of onset of cardiomyopathy in dystrophic children varies considerably and because skeletal muscle weakness and heart disease do not correlate, cellular factors other than dystrophin deficiency are believed to contribute to cardiomyopathy (Kaspar *et al.,* 2009). Overt cardiomyopathy drastically increases with age. More than 80% of teenage boys with muscular dystrophy show abnormal systolic function, resulting in fatal cardiac complications in a large number of cases (Cox and Kunkel, 1997). Pathological hallmarks of cellular changes in muscular dystrophy-associated cardiomyopathy

include interstitial inflammation, fatty tissue replacement, fibrosis and surface membrane degradation of cardiac tissue (Finsterer and Stöllberger, 2003). Since dystrophin-deficient cardiac fibres have only a limited regenerative capacity, the gradual replacement of cardiac fibres by non-contractile tissue results in progressive functional decline of the dystrophic heart (Judge *et al.,* 2011).

Previous proteomic investigations of dystrophin-deficient muscle tissues have focused on mildly affected extraocular muscle, moderately necrotic limb muscles and severely dystrophic diaphragm muscle from the *mdx* mouse (Lewis *et al.,* 2009; Gardan-Salmon *et al.,* 2011; Rayavarapu *et al.,* 2013), an established animal model of Duchenne muscular dystrophy (Sicinski *et al.,* 1989). With respect to cardiac muscle, proteomic profiling of the immunoprecipitated dystrophin complex has established potential new binding partners of cardiac Dp427 (Johnson *et al.,* 2012) and metabolomic and proteomic studies have established the diverse effects of dystrophin deficiency on 9-month-old dystrophic heart tissue (Gulston *et al.,* 2008; Lewis *et al.,* 2010). Importantly, the natural aging process itself is a major risk factor for cardiovascular disease. Intrinsic cardiac aging is associated with ventricular hypertrophy, increased fibrosis, atrial fibrillation and decreased maximal contractile capacity (Shioi and Inuzuka, 2012).

This makes the determination of protein changes in the senescent mouse model of severe muscular dystrophy-associated cardiomyopathy a crucial undertaking for the characterization of this naturally occurring genetic animal model. Proteomic studies of the aging rodent heart have established changes in the concentration of metabolic enzymes, as well as components of cell signaling, the immune response, oxidative stress and structural support (Richardson *et al.,*

2008; Dai *et al.,* 2008; Grant *et al.,* 2009). In analogy to these investigations of normal heart tissues during aging, this proteomic study has determined changes from 7-week-old to 20-month-old *mdx* hearts that lack dystrophin.

5.1.1 Experimental design

As the majority of patients afflicted with DMD develop cardiomyopathic complications, large-scale proteomic studies of global cardiac changes for the identification of new protein markers of dystrophinopathy are crucial.

Cardiac tissue from young 7-week old *mdx* mice (n = 4) and old 20-month old *mdx* (n = 4), in addition to age-matched normal WT mice, were prepared for this proteomic study. In order to establish age-related alterations in the proteome of dystrophin-deficient hearts, cardiomyopathic tissue from young versus aged *mdx* mice were examined by label-free LC-MS/MS in the Proteomics Facility of the National Institute for Cellular Biotechnology, Dublin City University. To determine the initial differences between unaffected and dystrophin deficient cardiac tissue, label-free mass spectrometry was first carried out on 7-week old *mdx* versus normal aged-matched WT samples. The samples analysed by label-free mass spectrometry were relatively quantified by label-free Progenesis software, identified with MASCOT and searched against the UniProtKB-SwissProt database. This revealed moderate changes in cardiac-associated proteins, agreeing with the mild cariomyopathic phenotype in young *mdx* mice. To determine the age-related changes cardiomyopathy has on the *mdx* heart proteome 7-week old versus 20-month old *mdx* dystrophin deficient hearts were analyzed by label-free LC-MS/MS in a similar way as before. Following this

an immunoblotting survey of young and old wild-type, WT, versus age matched *mdx* hearts was employed to verify key proteomic hits and to differentiate between the effects of natural aging versus aging of dystrophin deficient *mdx* cardiac tissue. The bioinformatics STRING software was applied to identify the potential protein interactions of the MS-identified muscle proteins with a changed abundance in the *mdx* mouse. This software can visualise known and predicted proteins interactions of direct physical and indirect functional protein associations.

5.2 Results

Proteomic profiling of 7-week-old versus 20-month-old *mdx* hearts was carried out to determine the extent of age-related protein changes in muscular dystrophy-associated cardiomyopathy. Following the determination of protein alterations by a label-free LC-MS/MS approach, key proteomic findings were verified by immunblotting of young and aged wild-type (WT) versus age-matched *mdx* hearts to differentiate between the effects of the natural aging process versus the severe reduction of dystrophin in the *mdx* heart.

5.2.1 Proteomic profiling of 7-week-old heart tissue from normal WT versus *mdx* mice

Label-free LC-MS/MS analysis of 7-week-old normal cardiac samples versus age-matched *mdx* samples was used to establish primary proteomic differences between unaffected and dystrophin-deficient heart tissue. The comparative proteomic profiling study revealed moderate changes, in 20 heart-associated proteins (Table 5.1), agreeing with the mild cardiomyopathic phenotype in young dystrophic *mdx* mice. An increased abundance was shown for actin, biglycan, protein disulphide isomerase isoforms, calreticulin, the mitochondrial enzymes succinyl-CoA:3-ketoacid-coenzyme A transferase, 2-oxoglutarate dehydrogenase and isocitrate dehydrogenase, as well as the glycolytic enzyme phosphofructokinase. In contrast, slightly decreased levels were found for troponin TnT, aortic actin, selenium-binding protein and glyceraldehyde-3-phosphate dehydrogenase, as well as the mitochondrial enzymes succinyl-CoA ligase, methylmalonate-semialdehyde dehydrogenase, 3-

hydroxyacyl-CoA dehydrogenase, 2,4-dienoyl-CoA reductase, 3-ketoacyl-CoA thiolase and glutamate dehydrogenase.

Table 5.1 List of changed proteins in 7-week-old *mdx* heart tissue versus age-matched normal WT controls as determined by label-free LC-MS/MS analysis

Accession number	Protein name	Peptides	Score	ANOVA	Fold change
P68134	Actin, alpha, muscle	3	141.67	3.00E-02	2.30
P28653	Biglycan	2	104.16	2.00E-02	1.77
P09103	Protein disulfide-isomerase	3	127.77	1.00E-02	1.51
P27773	Protein disulfide-isomerase A3	3	145.22	2.00E-02	1.47
Q9D0K2	Succinyl-CoA:3-ketoacid-coenzyme A transferase 1, mitochondrial	2	143.54	2.00E-02	1.43
Q8BFZ3	Beta-actin-like protein 2	2	93.12	5.00E-02	1.41
Q60597	2-oxoglutarate dehydrogenase, mitochondrial	2	97.42	2.00E-02	1.38
P14211	Calreticulin	2	90.70	3.71E-03	1.29
P54071	Isocitrate dehydrogenase [NADP], mitochondrial	3	215.87	3.00E-02	1.28
P47857	6-phosphofructokinase, muscle type	2	138.74	3.00E-02	1.25
P26443	Glutamate dehydrogenase 1, mitochondrial	2	102.33	2.00E-02	-1.23
Q8BWT1	3-ketoacyl-CoA thiolase, mitochondrial	3	220.83	2.00E-02	-1.24
P16858	Glyceraldehyde-3-phosphate dehydrogenase	3	245.05	1.00E-02	-1.25
P17563	Selenium-binding protein 1	3	144.51	2.00E-02	-1.36
Q9CQ62	2,4-dienoyl-CoA reductase, mitochondrial	2	147.96	8.71E-03	-1.38
O08756	3-hydroxyacyl-CoA dehydrogenase type-2	2	154.83	3.00E-02	-1.41
Q9EQ20	Methylmalonate-semialdehyde dehydrogenase [acylating], mitochondrial	4	198.45	2.62E-03	-1.43
Q9Z2I9	Succinyl-CoA ligase [ADP-forming] subunit beta, mitochondrial	3	152.40	7.12E-03	-1.49
P62737	Actin, aortic smooth muscle	2	95.23	1.12E-03	-1.62
P50752	Troponin T, cardiac muscle	2	101.51	1.00E-02	-1.68

* 7-week old *mdx* versus normal cardiac tissue
** UniProtKB SwissProt database (downloaded April 2012) with 16,521 proteins (*Mus musculus*)

5.2.2 Label-free LC-MS/MS analysis of the aged dystrophin-deficient *mdx* heart

As aging drastically accelerates the dystrophy-related cardiomyopathic phenotype of the *mdx* model of Duchenne muscular dystrophy, label-free LC-MS/MS analysis of 7-week- old versus 20-month-old *mdx* hearts was performed to determine global changes in dystrophin-deficient cardiac tissue. Significant changes were found in 67 proteins, with 39 proteins shown to be increased in abundance and a decreased expression was determined for 28 proteins (Table 5.2). Besides moderate changes in 50 heart-associated proteins, positive or negative alterations above a 2.5-fold change were shown in 17 proteins. Proteins with a drastically increased density were identified as various Ig chains, mitochondrial β-hydroxybutyrate dehydrogenase, ferritin light and heavy chain, catalase and transferrin. Considerable reductions were shown for lamin, laminin, myosin light chain, nidogen, vimentin and long chain fatty acid ligase. A variety of cardiac proteins were marginally affected in a differential manner and MS analysis identified them as proteins involved in muscle contraction, mitochondrial metabolism, glycolysis, ion handling, cytoskeletal organisation and the cellular stress response.

Dystrophin and other components of the DGC were not shown to have a statically significant reduction in either of the MS hit lists (Table 5.1 and 5.2). This is consistent with other global proteomic-screening experiments (Lewis *et al.,* 2010; Rayavarapu *et al.,* 2013). These proteins can be difficult to identify during global proteomic screening due to the individual molecular weights, the proteins are part of a complex that can be more difficult to digest. Cellular fractionation methods including ultra centrifugation are a way to overcome this.

Table 5.2 List of changed proteins in aging *mdx* heart tissue as determined by label-free LC-MS/MS analysis

Accession number	Protein name	Peptides	Score	ANOVA	Fold change
P01864	Ig gamma-2A chain C region	4	238.19	1.43E-03	19.59
Q80XN0	D-beta-hydroxybutyrate dehydrogenase, mitochondrial	3	201.56	7.48E-04	10.63
P01867	Ig gamma-2B chain C region	3	130.75	1.59E-03	9.32
P01872	Ig mu chain C region	2	129.15	5.20E-03	8.83
P01837	Ig kappa chain C region	3	192.25	2.37E-03	4.98
P29391	Ferritin light chain 1	4	248.68	9.40E-04	4.54
P24270	Catalase	2	112.04	3.00E-02	2.90
P09528	Ferritin heavy chain	4	281.25	1.81E-03	2.82
Q921I1	Transferrin	2	103.14	3.00E-02	2.56
P15626	GSH (Glutathione S-transferase) Mu 2	6	340.24	9.70E-04	2.14
Q9DBJ1	Phosphoglycerate mutase 1	3	154.49	2.00E-02	1.91
Q9DCM2	GSH (Glutathione S-transferase) kappa 1	2	128.36	5.24E-03	1.86
P54071	Isocitrate dehydrogenase [NADP], mitochondrial	23	2050.16	5.98E-04	1.85
Q6P8J7	Creatine kinase S-type, mitochondrial	2	137.95	4.00E-02	1.79
P17742	Peptidyl-prolyl cis-trans isomerase A	3	186.40	1.57E-03	1.76
P68134	Actin, alpha, muscle	4	273.36	3.98E-03	1.75
Q9JHI5	Isovaleryl-CoA dehydrogenase, mitochondrial	8	572.22	8.73E-04	1.68
P47738	Aldehyde dehydrogenase, mitochondrial	4	213.46	1.91E-03	1.67
P51174	Long-chain specific acyl-CoA dehydrogenase, mitochondrial	8	513.47	2.89E-03	1.66
O70250	Phosphoglycerate mutase 2	5	269.27	2.00E-02	1.66
P10649	GSH (Glutathione S-transferase) Mu 1	7	472.38	1.00E-02	1.65
P16125	L-lactate dehydrogenase B chain	2	199.75	7.91E-04	1.58
P26041	Moesin	3	134.23	1.00E-02	1.58
P19157	GSH (Glutathione S-transferase) P 1	2	171.48	3.00E-02	1.56
P04247	Myoglobin	8	971.05	4.14E-03	1.54
P05064	Fructose-bisphosphate aldolase A	2	89.51	4.00E-02	1.54
P62737	Actin, aortic smooth muscle	2	207.26	5.91E-03	1.53
P62962	Profilin-1	3	190.16	1.11E-03	1.46
P60710	Actin, cytoplasmic 1	4	256.28	8.91E-03	1.45
O70468	Myosin-binding protein C, cardiac-type	3	190.42	1.00E-02	1.45
P56565	Protein S100-A1	2	174.38	3.90E-05	1.45
Q9D0K2	Succinyl-CoA:3-ketoacid-coenzyme A transferase 1, mitochondrial	3	333.51	7.79E-03	1.44
Q60597	2-oxoglutarate dehydrogenase, mitochondrial	3	156.25	6.77E-03	1.41
P45376	Aldose reductase	3	177.39	2.00E-02	1.38
Q99KI0	Aconitate hydratase, mitochondrial	17	1228.30	5.62E-05	1.36
P05201	Aspartate aminotransferase, cytoplasmic	7	504.11	2.22E-03	1.35
P06745	Glucose-6-phosphate isomerase	4	346.71	4.29E-05	1.35
P17751	Triosephosphate isomerase	2	116.97	2.00E-02	1.29
Q8QZT1	Acetyl-CoA acetyltransferase, mitochondrial	3	164.07	6.03E-03	1.27
P52503	NADH dehydrogenase [ubiquinone] iron-sulfur protein 6, mitochondrial	2	137.35	1.00E-02	-1.23
P62631	Elongation factor 1-alpha 2	4	296.15	4.00E-02	-1.26
Q9D3D9	ATP synthase subunit delta, mitochondrial	2	185.13	3.00E-02	-1.37
Q9CQA3	Succinate dehydrogenase [ubiquinone] iron-sulfur subunit, mitochondrial	3	201.11	5.00E-02	-1.40
P56480	ATP synthase subunit beta, mitochondrial	10	854.08	4.00E-02	-1.42
P10126	Elongation factor 1-alpha 1	4	232.69	3.00E-02	-1.47
P63038	60 kDa heat shock protein, mitochondrial	4	280.95	2.00E-02	-1.55
P57776	Elongation factor 1-delta	2	111.73	3.00E-02	-1.60

Table 5.2 Continued

Accession number	Protein name	Peptides	Score	ANOVA	Fold change
P68372	Tubulin beta-4B chain	2	102.84	5.00E-02	-1.72
Q9D855	Cytochrome b-c1 complex subunit 7	5	280.00	1.07E-03	-1.76
P12787	Cytochrome c oxidase subunit 5A, mitochondrial	5	319.85	1.00E-02	-1.81
Q9CXZ1	NADH dehydrogenase [ubiquinone] iron-sulfur protein 4, mitochondrial	4	229.86	3.00E-02	-1.86
Q9DB15	39S ribosomal protein L12, mitochondrial	2	113.08	2.00E-02	-1.88
P51667	Myosin regulatory light chain 2, ventricular/cardiac muscle isoform	4	267.78	3.00E-02	-1.96
P14824	Annexin A6	2	112.82	4.00E-02	-1.96
P97450	ATP synthase-coupling factor 6, mitochondrial	5	403.38	3.00E-02	-2.05
P61979	Heterogeneous nuclear ribonucleoprotein K	2	96.70	5.93E-03	-2.05
Q9Z2I9	Succinyl-CoA ligase [ADP-forming] subunit beta, mitochondrial	3	172.20	3.00E-02	-2.07
P70670	Nascent polypeptide-associated complex subunit alpha, muscle-specific form	3	171.72	3.00E-02	-2.08
Q99020	Heterogeneous nuclear ribonucleoprotein A/B	2	102.84	2.43E-03	-2.11
P48678	Prelamin-A/C	3	177.88	4.00E-02	-2.67
P41216	Long-chain-fatty-acid--CoA ligase 1	2	120.37	2.85E-03	-2.77
P20152	Vimentin	3	146.10	5.00E-02	-3.04
P10493	Nidogen-1	2	100.17	6.04E-03	-3.36
Q3THE2	Myosin regulatory light chain 12B	2	105.15	6.44E-03	-4.03
P02468	Laminin subunit gamma-1	5	277.53	8.68E-04	-4.22
P02469	Laminin subunit beta-1	3	171.32	5.45E-04	-4.71
P14733	Lamin-B1	2	100.13	1.00E-02	-12.91

* 7-week old versus 20-month old *mdx* cardiac tissue
** UniProtKB SwissProt database (downloaded April 2012) with 16,521 proteins (*Mus musculus*)

5.2.3 Immunoblot analysis of aged normal WT versus aged *mdx* cardiac tissue

As the label-free LC-MS/MS analysis shown in Table 5.2 focuses on age-related effects in the *mdx* heart, immunoblotting was used to verify key proteomic findings and also to compare the expression levels of identified proteins in normal versus dystrophic *mdx* preparations. Figures 5.3-5.5 show the immunoblot survey of 7-week-old normal hearts, 20-month-old normal hearts, 7-week-old *mdx* hearts, and 20-month-old *mdx* hearts. Silver staining of crude tissue extracts from the four different heart preparations under investigation did not show extensive differences in their overall 1D banding pattern following SDS-PAGE analysis, but slight variations in the intensity of individual bands (Figure 5.1). Ponceau was used to stain membranes prior to immunoblotting and confirmed equal loading of the cardiac samples under investigation, as seen in Figure 5.2. A variety of antibodies were evaluated and representative immunoblots with reliable staining patterns are shown in Figures 5.3-5.5. The increase in transferrin was confirmed by immunoblotting, although differences were not found to be statistically significant (Figure 5.3 A, B). The drastic decrease in the expression levels of laminin (Figure 5.3 C, D), nidogen (Figure 5.3 E, F) and annexin (Figure 5.3 G, H) during senescence of the *mdx* heart were found to be statistically significant. Labeling with specific antibodies to these three cardiac proteins clearly verified the proteomic findings listed in Table 5.2. Importantly, while the concentration of laminin, nidogen and annexin increased during natural aging, the deficiency in dystrophin caused the opposite effect (Figure 5.3 A-H, respectively). No significant alterations in the expression of ATP synthase were found (Figure 5.4 A, B).

A previous 2D-DIGE gel-based study of the dystrophic heart at 9-months old has shown reduced levels of many mitochondrial and metabolic proteins (Lewis *et al.,* 2010). To correlate the findings from the aging study presented here to these previously established alterations in the *mdx* heart, antibody labeling of crucial metabolic enzymes and mitochondrial markers was employed. Immunoblotting of pyruvate dehydrogenase (Figure 5.4 C, D), aconitase (Figure 5.4 E, F) and malate dehydrogenase (Figure 5.5 A, B) demonstrated a significant reduction of these metabolic enzymes during aging of cardiac muscle from the *mdx* mouse. The mitochondrial marker protein VDAC-1 also showed reduced levels in 20-month-old *mdx* hearts as compared to younger dystrophic hearts, as illustrated in Figure 5.5 C, D. The analysis of antibody labeling to lamin, myosin light chain and vimentin did not result in significant differences between young versus aged *mdx* samples, not shown. The core element of the dystrophin-glycoprotein complex, DGC, consists of the integral 43 kDa glycoprotein β-dystroglycan. In the subsarcolemmal domain β-dystroglycan directly interacts with the actin-binding protein dystrophin and likewise with the extracellular laminin receptor α-dystroglycan (Ohlendieck and Campbell 1991). Absence of dystrophin causes a reduction in DGC associated proteins as seen in the immunoblot for β-dystroglycan, Figure 5.5 E, F. Dp427 immunoblots had major background staining (not shown).

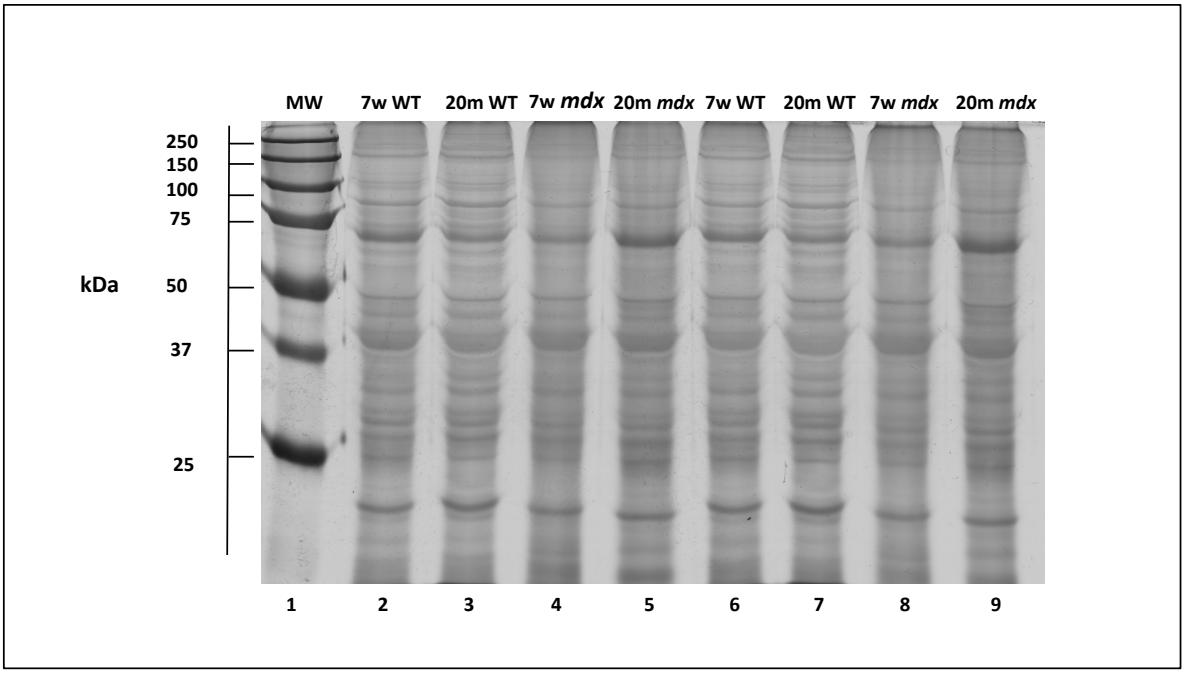

Figure 5.1 Gel electrophoretic analysis of cardiac proteins in young versus aged normal and dystrophic *mdx* mice.
Shown is a representative 1D silver-stained gel. Lane 1 shows molecular weight (MW) standards with their values in kDa on the left of the panel. Lanes 2 to 5, and duplicated in lanes 6 to 9, represent normal WT 7-week-old hearts, normal WT 20-month-old hearts, 7-week-old *mdx* hearts and 20-month-old *mdx* hearts, respectively.

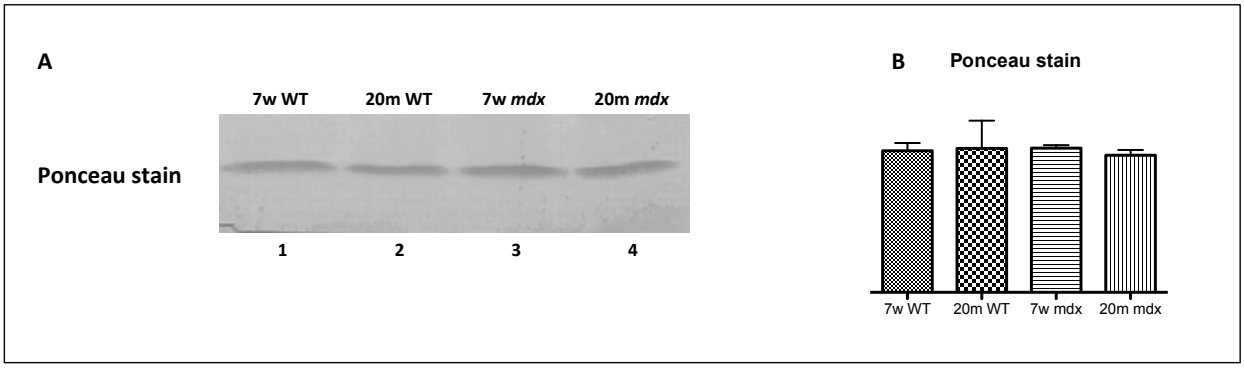

Figure 5.2 Equal loading Ponceau stain of cardiac proteins in young versus aged normal and dystrophic *mdx* mice.
Shown is an equally loaded membrane of cardiac proteins in young versus aged normal and dystrophic *mdx* mice, stained with Ponceau. Lanes 1 to 4 represent normal 7-week old hearts, normal 20-month old hearts, 7-week old *mdx* hearts and 20-month old *mdx* hearts, respectively at 20 kDa (unpaired Student's *t*-test; $n = 4$; NS).

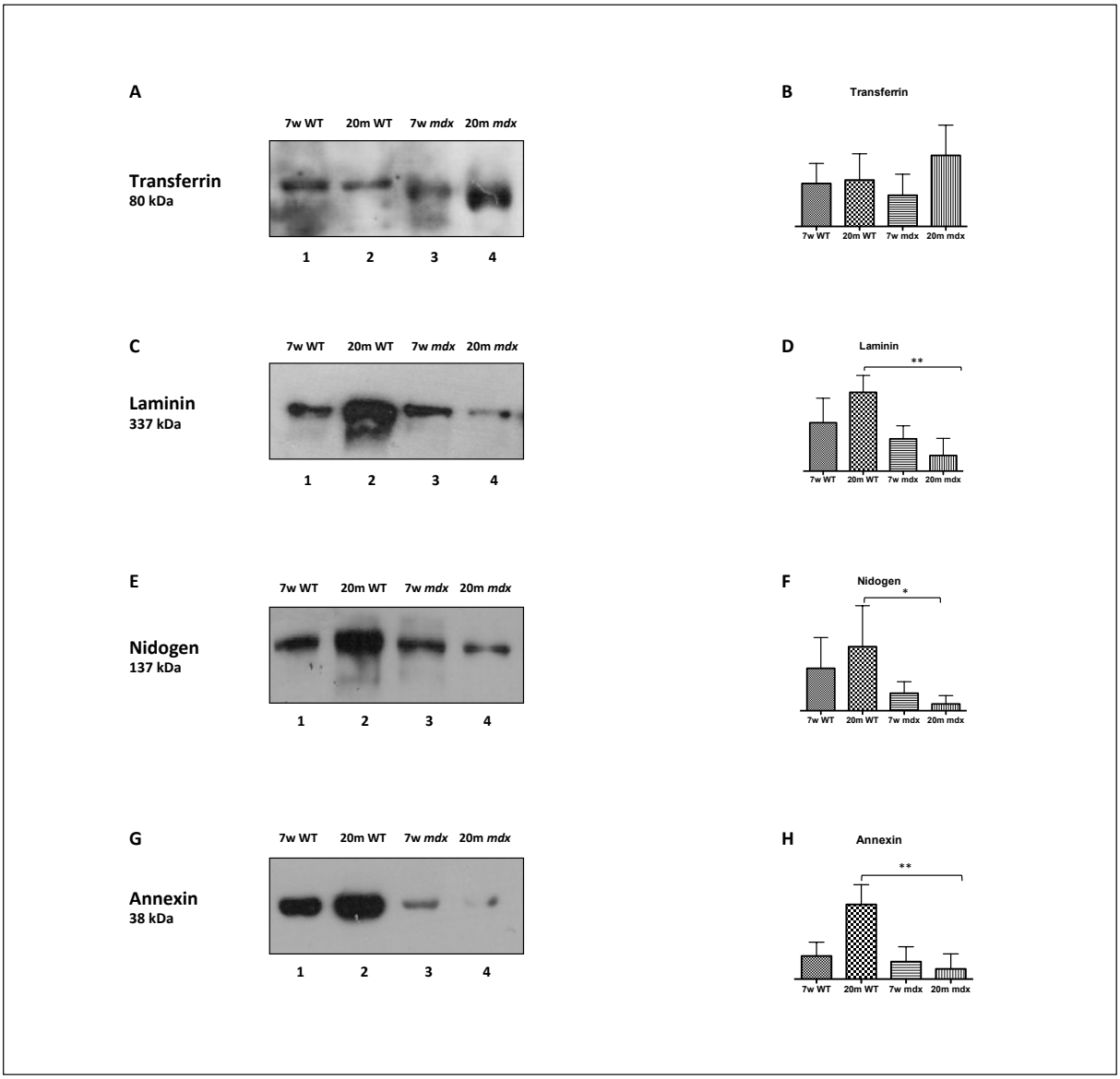

Figure 5.3 Immunoblot and quantitative analysis of select *mdx* proteins with an altered abundance during aging.

Shown are representative immunoblots with an expanded view of immuno-decorated bands (A, C, E and G). The immunoblot analysis of heart-associated proteins was performed with antibodies to transferrin (A), laminin (C), nidogen (E) and annexin (G). Lanes 1 to 4 represent normal 7-week-old hearts, normal 20-month-old hearts, 7-week-old *mdx* hearts and 20-month-old *mdx* hearts, respectively. Beside individual immunolots are the graphical representation (B, D, F and H) of the statistical evaluation of immunoblots. The comparative blotting of WT and *mdx* hearts were statistically evaluated using an unpaired Student's *t*-test ($n \geq 4$; *$p < 0.05$; **$p < 0.01$).

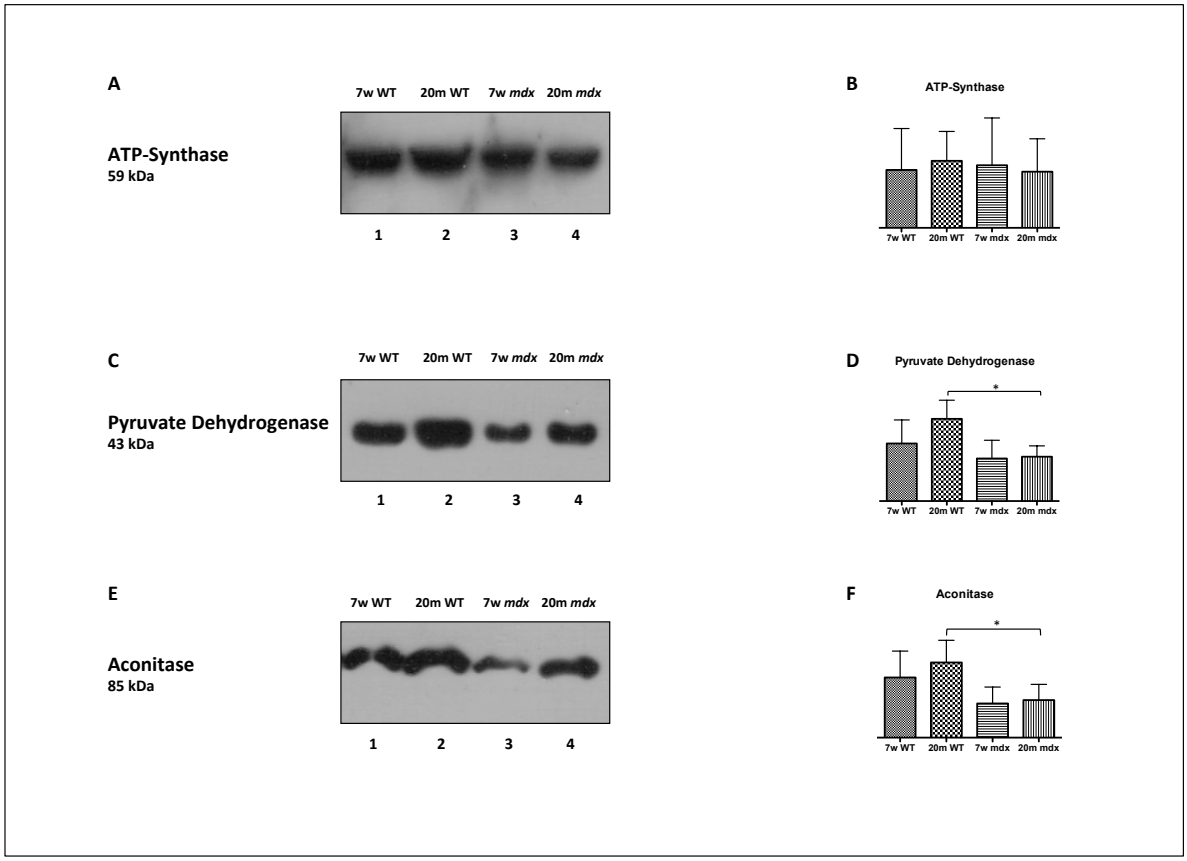

Figure 5.4 Immunoblot and quantitative analysis of select *mdx* proteins with an altered abundance during aging.

Shown are representative immunoblots with an expanded view of immuno-decorated bands (A, C and E). The immunoblot analysis of heart-associated proteins was performed with antibodies to ATP-synthase (A), pyruvate dehydrogenase (C) and aconitase (E). Lanes 1 to 4 represent normal 7-week-old hearts, normal 20-month-old hearts, 7-week-old *mdx* hearts and 20-month-old *mdx* hearts, respectively. Beside individual immunolots are the graphical representation (B, D and F) of the statistical evaluation of immunoblots. The comparative blotting of WT and *mdx* hearts were statistically evaluated using an unpaired Student's *t*-test ($n \geq 4$; $^{*}p < 0.05$; $^{**}p < 0.01$).

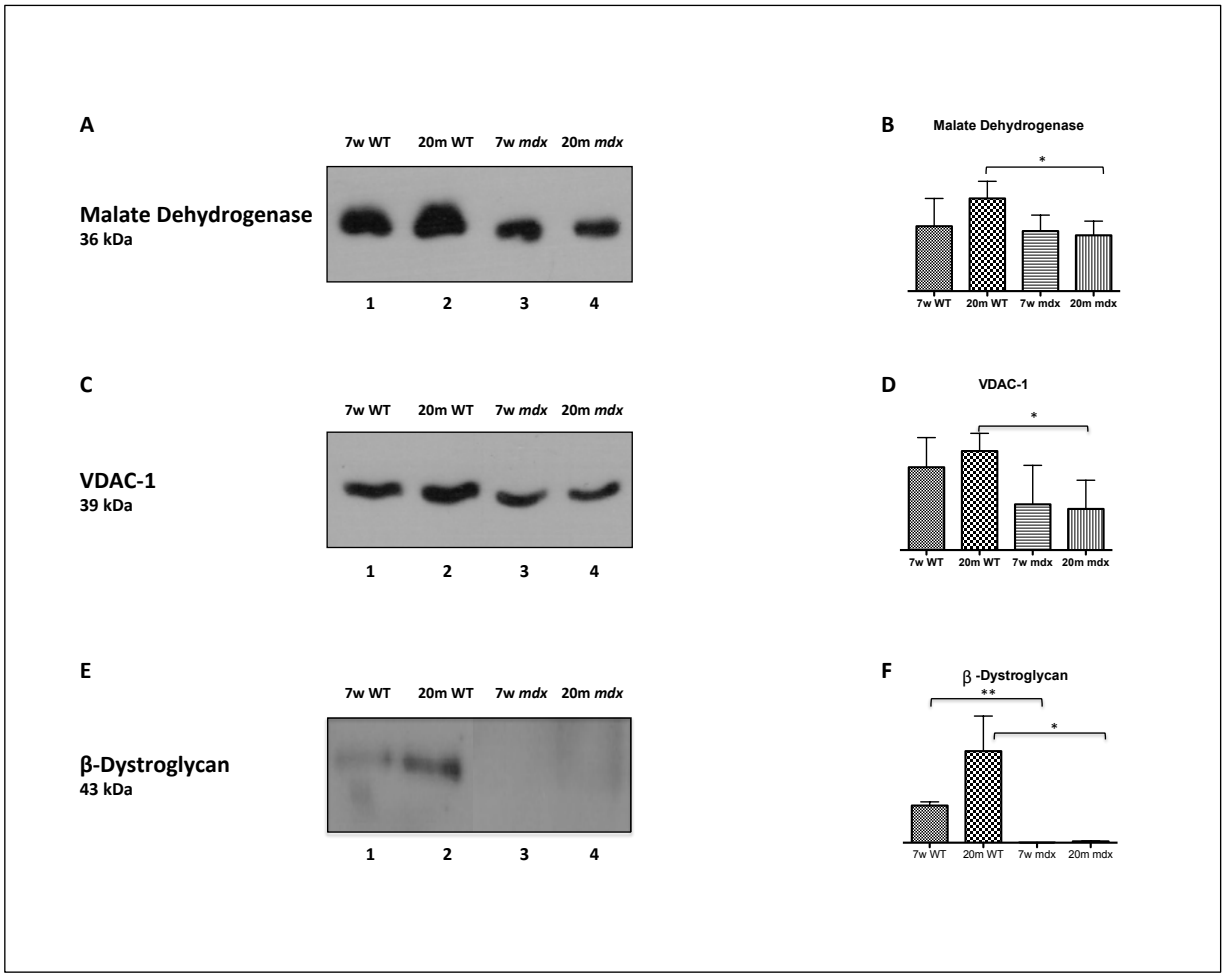

Figure 5.5 Immunoblot and quantitative analysis of select *mdx* proteins with an altered abundance during aging.

Shown are representative immunoblots with an expanded view of immuno-decorated bands (A, C and E). The immunoblot analysis of heart-associated proteins was performed with antibodies to malate dehydrogenase (A), VDAC-1 (C) and β-dystroglycan (E). Lanes 1 to 4 represent normal 7-week-old hearts, normal 20-month-old hearts, 7-week-old *mdx* hearts and 20-month-old *mdx* hearts, respectively. Beside individual immunolots are the graphical representation (B, D and F) of the statistical evaluation of immunoblots. Beside individual immunolots are the graphical representation (B, D, F and H) of the statistical evaluation of immunoblots ($n \geq 4$; *$p < 0.05$; **$p < 0.01$).

5.2.4 Protein interaction analysis of proteins with a changed concentration during senescence in the *mdx* heart

Figure 5.6 shows the bioinformatic STRING analysis of the proteomic data from label-free mass spectrometric results of the aging *mdx* heart outlined in Table 5.2. For the evaluation of potential protein-protein interactions of the label-free mass spectrometrically identified proteins with a changed abundance in the dystrophic *mdx* heart, bioinformatic analysis was carried out with the publically available STRING (http://string-db.org/; version 9.1) database of known and predicted protein interactions that include direct physical and indirect functional protein associations (Franceschini *et al.,* 2013). The interaction map illustrates the enormous complexity of potential protein interactions, especially with respect to mitochondrial components.

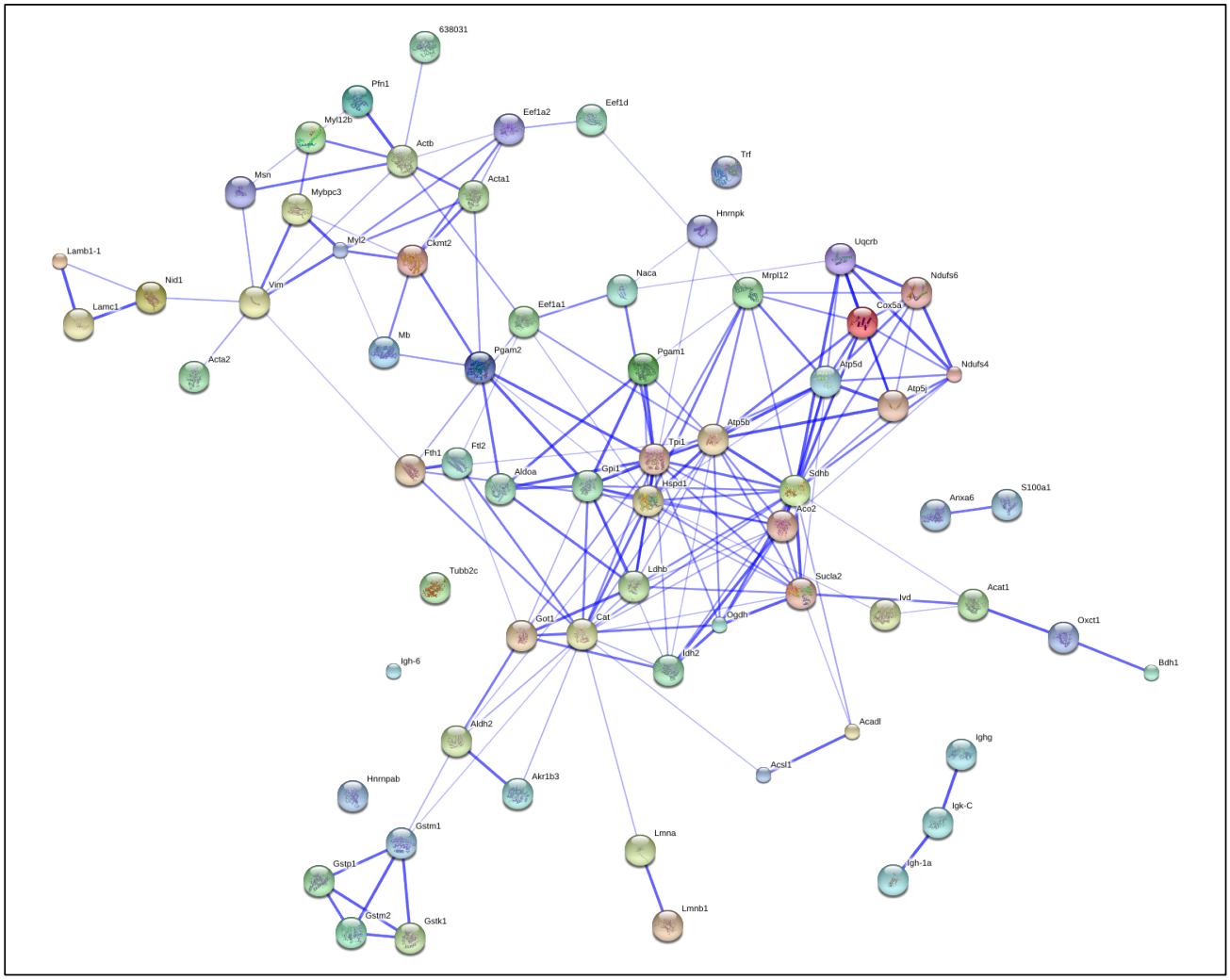

Figure 5.6 Bioinformatic STRING analysis of cardiac associated proteins with an altered abundance during aging of the *mdx* heart.
For the evaluation of protein-protein interactions of the mass spectrometrically identied proteins with a changed abundance in the dystrophic *mdx* heart, bioinformatic analysis was carried out with the publically available STRING (version 9.1) database of known and predicted protein interactions that include direct physical and indirect functional protein associations (Franceschini *et al.,* 2013).
*Image from Holland and Ohlendieck, 2014A

5.3 Discussion

A variety of novel pharmacological, cellular and genetic approaches are currently tested to counteract the symptoms of dystrophinopathies (Partridge, 2011; Benedetti *et al.,* 2013), including the treatment of muscular dystrophy related cardiomyopathic complications (Judge *et al.,* 2011). To better monitor the therapeutic success of experimental treatments and evaluate potential side effects, as well as generally improve diagnostic procedures, there is an urgent need for superior biomarkers of X-linked muscular dystrophy and associated cardiomyopathy. Experimental models of Duchenne muscular dystrophy, including the *mdx* mouse, exhibit many of the symptoms of cardiovascular disease seen in patients and are therefore frequently employed in pre-clinical investigations (Ameen and Robson, 2010). Dystrophin-deficient tissues are widely used as drug testing systems, including *mdx* heart preparations (De Luca, 2012). The *mdx* mouse is missing dystrophin due to a point mutation in exon 23 (Sicinski *et al.,* 1989) and shows many secondary abnormalities of the dystrophic phenotype (Durbeej and Campbell, 2002). Deficiency in cardiac dystrophin is associated with a variety of biochemical, physiological and cellular abnormalities, including a reduction in dystrophin-associated glycoproteins, disturbed Ca^{2+}-signaling, a substantial decrease in luminal Ca^{2+}-buffering proteins, amplification of ROS-generating pathways (Bia *et al.,* 1999; Jung *et al.,* 2008), broad infiltration of inflammatory cells (Lohan *et al.,* 2005; Lohan and Ohlendieck, 2004), greater amounts of adipose tissue (Au *et al.,* 2011), fibre necrosis and fibrosis (Fanchaouy *et al.,* 2009), as well as tachycardia and abnormal excitation–contraction–relaxation cycles in the *mdx* heart (Koenig *et al.,* 2011; Barnabei and Metzgerm, 2012; Stuckey *et al.,* 2012).

Since aging appears to accelerate the degenerative phenotype of the *mdx* heart (Quinlan *et al.,* 2004; Spurney *et al.,* 2008; Van Erp *et al.,* 2010), we have applied label-free MS-based proteomics to study the altered protein expression profile of 7-week-old versus 20-month-old dystrophic hearts. Both, the subcellular localization and the composition of the cardiac dystrophin–glycoprotein complex differs from skeletal muscle (Johnson *et al.,* 2012; Klietsch *et al.,* 1993), which might explain how the heart and skeletal muscle tissue are differently affected in dystrophinopathy. The MS proteomic findings presented in Table 5.2 indicate aging-associated alterations in components involved in the contraction–relaxation cycle, bioenergetics, iron binding, nuclear integrity, extracellular matrix organization, cytoskeletal maintenance and the cellular stress response.

5.3.1 Mass spectrometry based identification of antibodies in the aged *mdx* heart

High concentrations of antibodies were found in cardiac *mdx* preparations by MS analysis in Table 5.2. This agrees with the general idea of autoimmune mechanisms being involved in the molecular pathogenesis of cardiomyopathy (Zhao *et al.,* 2009). Possibly the deficiency in cardiac dystrophin leads to structural damage and tissue injury which in turn provokes autoimmunity or triggers infiltration of antibodies. Proteomic profiling of the dystrophin-deficient heart showed a drastic increase of antibodies during aging of the *mdx* mouse. This finding suggests a possible role of autoimmunity in muscular dystrophy-related cardiomyopathy or antibody penetration into

muscle cells through leaky membranes. It is not known, and difficult to determine, whether the increased antibody levels are a pathophysiological effect or a triggering factor of cardiomyopathy.

5.3.2 Iron binding proteins and the *mdx* heart during senescence

Other interesting proteins with elevated levels in the senescent dystrophic heart are represented by transferrin, ferritin and GSH transferase (Table 5.2). Since mammalian cells require sufficient iron levels for metabolic maintenance, transferrin levels are an important indicator of potential changes in iron absorption and usage (Szőke *et al.,* 2012). Transferrin (Figure 5.3 A, B) is an essential circulating protein that delivers iron to tissue proteins (Wang and Pantopoulos, 2011), thus changed levels of this transporter protein is indicative of disturbed cardiac iron homeostasis in muscular dystrophy. Another key player in iron metabolism is ferritin, a ubiquitous intracellular iron-binding protein (Crichton and Declercq, 2010). Ferritins sequester and release iron in a highly regulated fashion, thereby serving the dual physiological functions of iron detoxification and iron reserve (Harrison and Arosio, 1996). Its elevated level in the *mdx* heart suggests that ferritin buffers against a potential iron overload in the dystrophic phenotype.

5.3.3 Stress response

GSH transferase is a crucial catalyst in the GSH-dependent biotransformation of xenobiotics (Board and Menon, 2013) and elevated levels seen here therefore suggest increased stress levels in the *mdx* heart. In skeletal and cardiac muscle, GSH transferases also form ion channels in intracellular membrane systems and have been shown to modulate the ryanodine receptor Ca^{2+}-release channel (Dulhunty *et al.,* 2011). Thus, a higher concentration of GSH transferases could also be a compensatory mechanism to counteract abnormal Ca^{2+}-handling in muscular dystrophy. The fact that increased protein oxidation by reactive-free radical species induces muscle cell damage in both Duchenne patients (Haycock *et al.,* 1996) and the *mdx* mouse (Hauser *et al.,* 1995) and the establishment of altered GSH metabolism in oxidative damage (Renjini *et al.,* 2012), makes the proteomic identification of GSH transferase and catalase an interesting finding. As reviewed by Tidball and Wehling-Henricks (2007), the collapse of the dystrophin–glycoprotein complex appears to disrupt the normal production of free radicals and thereby contributes to the pathophysiology of muscular dystrophies. This might be due to constitutive differences in free radical production and concomitant disruption of crucial signaling processes in contractile fibres and/or a shift in free radical production, which promotes cellular injury and contractile dysfunction (Tidball and Wehling-Henricks, 2007). With respect to the *mdx* heart, changes in ROS and oxidative damage were shown to be involved in the molecular pathogenesis of cardiac dysfunction (Williams and Allen, 2007). It is therefore possible that GSH transferase might be involved in an antioxidant response in the dystrophic heart. Increased catalase levels for the enhanced removal of hydrogen peroxide would also agree with this concept

of an antioxidant mechanism in *mdx* tissue. A recent study by Selsby (2011) suggests that an elevated expression of catalase improves muscle function in *mdx* mice, hence a high concentration of catalase could play a crucial role in decreasing cellular injury in the dystrophin-deficient myocardium.

5.3.4 Abnormalities in the ECM, basement membrane and cytoskeletal network

Both proteomics (Table 5.2) and immunoblotting demonstrated differential expression levels of laminin (Figure 5.3 C, D), nidogen (Figure 5.3 E, F) and annexin (Figure 5.3 G, H) in normal versus dystrophic hearts at the two different ages studied. This indicates abnormalities in the extracellular matrix, ECM, basement membrane and cytoskeletal network of the dystrophin-deficient heart. Laminin is an essential component of the basement membrane and critical for the structural integrity of the ECM. Changes in laminin affect interactions between associated cells due to altered patterns of adhesion, differentiation and migration (Domogatskaya *et al.,* 2012). An abnormal laminin function is clearly involved in altered cell-matrix interactions in muscle disease (Carmignac and Durbeej, 2012). Laminin forms complexes with nidogen, a sulphated glycoprotein (Dziadek, 1995), in specialised basement membranes (Ho *et al.,* 2008). In general, changes in basement membrane composition facilitate pathological mechanisms (Kruegel and Miosge, 2010). In addition, annexins play a central role in maintenance of cytoskeleton and ECM integrity (Bizzarro *et al.,* 2012), as well as Ca^{2+}-handling in the heart (Camors *et al.,* 2005). A previous analysis of annexin in dystrophin-deficient skeletal muscles has indicated that

certain annexin isoforms are gradually released from the sarcolemmal membrane into the cytosol and into the extracellular space during the progression of dystrophinopathy (Selbert *et al.,* 1996). In analogy, dystrophy-associated cardiomyopathy appears to be also characterised by a drastic reduction in annexin-which in turn might be responsible for the decreased levels of the cytoskeletal protein vimentin. While the natural aging process is associated with an increased density of cardiac laminin, nidogen and annexin, muscular dystrophy triggers a severe reduction in these structural heart proteins. Thus, the deficiency in cardiac dystrophin seems to have a major destabilizing effect on the fibre periphery and its linkage to the ECM and cytoskeleton. These molecular and cellular changes are probably key events that cause cardiomyopathic complications and might explain the severe clinical phenotype of the heart in dystrophinopathy (Judge *et al.,* 2011). Furthermore, the age-dependent decrease in the nuclear protein lamin in the dystrophic *mdx* heart might destabilize nuclear integrity, transcriptional control and chromatin organization (Broers *et al.,* 2006), as well as trigger premature aging in the dystrophin-deficient heart (Reddy *et al.,* 2012).

5.3.5 Perturbed expression in mitochondrial proteins

The label-free LC-MS/MS analysis presented here of the aged *mdx* heart has identified disturbed levels of a variety of mitochondrial proteins and a general trend of increased glycolytic enzymes. This suggests considerable metabolic changes and potential adaptations in dystrophin-deficient heart tissue. The protein interaction map of cardiac proteins with an altered abundance in the

senescent *mdx* heart (Figure 5.6) illustrates the enormous complexity of potential protein interactions, most notably with respect to mitochondrial proteins. Increased mitochondrial enzymes included isocitrate dehydrogenase, creatine kinase, isovaleryl-CoA dehydrogenase, aldehyde dehydrogenase and long-chain specific acyl-CoA dehydrogenase. In contrast, reduced levels were established for the mitochondrial proteins ATP synthase (see also, Figure 5.4 A, B), NADH dehydrogenase, succinate dehydrogenase, cytochrome b-c1 complex, cytochrome c oxidase, succinyl-CoA ligase and long-chain fatty acid CoA ligase.

The reduction in key components of the mitochondrial electron transport chain suggests impaired oxidative phosphorylation. Lower levels of the mitochondrial complex V enzyme ATP synthase, which plays a central role in the biochemical generation of ATP, would agree with a reduced ATP production in *mdx* hearts (Zhang *et al.,* 2008). A reduction in critical elements of cardiac mitochondria would contribute in a major way to a bioenergetic crisis in dystrophin-deficient tissue, as previously suggested by a gel electrophoresis-based proteomic study of the *mdx* heart (Lewis *et al.,* 2010). It has long been established that impaired mitochondrial metabolism plays an important pathogenic feature in dystrophinopathy. Mitochondria from *mdx* skeletal muscle were shown to exhibit significant uncoupling of oxidative phosphorylation and a reduction in maximal ATP-synthesis capacity, which results in decreased intramuscular ATP levels (Kuznetsov *et al.,* 1998). A recent study by Percival and co-workers (2013) has shown that the lack of the membrane cytoskeletal protein dystrophin disrupts the subsarcolemmal localization of mitochondria, promotes mitochondrial inefficiency and restricts maximal mitochondrial ATP-generating capacity. The proteomic analysis of the aged *mdx* heart presented here agrees

with this idea of a bioenergetic dysfunction of mitochondria and suggests that the inability of *mdx* heart mitochondria to meet ATP demand increases during aging. The observed increased expression of glycolysis-associated enzymes could be interpreted as a compensatory mechanism to stabilize ATP levels. Thus, the increase in phosphoglycerate mutase, aldolase, glucose-6-phosphate isomerase, triosephosphate isomerase and lactate dehydrogenase might be a natural mechanism to counteract the pathophysiological loss of mitochondrial ATP production and at least partially balance the metabolic need for ATP in the dystrophic heart. This would suggest a general tendency to an oxidative-to-glycolytic shift in cardiac *mdx* metabolism. Based on the previous finding that dystrophin deficiency causes a drastic decrease in the dystrophin-connected α/β-dystroglycan complex in the *mdx* heart (Bia *et al.,* 1999), we could show here that additional secondary changes appear to trigger the loss in key ECM linker proteins. Alterations down-stream from the direct binding partners of the dystrophin complex have previously been established, including lower levels of the sarcoplasmic reticulum Ca^{2+}-buffering proteins sarcalumenin and calsequestrin in the membrane fraction from dystrophic hearts (Lohan and Ohlendieck, 2004). In addition, here we could show by label-free LC-MS/MS analysis that secondary effects influence the concentration of ferritin, tranferrin, catalase, GSH transferase, laminin, nidogen and annexin, as well as a large number of enzymes involved in both anaerobic and oxidative metabolism.

5.3.6 Conclusion

Aging of the *mdx* heart appears to have a profound influence on many structural proteins and metabolic enzymes. Ion transportation, the cellular stress response, ion handling and the maintenance of the contractile apparatus seem to be affected in dystrophin-deficient heart muscle. Dystrophinopathy-associated changes in a broad range of cardiac proteins supports the idea of severe pathobiochemical complications in aged *mdx* mice and establishes this *mdx* genetic model as a suitable system to evaluate new and potential drug treatments to counteract cardiomyopathy. Aged dystrophic hearts clearly exhibited a generally perturbed protein expression pattern with drastic changes in cardiac proteins involved in basal lamina stabilization, cytoskeletal organization, iron binding, antibody response, fibre contraction and energy metabolism.

Chapter 6

Label-Free Mass Spectrometry Analysis of the *mdx-4cv* Diaphragm

6.1 Introduction

The neuromuscular disorder Duchenne muscular dystrophy, DMD, is one of the most frequently inherited lethal diseases of childhood (Muntoni *et al.,* 2003). Approximately 1 in 3,500 live male births are affected by this form of contractile dysfunction, whereby considerable regional differences exist in the occurrence of DMD (Mah *et al.,* 2014). Early indicators of the disease, such as a waddling gait, toe walking, slow running patterns or frequent falls, are usually seen before the age of 5 years (Chelly and Desguerre, 2013). Besides an early-onset and highly progressive skeletal muscle wasting pathology (Chelly and Desguerre, 2013), the X-linked recessively inherited disorder is also characterized by respiratory impairments and a delayed onset of cardiomyopathic complications in almost all Duchenne patients (Mosqueira *et al.,* 2013).

DMD results from primary abnormalities in the gene coding for dystrophin, a large membrane cytoskeletal protein of the fibre periphery (Hoffman *et al.,* 1987). Since the full-length dystrophin isoform of 427 kDa (Dp427) functions as a molecular anchor providing an indirect linkage between the basal lamina and the actin membrane cytoskeleton, deficiency in Dp427 is believed to primarily cause the disintegration of sarcolemmal integrity (Holland *et al.,* 2013B). This pathobiochemical concept is supported by the fact that all members of the dystrophin-associated glycoprotein complex are greatly reduced in muscular dystrophy (Ohlendieck *et al.,* 1993) and that dystrophic fibres are fragile and exhibit sarcolemmal micro-rupturing (Allen and Whitehead, 2011). Abnormal calcium handling and a concomitant increase in calpain activity were shown to play a critical secondary role in the molecular pathogenesis of DMD

(Fong *et al.,* 1990; Hopf *et al.,* 2007; Holland and Ohlendieck, 2014D; Vallejo-Illarramendi *et al.,* 2014). Importantly, extensive accumulation of collagen and the substitution of contractile fibres with non-functional fibrotic tissue are a critical myopathological parameter in dystrophinopathy (Zanotti *et al.,* 2007; Vidal *et al.,* 2008; Sabatelli *et al.,* 2012) and endomysial fibrosis significantly correlates with poor motor outcome in X-linked muscular dystrophy (Desguerre *et al.,* 2009; Klingler *et al.,* 2012; Kharraz *et al.,* 2014).

In order to fully comprehend the complexity of the various pathophysiological steps involved in this monogenic disorder, comparative proteomics has made crucial contributions to the field of muscular dystrophy research. Dystrophinopathies have been investigated by MS-based surveys using both muscle tissue samples and bio-fluids from animal models and human patient material, as reviewed by Dowling *et al.,* (2014). Recently, the proteomic profiling of serum, plasma and urine samples from Duchenne patients has identified a variety of new biomarker candidates for improving diagnosis, prognosis and therapy monitoring (Nadarajah *et al.,* 2011; Martin *et al.,* 2014; Hathout *et al.,* 2014; Ayoglu *et al.,* 2014; Rouillon *et al.,* 2014). Muscle-derived proteins with an elevated concentration in body fluids include the matrix metalloproteinase MMP-9, fibronectin, carbonic anhydrase CA-3, creatine kinase, myosin light chain MLC3, malate dehydrogenase MDH2, transforming growth factor TGFβ1, electron transfer flavoprotein ETFA and various glycolytic enzymes in serum (Nadarajah *et al.,* 2011; Martin *et al.,* 2014; Hathout *et al.,* 2014; Ayoglu *et al.,* 2014). Interestingly, N- and C-terminal fragments of the contractile protein titin have been identified in urine samples from Duchenne patients (Rouillon *et al.,* 2014). The proteomic survey of the secretome from

dystrophin-deficient myotubes has demonstrated disturbances in vesicles that contain the lysosomal-associated membrane protein LAMP1 and an over-secretion of myosin light chain MLC1 (Duguez *et al.,* 2013). In addition, tissue proteomics of established animal models of DMD, such as the *grmd* dog and the *mdx* mouse, have revealed concentration changes in muscle-associated proteins especially associated with excitation, contraction, relaxation, signaling, ion handling, metabolic pathways, metabolite transportation and the cellular stress response (Doran *et al.,* 2006A; Doran *et al.,* 2009A; Guevel *et al.,* 2011; Carberry *et al.,* 2013A; Rayavarapu *et al.,* 2013).

Building on the extensive proteomic characterization of muscle specimens and body fluids from dystrophic organisms, here we have carried out a label-free MS study of the severely affected diaphragm from the *mdx-4cv* mouse (Banks *et al.,* 2010). This alternative DMD model to the *mdx* mouse exhibits very few dystrophin-positive revertant fibres (Danko *et al.,* 1992; Judge *et al.,* 2006) making it an excellent pathophysiological system for the evaluation of experimental gene therapies, such as exon skipping (Mitrpant *et al.,* 2009), artificial chromosomes (Tedesco, 2015) or viral vector transfer approaches (Kimura *et al.,* 2010). Interesting new results from the proteomic survey of this not extensively studied rodent model of dystrophinopathy included a major increase in numerous extracellular matrix, ECM, proteins and elements of the cytoskeleton. These findings agree with the idea of severe tissue damage, fibrotic scaring and cytoskeletal remodeling in dystrophin-deficient muscle.

6.1.1 Experimental design

Proteomic profiling plays a decisive role in the identification of novel biomarkers of muscular dystrophy and the elucidation of new pathobiochemical mechanisms that underlie progressive muscle wasting. Building on recent findings from comparative analyses from dystrophic animals and patients with DMD, we have here used label-free MS to study the severely dystrophic diaphragm from the *mdx-4cv* mouse. Wild type, WT, controls and *mdx-4cv* mice, as well as conventional *mdx* mice for comparative studies, were obtained from the Animal Facility of the University of Bonn, Germany.

Crude diaphragm muscle specimens from 3-month old *mdx-4cv* mice (n = 4) and age-matched normal WT mice (n = 4) were prepared for label-free LC-MS/MS analysis and analyzed using an Ultimate 3000 nanoLC system coupled to a an LTQ Orbitrap XL mass spectrometer in the Proteomics Facility of the National Institute for Cellular Biotechnology, Dublin City University. Progenesis label-free LC-MS software was used to process the raw data generated from LC-MS/MS analysis and peptides were identified with MASCOT and searched against the UniProtKB-SwissProt database. Standard bioinformatics software programs were applied to catalogue the clustering of molecular functions and to identify potential protein interactions of the MS-identified muscle proteins with a changed concentration in the dystrophic *mdx-4cv* diaphragm compared to WT. In order to verify potential concentration changes in diaphragm proteins, as indicated by proteomic analysis, the expression levels of select protein species of interest were determined by immunoblotting. Following this, the main focus of verification analysis in this study was on the substantially increased matricellular protein periostin. Periostin levels were compared in *mdx-4cv*

versus WT and also in *mdx* versus WT diaphragm preparations by immunoblotting. Indirect immunofluorescence microscopy was further employed to look at select proteins in the dystrophic *mdx-4cv* diaphragm. In order to evaluate potential changes during aging of dystrophic versus normal muscle, diaphragm samples over a 2 to 15 month senescent period were analyzed by comparative immunoblotting.

6.2 Results

A comparative proteomic analysis of dystrophic diaphragm muscle from the *mdx-4cv* mouse model of X-linked muscular dystrophy was performed in order to identify novel protein changes in dystrophinopathy. Following label-free LC-MS/MS analysis, the most drastic alteration in a fibrosis-related matricellular protein was further characterized by immunofluorescence microscopy and comparative immunoblotting of *mdx-4cv* preparations of differing age versus wild type muscle. Standard bioinformatics software programs were used to outline the molecular functions of the identified muscle proteins and determine their potential interaction patterns.

6.2.1 Proteomic profiling of 3-month old diaphragm muscle from *mdx-4cv* versus wild type mice

Label-free LC-MS/MS analysis revealed significant changes (ANOVA score of $p \leq 0.05$) in 158 diaphragm-associated proteins including identifications based on only 1 matched peptide (not shown). Stringent conditions were applied for the quantitative profiling by label-free LC-MS/MS data and the identification of peptides and corresponding muscle proteins using the Label-Free Progenesis software programme, the MASCOT search engine and the UniProtKB-SwissProt database. For the final established list of altered components, only proteins with ≥ 2 matched peptides and a MASCOT score above 40 were assigned as properly identified protein species, outline in Table 6.1. Excluding protein hits with only 1 matched peptide, 67 altered proteins were clearly identified in in 3-month old *mdx-4cv* diaphragm samples as compared to age-matched control WT specimens.

As listed in Table 6.1, 50 proteins exhibited an increased abundance and 17 proteins a decreased density in dystrophic muscle. The most significant changes with values of 3-fold or higher were established for increases in myosin-8, periostin, myosin-3, mitochondrial NADP transhydrogenase, aminopeptidase N, collagen α-1(I) chain, asporin, the heterogeneous nuclear ribonucleoprotein K, dermatopontin and prelamin-A/C, and decreases in myosin-4, fast-type parvalbumin and myosin-binding protein MBP-C. Moderately elevated expression levels were shown for cytoplasmic actin, vimentin, protein disulphide isomerase, prolargin, elongation factor 1-alpha 1 and 2, serotransferrin, decorin, desmin, myosin light chains MLC-6B and MLC2, 14-3- 3 protein beta and theta, serum albumin, myosin-9, histones H1.2, H2B, H3.3C and H2A.Z, collagen alpha-1(VI) chain and alpha-2(I) chain, tubulin beta-2A, tropomyosin TMα3 chain, vinculin, polyubiquitin-B GTP-binding nuclear protein Ran, spectrin alpha, heterogeneous nuclear ribonucleoproteins A2/B1, myosin-7, tropomyosin alpha-4, enolase, filamin-C, heat shock proteins Hsp71 cognate and HSP90-beta, transitional endoplasmic reticulum ATPase, sarcalumenin, obscurin, plectin, mitochondrial succinyl-CoA:3-ketoacid coenzyme A transferase and titin. Minor decreases were identified in myomesin-1, long-chain-fatty-acid-CoA ligase, fast Troponin TnT, phosphofructokinase, mitochondrial electron transfer flavoprotein-ubiquinone oxidoreductase, myosin-1, phosphoglycerate mutase, myozenin, glycogen phosphorylase, creatine kinase, tropomyosin alpha-1, medium-chain specific acyl-CoA dehydrogenase, α- actinin-3 and perilipin-4.

Dystrophin and other major components of the DGC were not shown to have a statically significant reduction in the MS hit list (Table 6.1). This is consistent with previous global proteomic-screening experiments (Lewis *et al.,*

2010; Carberry *et al.,* 2012A; Rayavarapu *et al.,* 2013). These proteins can be difficult to identify during global proteomic screening due to the individual molecular weights, the proteins are part of a complex that can be more difficult to digest. Cellular fractionation methods including ultra centrifugation are a way to overcome this.

Table 6.1 List of muscle-associated proteins with an altered abundance in the diaphragm muscle from *mdx-4cv* mice

Accession number	Protein name	Peptides	Score	ANOVA	Fold change
P13542	Myosin-8	2	286.71	1.98E-06	36.00
Q62009	Periostin	2	125.21	1.54E-06	21.96
P13541	Myosin-3	5	309.32	1.12E-03	19.53
Q61941	NAD(P) transhydrogenase, mitochondrial	5	226.04	1.00E-02	9.82
P97449	Aminopeptidase N	2	137.61	2.00E-06	6.15
P11087	Collagen alpha-1(I) chain	2	111.18	3.00E-02	5.52
Q99MQ4	Asporin	2	46.03	1.48E-06	4.46
P61979	Heterogeneous nuclear ribonucleoprotein K	2	111.6	3.63E-04	3.68
Q9QZZ6	Dermatopontin	3	130.04	1.38E-06	3.43
P48678	Prelamin-A/C	13	728.51	1.19E-03	3.19
P60710	Actin, cytoplasmic 1	2	159.08	4.00E-02	2.96
P20152	Vimentin	4	248.62	4.11E-05	2.90
P27773	Protein disulfide-isomerase A3	3	47.58	9.59E-04	2.84
Q9JK53	Prolargin	3	120.54	2.48E-03	2.62
P10126	Elongation factor 1-alpha 1	2	80.79	2.18E-03	2.61
Q921I1	Serotransferrin	2	96.53	2.00E-02	2.56
P28654	Decorin	4	151.38	2.92E-05	2.44
P31001	Desmin	7	262.69	2.79E-03	2.40
Q8CI43	Myosin light chain 6B	2	43.68	1.81E-06	2.40
Q9CQV8	14-3-3 protein beta/alpha	2	114.95	1.84E-03	2.39
P10853	Histone H2B type 1-F/J/L	2	90.58	5.60E-05	2.15
P07724	Serum albumin	4	188.46	1.11E-03	2.13
Q8VDD5	Myosin-9	2	126.54	3.57E-05	2.11
P15864	Histone H1.2	2	131.63	1.65E-03	2.07
P68254	14-3-3 protein theta	2	200.85	7.65E-04	2.05
Q04857	Collagen alpha-1(VI) chain	5	221.01	1.11E-05	2.01
Q7TMM9	Tubulin beta-2A chain	3	144.06	2.23E-03	2.01
P21107	Tropomyosin alpha-3 chain	4	17.63	4.71E-04	1.95
P02301	Histone H3.3C	3	106.11	7.25E-05	1.89
Q64727	Vinculin	4	145.48	1.51E-03	1.88
P0CG49	Polyubiquitin-B	2	4.14	2.44E-03	1.88
P62827	GTP-binding nuclear protein Ran	2	84.98	4.05E-04	1.87
P16546	Spectrin alpha chain, non-erythrocytic 1	2	117.17	2.00E-02	1.84
P58252	Elongation factor 2	4	225.21	3.50E-03	1.78
O88569	Heterogeneous nuclear ribonucleoproteins A2/B1	2	60.79	9.77E-04	1.78
P0C0S6	Histone H2A.Z	2	115.98	1.10E-03	1.76
Q91Z83	Myosin-7	15	696.21	2.60E-04	1.74
Q6IRU2	Tropomyosin alpha-4 chain	2	100.58	8.54E-05	1.74
Q01149	Collagen alpha-2(I) chain	2	149.41	2.00E-02	1.64
P17182	Alpha-enolase	4	181.63	4.14E-03	1.59
P51667	Myosin regulatory light chain 2, ventricular/cardiac muscle isoform	2	61.17	3.00E-02	1.58
Q8VHX6	Filamin-C	15	579.09	9.27E-04	1.55

Table 6.1 Continued

Accession number	Protein name	Peptides	Score	ANOVA	Fold change
P63017	Heat shock cognate 71 kDa protein	2	148.17	3.00E-02	1.46
Q01853	Transitional endoplasmic reticulum ATPase	2	135.98	4.37E-03	1.45
P11499	Heat shock protein HSP 90-beta	3	162.72	9.34E-03	1.44
Q7TQ48	Sarcalumenin	2	92.76	2.29E-03	1.39
A2AAJ9	Obscurin	2	109.12	3.46E-03	1.38
Q9QXS1	Plectin	22	1015.84	2.84E-04	1.36
Q9D0K2	Succinyl-CoA:3-ketoacid coenzyme A transferase 1, mitochondrial	2	111.98	3.00E-02	1.25
A2ASS6	Titin	45	2212.08	4.88E-04	1.21
Q62234	Myomesin-1	6	275.12	1.58E-03	-1.12
P41216	Long-chain-fatty-acid--CoA ligase 1	3	115.26	1.77E-03	-1.23
Q9QZ47	Troponin T, fast skeletal muscle	2	95.54	1.00E-02	-1.24
P47857	6-phosphofructokinase, muscle type	2	112.1	4.97E-03	-1.26
Q921G7	Electron transfer flavoprotein-ubiquinone oxidoreductase, mitochondrial	3	191.07	8.54E-04	-1.38
Q5SX40	Myosin-1	3	271.46	6.53E-03	-1.39
O70250	Phosphoglycerate mutase 2	2	129.66	2.00E-02	-1.40
Q9JK37	Myozenin-1	2	68.41	4.17E-03	-1.41
Q9WUB3	Glycogen phosphorylase, muscle form	5	147.42	1.79E-03	-1.43
P07310	Creatine kinase M-type	2	46.24	3.00E-02	-1.46
P58771	Tropomyosin alpha-1 chain	2	149.5	7.54E-03	-1.53
P45952	Medium-chain specific acyl-CoA dehydrogenase, mitochondrial	2	111.99	2.27E-03	-1.65
O88990	Alpha-actinin-3	4	150.35	8.25E-03	-1.99
O88492	Perilipin-4	2	103.41	1.49E-05	-2.03
Q5XKE0	Myosin-binding protein C, fast-type	2	80.59	1.79E-03	-3.26
P32848	Parvalbumin alpha	4	114.94	9.26E-04	-5.60
Q5SX39	Myosin-4	2	316.02	1.00E-02	-6.55

* *mdx-4cv* versus normal diaphragm

** UniProtKB-SwissProt database (downloaded in January 2013) with 16,638 proteins (*Mus musculus*)

6.2.2 Bioinformatic protein cataloguing and protein interaction analysis

Standard bioinformatics software programs were applied to catalogue the clustering of molecular functions and to identify potential protein interactions of the MS-identified muscle proteins with a changed concentration in the dystrophic *mdx-4cv* diaphragm (Table 6.1).

The application of the PANTHER database of protein families (Mi *et al.,* 2013) resulted in the cataloging of molecular classes of the identified *mdx-4cv* muscle proteins (Table 6.1) with a changed concentration as follows: cytoskeletal protein (21.5%), enzyme modulator (11.2%), extracellular matrix protein (7.6%) transferase (5.9%), nucleic acid binding protein (5.9%), cell adhesion molecule (5.1%), cell junction protein (5.1%), receptor (5.1%), calcium-binding protein (3.4%), molecular chaperone (3.4%), structural protein (3.4%), kinase (3.4%), transporter (2.5%), transfer/carrier protein (2.5%), hydrolase (2.5%), surfactant (2.5%), defense/immunity protein (2.5%), oxidoreductase (1.7%), signaling molecule (0.8%), protease (0.8%), membrane traffic protein (0.8%), lyase (0.8%), isomerase (0.8%) and ligase (0.8%) (Figure 6.1).

Further bioinformatics analysis was performed with the help of the STRING database of known and predicted protein interactions that include direct physical and indirect functional protein associations (Franceschini *et al.,* 2013). The prediction of muscle-associated protein interactions is based on published data with respect to neighborhood, gene fusion, co-occurrence, co-expression, experiments, databases, text-mining and homology data (Franceschini *et al.,* 2013). The existence of potential interactions between proteins with a changed abundance in the *mdx-4cv* diaphragm, as identified by the proteomics survey

presented here, was evaluated. The STRING analysis resulted in a complex interaction map (Figure 6.2). The predicted cluster of components of the extracellular matrix, ECM, complex is highlighted in Figure 6.2. The main focus of the below described immunoblot analyses (Section 6.2.4), the matricellular protein periostin, is predicted to form strong interactions patterns with key elements of the extracellular matrix, such as collagen, dermatopontin, asporin and decorin. In addition, a main interaction hub was shown to include proteins of the contractile apparatus and the cytoskeleton.

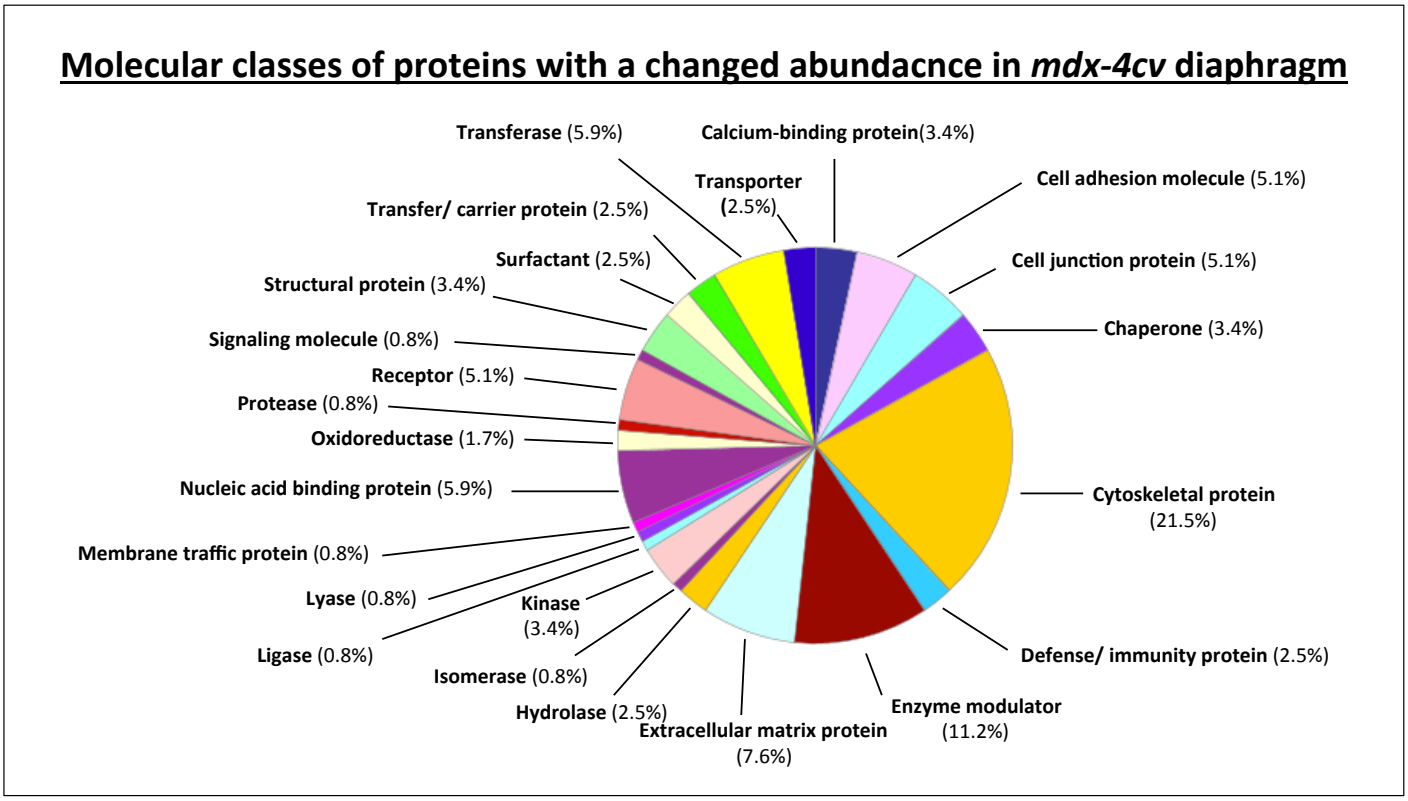

Figure 6.1 Molecular classes of proteins with a changed abundance in *the mdx-4cv* diaphragm.

Bioinformatics software was used to identify the clustering of the molecular classes of the MS-identified proteins with an altered concentration in the dystrophic *mdx-4cv* diaphragm (Table 6.1). The analysis was carried out with the PANTHER database (version 8.1) of protein families for the cataloging of molecular classes (Mi *et al.,* 2013).

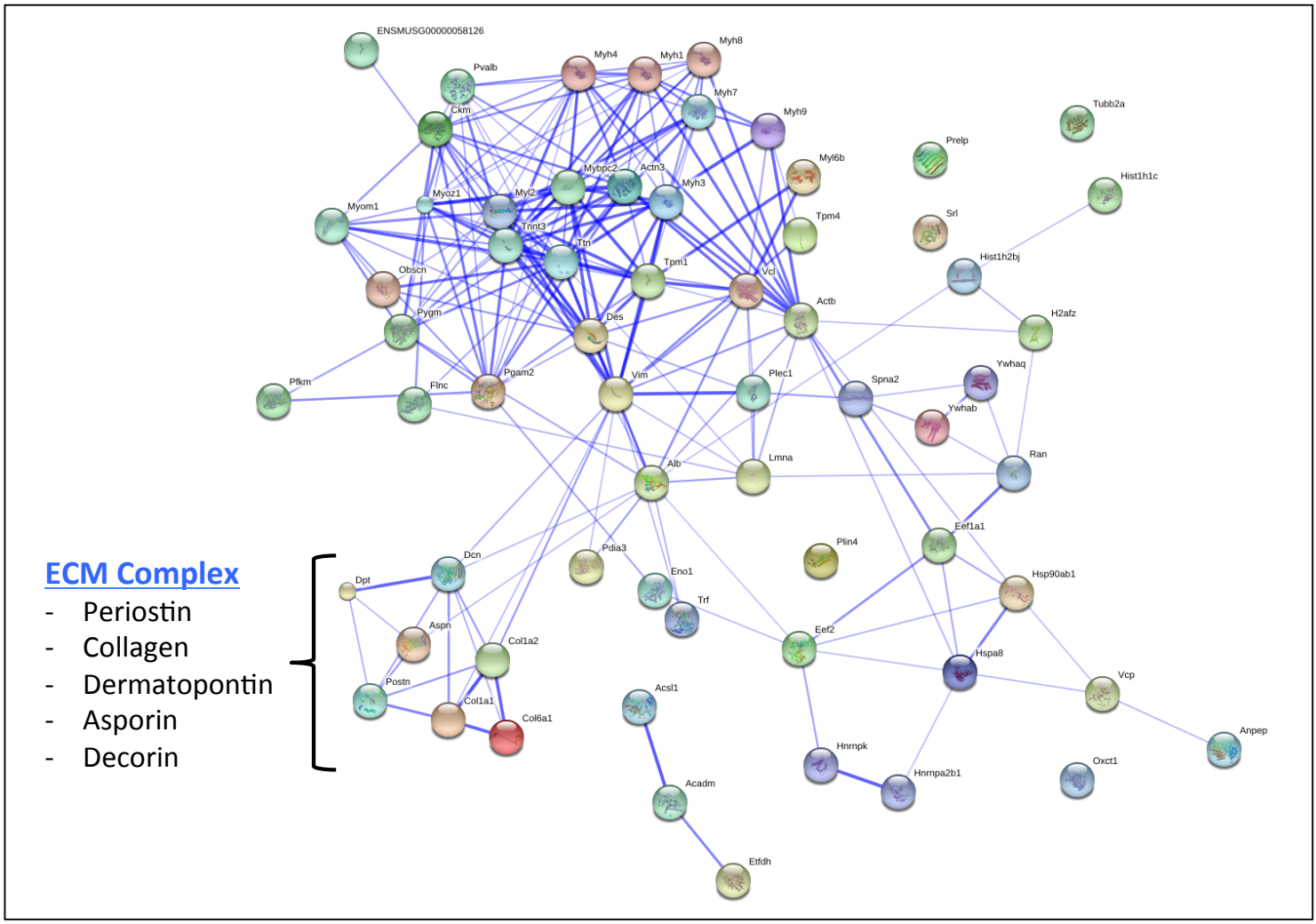

Figure 6.2 Protein interaction map of proteins with a changed abundance in the *mdx-4cv* diaphragm.

Shown is a map of potential protein interactions generated with the STRING database (version 9.1) of known and predicted protein associations that include direct physical and indirect functional protein linkages (Franceschini *et al.,* 2013). The analysis was performed with proteins that exhibited a changed concentration in the dystrophic *mdx-4cv* diaphragm muscle (Table 6.1). The predicted cluster of components of the extracellular matrix, ECM, complex is highlighted.

6.2.3 Verification of proteomic findings by comparative immunoblotting of *mdx-4cv* versus WT diaphragm

In order to verify key findings form the proteomic survey of the *mdx-4cv* diaphragm (Table 6.1), immunoblotting was carried out with primary antibodies to markers of the sarcolemma, the basal lamina, the nuclear envelope, the intermediate filament, the sarcosol, muscle metabolism and the contractile apparatus. Silver-stained 1D gels indicated no major differences in the overall composition of major proteins bands (Figure 6.3). Comparable levels of the basal lamina component laminin (Figure 6.4 A, B). Laminin was used to confirm equal loading between the dystrophic *mdx-4cv* diaphragm and WT diaphragm muscle preparations. In contrast, immuno-detection confirmed the major decrease of β-dystroglycan (Figure 6.4 C, D) in the sarcolemma of dystrophic diaphragm muscle. β-dystroglycan is a transmembrane protein and a component of the DGC. Dystrophin deficiency in DMD patients and *mdx-4cv* mice (Figure 6.8 and 6.9 C) causes an overall reduction in the components of the DGC. β-dystroglycan is routinely used for immunoblotting, as it is an appropriate alternative protein used as a disease control (Ohlendieck and Campbell, 1991). Dp427 immunoblots had major background staining (not shown). In agreement with the proteomic findings presented in this study, the nuclear envelope protein lamin A/C (Figure 6.4 E, F) and the intermediate filament desmin (Figure 6.4 G, H) showed greatly increased levels in *mdx-4cv* muscle. Significant reductions in concentration were shown for the sarcosol Ca^{2+}-binding protein parvalbumin (Figure 6.5 A, B) and the metabolic enzyme creatine kinase (Figure 6.5 C, D). For control purposes, immuno-detection with an antibody against carbonic anhydrase CA-3 was carried out. A reduced concentration in dystrophic muscle was confirmed

(Figure 6.5 E, F). Immunoblotting analysis of markers of the contractile apparatus revealed no major alterations in the MLC2 isoform of myosin light chain (Figure 6.5 G, H), but a drastic reduction in the myosin binding protein MBP-C (Figure 6.6 A, B). Comparable levels of myoglobin were identified in both sample preparations (Figure 6.6 C, D). The statistical evaluation of the immunoblot survey of laminin, β-dystroglycan, lamin A/C, desmin, parvalbumin, creatine kinase M-type, carbonic anhydrase isoform CA-3, myosin light chain MLC-2, myosin binding protein MBP-C, and myoglobin was carried out using an unpaired Student's *t*-test.

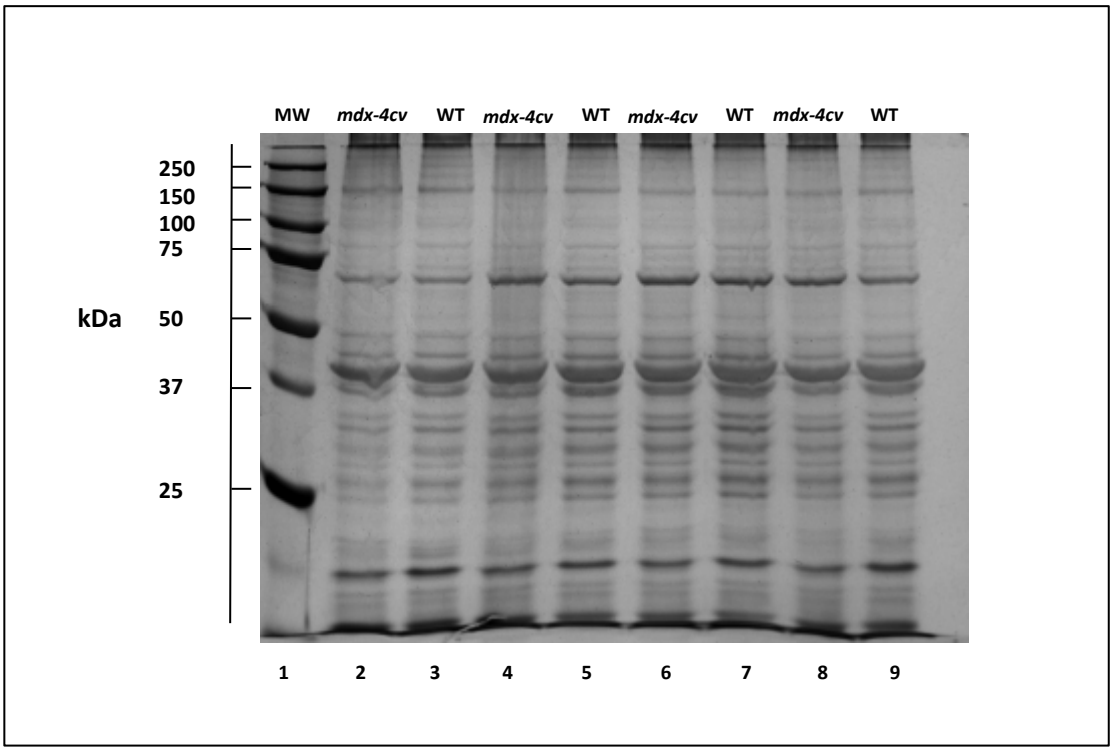

Figure 6.3 Gel electrophoretic analysis of *mdx-4cv* and WT diaphragm muscle. Shown is a representative 1D silver-stained gel. Lane 1 shows the molecular weight (MW) standards with their values (kDa) indicated on the left. Lanes 2, 4, 6 and 8 represent 3-month old *mdx-4cv* diaphragm preparations and lanes 3, 5, 7 and 9 represent wild type (WT) diaphragm preparations, respectively.

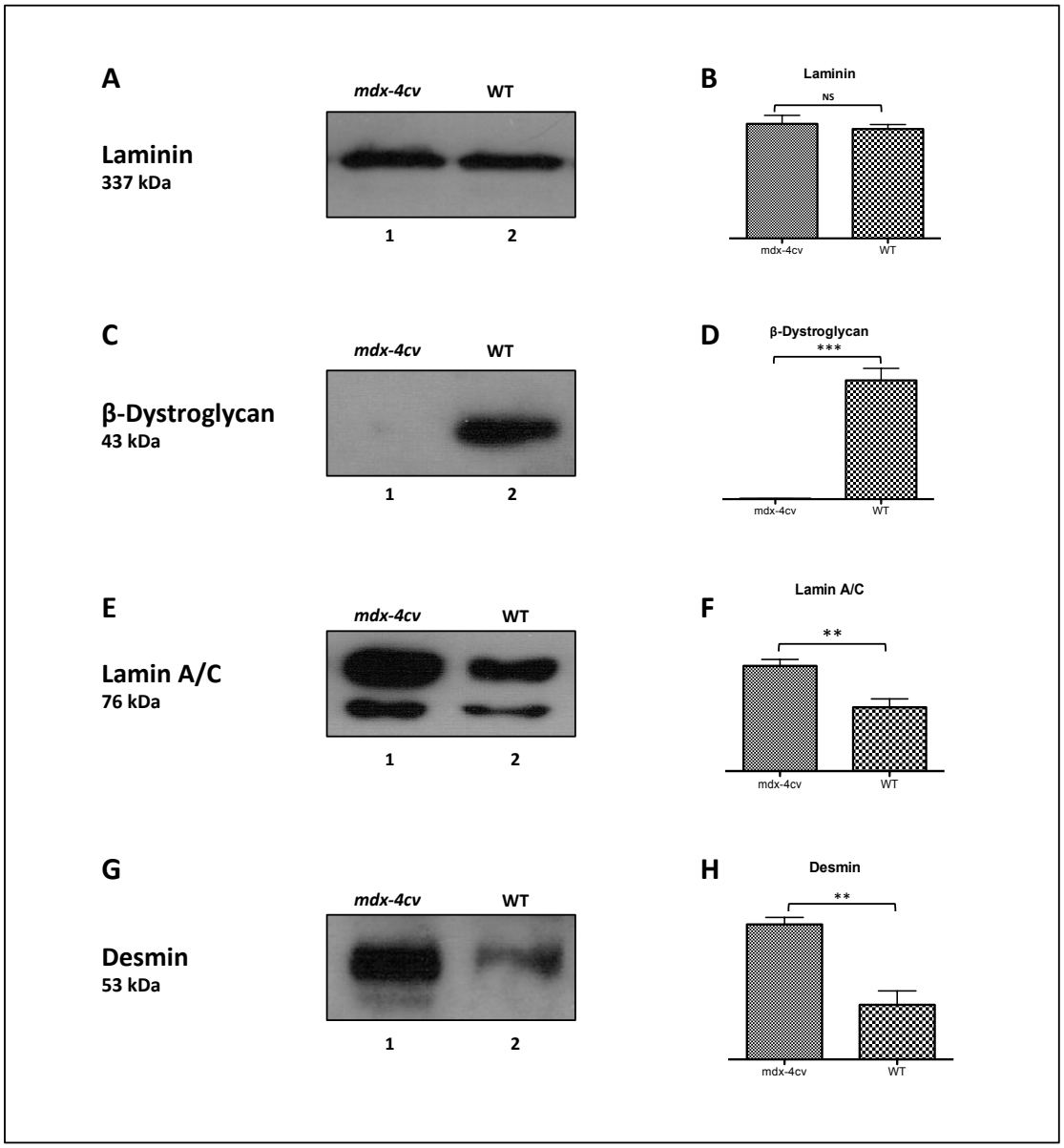

Figure 6.4 Immunobloting survey and quantitative analysis of proteins with an altered abundance in *mdx-4cv* diaphragm muscle.

Shown are representative immunoblots with expanded views to illustrate antibody-labeled bands to laminin (A), β-dystroglycan (C), lamin A/C (E) and desmin (G). Lanes 1 and 2 represent *mdx-4cv* versus WT diaphragm muscle preparations, respectively. The graphical presentation represents the statistical analysis of immunoblotting to laminin (B), β-dystroglycan (D), lamin A/C (F) and desmin (H). (Student's *t*-test, unpaired; $n \geq 4$; NS = not significant; $^{**}p < 0.01$; $^{***}p < 0.001$).

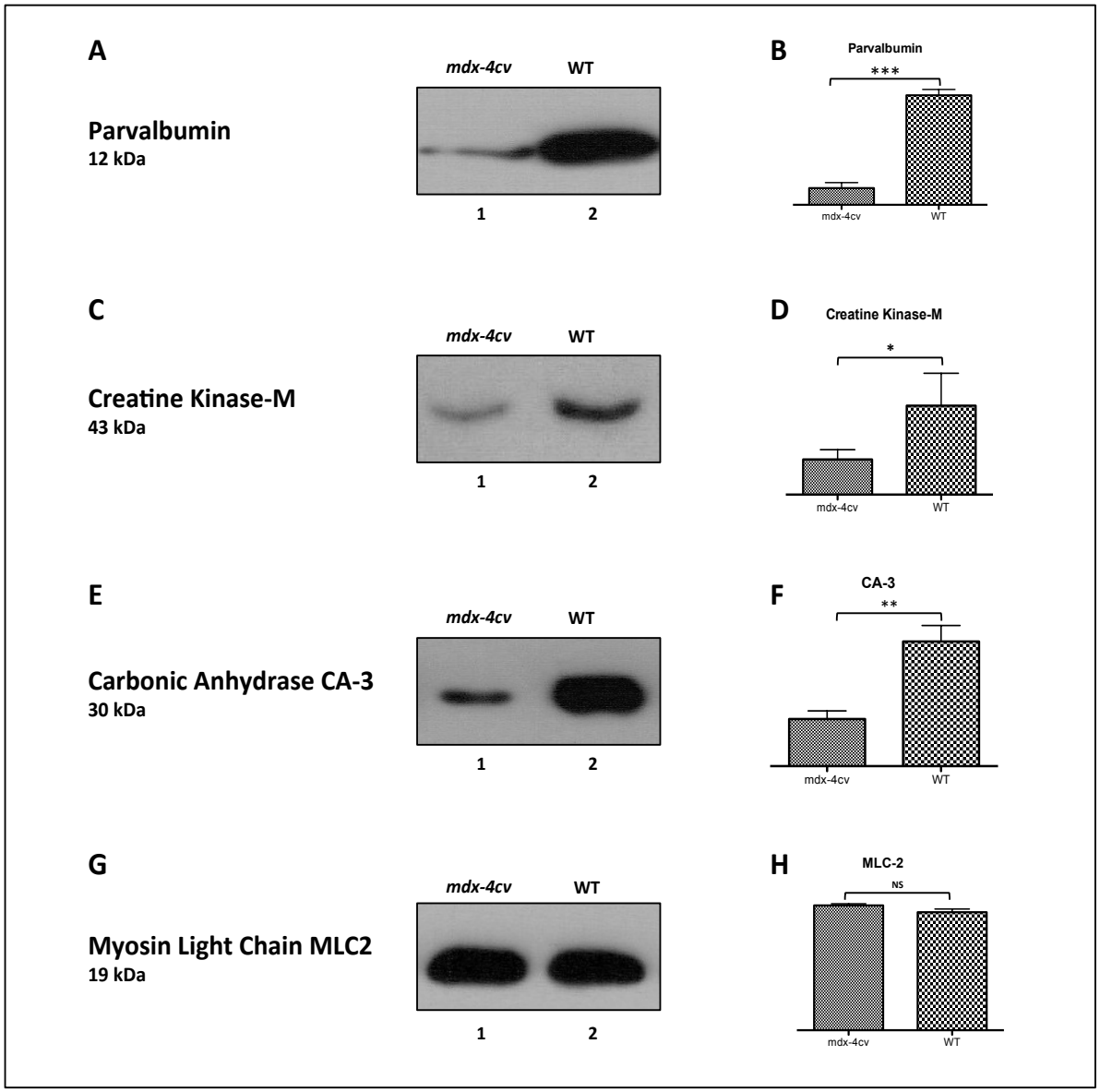

Figure 6.5 Immunobloting survey and quantitative analysis of proteins with an altered abundance in *mdx-4cv* diaphragm muscle.
Shown are representative immunoblots with expanded views to illustrate antibody-labeled bands to parvalbumin (A), creatine kinase-M (C), carbonic anhydrase CA-3 (E) and myosin light chain MLC-2 (G). Lanes 1 and 2 represent *mdx-4cv* versus WT diaphragm muscle preparations, respectively. The graphical presentation represents the statistical analysis of immunoblotting to parvalbumin (B), creatine kinase-M (D), carbonic anhydrase CA-3 (F) and myosin light chain MLC-2 (H). (Student's *t*-test, unpaired; $n \geq 4$; NS = not significant; *$p < 0.05$; **$p < 0.01$; ***$p < 0.001$).

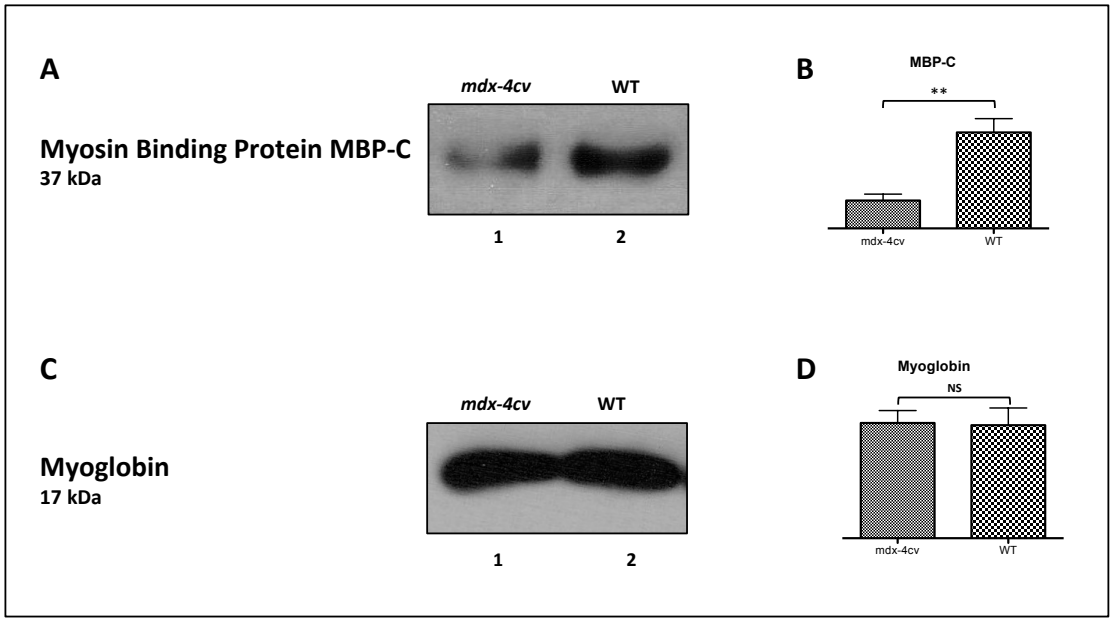

Figure 6.6 Immunobloting survey and quantitative analysis of proteins with an altered abundance in *mdx-4cv* diaphragm muscle.
Shown are representative immunoblots with expanded views to illustrate antibody-labeled bands to myosin binding protein MBP-C (A) and myoglobin (C). Lanes 1 and 2 represent *mdx-4cv* versus WT diaphragm muscle preparations, respectively. The graphical presentation represents the statistical analysis of immunoblotting to myosin binding protein MBP-C (B) and myoglobin (D) (Student's *t*-test, unpaired; $n \geq 4$; NS = not significant; $^{**}p < 0.01$).

6.2.4 Immunoblot analysis of the dystrophin-deficient *mdx-4cv* and *mdx* diaphragm muscle

A very unexpected and interesting finding of the proteomic profiling of the severely dystrophic *mdx-4cv* diaphragm muscle was the drastic increase in periostin (Table 6.1). Immunoblotting clearly confirmed the increased concentration of this matricellular protein in dystrophin-deficient muscle (Figure 6.7 D-G, K-N). Shown are silver-stained 1D gels of *mdx-4cv* versus normal and *mdx* versus normal diaphragm preparations (Figure 6.7 A and H, respectively) and representative immunoblots of collagen-VI (Figure 6.7 B-C, I-J) and periostin (Figure 6.7 D-F, K-N). The two different antibodies for periostin display a slightly differing specificity. The antibody in Figure 6.7 D-E, K-L (antibody ab92460) distinguished two proteins bands, the periostin doublet, while the alternative immune-detection shown in Figure 6.7 F-G, M-N (NBP1-30042) recognized only a single periostin band. Both equally loaded *mdx-4cv* and *mdx* animal models of DMD exhibited greatly elevated levels of the extracellular matrix protein collagen and the matricellular component periostin. The analysis of perisotin and collagen agrees with the proteomic data presented in Table 6.1 and strongly suggest greatly elevated levels of the extracellular matrix and matricellular factors in dystrophinopathy.

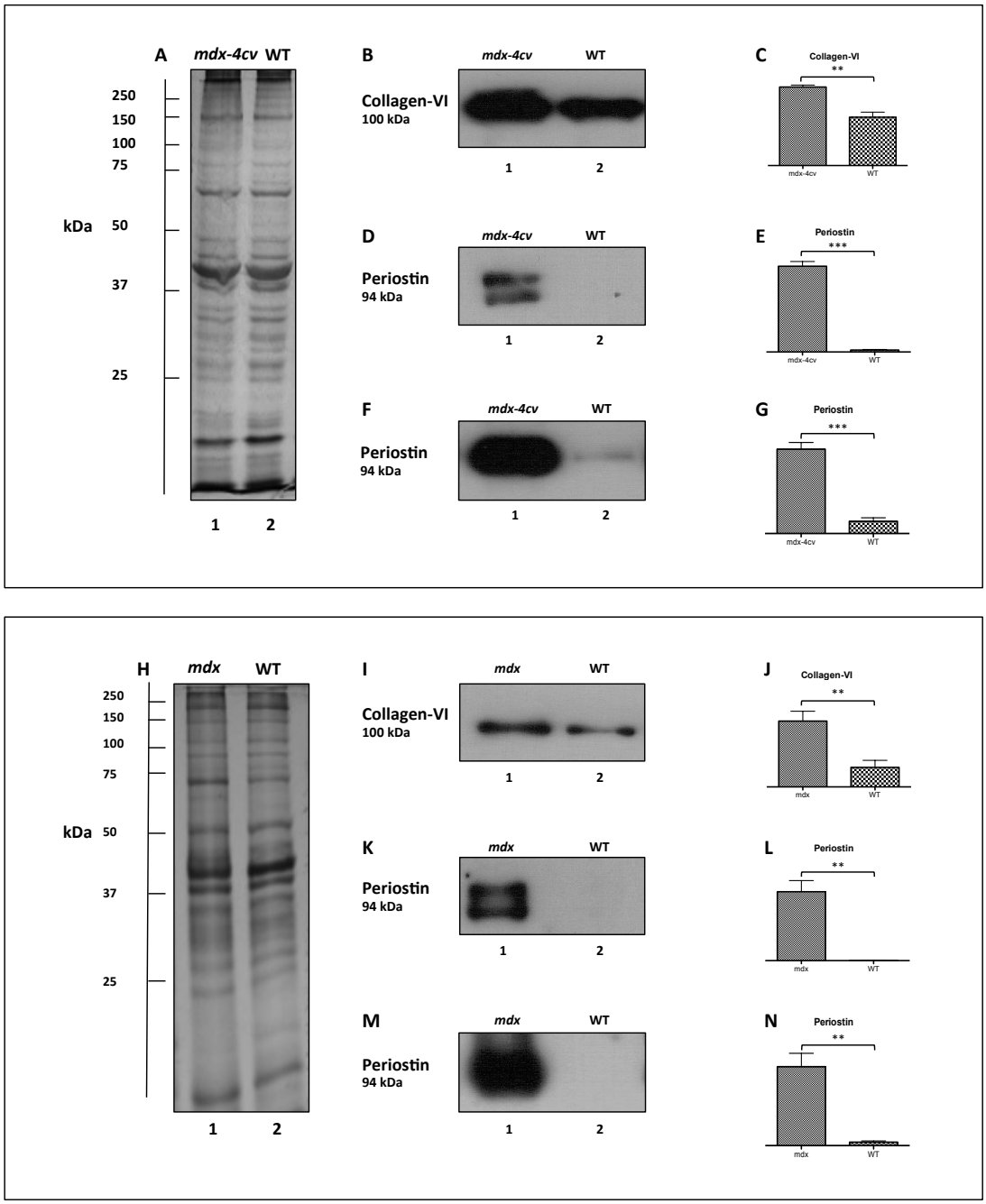

Figure 6.7 Immunoblot analysis of collagen and periostin in *mdx-4cv* and *mdx* diaphragm.

Shown are silver-stained 1D gels (A, H) and representative immunoblots with expanded views of antibody-labelled bands (B, D, F, I, K, M). Immunoblotting was carried out with antibodies to collagen-VI (B-C, I-J) and periostin (D-E, K-L: antibody ab92460; F-G, M-N: antibody NBP1-30042). Lanes 1 and 2 in (A-G) represent 3-month old *mdx-4cv* diaphragm and 3-month old wild-type (WT) diaphragm, and lanes 1 and 2 in (I-N) represent 3-month old *mdx* diaphragm and 3-month old wild-type (WT) diaphragm, respectively. The graphical presentation represents the statistical analysis of immunoblotting to collagen-VI (C, J) and periostin (E, G, L, N). Student's *t*-test, unpaired; $n \geq 4$; $^{**}p < 0.01$; $^{***}p < 0.001$).

6.2.5 Histological and immunofluorescence microscopy analysis of *mdx-4cv* diaphragm muscle

Initial histological and immunofluorescence microscopical examinations of dystrophin-deficient *mdx-4cv* diaphragm sections confirmed the presence of fibrosis, necrosis, and central nucleation (Figure 6.8). Since the label-free LC-MS/MS analysis of the dystrophic *mdx-4cv* versus normal diaphragm has revealed changes in several notable proteins associated with disease related fibrosis, it was important to confirm these findings by an alternative method to immunoblotting, as seen in Figure 6.7. Figure 6.9 illustrates the findings from an immunofluorescence microscopy survey of *mdx-4cv* versus normal diaphragm muscle tissue. Cryosections of *mdx-4cv* and WT diaphragm muscle showed comparable levels of the extracellular matrix protein laminin (Figure 6.9 A, B) and complete absence of the dystrophin isoform Dp427 (Figure 6.9 C, D) in the diseased *mdx-4cv* diaphragm compared to the normal WT. Collagen-VI (Figure 6.9 E, F) and periostin (Figure 6.9 G, H) both exhibited up-regulation in the *mdx-4cv* diaphragm compared to WT sections. Immunofluorescence microscopy was also employed to illustrate localization of these select proteins, and revealed similar extracellular matrix/surface localization patterns both dystrophic and WT sections for each of the proteins under investigation (green). Sections were counter stained with the nuclear binding dye DAPI (blue), and shown in Figure 6.9 are the merged images containing staining for both protein of interest and nuclear component. This immunofluorescence microscopy analysis confirms and further validates the findings from the label-free LC-MS/MS analysis (Table 6.1) and immunoblotting surveys presented in this study (Figure 6.4 A-D; Figure 6.7 B-G and I-N).

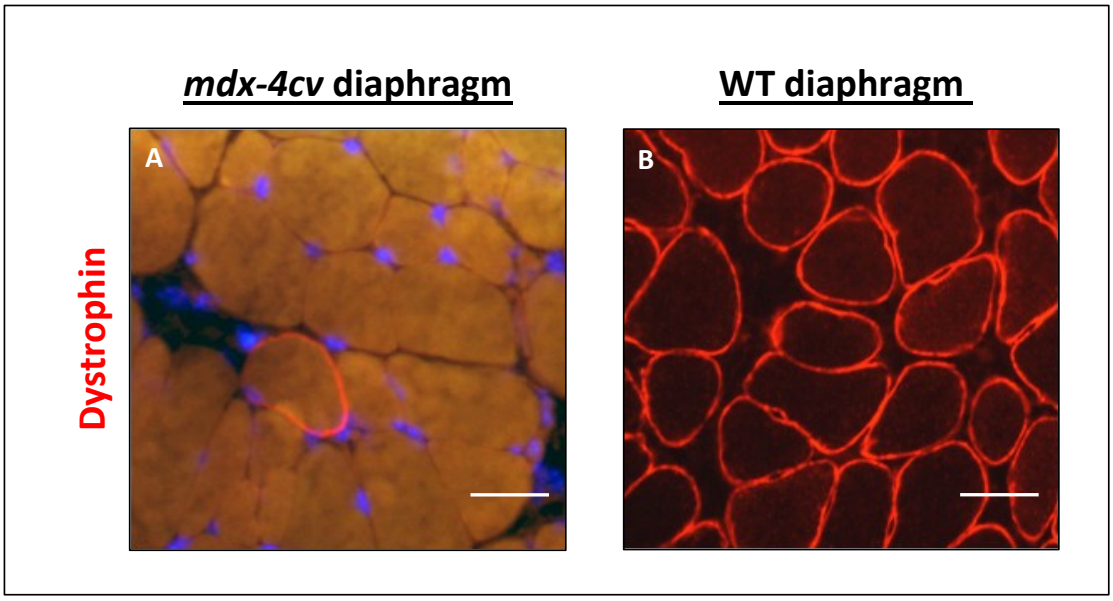

Figure 6.8 Histological and immunofluorescence microscopical examinations of dystrophin-deficient *mdx-4cv* diaphragm.
Shown above in panel A is a histological *mdx-4cv* diaphragm section in which the cytoskeletal protein dystrophin, red, is scarce. Blue shading indicates staining of the nuclei with DAPI. On the right in panel B is an immunofluorescently stained section of normal WT diaphragm mouse muscle, colored red is the structural muscle fibre protein dystrophin. Bars equal 30 µm.
*Image kindly provided by collaborator Margit Zweyer from the Department of Physiology II, University of Bonn, Germany.

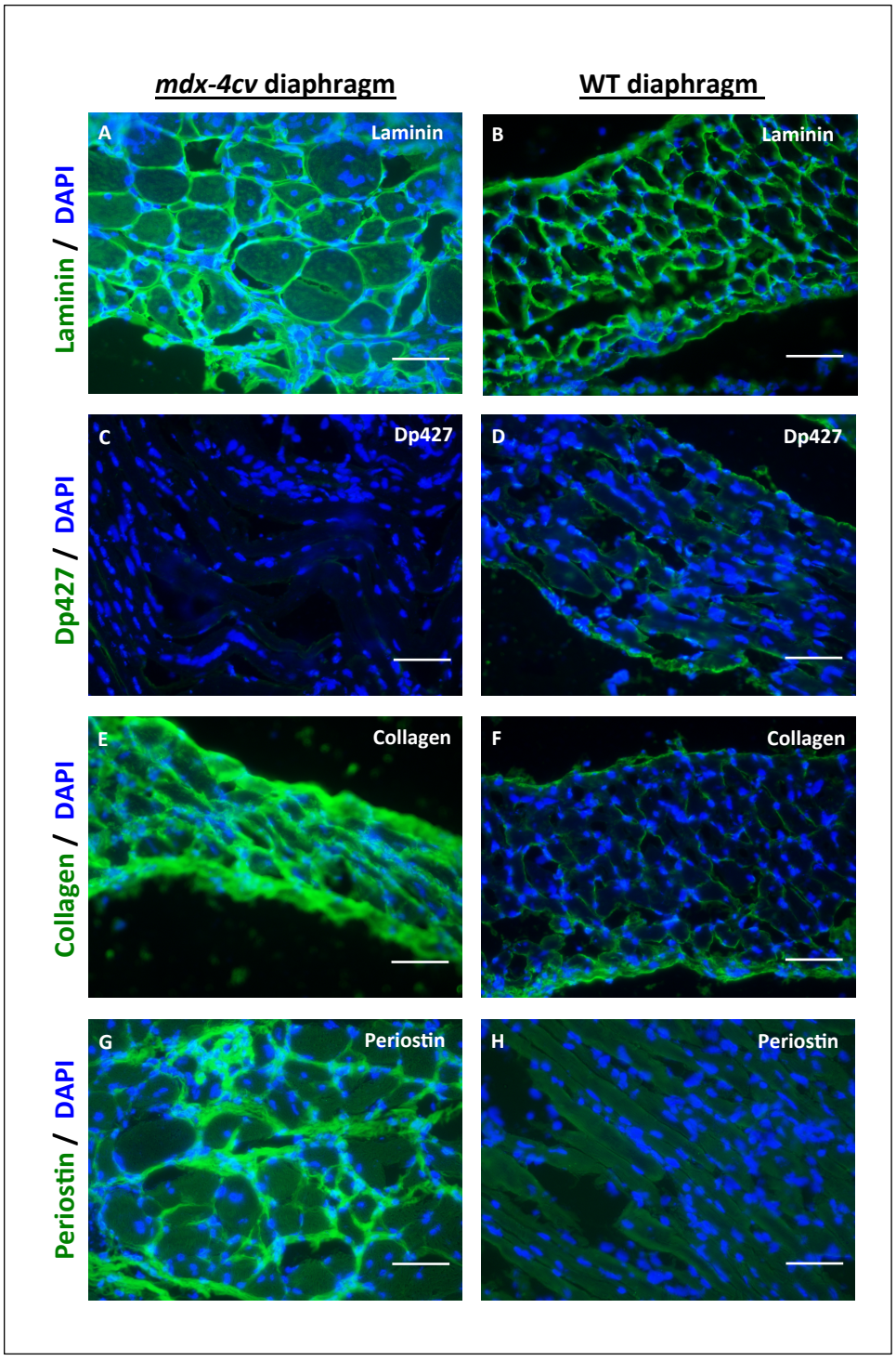

Figure 6.9 Immunofluorescence microscopy of select proteins with an altered abundance in *mdx-4cv* versus WT diaphragm muscle cryosections.
Shown are overlaid indirect immunofluorescence microscopy images of *mdx-4cv* (A, C, E and G) versus WT (B, D, F and H) diaphragm muscle tissue cryocestions. Immunofluorescence staining was carried out with select extracellular matrix/surface membrane primary antibodies to laminin (A, B), dystrophin isoform Dp427 (C, D), collagen-VI (E, F) and periostin (G, H), shown in green and the nuclear stain DAPI in blue. Staining with secondary antibody alone was carried out as negative control (not shown). Bars equal 50 µm.

6.2.6 Immunoblot analysis of aged *mdx-4cv* versus WT diaphragm muscle

The main focus of our independent verification analysis of proteomic findings by immunoblotting was the matricellular protein periostin, an apparent marker of tissue damage and fibrosis (Conway *et al.,* 2014; Norris *et al.,* 2007; Frangogiannis *et al.,* 2012; Conway and Molkentin, 2008). In order to evaluate potential changes during aging of dystrophic versus normal muscle, diaphragm preparations from mice of 2 to 15 months of age were prepared and analyzed by comparative immunoblotting. Figure 6.10 A and B shows the overall protein expression pattern in a 1D silver stained gel and comparable levels of laminin (Figure 6.10 C, D) in the dystrophic *mdx-4cv* diaphragm versus wild type (WT) controls. These dystrophic preparations exhibited a typically greatly reduced concentration in the dystrophin-associated glycoprotein β-dystroglycan at all ages studied (Figure 6.10 E, F). However in the same preparations showed elevated levels of the matricellular protein periostin whereby this effect decreased during aging (Figure 6.10 G, H).

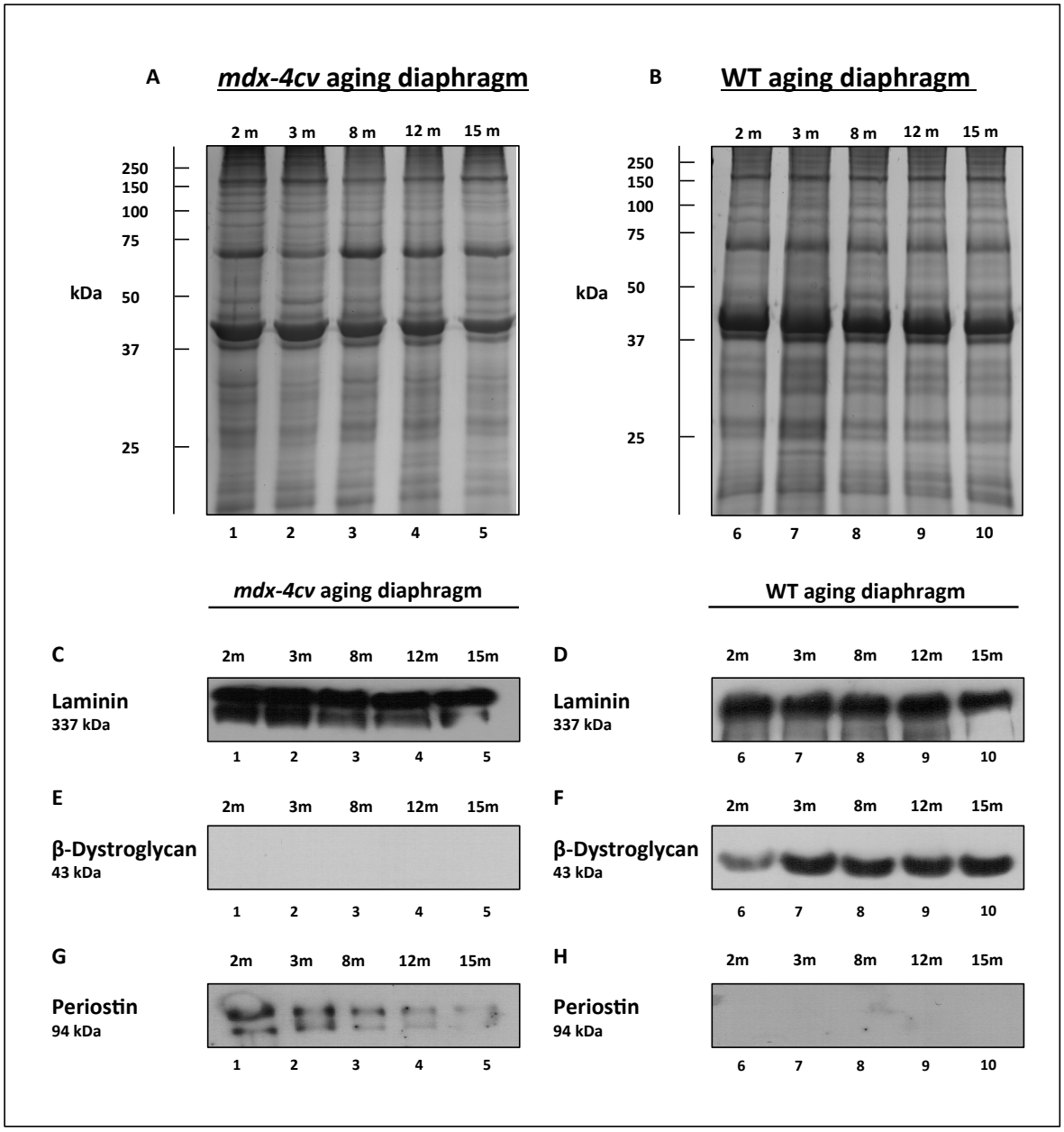

Figure 6.10 Immunoblot analysis of periostin in the aging dystrophic *mdx-4cv* diaphragm.

Shown are silver-stained 1D gels (A, B) and representative immunoblots with expanded views of immuno-decorated bands (C-H). Immunoblotting was carried out with antibodies to laminin (C, D), β-dystroglycan (E, F) and periostin (G, H). Lanes 1 to 5 and 6 to 10 represent 2, 3, 8, 12 and 15-month old *mdx-4cv* diaphragm versus wild type (WT) diaphragm preparations, respectively.

6.3 Discussion

The histopathological hallmarks of X-linked muscular dystrophy encompass substantial variations in myofiber diameter, significantly increased central nucleation, fibre splitting and degeneration-regeneration cycles in affected fibre populations (Chelly and Desguerre, 2013). In addition, one of the most striking cytoarchitectural alterations in dystrophin-deficient skeletal muscles is the extensive connective tissue proliferation in the perimysium and endomysium. Importantly, fibrosis was shown to significantly correlate with poor motor outcome in Duchenne patients (Desguerre *et al.,* 2009). Thus, dysregulation of the synthesis, assembly, accumulation and controlled degradation of collagen fibrils and resulting fibrosis probably play a critical role in the progressive pathogenesis of DMD (Kharraz *et al.,* 2014). Although DMD is due to a single gene defect that primarily affects the membrane cytoskeleton, dystrophinopathy manifests itself as a fibrosis disease causing loss of cellular elasticity and tissue scaring and forming a barrier that may hamper cell- or gene-based therapies (Partridge, 2011; Benedetti *et al.,* 2013). In order to better understand the molecular mechanisms that underlie fibrosis and the decreased ability to voluntarily move muscles, proteomic profiling was used to identify global changes in the severely dystrophic *mdx-4cv* diaphragm.

6.3.1 Collagen and the *mdx-4cv* diaphragm

The considerable changes in markers of the extracellular matrix and the cytoskeletal network agree with a general tendency of dystrophin-deficient skeletal muscle to undergo both a massive collagen deposition and substitution

of contractile fibres with fibrotic tissue and compensatory restructuring of the cytoskeleton. The label-free MS analysis of the *mdx-4cv* diaphragm presented here in Table 6.1 has clearly shown a drastic increase in collagen, i.e. collagen alpha-1(I) chain, collagen alpha-2(I) chain and collagen alpha- 1(VI) chain. This agrees with previous gene expression studies (Goldspink *et al.,* 1994) and proteomic surveys of the *mdx soleus* muscle (Carberry *et al.,* 2013A) and the aged *mdx* diaphragm (Carberry *et al.,* 2012A). Immunoblotting for collagen VI found elevated levels in both *mdx-4cv* and *mdx* diaphragm preparations at 3-months of age (Figure 6.7 B-C and I-J) and similarly via immunofluorescence microscopy for *mdx-4cv* cryosections (Figure 6.9 E, F). Although natural aging is also associated with an increased accumulation of collagen (Carberry and Ohlendieck, 2013), X-linked muscular dystrophy exhibits a much greater degree of fibrotic changes in dystrophin-deficient muscle tissue (Holland *et al.,* 2014B). Collagen deposition and fibrosis are related to the increased expression of TGF-β1 (Vidal *et al.,* 2008) and appear to occur prior to substantial muscle degeneration (Graham *et al.,* 2010) and have been clearly linked to abnormal functioning of the *mdx* diaphragm and respiratory impairment (Ishizaki *et al.,* 2008). Collagen functions as a major structural element in skeletal muscle and exists in a variety of isoforms, i.e. collagen I to XVIII (Gillies and Lieber, 2011). A great variety of theses isoforms is transiently expressed during myogenesis, but adult muscle exhibits predominantly collagen type I in the perimysium and collagen type III in the endomysium and epimysium. The main collagen present in the muscle basement membrane is type IV, but the types VI, XV and XVIII have also been shown to be part of the collagen network close to the sarcolemma (Gillies and Lieber, 2011). The filament-forming collagen type VI is a crucial interstitial

matrix component interacting with collagen IV and perlecan of the basal lamina, as well as biglycan, fibronectin, decorin and sarcolemmal integrins (Carmignac and Durbeej, 2012). Since the major increase in collagen isoforms of the fibrillar extracellular matrix was accompanied by the apparent up-regulation of several related extracellular matrix proteins, such as decorin, dermatopontin, asporin and prolargin, extensive alterations in the extracellular matrix seem to play a crucial role in the secondary pathogenesis of dystrophinopathy (Lieber and Ward, 2013). Fibrosis can therefore be considered a key histopathological process in the contractile dysfunction of dystrophic muscles (Desguerre *et al.,* 2009; Klingler *et al.,* 2012; Kharraz *et al.,* 2014).

6.3.2 Matricellular proteins

A crucial finding of this proteomic survey of the dystrophic diaphragm muscle is the most substantially increased protein periostin. Periostin is a matricellular component of approximately 93 kDa (Conway *et al.,* 2014). The mass spectrometric identification (Table 6.1) of this protein and its elevated expression levels in both the *mdx* and the *mdx-4cv* diaphragm (Figure 6.7 K-N and D-G, respectively) agree with a previous transcriptomic study of the *mdx* mouse model of DMD (Marotta *et al.,* 2009). This finding was our main focus of verification analysis of the *mdx-4cv* diaphragm. Periostin is a crucial regulatory factor of collagen fibrillogenesis and thus influences the biomechanical properties of connective tissues (Norris *et al.,* 2007). In contrast to structural matrix proteins, matricellular proteins probably do not play a primary role in tissue architecture, but regulate collagen fibrillogenesis and the biomechanical

properties of connective tissues (Norris *et al.,* 2007). The expression of matricellular proteins is greatly induced following injury, such as observed after cardiac infarction (Frangogiannis, 2012), and is believed to modulate cell-cell and cell-matrix interactions. Released matricellular proteins were shown to associate with a variety of signaling molecules, such as growth factors, cytokines and cell surface receptors involved in the transduction of cellular signaling cascades (Conway and Molkentin, 2008; Kühn *et al.,* 2007). Thus, although periostin is not a structural component of the ECM with a primary role in tissue architecture, its up-regulation in muscular dystrophy is probably closely related to fibre injury and the resulting modulation of cell-matrix interactions.

In analogy to increased periostin levels in heart muscle following cardiac infarction (Frangogiannis, 2012) and β1KO*mdx* hearts that are missing both dystrophin and integrin (Elsherif *et al.,* 2008), its elevated release might be coupled to disease-induced changes in growth factor and cytokine signalling at the level of the extracellular matrix (Conway and Molkentin, 2008; Kühn *et al.,* 2007).

With respect to the role of periostin in skeletal muscle, it is important to mention that this extracellular protein is present at a very low concentration in normal adult fibres. A recent study by Özdemir *et al.,* (2014) suggests that up-regulation of periostin is a function of the ECM remodeling and that periostin is a mediator with deleterious impact on conditions exhibiting fibrosis. Periostin appears to play a part in the dysregulation of the matricellular network in laminin-deficient muscular dystrophy (Mehuron *et al.,* 2014; Menezes de Oliveira *et al.,* 2014) and its deletion reduces dystrophic symptoms and fibrosis in mice by modulating the TGF-β pathway (Lorts *et al.,* 2012).

The proteomic identification of changed periostin levels in dystrophin-deficient *mdx* and *mdx-4cv* diaphragm muscle, and the verification of this finding by immunoblotting (Figure 6.7 K-N and D-G respectively) and immunofluorescence microscopy (Figure 6.9 G, H), strongly suggests that this matricellular protein is involved in secondary steps of the molecular pathogenesis of muscular dystrophy. Interestingly, the degree of elevated periostin levels appears to be highest in 2 to 3 month old *mdx-4cv* mice, but decreases in 8 to 15 month old dystrophic animals, as judged by immunoblotting (Figure 6.10 G, H). Periostin might therefore represent a useful indicator of transient changes within the ECM during dystrophic pathology. This proteomic identification of increased periostin levels in the dystrophic diaphragm has potential implications for (i) our general understanding of the crucial role of fibrosis in the pathophysiological mechanisms that underlie progressive skeletal muscle wasting in DMD, (ii) the design of improved treatment strategies that take into account the essential elimination of physical fibrosis-induced barriers to a successful pharmacological or gene therapy of dystrophinopathies (Partridge, 2011; Benedetti *et al.,* 2013) and (iii) the establishment of a comprehensive biomarker signature of muscular dystrophy (Ohlendieck, 2013). In order to improve diagnostic and prognostic methodologies and facilitate efficient therapy monitoring, ideally a panel of proteomic biomarkers would be available that includes tissue injury markers and distinct indicators of muscular dystrophy-related fibrosis. Thus, in conjunction with elevated collagen levels, periostin testing could potentially be used as a tissue-based biomarker of fibrotic changes in dystrophinopathy. This could then be correlated to altered expression levels of other marker proteins (Dowling *et al.,* 2014).

6.3.3 Additional changes in the *mdx-4cv* diaphragm

As illustrated in the PANTHER diagram, Figure 6.1, the main molecular classes of proteins with an altered abundance in the *mdx-4cv* diaphragm (Table 6.1) belong to the ECM, the cytoskeleton, cell adhesion and junction formation, ion handling, metabolite transportation, cellular signaling and enzymatic regulation. In addition to the many changes in elements of the ECM (periostin, collagen, asporin, decorin, dermatopontin, prolargin) as revealed by label-free MS, this proteomic study also suggests compensatory remodelling of the cytoskeletal networks in dystrophic fibres (Figure 6.4 C, D), including desmin (Figure 6.4 G, H), filamin, obscurin, plectin, spectrin, tubulin, vimentin and vinculin. Additional changes in lamin (Figure 6.4 E, F) might be due to alterations in the nuclear envelope. In agreement with the idea that disturbed calcium handling is involved in muscular dystrophy (Allen and Whitehead, 2011; Fong *et al.,* 1990; Hopf *et al.,* 2007; Holland and Ohlendieck, 2014D; Vallejo-Illarramendi *et al.,* 2014), a significant decrease in the cytosolic calcium binding protein parvalbumin was confirmed (Figure 6.5 A, B). The differential expression of many contractile proteins, such as myosin heavy chains, myosin light chains (Figure 6.5 G, H) and myosin binding proteins (Figure 6.6 A, B) indicates considerable rearrangements within the actomyosin apparatus (Holland and Ohlendieck, 2013). Changes in the abundant enzymes creatine kinase M-type (Figure 6.5 C, D) and carbonic anhydrase isoform CA-3 (Figure 6.5 E, F) support the concept of pathophysiological disturbances in nucleotide metabolism and CO_2-removal, respectively. Altered concentration levels of metabolic enzymes, belonging both to the glycolytic pathway and mitochondrial bioenergetics mechanisms, do no indicate a clear switch in muscle metabolism due to

deficiency in dystrophin isoform Dp427 (Carberry *et al.,* 2013A). The increase in the molecular chaperones HSP-71 and HSP-90α agrees with the pathobiochemical concept of increased cellular stress in muscular dystrophy (Doran *et al.,* 2006A; Brinkmeier and Ohlendeick, 2014).

6.3.4 Potential biomarkers of muscular dystrophy

The results from the label-free LC-MS/MS analysis of the severely dystrophic diaphragm are highly interesting in relation to establishing a potentially disease stage-specific and muscle subtype-relevant biomarker signature of dystrophinopathy. In contrast to the dystrophic diaphragm, the recent proteomic profiling and comparative immunoblot survey of cardiomyopathic tissue from the aged *mdx* mice revealed the disintegration of the basal lamina structure and the cytoskeletal network in the dystrophin-deficient cardiac fibres (Holland *et al.,* 2013B; see also Chapter 5). The heart of senescent *mdx* mice showed a considerable reduction in laminin, which is not the case in *mdx* skeletal muscle (Carberry *et al.,* 2013A; Carberry *et al.,* 2013B). In addition, drastically increased levels of antibodies in a potential autoimmune reaction of the degenerating heart, compensatory binding of excess iron and a general perturbation of metabolic pathways were established as characteristic features of dystrophy-associated cardiomyopathy (Holland *et al.,* 2013B; Lewis *et al.,* 2010). The fact that the aged heart from *mdx* mice exhibit distinct pathological changes agrees with the clinical finding that the majority of DMD patients develop serious cardiomyopathic complications in the second decade of life (Holland and Ohlendieck, 2014D). In the future, it will be of interest to

perform label-free LC-MS/MS studies that directly compare mildly versus severely affected muscles that are dystrophin deficient. The various *mdx* type mouse models of DMD are ideal systems to carry out such a large comparative survey, since they exhibit age-dependent variations in the degree of fibre degeneration in different sub-types of muscles (Holland *et al.,* 2014B). It might then be possible to establish a muscle type-specific marker panel in relation to secondary changes in cellular signaling, metabolite transportation, antibody response, excitation-contraction-relaxation cycles, basal lamina stabilization, metabolic regulation and cytoskeletal organization.

6.3.5 Conclusion

The label-free MS analysis of the dystrophin-deficient *mdx-4cv* diaphragm has revealed a highly complex pattern of proteome-wide changes in the dystrophic skeletal muscle protein constellation. The proteomic identification and immunoblot and immunofluorescence validation of a significant up-regulation of the matricellular protein periostin agrees with the idea of progressive fibrosis being a major histopathological feature of X-linked muscular dystrophy. In the future, the altered concentration of periostin in dystrophinopathy and related signaling molecules and regulatory enzymes might be exploitable for improving diagnostic, prognostic and therapy monitoring approaches in DMD research.

Chapter 7

General Discussion

7. General Discussion

Over the past decade skeletal muscle proteomics has developed into a new discipline within the field of basic and applied myology (Gelfi *et al.,* 2011). The systematic application for proteomics in the field of neuromuscular disorders such as amyotrophic lateral sclerosis, ALS, and Duchenne muscular dystrophy, DMD, has (i) resulted in the confirmation of the complexity of the muscle proteome due to the disease (Dowling *et al.,* 2014), and (ii) the identification of a large number of new biomarker candidates of secondary changes in denervated (Ekegren *et al.,* 2008) or dystrophin deficient tissue (Rouillon *et al.,* 2014; Martin *et al.,* 2014), respectively.

Pathobiochemical insights from label-free mass spectrometry and fluorescent 2D-DIGE analyses are of crucial interest to the field of muscle pathology but are also crucial for furthering the discovery of specific protein biomarkers of ALS (Staunton *et al.,* 2011; Holland *et al.,* 2014A; Dowling *et al.,* 2014). Figure 7.1 summaries the main groups of muscle-associated proteins altered in the wobbler model of motor neuron disease as determined from Chapter 3. Interesting new findings from this research include the identification of increased levels of certain mitochondrial proteins, suggesting that muscular atrophy in WR muscle is not directly linked to the slow-to-fast fibre type shifting, but probably initially involves a preferential loss of neuromuscular synapses that function under normal conditions within a fast type of innervation process.

A promising new muscle-associated biomarker of motor neuron disease is the fast isoform of MBP-C. A decrease in this major auxiliary protein of the contractile apparatus was demonstrated by the fluorescent 2D-DIGE technique (Staunton *et al.,* 2011), label free mass spectrometry analysis (Chapter 3; Holland

et al., 2014A) and the transcriptomic screening of ALS muscle biopsies (Shtilbans *et al.,* 2011), making this filament-associated component a suitable biomarker candidate of ALS.

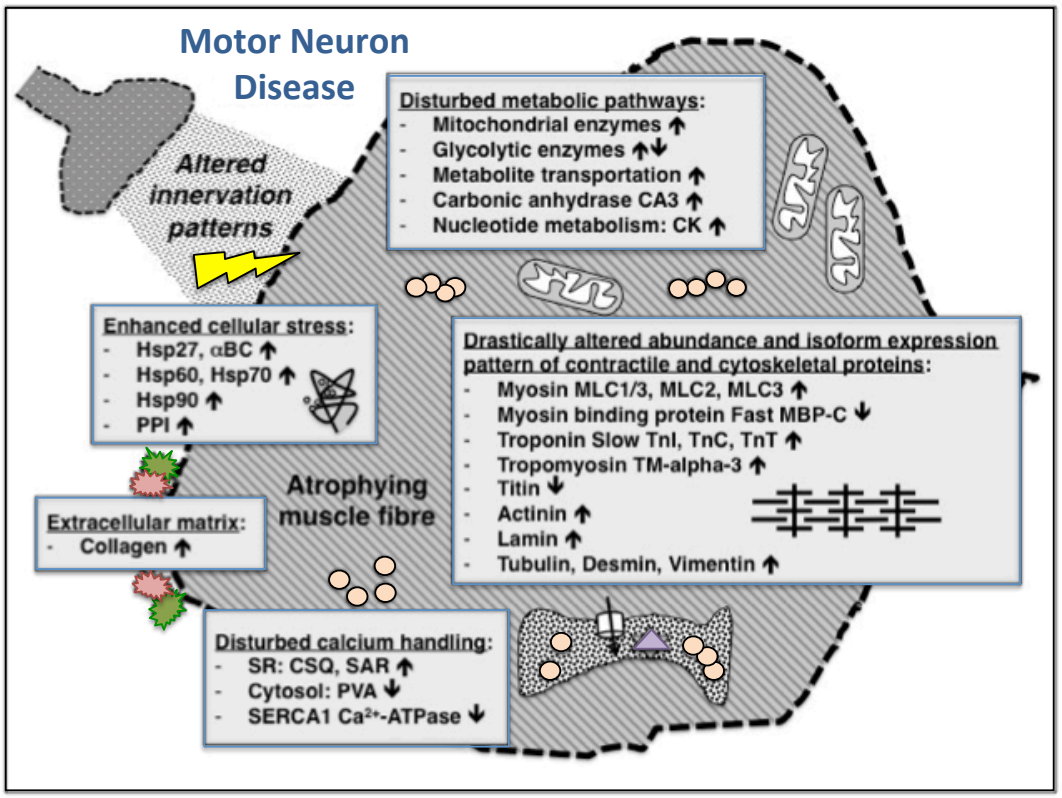

Figure 7.1 Overview of the major pathobiochemical changes in motor neuron disease as revealed by mass spectrometry based proteomics.
Listed are the subcellular regions, metabolic pathways, cellular processes and protein families that are majorly altered in skeletal muscle due to the progressive neurodegeneration. Various newly identified muscle-associated proteins with a changed abundance may be useful as novel biomarker candidates for the design of improved diagnostic, prognostic or therapy monitoring assay systems.
*Image from Holland and Ohlendieck, 2014C

The future screening of large numbers of human ALS patient muscle samples will be needed to fully establish the newly identified proteomic markers as reliable indicators of disease related muscular atrophy. These proteins show promise and could potentially be exploitable to design superior prognostic and

therapy monitoring assay systems consisting of a meaningful and diagnostically conclusive biomarker signature.

Going forward, it can be expected that ALS specific biomarkers will play a prominent role for a more accurate diagnosis, the proper monitoring of muscular atrophy and the determination of clinical outcome measures (Elf *et al.,* 2014).

The 2D-DIGE proteomic profiling of WR testis presented in Chapter 4 revealed distinct changes in spermatid specific proteins. It is reasonable to conclude these proteome-wide alterations in testis tissue are probably due to variations in the WR sperm population. Future comparative studies will hopefully determine distinct alterations in proteins in isolated preparations from WR versus WT mouse sperm. Based on the findings from the proteomic data in Chapter 4, it can be concluded that the reduced concentration of the GARP component VPS-54 is linked to secondary disturbances in crucial metabolic pathways, including an impaired utilization of fatty acid molecules. This could indirectly be linked with defects in WR sperm assembly and a failure to properly form an acrosome and an elongated sperm head. The complexity of the proteome wide changes in WR testis and probable relation to sperm abnormalities is summarised in Figure 7.2.

The currently available proteomic datasets, including the dataset presented here in Chapter 4, of normal and diseased spermatozoa from human and animals are of crucial importance to the field of biomedicine (Rahman *et al.,* 2013) and agriculture (Peddinti *et al.,* 2008). Biochemical, physiological and cell biological studies can potentially be planned in detail to further characterise the biological functions and/or pathobiochemical roles of newly identified sperm-associated proteins (Hamada *et al.,* 2012). The exploration for reliable proteomic

biomarkers of fertility and infertility are vital for improving diagnostic and prognostic procedures and recognising new therapeutic routes to treat sperm abnormalities such as globozoospermia (Holland and Ohlendieck, 2015).

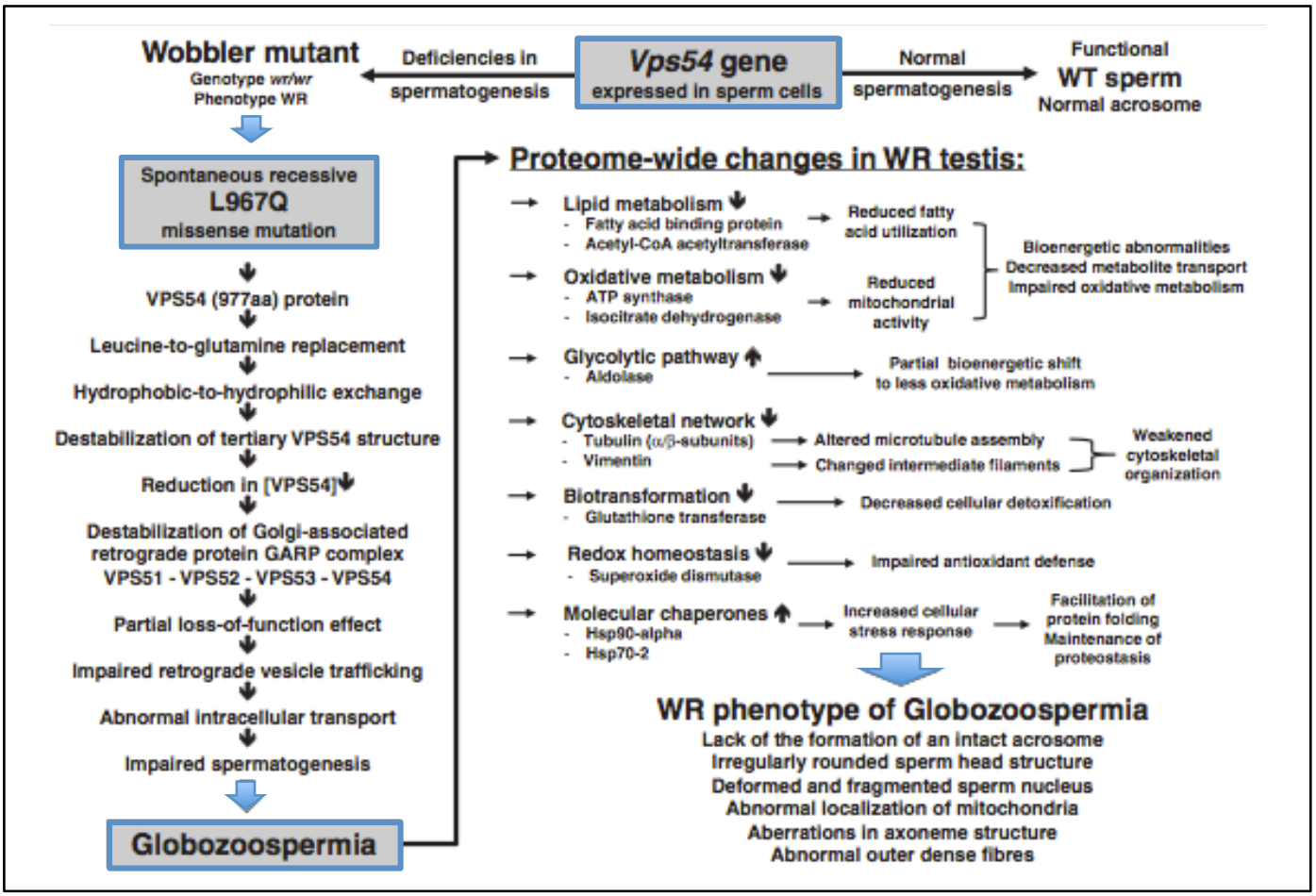

Figure 7.2 Proteomic consequences due to mutation in the *Vps54* gene in WR mice. Flowchart of proteome wide changes in WR testis and the potential relationship to the globozoospermia phenotype based on mutation in the *Vps54* gene.
*Image from Holland and Ohlendieck, 2014B

Globozoospermia is a rare, but not uncommon, sperm abnormality (Dam *et al.,* 2007). The comparative proteomic screening of isolated sperm cells or testis samples has great biomedical potential for the swift identification of novel markers of down-stream alterations in spermatozoa and supportive cells due to inherited abnormalities (Holland and Ohlendieck, 2015). The establishment of a biomarker signature of male fertility includes the elucidation of protein factors involved in capacitation, sperm motility, the acrosomal reaction, gamete interactions, and egg–sperm fusion (Holland and Ohlendieck, 2015). Protein factors with a great potential for being exploitable to improve male contraceptive strategies are cellular antigens for antibody-based sperm neutralization, in-addition to pharmacological blockers of sperm receptor complexes involved in gamete recognition or biochemical modifiers of essential enzyme activities involved in sperm metabolism and cellular motility, as illustrated in Figure 7.3. Identifying new targets to counteract male infertility is an important biomedical factor; key protein families of interest identified in Chapter 4 include sperm receptors, molecular chaperones, metabolic enzymes, metabolite transporters, cytoskeletal proteins, ion channels and proteasome components.

Proteomics-based discovery of new molecular targets will be essential to guide the future advancement of innovative pharmacological approaches, including the support of hormonal treatments, anti-inflammatory therapy, antibiotic procedures, antioxidant therapy, and enzyme modulation (Hamada *et al.,* 2012).

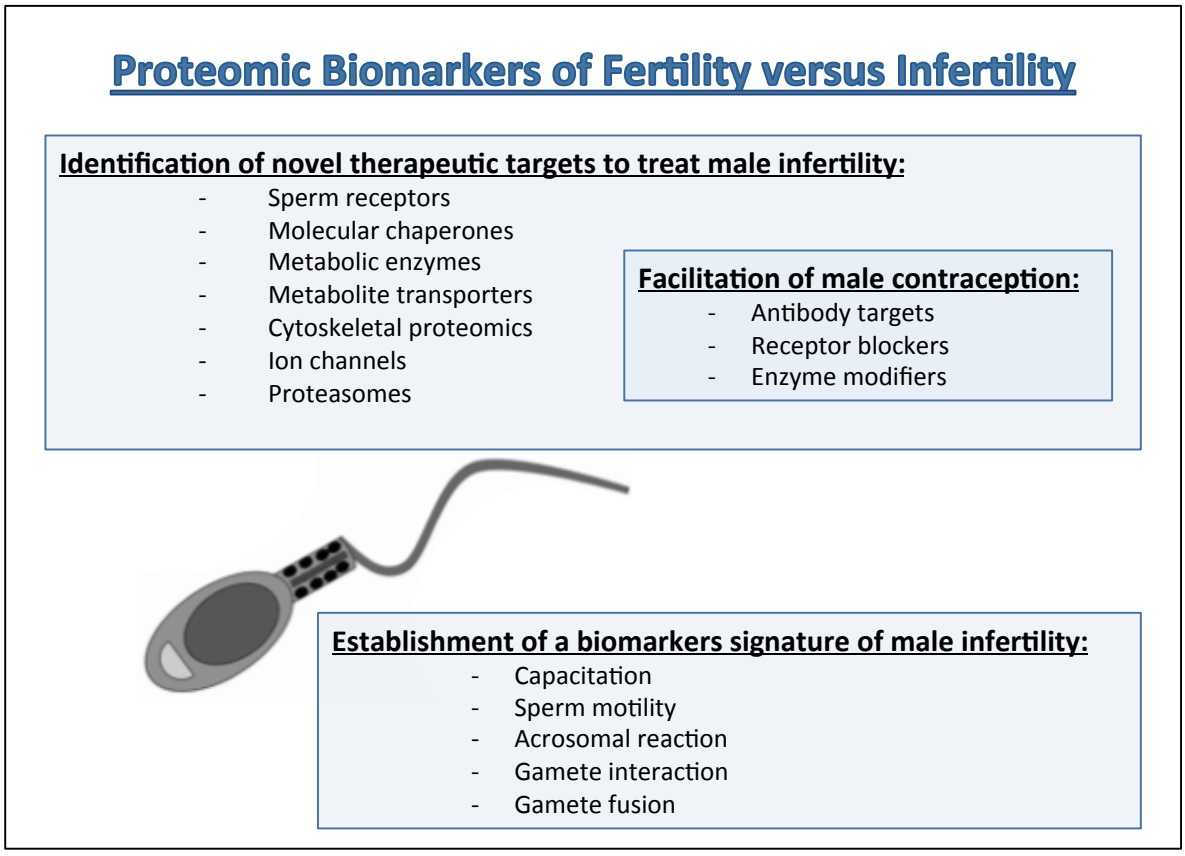

Figure 7.3 Proteomic biomarkers of fertility versus infertility.
Summary of the importance of sperm proteomics with respect to establishing a biomarker signature of male infertility, male contraceptive strategies and the treatment of male infertility.
*Image from Holland and Ohlendieck, 2014B

As illustrated and verified in Chapter 5, label-free mass spectrometry based proteomic profiling has clearly established the *mdx* mouse as a suitable and ideal animal model for exploring molecular and cellular aspects of cardiac pathogenesis. Further to that, the *mdx* heart was shown as a highly appropriate organ system for studying the progressive aspects of muscular dystrophy associated cardiomyopathy.

Figure 7.4 contains a flowchart summarising the variety of biochemical, physiological and cellular abnormalities that result in cardiac fibrosis and the progressive functional decline of the cardiovascular system (Holland and Ohlendieck, 2014A). The application of comparative proteomics present in Chapter 5 has identified a large number of new modifications in cardiac proteins associated with cellular signalling mechanisms, mitochondrial energy metabolism, glycolysis, antibody response, iron binding, the contraction-relaxation cycle, basal lamina stabilisation and organisation of the cytoskeleton. These novel protein marker candidates from Chapter 5 can now be used for the systematic screening of the cardiac *mdx* heart following experimental therapeutic interventions.

The combination of employing both gel-based and label-free mass spectrometry promises the most comprehensive coverage of the cardiac proteome, including highly hydrophobic components, low-abundance elements, proteins with extreme p*I,* and proteins with extensive PTMs (Lewis *et al.,* 2010; Dowling *et al.,* 2014; Holland and Ohlendieck, 2014A).

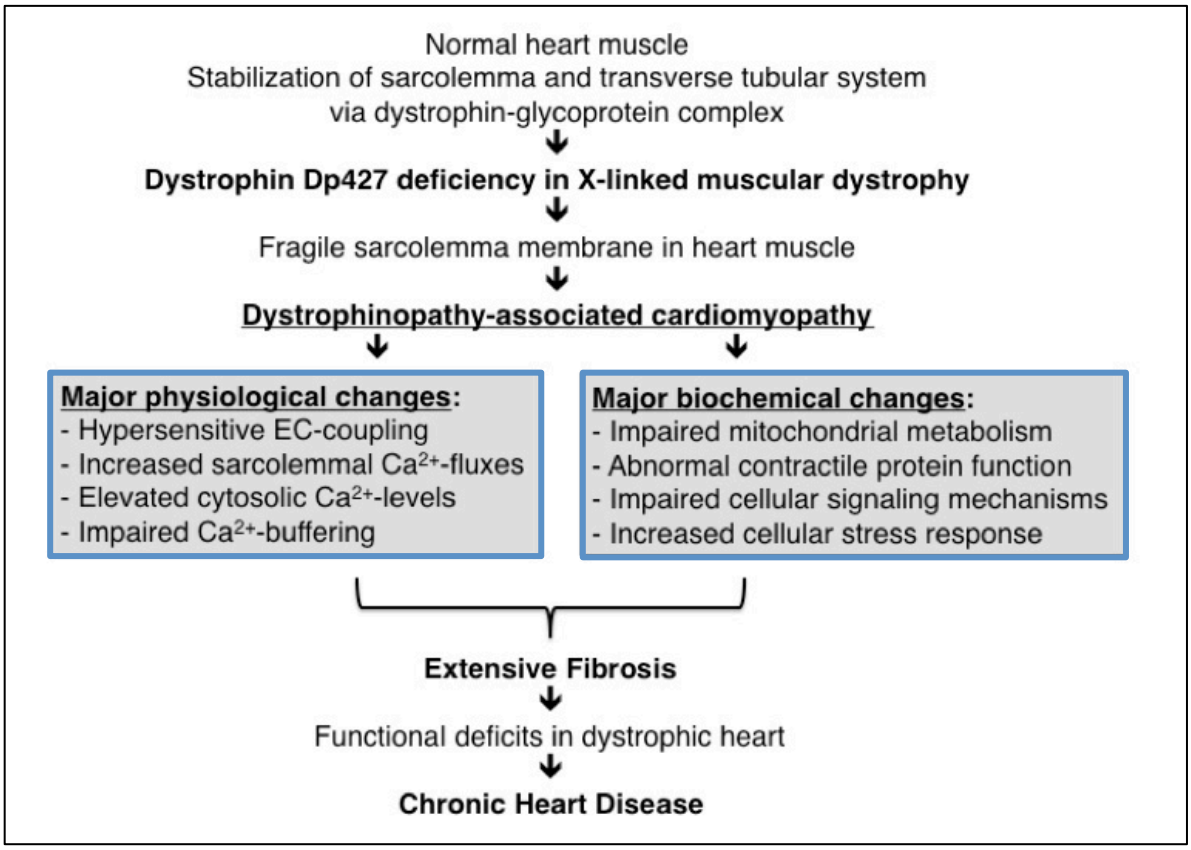

Figure 7.4 Molecular pathogenesis of muscular dystrophy-associated cardiomyopathy.
Shown is a flowchart of major pathophysiological and pathobiochemical changes that render the dystrophin-deficient heart more susceptible to fibre degeneration and fibrosis, which in turn eventually triggers chronic heart disease in dystrophinopathies. Key changes in the physiological regulation of the dystrophic heart are associated with abnormal calcium handling and hypersensitive excitation-contraction, EC, coupling. *Image from Holland and Ohlendieck, 2014A

Chapter 6 employed label-free proteomic profiling methodologies for the identification of novel biomarkers and the elucidation of new pathobiochemical mechanisms that underlie the progressive muscle wasting in dystrophic animals. This study focused on the severely dystrophic diaphragm from the not extensively characterised *mdx-4cv* mouse and identified an interesting pathoproteomic signature. The revelation of a highly complex pattern of proteome wide alterations and the recognition of the matricellular protein periostin as a potential factor involved in dystrophinopathy-related fibrosis has huge potential for future exploitation. The altered concentration of periostin in dystrophinopathy and related signalling molecules and regulatory enzymes has significance in disease related fibrosis can potentially be exploitable for improving diagnostic, prognostic and therapy monitoring approaches in future DMD research (Dowling *et al.,* 2014).

The altered proteomic expression patterns present in dystrophic skeletal muscle fall into a broad range of categories including impaired excitation-contraction coupling, disturbed ion homeostasis altered surface marker proteins, reduction in the dystrophin complex, loss of sarcolemmal integrity, disturbed metabolic pathways, elevated stress response and increases in the extracellular matrix (Doran *et al.,* 2004; Doran *et al.,* 2006B; Lewis *et al.,* 2010; Carberry *et al.,* 2012A; Holland *et al.,* 2013B). Figure 7.5 provides an overview of the subcellular localisation and disease related concentration changes of these major biomarker candidates of dystrophinopathies (Dowling *et al.,* 2014). The majority of protein families outlined here have been identified by mass-spectrometry based proteomics, and can potentially be employed as biomarker candidates for dystrophinopathies.

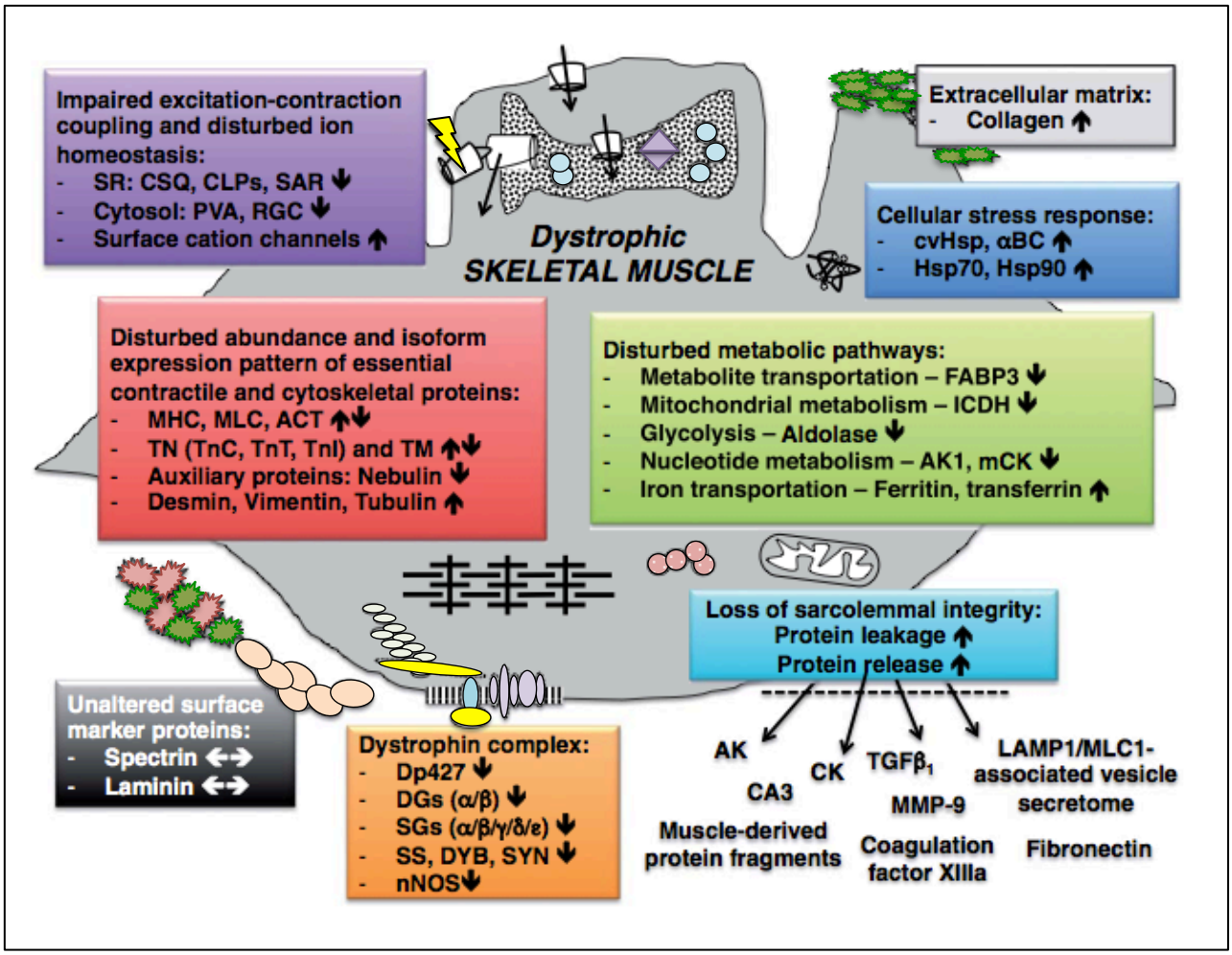

Figure 7.5 Dystrophic skeletal muscle.
Shown is an overview of the subcellular localisation and disease-related concentration changes of major biochemical candidates of dystrophinopathies. This illustration summarises the majority of protein families that have been identified by mass spectrometry-based proteomics as potential biomarker candidates.
*Image from Dowling *et al.,* 2014

Recent experiments in biomarker discovery for muscular dystrophies have used alternative sources to the invasive method of muscle biopsies presented here, including the minimally invasive serum markers (Hathout *et al.,* 2015; Rouillon *et al.,* 2015) and non-invasive urine markers (Rouillon *et al.,* 2014). Current potential urine markers include specific fragments of the contractile apparatus protein titin in DMD patients (Rouillon *et al.,* 2014). Proteomic profiling of serum from DMD patients has revealed MYOM3 fragments as a potential biomarker for monitoring the outcome of therapeutic interventions in muscular dystrophies (Rouillon *et al.,* 2015). Combinations of these potential novel biomarkers combined with the biomarkers presented in Chapters 5 and 6 could potentially be employed as a superior biomarker signature for dystrophinopathies.

7.1 Concluding remarks

The muscle specific and disease associated proteins presented throughout this research will be extremely useful for the evaluation of novel biomarkers signatures of neuromuscular disorders and the identification of new therapeutic targets. In order to progress this research and drive it forward towards more clinically relevant biomarkers further experimentation and validation in human muscle biopsies is crucial. These results should ideally be cross-checked with protein levels in minimally invasive serum markers (Hathout *et al.,* 2015; Rouillon *et al.,* 2015; Anaya-Segura *et al.,* 2015) and non-invasive urine markers (Rouillon *et al.,* 2014). In addition to this, with respect to biomarker signatures, further exploration and validation should ideally include DNA, RNA, protein and metabolites, spanning the multiple biomolecular levels.

The research presented here is an ideal first step at creating this on a proteomic level and advancing the field towards a reliable disease specific biomarker signature. However future combinations of parallel tests that determine significant changes in disease specific muscle associated proteomic biomarkers, muscle derived proteins or protein fragments are required. This combination appears to be the most appropriate approach for the comprehensive diagnostic, prognostic and therapeutic evaluation of neuromuscular disorders.

Chapter 8

Bibliography

8. Bibliography

Agbulut, O., Noirez, P., Butler-Browne, G. and Jockusch, H. 2004. Specific isomyosin proportions in hyperexcitable and physiologically denervated mouse muscle. *FEBS Letters.* 561, 191–194.

Alfaro, L.A., Dick, S.A., Siegel, A.L., Anonuevo, A.S. *et al.* 2011. CD34 promotes satellite cell motility and entry into proliferation to facilitate efficient skeletal muscle regeneration. *Stem Cells.* 29(12), 2030–2041.

Allen, D.G. and Whitehead, N.P. 2011. Duchenne muscular dystrophy - what causes the increased membrane permeability in skeletal muscle? *International Journal of Biochemistry and Cell Biology.* 43, 290-294.

Allen, D.G., Gervasio, O.L., Yeung, E.W. and Whitehead, N.P. 2010. Calcium and the damage pathways in muscular dystrophy. *Canadian Journal of Physiology and Pharmacology.* 88, 83–91.

Altelaar, A.F. and Heck, A.J. 2012. Trends in ultrasensitive proteomics. *Current Opinions Chem Biol.* 16(2), 206-213.

Altelaar, A.F., Munoz, J. and Heck, A.J. 2013. Next-generation proteomics: towards an integrative view of proteome dynamics. *Nature Reviews Genetitics.* 14, 35-48.

Alvarez Sedo, C., Rawe, V.Y. and Chemes, H.E. 2012. Acrosomal biogenesis in human globozoospermia: immunocytochemical, ultrastructural and proteomic studies. *Human Reproduction.* 27, 1912–1921.

Ameen, V. and Robson, L.G. 2010. Experimental models of Duchenne muscular dystrophy: relationship with cardiovascular disease. *Open Cardiovascular Medical Journal.* 4, 265–77.

Amlani, S. and Vogl, A.W. 1988. Changes in the distribution of microtubules and intermediate filaments in mammalian Sertoli cells during spermatogenesis. *Anatomical Record.* 220, 143–160.

Anaya-Segura, M.A., García-Martínez, F.A., Montes-Almanza, L.A., Díaz, B.G., *et al.* 2015. Non-invasive biomarkers for Duchenne muscular dystrophy and carrier detection. *Molecules.* 20(6), 11154-11172.

Andrews, J.M., Gardner, M.B., Wolfgram, F.D., Ellison, G.W., *et al.* 1974. Studies on a murine form of spontaneous lower motor neuron degeneration-the wobbler (wr) mouse. *American Journal of Pathology.* 76**,** 63–78.

Au, C.G., Butler, T.L., Sherwood, M.C., Egan, J.R. *et al.* 2011. Increased connective tissue growth factor associated with cardiac fibrosis in the *mdx* mouse model of dystrophic cardiomyopathy. *International Journal of Experimental Pathology.* 92, 57–65.

Ayoglu, B., Chaouch, A., Lochmüller, H., Politano, L., *et al.* 2014. Affinity proteomics within rare diseases: a BIO-NMD study for blood biomarkers of muscular dystrophies. *EMBO Molecular Medicine.* 6, 918-936.

Bach, J.R. and Martinez, D. 2011. Duchenne muscular dystrophy: continuous noninvasive ventilatory support prolongs survival. *Respiratory Care*. 56, 744-750.

Baker, M.A., Hetherington, L., Reeves, G.M. and Aitken, R.J. 2008. The mouse sperm proteome characterized via IPG strip pre-fractionation and LC-MS/MS identification. *Proteomics.* 8, 1720–1730.

Baker, M.A., Naumovski, N., Hetherington, L., Weinberg, A. *et al.* 2013. Head and flagella sub-compartmental proteomic analysis of human spermatozoa. *Proteomics.* 13*,* 61–74.

Baker, M.A., Nixon, B., Naumovski, N. and Aitken, R.J. 2012. Proteomic insights into the maturation and capacitation of mammalian spermatozoa. *Systems Biology in Reproductive Medicine. 58,* 211–217.

Baker, M.A., Reeves, G., Hetherington, L. and Aitken, R.J. 2010. Analysis of proteomic changes associated with sperm capacitation through the combined use of IPG-strip pre-fractionation followed by RP chromatography LC-MS/MS analysis. *Proteomics.* 10, 482–495.

Baker, M.A., Witherdin, R., Hetherington, L., Cunningham-Smith, K., *et al.* 2005. Identification of post-translational modifications that occur during sperm maturation using difference in two-dimensional gel electrophoresis. *Proteomics*. 5, 1003–1012.

Banks, G.B. and Chamberlain, J. S. 2008. The value of mammalian models for Duchenne muscular dystrophy in developing therapeutic strategies. *Current Topics in Developmental Biology.* 84, 431-453.

Banks, G.B., Combs, A.C. and Chamberlain, J.S. 2010. Sequencing protocols to genotype *mdx*, *mdx (4cv)* and *mdx (5cv)* mice. *Muscle Nerve.* 42, 268-270.

Bar, S., Barnea, E., Lavy, Z., Neuman, *et al.* 1990. A novel protein product of the Duchenne muscular dystrophy gene which greatly differs from known isoforms in its structure and tissue distribution. *Biochemistry Journal.* 272, 557-560.

Barnabei, M.S. and Metzgerm, J.M. 2012. Ex vivo stretch reveals altered mechanical properties of isolated dystrophin-deficient hearts. *PLoS One.* 7, e32880.

Bastone, A., Fumagalli, E., Bigini, P., Perini, P., *et al.* 2009. Proteomic profiling of cervical and lumbar spinal cord reveals potential protective mechanisms in the wobbler mouse, a model of motor neuron degeneration. *Journal of Proteome Research.* 8, 5229–5240.

Beghi, E., Mennini, T., Bendotti, C., Bigini, P., *et al.* 2007. The heterogeneity of amytrophic lateral sclerosis: a possible explaination of the treatment failure. *Current Medicinal Chemistry.* 14(30), 3185-3200.

Benedetti, S., Hoshiya, H. and Tedesco, F.S. 2013. Repair or replace? Exploiting novel gene and cell therapy strategies for muscular dystrophies. *FEBS Journal.* 280, 4263-4280.

Berger, M.J. and Doherty, T.J. 2010. Sarcopenia: prevelance, mechanisms, and functional consequences. *Interdiscip. Top. Gerontology.* 37, 94-114.

Bia, B.L., Cassidy, P.J., Young, M.E., Rafael, J.A., *et al.* 1999. Decreased myocardial nNOS, increased iNOS and abnormal ECHs in mouse models of Duchenne muscular dystrophy. *Journal of Molecular and Cellular Cardiology.* 31, 1857-1862.

Bizzarro, V., Petrella, A. and Parente, L. 2012. Annexin A1: novel roles in skeletal muscle biology. *Journal of Cell Physiology.* 227, 3007–3015.

Board, P.G. and Menon, D. 2013. Glutathione-transferases, regulators of cellular metabolism and physiology. *Biochimica et Biophysica Acta*. 1830, 3267–3288.

Bogdanov, B. and Smith, R.D. 2005. Proteomics by FTICR mass spectrometry: top down and bottom up. *Mass Spectrometry Reviews*. 24, 168-200.

Boillée, S., Berruti, G., Meccariello, R., Grannec, G., *et al.* 2002. Early defect in the expression of mouse sperm DNAJ 1, a member of the DNAJ/heat shock protein 40 chaperone protein family, in the spinal cord of the wobbler mouse, a murine model of motoneuronal degeneration. *Neuroscience.* 113, 825–835.

Boillée, S., Peschanski, M. and Junier, M.P. 2003. The wobbler mouse: a neurodegeneration jigsaw puzzle. *Molecular Neurobiology.* 28:65–106.

Bonifacino, J.S. and Hierro, A. 2011. Transport according to GARP: receiving retrograde cargo at the trans-Golgi network. *Trends Cell Biology. 21*, 159–167.

Bose, P., Fielding, R. and Vacca-Galloway, L.L. 1999. Effects of assisted feeding on wobbler mouse motoneuron disease and serotoninergic and peptidergic sprouting in the cervical spinal horn. *Brain Research Bullitin.* 48, 429–439.

Bowser, R., Cudkowicz, M. and Kaddurah-Daouk, R. 2006. Biomarkers for amyotrophic lateral sclerosis. *Expert Reviews of Molecular Diagnostics.* 387-398.

Bozzi, M., Morlacchi, S., Bigotti, M.G., Sciandra, F., *et al.* 2009. Functional diversity of dystroglycan. *Matrix Biology*. 28, 179-187.

Bradford, M. 1976. A rapid and sensitive method for the quantitation of microgram quantities of protein utilizing the principle of protein-dye binding. *Analytical Biochemistry.* 72, 248-254.

Bradley, W.G., Hudgson, P., Larson, P.F., Papapetropoulos, T.A., *et al.* 1972. Structural changes in the early stages of Duchenne muscular dystrophy. *Journal of Neurology, Neurosurgery and Psychiatry.* 35, 451-455.

Brancaccio, P., Lippi, G. and Maffulli, N. 2010. Biochemical markers of muscular damage. *Clinical Chemistry and Laboratory Medicine*. 48, 757-767.

Brenman, J.E., Chao, D.S., Gee, S.H., McGee, A.W., *et al.* 1996. Interaction of nitric oxide synthase with the postsynaptic density protein PSD-95 and α1-syntrophin mediated by PDZ domains. *Cell*. 84, 757-767.

Brewis, I.A. and Gadella, B.M. 2010. Sperm surface proteomics: from protein lists to biological function. *Molecular Human Reproduction.* 16, 68–79.

Bridges, L.R. 1986. The association of cardiac muscle necrosis and inflammation with the degenerative and persistent myopathy of *mdx* mice. *Journal of the Neurological Sciences.* 72, 147-157.

Brinkmeier, H. and Ohlendieck, K. 2014. Chaperoning heat shock proteins: proteomic analysis and relevance for normal and dystrophin-deficient muscle. *Proteomics Clinical Applications.* 8, 875-895.

Broch-Lips, M., Pedersen, T.H., Riisager, A., Schmitt-John, T., *et al.* 2013. Neuro-muscular function in the wobbler murine model of primary motor neuronopathy. *Experimental Neurology*. 248, 406–415.

Broderick, M.J. and Winder, S.J. 2005. Spectrin, alpha-actinin, and dystrophin. *Advanced Protein Chemistry.* 70, 203-246.

Broers, J.L., Ramaekers, F.C., Bonne, G., Yaou, R.B., *et al.* 2006. Nuclear lamins: laminopathies and their role in premature ageing. *Physiological Reviews.* 86, 967–1008.

Buckingham, M., Bajard, L., Chang, T., Daubas, P., *et al*. 2003. The formation of skeletal muscle: from somite to limb. *Journal of Anatomy.* 202, 59–68.

Bulfield, G., Siller, W.G., Wight, P.A. and Moore, K.J. 1984. X chromosome-linked muscular dystrophy (*mdx*) in the mouse. *Proceeding of the National Academy of Science, USA*. 81, 1189–1192.

Burkholder, T.J. and Lieber, R.L. 2001. Sarcomere length operating range of vertebrate muscles during movement. *Journal of Experimental Biology.* 204, 1529-1536.

Burniston, J.G., Connolly, J., Kainulainen, H., Britton, S.L., *et al.* 2014. Label-free profiling of skeletal muscle using high-defination mass spectrometry. *Proteomics.* 14, 2339-2344.

Bushby, K., Finkel, R., Birnkrant, D.J., Case, L.E., *et al.* 2010. DMD Care Considerations Working Group. Diagnosis and management of Duchenne muscular dystrophy, part 2: implementation of multidisciplinary care. *Lancet Neurology.* 9, 177-189.

Byers, T.J., Lidov, H.G.W. and Kunkel, L.M. 1993. An alternative dystrophin transcript specific to peripheral nerve. *Nature Genetics.* 4, 77-81.

Calligaris, D., Villard, C. and Lafitte, D. 2011. Advances in top-down proteomics for disease biomarker discovery. *Journal of Proteomics.* 74; 920-934.

Camors, E., Monceau, V. and Charlemagne, D. 2005. Annexins and Ca^{2+} handling in the heart. *Cardiovascular Research.* 65, 793–802.

Campbell, K.P. 1995. Three muscular dystrophies: loss of cytoskeleton-extracellular matrix linkage. *Cell*. 80, 675-679.

Campbell, K.P. and Kahl, S.D. 1989. Association of dystrophin and an integral membrane glycoprotein. *Nature*. 338, 259-262.

Canepari, M., Pellegrino, M. A., D'Antona, G. and Bottinelli, R. 2010. Skeletal muscle fibre diversity and the underlying mechanisms. *Acta Physiologica (Oxford).* 199, 465–476.

Canzi, L., Castellaneta, V., Navone, S., Nava, S., *et al.* 2012. Human skeletal muscle stem cell anti-inflammatory activity ameliorates clinical outcome in amyotrophic lateral sclerosis models. *Molecular Medicine*. 18, 401–411.

Capetanaki, Y., Bloch, R.J., Kouloumenta, A., Mavroidis, M., *et al.* 2007. Muscle intermediate filaments and their links to membranes and membranous organelles. *Experimental Cell Research.* 313, 2063–2076.

Capitanio, D., Vasso, M., Ratti, A., Grignaschi, G. *et al.* 2012. Molecular signatures of amyotrophic lateral sclerosis disease progression in hind and forelimb muscles of an SOD1(G93A) mouse model. *Antioxidants and Redox Signaling.* 17, 1333–1350.

Carberry, S. and Ohlendieck, K. 2013. Gel electrophoresis-based proteomics of senescent tissues. *Methods Molecular Biology.* 1048, 229-246.

Carberry, S., Brinkmeier, H., Zhang, Y., Winkler, C.K., *et al.* 2013A. Comparative proteomic profiling of *soleus*, *extensor digitorum longus*, *flexor digitorum brevis* and *interosseus* muscles from the *mdx* mouse model of Duchenne muscular dystrophy. *International Journal of Molecular Medicine.* 32, 544-556.

Carberry, S., Zweyer, M., Swandulla, D. and Ohlendieck, K. 2013B. Application of Fluorescence Two-Dimensional Difference In-Gel Electrophoresis as a Proteomic Biomarker Discovery Tool in Muscular Dystrophy Research. *Biology.* 2, 1438-1464.

Carberry, S., Zweyer, M., Swandulla, D. and Ohlendieck, K. 2012A. Proteomics reveals drastic increase of extracellular matrix proteins collagen and dermatopontin in the aged *mdx* diaphragm model of Duchenne muscular dystrophy. *International Journal of Molecular Medicine. 30,* 229–234.

Carberry, S., Zweyer, M., Swandulla, D. and Ohlendieck, K. 2012B. Profiling of age-related changes in the tibialis anterior muscle proteome of the *mdx* mouse model of dystrophinopathy. *Journal of Biomedical Bioeng*ineering. Article ID 691641.

Carmignac, V. and Durbeej, M. 2012. Cell-matrix interactions in muscle disease. *Journal of Pathology.* 226, 200–218.

Chamberlain, J.S., Metzger, J., Reyes, M., Townsend, D., *et al.* 2007. Dystrophin-deficient *mdx* mice display a reduced life span and are susceptible to spontaneous rhabdomyosarcoma. *FASEB Journal.* 21, 2195-2204.

Chapman, V.M., Miller, D.R., Armstrong, D. and Caskey C.T. 1989. Recovery of induced mutations for X-chromosome linked muscular dystrophy in mice. *Proceeding of the National Academy of Science, USA*. 86, 1292–1296.

Chelly, J. and Desguerre, I. 2013. Progressive muscular dystrophies. *Handbook of Clinical Neurology.* 113, 1343-1366.

Chen, H., Guo, Y., Hu, M., Duan, W., *et al.* 2010. Differential expression and alternative splicing of genes in lumbar spinal cord of an amyotrophic lateral sclerosis mouse model. *Brain Research*. 1340, 52–69.

Cheng, Y.J., Lang, D., Caruthers, S.D., Efimov, I.R., *et al.* 2012. Focal but reversible diastolic sheet dysfunction reflects regional calcium mishandling in dystrophic *mdx* mouse hearts. *The American Journal of Physiology—Heart and Circulatory Physiology*. 303, 559-568.

Chevallet, M., Luche, S. and T. Rabilloud. 2006. Silver staining of proteins in polyacrylamide gels. *Nature Protocols.* 4, 1852-8.

Chianese, R., Scarpa, D., Berruti, G., Cobellis, G., *et al.* 2010. Expression and localization of the deubiquitinating enzyme mUBPy in wobbler mouse testis during spermiogenesis. *General and Comparative Endocrinology. 166*, 289–295.

Chmurzyñska, A. 2006. The multigene family off fatty acid-binding proteins (FABPs): function, structure and polymorphism. *Journal of Applied Genetics.* 47, 39–48.

Chu, V., Otero, J.M., Lopez, O., Sullivan, M.F., *et al.* 2002. Electrocardiographic findings in *mdx* mice: a cardiac phenotype of Duchenne muscular dystrophy. *Muscle and Nerve.* 26, 513-519.

Clark, K.A., McElhinny, A.S.,Beckerle, M.C. and Gregorio, C.C. 2002. Striated muscle cytoarchitecture: an intricate web of form and function. *Annual review of Cell Biology.* 18,637-706.

Conway, S.J. and Molkentin, J.D. 2008. Periostin as a heterofunctional regulator of cardiac development and disease. *Current Genomics.* 9, 548-555.

Conway, S.J., Izuhara, K., Kudo, Y., Litvin, J., *et al,* 2014. The role of periostin in tissue remodeling across health and disease. *Cellular and Molecular Life Sciences.* 71, 1279-1288.

Cornelison, D.D. and Wold, B.J. 1997. Single-cell analysis of regulatory gene expression in quiescent and activated mouse skeletal muscle satellite cells. *Developmental Biology*. 191(2), 270–283.

Coughlan, H.C. and Coughlan, L. 2001. Cardiac architecture: Gothic versus Romanesque. A cardiologist's view. *Semin. Thorac Cardiovase. Surg.* 13, 417-430.

Coulpier, M., Junier, M.P., Peschanski, M. and Dreyfus, P.A. 1996. Bcl-2 sensitivity differentiates two pathways for motoneuronal death in the wobbler mouse. *Journal of Neuroscience.* 16, 5897–5904.

Cox, G.F. and Kunkel, L.M. 1997. Dystrophies and heart disease. *Current Opinion in Cardiology*. 12, 329-343.

Crichton, R.R. and Declercq, J.P. 2010. X-ray structures of ferritins and related proteins. *Biochimica et Biophysica Acta.* 1800, 706–718.

Crosbie, R.H., Lim, L.E., Moore, S.A., Hirano, M., *et al.* 2000. Molecular and genetic characterization of sarcospan: insights into sarcoglycan-sarcospan interactions. *Human Molecular Genetics.* 9, 2019-2027.

Culligan, K. and Ohlendieck, K. 2002. Distal *mdx* muscle groups exhibiting up-regulation of utrophin and rescue of dystrophin-associated glycoproteins exemplify a protected phenotype in muscular dystrophy. *Naturwissenschaften*. 89, 75-78.

Culligan, K. and Ohlendieck, K. 2002. Diversity of the Brain Dystrophin-Glycoprotein Complex. *Journal of Biomedicine and Biotechnology.* 2, 31-36.

Culligan, K., Banville, N., Dowling, P. and Ohlendieck, K. 2002. Drastic reduction of calsequestrin-like proteins and impaired calcium binding in dystrophic *mdx* muscle. *Journal of Applied Physiology.* 92, 435-445.

Culligan, K.G., Mackey, A.J., Finn, D.M., Maguire, P.B., *et al.* 1998. Role of dystrophin isoforms and associated proteins in muscular dystrophy (review). *International Journal of Molecular Medicine.* 2, 639-648.

D'Souza, V.N., Nguyen, T.M., Morris, G.E., Karges, W., *et al.* 1995. A novel dystrophin isoform is required for normal retinal electrophysiology. *Human Molecular Genetics.* 4, 837-842.

Da Cruz, S. and Cleveland, D.W. 2011. Understanding the role of TDP-43 and FUS/TLS in ALS and beyond. *Current Opinion in Neurobiology.* 21, 904–919.

Dacheux, J.L., Belleannée, C., Guyonnet, B., Labas, V., *et al.* 2012. The contribution of proteomics to understanding epididymal maturation of mammalian spermatozoa. *Systems Biology in Reproductive Medicine.* 58, 197–210.

Dai, Q., Escobar, G.P., Hakala, K.W., Lambert, J.M., *et al.* 2008. The left ventricle proteome differentiates middle-aged and old left ventricles in mice. *Journal of Proteome Research.* 7, 756–765.

Dalkilic, I. and Kunkel, L.M. 2003. Muscular dystrophies: genes to pathogenesis. *Current Opinions in Genetic Development.* 13, 231–238.

Dam, A.H., Pijnenburg, A.J., Hendriks, J.C., Westphal, H., *et al.* 2012. Intracytoplasmic sperm injection in partial globozoospermia. *Fertility and Sterility.* 97, 60–66.

Dam, A.H., Ramos, L., Dijkman, H.B., Woestenenk, R., *et al.* 2011. Morphology of partial globozoospermia. *Journal of Andrology. 32*, 199–206.

Dam, A.H., Feenstra, I., Westphal, J.R., Ramos, L., *et al.* 2007. Globozoospermia revisited. *Human Reproduction Update*. *13*, 63–75.

Danko, I., Chapam, V. and Wolff, J.A. 1992. The frequency of revertants in the *mdx* mouse genetic models for Duchenne muscular dystrophy. *Pediatriac Research.* 32, 128-131.

De Luca, A. 2012. Pre-clinical drug tests in the mdx mouse as a model of dystrophinopathies: an overview. *Acta Myologica.* 31, 40–47.

de Oliveira, G.P., Maximino, J.R., Maschietto, M., Zanoteil, E., *et al.* 2014. Early gene expression changes in skeletal muscle from SOD1 (G93A) amyotrophic lateral sclerosis animal model. *Cellular & Molecular Neurobiology.* 3, 451–462.

De Paola, M., Mariani, A., Bigini, P., *et al.* 2012. Neuroprotective effects of toll-like receptor 4 antagonism in spinal cord cultures and in a mouse model of motor neuron degeneration. *Molecular Medicine.* 18, 971–981.

Desguerre, I., Mayer, M., Leturcq, F., Barbet, J.P., *et al.* 2009. Endomysial fibrosis in Duchenne muscular dystrophy: a marker of poor outcome associated with macrophage alternative activation. *Journal of Neuropathology and Experimental Neurology.* 68, 762-773.

Deshmukh, A.S., Murgia, M., Nagaraja, N., Treebak, J.T., *et al.* 2015. Deep proteomics of mouse skeletal muscle enables quantitation of protein isoforms, metabolic pathways and transcription factors. *Molecular and Cellular Proteomics.* In press.

Dion, P.A., Daoud, H. and Rouleau, G.A. 2009. Genetics of motor neuron disorders: new insights into pathogenetic mechanisms. *Nature Reviews Genetics.* 10;11 769-782.

Dix, D.J. 1997. Hsp70 expression and function during gametogenesis. *Cell Stress Chaperones.* 2, 73–77.

Dix, D.J., Allen, J.W., Collins, B.W., Mori, C., *et al.* 1996A. Targeted gene disruption of Hsp70–2 results in failed meiosis, germ cell apoptosis, and male infertility. *Proceeding of the National Academy of Sciences USA.* 93, 3264–3268.

Dix, D.J., Rosario-Herrle, M., Gotoh, H., Mori, C., *et al.* 1996B. Developmentally regulated expression of hsp70–2 and a hsp70–2/lacZ transgene during spermatogenesis. *Developmental Biol*ogy. 174, 310–321.

Domogatskaya, A., Rodin, S. and Tryggvason, K. 2012. Functional diversity of laminins. *Annual Review of Cell Developmental Bioogyl.* 28, 523–553.

Donoghue, P., Ribaric, S., Moran, B., Cebasek, V., *et al.* 2004. Early effects of denervation on Ca^{2+}-handling proteins in skeletal muscle. *International Journal of Molecular Medicine*. 13(6), 767-772.

Doppler, K., Mittelbronn, M. and Bornemann, A. 2008. Myogenesis in human denervated muscle biopsies. *Muscle Nerve.* 37, 79–83.

Doran, P., Donoghue, P., O'Connell, K., Gannon, J., *et al.* 2009A. Proteomics of skeletal muscle aging. *Proteomics.* 9, 989–1003.

Doran, P., Wilton, S.D., Fletcher, S. and Ohlendieck, K. 2009B. Proteomic profiling of antisense-induced exon skipping reveals reversal of pathobiochemical abnormalities in dystrophic *mdx* diaphragm. *Proteomics.* 9, 671-685.

Doran, P., O'Connell, K., Gannon, J., Kavanagh, M., *et al.* 2008. Opposite pathobiochemical fate of pyruvate kinase and adenylate kinase in aged rat skeletal muscle as revealed by proteomic DIGE analysis. *Proteomics.* 8, 364–377.

Doran, P., Gannon, J., O'Connell, K. and Ohlendieck, K. 2007A. Proteomic profiling of animal models mimicking skeletal muscle disorders. *Proteomics- Clinical Applications.* 1, 1169-1184.

Doran, P., Gannon, J., O'Connell, K. and Ohlendieck, K. 2007B. Aging skeletal muscle shows a drastic increase in the small heat shock proteins alphaB- crystallin/HspB5 and cvHsp/HspB7. *European Journal of Cell Biology.* 86, 629–640.

Doran, P., Martin, G., Dowling, P., Jockusch, H., *et al.* 2006A. Proteome analysis of the dystrophin-deficient MDX diaphragm reveals a drastic increase in the heat shock protein cvHSP. *Proteomics.* 6, 4610–4621.

Doran, P., Dowling, P., Donoghue, P., Buffini, M., *et al.* 2006B. Reduced expression of regucalcin in young and aged *mdx* diaphragm indicates abnormal cytosolic calcium handling in dystrophin-deficient muscle. *Biochimica et Biophysica Acta*. 1764, 773- 785.

Doran, P., Dowling, P., Lohan, J., McDonnell, K., *et al.* 2004. Subproteomics analysis of Ca^{2+}-binding proteins demonstrates decreased calsequestrin expression in dystrophic mouse skeletal muscle. *European Journal of Biochemistry.* 271, 3943-3952.

Dowling, P., Holland, A. and Ohlendieck, K. 2014. Mass spectrometry-based identification of muscle-associated and muscle-derived proteomic biomarkers of dystrophinopathies. *Journal of Neuromuscular Disorders.* 1, 15-40.

Dowling, P., Doran, P. and Ohlendieck, K. 2004. Drastic reduction of sarcalumenin in Dp427 (dystrophin of 427 kDa)-deficient fibres indicates that abnormal calcium handling plays a key role in muscular dystrophy. *Biochemistry Journal.* 379, 479-488.

Dowling, P., Lohan, J. and Ohlendieck, K. 2003. Comparative analysis of Dp427-deficient *mdx* tissues shows that the milder dystrophic phenotype of extraocular and toe muscle fibres is associated with a persistent expression of beta-dystroglycan. *European Journal of Cell Biology.* 82, 222-230.

Dubowitz, V., Sewry, C.A. and Oldfors, A. 2013. Muscle Biopsy: a practical approach. *(4th edition) Saunders Elsevier, Oxford, UK.*

Duchen, L.W. and Strich, S.J. 1968. A hereditary motor neuron disease with progressive denervation of muscle in the mouse: the mutant 'wobbler'. *Journal of Neurology, Neurosurgery & Psychiatry.* 31, 535–542.

Duguez, S., Duddy, W., Johnston, H., Lainé, J., *et al.* 2013. Dystrophin deficiency leads to disturbance of LAMP1-vesicle-associated protein secretion. *Cellular and Molecular Life Sciences.* 70, 2159-2174.

Dulhunty, A.F., Hewawasam, R., Liu, D., Casarotto, M. G., *et al*. 2011. Regulation of the cardiac muscle ryanodine receptor by glutathione transferases. *Drug Metabolism Review.* 43, 236–252.

Durbeej, M. and Campbell, K.P. 2002. Muscular dystrophies involving the dystrophin-glycoprotein complex: an overview of current mouse models. *Current Opinion of Genetic Development.* 12, 349–361.

Dziadek, M. 1995. Role of laminin-nidogen complexes in basement membrane formation during embryonic development. *Experientia.* 51, 901–913.

Eddy, E.M. 1999. Role of heat shock protein HSP70–2 in spermatogenesis. *Reviews of Reproduction*. 4, 23–30.

Edström, E., Altun, M., Bergman, E., Johnson, H., *et al*. 2007. Factors contributing to neuromuscular impairment and sarcopenia during aging. *Physiological Behavior.* 92, 129–135.

Ekegren, T., Hanrieder, J. and Bergquist, J. 2008. Clinical perspectives of high-resolution mass spectrometry-based proteomics in neuroscience: exemplified in amyotrophic lateral sclerosis biomarker discovery research. *Journal of Mass Spectrometry.* 43, 559–571.

Elf, K., Shevchenko, G., Nygren, I., Larsson, L., *et al.* 2004. Alterations in muscle proteome of patients diagnosed with amyotrophic lateral sclerosis. *Journal of Proteomics.* 108, 55-64.

Elsherif, L., Huang, M.S., Shai, S.Y., Yang, Y., *et al.* 2008. Combined deficiency of dystrophin and beta1 integrin in the cardiac myocyte causes myocardial dysfunction, fibrosis and calcification. *Circulation Research.* 102, 1109-1117.

Ervasti, J.M. and Campbell, K.P. 1993. A role for the dystrophin- glycoprotein complex as a transmembrane linker between laminin and actin. *Journal of Cell Biology.* 122, 809-823.

Ervasti, J.M. and Sonnemann, K.J. 2008. Biology of the striated muscle dystrophin-glycoprotein complex. *International Review of Cytology.* 265, 191-225.

Fairclough, R.J., Perkins, K.J. and Davies, K.E. 2012. Pharmacologically targeting the primary defect and downstream pathology in Duchenne muscular dystrophy. *Current Gene Therapies.* 12, 206- 244.

Fanchaouy, M., Polakova, E., Jung, C., Ogrodnik, J., *et al.* 2009. Pathways of abnormal stress-induced Ca^{2+}-influx into dystrophic *mdx* cardiomyocytes. *Cell Calcium.* 46, 114–121.

Farley, J. and Miles, P.R. 1977. Role of depolarization in acetylcholine-induced contractions of dog trachealis muscle. *Journal of Pharmacology and Experimental Therapeutics*. 201, 199-205.

Faulkner, J.A., Larkin, L.M., Claflin, D.R. and Brooks, S.V. 2007. Age-related changes in the structure and function of skeletal muscles. *Clinical and Experimental Pharmacology and Physiology.* 34, 1091–1096.

Fayssoil, A., Nardi, O., Orlikowaki, D. and Annane, D. 2010. Cardiomyopathy in Duchenne muscular dystrophy: pathogenesis and therapeutics. *Heart Failure Reviews.* 15, 103-107.

Ferreira, R., Vitorino, R., Neuparth, M.J., Appell, H.J., *et al.* 2009. Proteolysis activation and proteome alterations in murine skeletal muscle submitted to 1 week of hind limb suspension. *European Journal of Applied Physiol*ogy. 107, 553–563.

Ficarro, S., Chertihin, O., Westbrook, V.A., White, F., *et al.* 2003. Phosphoproteome analysis of capacitated human sperm. Evidence of tyrosine phosphorylation of a kinase-anchoring protein 3 and valosin-containing protein/p97 during capacitation. *Journal of Biological* Chemistry. 278, 11579–11589.

Finsterer, J. and Stöllberger, C. 2003. The heart in human dystrophinopathies. *Cardiology*. 99, 1-19.

Fong, P.Y., Turner, P.R., Denetclaw, W.F. and Steinhardt, R.A. 1990. Increased activity of calcium leak channels in myotubes of Duchenne human and *mdx* mouse origin. *Science.* 250, 673-676.

Forbes, S.C., Walter, G.A., Rooney, W.D., Wang, D.J., *et al.* 2013. Skeletal muscles of ambulant children with Duchenne muscular dystrophy: validation of multicenter study of evaluation with MR imaging and MR spectroscopy. *Radiology*. 269, 198-207.

Franceschini, A., Szklarczyk, D., Frankild, S., Kuhn, M., *et al.* 2013. STRING v9.1: protein-protein interaction networks, with increased coverage and integration. *Nucleic Acids Research. 41,* D808–D815.

Frangogiannis, N.G. 2012. Matricellular proteins in cardiac adaptation and disease. *Physiological Reviews.* 92, 635-688.

Frankel, K.A. and Rosser, R.J. 1976. The pathology of the heart in progressive muscular dystrophy: epimyocardial fibrosis. *Human Pathology*. 7, 375-386.

Fremont, P., Charest, P.M., Cote, C. and Rogers, P.A. 1988. Carbonic anhydrase III in skeletal muscle fibers: an immunocytochemical and biochemical study. *Journal of Histochemistry & Cytochemistry.* 36, 775–782.

Fu, X., Wang, H. and Hu, P. 2015. Stem cell activation in skeletal muscle regeneration. *Cellular and Molecular Life Sciences.* 72, 1662-1677.

Gallagher, P., Trappe, S., Harber, M., Creer, A., *et al.* 2005. Effects of 84-days of bed rest and resistance training on single muscle fibre myosin heavy chain distribution in human *vastus lateralis* and *soleus* muscles. *Acta Physiolica Scandanivia*. 185, 61–69.

Galpin, A. J., Raue, U., Jemiolo, B., Trappe, T. A., *et al.* 2012. Human skeletal muscle fiber type specific protein content. *Analytical Biochemistry*. 425, 175–182.

Gannon, J., Doran, P., Kirwan, A. and Ohlendieck, K. 2009. Drastic increase of myosin light chain MLC-2 in senescent skeletal muscle indicates fast-to-slow fibre transition in sarcopenia of old age. *European Journal of Cell Biology.* 88, 685–700.

Gardan-Salmon, D., Dixon, J.M., Lonergan, S.M. and Selsby, J.T. 2011. Proteomic assessment of the acute phase of dystrophin deficiency in *mdx* mice. *European Journal of Applied Physiology.* 111, 2763–2773.

Gatto, L., Vizcaíno, J.A., Hermjakob, H., Huber, W., *et al.* 2010. Organelle proteomics experimental designs and analysis. *Proteomics.* 10, 3957-3969.

Gee, S.H., Gee, R., Madhaven, S.H., Levinson, S.R., *et al.* 1998. Interaction of muscle and brain sodium channels with multiple members of the syntrophin family of dystrophin-associated proteins. *Journal of Neuroscience.* 18, 128-137.

Gelfi, C., Vasso, M. and Cerretelli, P. 2011. Diversity of human skeletal muscle in health and disease: contribution of proteomics. *Journal of Proteomics.* 74, 774-795.

Gelfi, C., Vigano, A., De Palma, S., Ripamonti, M., *et al.* 2006. 2-D protein maps of rat *gastrocnemius* and *soleus* muscles: a tool for muscle plasticity assessment. *Proteomics.* 6, 321–340.

Gelfi, C., Vigano, A., Ripamonti, M., Pontoglio, A., *et al*. 2006. The human muscle proteome in aging. *Journal of Proteome Research.* 5, 1344–1353.

Gevaert, K., Van Damme, P., Ghesquière, B., Impens, F., *et al.* 2007. A la carte proteomics with an emphasis on gel-free techniques. *Proteomics*. 7, 2698-2718.

Gillies, A.R. and Lieber, R.L. 2011. Structure and function of the skeletal muscle extracellular matrix. *Muscle Nerve.* 44, 318-331.

Goldspink, G., Fernandes, K., Williams, P.E. and Wells, D.J. 1994. Age-related changes in collagen gene expression in the muscles of *mdx* dystrophic and normal mice. *Neuromuscular Disorders.* 4, 183-191.

Gordon, A.M., Homsher, E. and Regnier, M. 2000. Regulation of contraction in striated muscle. *Physiology Reviews.* 80, 853-924.

Gordon, P.H. 2013. Amyotrophic Lateral Sclerosis: An update for 2013 Clinical Features, Pathophysiology, Management and Therapeutic Trials. *Aging Disease*. 4, 295-310.

Gordon, P.H. and Mitsumoto, H. 2007. Chapter 20 Symptomatic therapy and palliative aspects of clinical care. *Handbook of Clinical Neurology*. 82, 389-424.

Gorecki, D.C., Monaco, A.P., Derry, J.M.J., Walker, A.P., *et al.* 1992. Expression of four alternative transcripts in human brain regions regulated by different promoters. *Human Molecular Genetics.* 1, 505-510.

Graham, K.M., Singh, R., Millman, G., Malnassy, G., *et al.* 2010. Excessive collagen accumulation in dystrophic (*mdx*) respiratory musculature is independent of enhanced activation of the NF-kappaB pathway. *Journal of Neurological Sciences.* 294, 43-50.

Grant, J.E., Bradshaw, A.D., Schwacke, J.H., Baicu, C.F., *et al.* 2009. Quantification of protein expression changes in the aging left ventricle of Rattus norvegicus. *Journal of Proteome Research.* 8, 4252–4263.

Greising, S.M., Gransee, H.M., Mantilla, C.B. and Sieck, G.C. 2012. System biology of skeletal muscle: fiber type as an organizing principle. *Wiley Interdiscip Rev Syst Biol Med.* 4, 457-473.

Gros-Louis, F., Gaspar, C., and Rouleau, G.A. 2006. Genetics of familial and sporadic amyotrophic lateral sclerosis. *Biochemical et Biophysica Acta*. 11, 956-972.

Gruppi, C. M., Zakeri, Z. F. and Wolgemuth, D. J. 1991. Stage and lineage-regulated expression of two hsp90 transcripts during mouse germ cell differentiation and embryogenesis. *Molecular Reproduction and Development.* 28, 209–217.

Guenet, J.L. 2011. Animal models of human genetic diseases: do they need to be faithful to be useful? *Molecular Genetics and Genomics*. 286, 1-20.

Guevel, L., Lavoie, J.R., Perez-Iratxeta, C., Rouger, K., *et al.* 2011. Quantitative proteomic analysis of dystrophic dog muscle. *Journal of Proteome Research.* 10, 2465-2478.

Gulston, M.K., Rubtsov, D.V., Atherton, H.J., Clarke, K., *et al.* 2008. A combined metabolomic and proteomic investigation of the effects of a failure to express dystrophin in the mouse heart. *Journal of Proteome Research.* 7, 2069–2077.

Gumerson, J.D. and Michele, D.E. 2011. The dystrophin-glycoprotein complex in the prevention of muscle damage. *Journal of Biomedicine and Biotechnology.* 2011, 210797.

Gunning, P., O'Neill, G. and Hardeman, E. 2008. Tropomyosin-based regulation of the actin cytoskeleton in time and space. *Physiology Reviews.* 88, 1-35.

Hamada, A., Sharma, R., du Plessis, S.S., Willard, B., *et al.* 2013. Two-dimensional differential in-gel electrophoresis-based proteomics of male gametes in relation to oxidative stress. *Fertility and Sterility.* 99, 1216–1226.

Hamada, A.J., Montgomery, B. and Agarwal, A. 2012. Male infertility: a critical review of pharmacologic management. *Expert Opinions in Pharmacotherapy.* 13, 2511–2531.

Harrison, P.M. and Arosio, P. 1996. The ferritins: molecular properties, iron storage function and cellular regulation. *Biochimica et Biophysica Acta.* 1275, 161–203.

Hathout, Y., Brody, E., Clemens, P.R., Cripe, L., *et al.* 2015. Large-scale serum protein biomarker discovery in Duchenne muscular dystrophy. *Proc. National Acad. Science.* 112(23), 7153-7158.

Hathout, Y., Marathi, R.L., Rayavarapu, S., Zhang, A., *et al.* 2014. Discovery of serum protein biomarkers in the *mdx* mouse model and cross-species comparison to Duchenne muscular dystrophy patients. *Human Molecular Genetics.* 23, 6458-6469.

Hauser, E., Höger, H., Bittner, R., Widhalm, K., *et al.* 1995. Oxyradical damage and mitochondrial enzyme activities in the *mdx* mouse. *Neuropediatrics.* 26, 260–272.

Haycock, J.W., MacNeil, S., Jones, P., Harris, J.B., *et al.* 1996. Oxidative damage to muscle protein in Duchenne muscular dystrophy. *Neuroreports.* 8, 357–361.

Head, S.I. 2010. Branched fibres in old dystrophic *mdx* muscle are associated with mechanical weakening of the sarcolemma, abnormal Ca^{2+}-transients and a breakdown of Ca^{2+}-homeostasis during fatigue. *Experimental Physiology.* 95, 641-656.

Heimann, P., Laage, S. and Jockusch, H. 1991. Defect of sperm assembly in a neurological mutant of the mouse, wobbler (WR). *Differentiation*. 47, 77–83.

Hermans, M.C., Pinto, Y.M., Merkies, I.S., de Die-Smulders, C.E., *et al.* 2010. Hereditary muscular dystrophies and the heart. *Neuromuscular Disord*ers. 20, 479–492.

Heytens, E., Schmitt-John, T., Moser, J.M., Jensen, N.M., *et al.* 2010. Reduced fertilization after ICSI and abnormal phospholipase C zeta presence in spermatozoa from the wobbler mouse. *Reproduction Biomedicine Online.* 21, 742–749.

Hnia, K., Zouiten, D., Cantel, S., Chazalette, D., *et al.* 2007. ZZ domain of dystrophin and utrophin: topology and mapping of a beta-dystroglycan interaction site. *Biochemistry Journal.* 401, 667-77.

Ho, M.S., Böse, K., Mokkapati, S., Nischt, R., *et al.* 2008. Nidogens-extracellular matrix linker molecules. *Microscopy Research and Technologies.* 71, 387–395.

Hochstrasser, D.F., Sanchez, J.C. and Appel, R.D. 2002. Proteomics and its trends facing nature's complexity. *Proteomics*. 2, 807-812.

Hodgkin, A. and Horowicz, P. 1960. Potassium contractures in single muscle fibres. *Journal of Physiology.* 153, 386-403.

Hoffman, E.P., Brown, R.H. Jr. and Kunkel, L.M. 1987. Dystrophin: the protein product of the Duchenne muscular dystrophy locus. *Cell.* 51, 919-928.

Højlund, K., Yi, Z., Hwang, H., Bowen, B., *et al.* 2008. Characterization of the human skeletal muscle proteome by one-dimensional gel electrophoresis and HPLC-ESI-MS/MS. *Molecular and Cell Proteomics.* 7, 257-267.

Holland, A., Dowling, P., Meleady, P., Henry, M., *et al.* 2015. Label-free mass spectrometric analysis of the *mdx-4cv* diaphragm identifies the matricellular protein periostin as a potential factor involved in the dystrophinopathy-related fibrosis. *Proteomics.* Doi: 10.1002/pmic.201400471.

Holland, A., Schmitt-John, T., Dowling, P., Jockusch, H., *et al.* 2014A. Intricate effects of primary motor neuropathy on contractile proteins and metabolic muscle enzymes as revealed by label-free mass spectrometry. *Bioscience Reports.* 34, Article ID: e00119.

Holland, A., Dowling, P. and Ohlendieck, K. 2014B. New pathobiochemical insights into dystrophinopathy from the proteomics of senescent *mdx* mouse muscle. *Frontiers in Aging Neuroscience.* 3,109.

Holland, A. and Ohlendieck, K. 2014A. Proteomic profiling of the dystrophin-deficient *mdx* heart, a phenocopy of dystrophinopathy-associated cardiomyopathy. *BioMed Research International.* Article ID: 246195

Holland, A. and Ohlendieck, K. 2014B. Comparative profiling of the sperm proteome. *Proteomics.* 15, 632–648.

Holland, A. and Ohlendieck, K. 2014C. Proteomic identification of muscle-associated biomarkers of amyotrophic lateral sclerosis using the wobbler mouse model of primary motor neuronopathy. *Journal of Integrated OMICS.* 4, 57-68.

Holland, A. and Ohlendieck, K. 2014D. Proteomic profiling of calsequestrin and the Ca^{2+}-related damage pathway on dystrophinopathy. *Calcium Signalling.* 1, 60-69.

Holland, A. and Ohlendieck, K. 2014E. Comparative proteomics for studying muscular dystrophy: Intrinsic biological and analytical issues associated with the systematic utilization of tissue specimens. *Journal of Proteomics and Bioinformatics*. S10, 002 In press.

Holland A. and Ohlendieck K. 2013. Proteomic profiling of the contractile apparatus from skeletal muscle. *Expert Reviews of Proteomics.* 10, 239-57.

Holland A., Carberry S. and Ohlendieck K. 2013A. Proteomics of the dystrophin-glycoprotein complex and dystrophinopathy. *Current Protein & Peptide Science.* 14, 680-697.

Holland A., Dowling P., Zweyer M., Swandulla D., *et al.* 2013B. Proteomic profiling of cardiomyopathic tissue from the aged *mdx* model of Duchenne muscular dystrophy reveals a drastic decrease in laminin, nidogen and annexin. *Proteomics.* 15, 2312-23.

Holmes, K.C. 1997. The swinging lever-arm hypothesis of muscle contraction. *Current Biology.* 7, 112-118.

Hopf, F.W., Turner, P.R. and Steinhardt, R.A. 2007. Calcium misregulation and the pathogenesis of muscular dystrophy. *Subcellular Biochemistry.* 45, 429-64.

Hortin, G.L. and Sviridov, D. 2010. The dynamic range problem in the analysis of the plasma proteome. *Journal of Proteomics*. 73, 629-636.

Hsu, J.D. and Quinlivan, R. 2013. Scoliosis in Duchenne muscular dystrophy (DMD). *Neuromuscular Disorders*. 23, 611-617.

Huang, S.Y., Tam, M.F., Hsu, Y.T., Lin, J.H., *et al.* 2005. Developmental changes of heat-shock proteins in porcine testis by a proteomic analysis. *Theriogenology.* 64, 1940–1955.

Hubner, G., Klein, H.J., Kleinsasser, O. and Schiefer, H.G. 1971. Role of myoepithelial cells in the development of salivary gland tumors. *Cancer.* 27, 1255-1261.

Ibraghimov-Beskrovnaya, O., Ervasti, J.M., Leveille, C.J., Slaughter, C.A., *et al.* 1992. Primary structure of dystrophin-associated glycoproteins linking dystrophin to the extracellular matrix. *Nature*. 355, 696-702.

Ikeda, K. and Mitsumoto, H. 1993. In vivo and in vitro muscle tensions in wobbler mouse motor neuron disease. *Muscle Nerve.* 16, 979–981.

Ilsley, J.L., Sudol, M. and Winder, S.J. 2002. The WW domain: linking cell signalling to the membrane cytoskeleton. *Cell Signaling.* 14, 183-189.

Im, W.B., Phelps, S.F., Copen, E.H., Adams, E.G., *et al.* 1996. Differential expression of dystrophin isoforms in strains of *mdx* mice with different mutations. *Human Molecular Genetics*. 5, 1149–1153.

Ino, Y. and Hirano, H. 2011. Mass spectrometric characterization of proteins transferred from polyacrylamide gels to membrane filters. *FEBS Journal.* 278, 3807-3814.

Irintchev, A., Zweyer, M. and Wernig, A. 1997. Impaired functional and structural recovery after muscle injury in dystrophic *mdx* mice. *Neuromuscular Disorders. 7,* 117-125.

Ishiyama, T., Klinkosz, B., Pioro, E.P. and Mitsumoto, H. 1997. Genetic transfer of the wobbler gene to a C57BL/6J X NZB hybrid stock: natural history of the motor neuron disease and the response to CNTF and BDNF cotreatment. *Experimental Neurology.* 148, 247–255.

Ishizaki, M., Suga, T., Kimura, E., Shiota, T., *et al.* 2008. *Mdx* respiratory impairment following fibrosis of the diaphragm. *Neuromuscular Disorders.* 18, 342-348.

Iwamoto, Y., Yoshii, K. and Ikeda, K. 2009. Atorvastatin treatment attenuates motor neuron degeneration in wobbler mice. *Amyotrophic Lateral Sclerosis*. 10, 405–409.

Jiang, C., Wen, Y., Kuroda, K., Hannon, K., *et al.* 2014. Notch signalling deficiency underlis age-dependent depletion of satellite cells in muscular dystrophy. *Disease Model Mechanisms.* 7, 997-1004.

Jockusch, H., Holland, A., Staunton, L., Schmitt-John, T., *et al.* 2014. Pathoproteomics of testicular tissue deficient in the GARP component VPS54: the wobbler mouse model of globozoospermia. *Proteomics.* 14, 839–852.

Johnson, E.K., Zhang, L., Adams, M.E., Philips, A., *et al.* 2012. Proteomic analysis reveals new cardiac-specific dystrophin-associated proteins. *PLoS ONE*. Article ID: e43515.

Johnston, D.S., Wooters, J., Kopf, G.S., Qiu, Y., *et al.* 2005. Analysis of the human spermproteome. *Annals of the New York Academy of Sciences.* 1061, 190–202.

Judge, D.P., Kass, D.A., Thompson, W.R. and Wagner, K.R. 2011. Pathophysiology and therapy of cardiac dysfunction in Duchenne muscular dystrophy. *American Journal of Cardiovascular Drugs.* 11, 287–294.

Judge, L.M. Haraguchiln, M. and Chamberlain, J.S. 2006. Dissecting the signaling and mechanical functions of the dystrophin-glycoprotein complex. *Journal of Cell Signalling.* 119, 1537-1546.

Jung, C., Martins, A.S., Niggli, E. and Shirokova, N. 2008. Dystrophic cardiomyopathy: amplification of cellular damage by Ca^{2+}-signaling and reactive oxygen species-generating pathways. *Cardiovascular Research.* 77, 766–773.

Kaprielian, R.R. and Severs, N.J. 2000. Dystrophin and the cardiomyocyte membrane cytoskeleton in the healthy and failing heart. *Heart Failure Reviews*. 5, 221-238.

Kaprielian, R.R., Stevenson, S., Rothery, S.M., Cullen, M.J., *et al.* 2000. Distinct patterns of dystrophin organization in myocyte sarcolemma and transverse tubules of normal and diseased human myocardium. *Circulation*. 101, 2586-2594.

Karlsson, P., Droce, A., Moser, J.M., Cuhlmann, S., *et al.* 2013. Loss of vps54 function leads to vesicle traffic impairment, protein mis-sorting and embryonic lethality. *International Journal of Molecular Science*. 14, 10908–10925.

Kaspar, R.W., Allen, H.D. and Montanaro, F. 2009. Current understanding and management of dilated cardiomyopathy in Duchenne and Becker muscular dystrophy. *Journal of American Academy of Nurse Practitioners.* 21, 241–249.

Kaupmann, K., Simon-Chazottes, D., Guénet, J.L., Jockusch, H., *et al.* 1992. Wobbler, a mutation affecting motoneuron survival and gonadal functions in the mouse, maps to proximal chromosome 11. *Genomics*. 13, 39–43.

Kerrien, S., Aranda, B., Breuza, L., Bridge, A., *et al.* 2012. The IntAct molecular interaction database in 2012. *Nucleic Acids Research. 40,* 841–846.

Khairallah, M., Khairallah, R., Young, M.E., Dyck, J.R.B., *et al.* 2007. Metabolic and signalling alterations in dystrophin-deficient hearts precede overt cardiomyopathy. *Journal of Molecular and Cellular Cardiology.* 43, 119-129.

Kharraz, Y., Guerra, J., Pessina, P., Serrano, A.L., *et al.* 2014. Understanding the process of fibrosis in Duchenne muscular dystrophy. *Biomedical Research International.* 2014, 965631.

Kido, T., Arata, S., Suzuki, R., Hosono, T., *et al.* 2005. The testicular fatty acid binding protein PERF15 regulates the fate of germ cells in PERF15 transgenic mice. *Development Growth and Differentiation.* 47, 15–24.

Kido, T. and Namiki, H. 2000. Expression of testicular fatty acid-binding protein PERF 15 during germ cell apoptosis. *Development Growth and Differentiation.* 42, 359–366.

Kim, M.S., Pinto, S.M., Getnet, D., Nirujogi, R.S., *et al.* 2014. A draft map of the human proteome. *Nature.* 509, 575-581.

Kim, Y.E., Hipp, M.S., Bracher, A., Hayer-Hartl, M., *et al.* 2013. Molecular chaperone functions in protein folding and proteostasis. *Annual Review of Biochemistry.* 82, 323–355.

Kimura, E., Li, S., Gregorevic, P., Fall, B.M., *et al.* 2010. Dystrophin delivery to muscles of *mdx* mice using lentiviral vectors leads to myogenic progenitor targeting and stable gene expression. *Molecular Therapy.* 18, 206-213.

Kinali, M., Messina, S., Mercuri, E., Lehovsky, J., *et al.* 2006. Management of scoliosis in Duchenne muscular dystrophy: a large 10-year retrospective study. *Developmental Medicine and Child Neurology*. 48, 513-518.

Klamut, H.J., Gangopadhyay, S.B., Worton, R.N. and Ray, P.N. 1990. Molecular and functional analysis of the muscle-specific promoter region of the Duchenne muscular dystrophy gene. *Molecular and Cellular Biology.* 10, 193-205.

Klietsch, R., Ervasti, J.M., Arnold, W., Campbell, K.P., *et al.* 1993. Dystrophin-glycoprotein complex and laminin co-localize to the sarcolemma and transverse tubules of cardiac muscle. *Circulation Research*. 72, 349–360.

Klingler, W., Jurkat-Rott, K., Lehmann-Horn, F. and Schleip, R. 2012. The role of fibrosis in Duchenne muscular dystrophy. *Acta Myologica.* 31, 184-195.

Koeing, M., Hoffman, E.P., Bertelson, C.J., Monaco, A.P., *et al.* 1987. Complete cloning of the Duchenne muscular dystrophy (DMD) cDNA and preliminary genomic organization of the DMD gene in normal and affected individuals. *Cell.* 50, 509-517.

Koenig, M., Beggs, A.H., Moyer, M., Scherpf, S., *et al.* 1989. The molecular basis for Duchenne versus Becker muscular dystrophy: Correlation of severity with type of deletion. *American Journal of Human Genetics.* 45, 498-506.

Koenig, X., Dysek, S., Kimbacher, S., Mike, A.K., *et al.* 2011. Voltage-gated ion channel dysfunction precedes cardiomyopathy development in the dystrophic heart. *PLoS One.* 6, e20300.

Kornegay, J.N., Bogan, J.R., Bogan, D.J., Childers, M.K., *et al.* 2012. Canine models of Duchenne muscular dystrophy and their use in therapeutic strategies. *Mammalian Genome.* 23, 85-108.

Kozicka, A., Prot, J. and Wasilewski, R. 1971. Mental retardation in patients with Duchenne progressive muscular dystrophy. *Journal of Neurological Science.* 14, 209-213.

Kravchenko, I.V., Furalyov, V.A. and Popov, V.O. 2012. Stimulation of mechano-growth factor expression by myofibrillar proteins in murine myoblasts and myotubes. *Molecular and Cellular Biochemistry.* 363, 347–355.

Kruegel, J. and Miosge, N. 2010. Basement membrane components are key players in specialized extracellular matrices. *Cellular and Molecular Life Sciences*. 67, 2879–2895.

Krüger, T., Lautenschläger, J., Grosskreutz, J. and Rhode, H. 2013. Proteome analysis of body fluids for amyotrophic lateral sclerosis biomarker discovery. *Proteomics Clinical Applications*. 7, 123–135.

Kuang, S., Chargé, S.B., Seale, P., Huh, M., *et al.* 2006. Distinct roles for Pax7 and Pax3 in adult regenerative myogenesis. *Journal of Cell Biology.* 172(1),103–113.

Kudo, L.C., Parfenova, L., Vi, N., Lau, K., *et al.* 2010. Integrative gene-tissue microarray-based approach for identification of human disease biomarkers: application to amyotrophic lateral sclerosis. *Human Molecular Genetics.* 19, 3233–3253.

Kühn, B., del Monte, F., Hajjar, R.J., Chang, Y.S., *et al.* 2007. Periostin induces proliferation of differentiated cardiomyocytes and promotes cardiac repair. *Nature Medicine.* 13, 962-969.

Kuznetsov, A.V., Winkler, K., Wiedemann, F.R., von Bossanyi, P., *et al.* 1998. Impaired mitochondrial oxidative phosphorylation in skeletal muscle of the dystrophin-deficient *mdx* mouse. *Molecular Cell and Biochemistry.* 183, 87–96.

Laage, S., Zobel, G. and Jockusch, H. 1988. Astrocyte overgrowth in the brain stem and spinal cord of mice affected by spinal atrophy, Wobbler. *Developmental Neuroscience*. 10, 190–198.

Laemmli, U.K. 1970. Cleavage of structural proteins during the assembly of the head of bacteriophage T4. *Nature.* 5259, 680-685.

Lander, E.S. 2011. Initial impact of the sequencing of the human genome. *Nature.* 470, 187-197.

Lane, C.S. 2005. Mass spectrometry-based proteomics in the life sciences. *Cellular and Molecular Life Science.* 62, 848-869.

Lapidos, K.A., Kakkar, R. and McNally, E.M. 2004. The dystrophin glycoprotein complex: signaling strength and integrity for the sarcolemma. *Circulation Research*. 94, 1023-1031.

Le Rumeur, E., Winder, S.J. and Hubert, J.F. 2010. Dystrophin: more than just the sum of its parts. *Biochimica et Biophysica Acta.* 1804,1713-1722.

Lee, Y.H., Tan, H.T. and Chung, M.C. 2010. Subcellular fractionation methods and strategies for proteomics. *Proteomics*. 10, 3935-3956.

Leestma, J.E. and Sepsenwol, S. 1980. Sperm tail axoneme alterations in the Wobbler mouse. *Journal of Reproduction and Fertility.* 58, 267–270.

Lefaucheur, J.P., Pastoret, C. and Sebille, A. 1995. Phenotype of dystrophinopathy in old MDX mice. *Anatomical Record*. 1, 70–76.

Lemieux, H. and Hoppel, C.L. 2009. Mitochondria in the human heart. *Journal of Bioenergetics and Biomembranes*. 41, 99–106.

Leslie, K.O., Mitchell, J.J., Woodcock-Mitchell, J.L. and Low, R.B. 1990. Alpha smooth muscle actin expression in developing and adult human lung. *Differentiation.* 44, 143-149.

Lewis, C., Carberry, S. and Ohlendieck, K. 2009. Proteomic profiling of X-linked muscular dystrophy. *Journal of Muscle Research and Cell Motility.* 30, 267–279.

Lewis, C., Doran, P. and Ohlendieck, K. 2012. Proteomic analysis of dystrophic muscle. *Methods of Molecular Biology.* 798, 357-369.

Lewis, C., Jockusch, H. and Ohlendieck, K. 2010. Proteomic profiling of the dystrophin-deficient *mdx* heart reveals drastically altered levels of key metabolic and contractile proteins. *Journal of Biomedicine and Biotechnology.* Article ID: 648501.

Lidov, H.G.W., Selig, S. and Kunkel, L.M. 1995. Dp140: a novel 140 kDa CNS transcript from the dystrophin locus. *Human Molecular Genetics.* 4, 329-335.

Lieber, R.L. and Ward, S.R. 2013. Cellular mechanisms of tissue fibrosis. 4. Structural and functional consequences of skeletal muscle fibrosis. *American Journal of Physiology, Cell Physiology.* 305, C241-C252.

Liu, R.Z., Li, X. and Godbout, R. 2008. A novel fatty acid-binding protein (FABP) gene resulting from tandem gene duplication in mammals: transcription in rat retina and testis. *Genomics.* 92, 436–445.

Lohan, J., Culligan, K. and Ohlendieck, K. 2005. Deficiency in cardiac dystrophin affects the abundance of the alpha/beta-dystroglycan complex. *Journal of Biomedicine and Biotechnology.* 2005, 28–36.

Lohan, J. and Ohlendieck, K. 2004. Drastic reduction in the luminal Ca^{2+}-binding proteins calsequestrin and sarcalumenin in dystrophin-deficient cardiac muscle. *Biochimica et Biophysica Acta.* 1689, 252–258.

Lorts, A., Schwanekamp, J.A., Baudino, T.A., McNally, E.M., *et al.* 2012. Deletion of periostin reduces muscular dystrophy and fibrosis in mice by modulating the transforming growth factor-β pathway. *Proceedings of the National Academy of Science, USA.* 109, 10978-10983.

Lynch, G.S., Hinkle, R.T., Chamberlain, J.S., Brooks, S.V., *et al.* 2001. Force and power output of fast and slow skeletal muscles from *mdx* mice 6-28 months old. *Journal of Physiology.* 535, 591-600.

Lynch, G.S., Rafael, J.A., Chamberlain, J.S. and Faulkner, J.A. 2000. Contraction-induced injury to single permeabilized muscle fibers from *mdx*, transgenic *mdx*, and control mice. *American Journal of Physiology- Cell Physiology.* 279, 1290-1294.

Mah, J.K., Korngut, L., Dykeman, J., Day, L., *et al.* 2014. A systematic reviewand meta-analysis on the epidemiology of Duchenne and Becker muscular dystrophy. *Neuromuscular Disorders.* 24, 482-491.

Mallick, P. and Kuster, B. 2010. Proteomics: a pragmatic perspective. *Nature Biotechnology*. 28, 695-709.

Marotta, M., Ruiz-Roig, C., Sarria, Y., Peiro, J.L., *et al.* 2009. Muscle genome-wide expression profiling during disease evolution in *mdx* mice. *Physiological Genomics.* 37, 119-132.

Marques, M.J., Ferretti, R., Vomero, V.U., Minatel, E., *et al.* 2007. Intrinsic laryngeal muscles are spared from myonecrosis in the *mdx* mouse model of Duchenne muscular dystrophy. *Muscle Nerve*. 35, 349-353.

Martin, C.F., Hiller, M., Spitali, P., Oonk, S., *et al.* 2014. Fibronectin is a serum biomarker for Duchenne muscular dystrophy. *Proteomics Clinical Applications.* 8, 269-278.

Martínez-Heredia, J., Estanyol, J.M., Ballescá, J.L. and Oliva, R. 2006. Proteomic identification of human sperm proteins. *Proteomics.* 6, 4356–4369.

Matsakas, A. and Patel, K. 2009. Skeletal muscle fibre plasticity in response to selected environmental and physiological stimuli. *Histology and Histopathology.* 24, 611–629.

Matsumura, K., Ervasti, J.M., Ohlendieck, K., Kahl, S.D., *et al.* 1992. Association of dystrophin-related protein with dystrophin-associated proteins in mdx mouse muscle. *Nature*. 360, 588-591.

Mauro, A. 1961. Satellite cell of skeletal muscle fibers. *J Bio-phys Biochem Cytol.* 9, 493–495.

McGoldrick, P., Joyce, P.I., Fisher, E.M. and Greensmith, L. 2013. Rodent models of amyotrophic lateral sclerosis. *Biochimicia et Biophysica Acta*. 1832, 1421–1436.

Meccariello, R., Cobellis, G., Berruti, G., Junier, M. P., *et al.* 2002. Mouse sperm cell-specific DnaJ first homologue: an evolutionarily conserved protein for spermiogenesis. *Biology of Reproduction.* 66, 1328–1335.

Mehuron, T., Kumar, A., Duarte, L., Yamauchi, J., *et al.* 2014. Dysregulation of matricellular proteins is an early signature of pathology in laminin-deficient muscular dystrophy. *Skeletal Muscle.* 4, 14.

Meisler, M.H., Russ, C., Montgomery, K.T., Greenway, M., *et al.* 2008. Evaluation of the Golgi trafficking protein VPS54 (wobbler) as a candidate for ALS. *Amyotrophic Lateral Sclerosis.* 9, 141–148.

Meleady, P., Gallagher, M., Clarke, C., Henry, M., *et al.* 2012. Impact of miR-7 over-expression on the proteome of Chinese hamster ovary cells. *Journal of Biotechnol*ogy. 160, 251–262.

Meleady, P., Hoffrogge, R., Henry, M., Rupp, O., *et al.* 2012. Utilization and evaluation of CHO-specific sequence databases for mass spectrometry based proteomics. *Biotechnology and Bioengineering.* 109, 1386–1394.

Mendell, J.R., Shilling, C., Leslie, N.D., Flanigan, K.M., *et al.* 2012 Evidence-based path to newborn screening for Duchenne muscular dystrophy. *Annals of Neurology*. 71: 304-313.

Mendonça, D.M., Pizzati, L., Mostacada, K., de S Martins, S.C., *et al.* 2012. Neuroproteomics: an insight into ALS. *Neurological Research.* 34, 937–943.

Menezes de Oliveira, B., Matsumura, C.Y., Fontes-Oliveira, C.C., Gawlik, K.I., *et al.* 2014. Quantitative proteomic analysis reveals metabolic alterations, calcium dysregulation and increased expression of extracellular matrix proteins in laminin α2 chain-deficient muscle. *Molecular and Cellular Proteomics.* In press.

Menke, A. and Jockusch, H. 1991. Decreased osmotic stability of dystrophin-less muscle cells from the *mdx* mouse. *Nature*. 349, 69-71.

Mi, H., Muruganujan, A. and Thomas, P.D. 2013. PANTHER in 2013: modeling the evolution of gene function, and other gene attributes, in the context of phylogenetic trees. *Nucleic Acids Research.* 41, D377–D386.

Milardi, D., Grande, G., Vincenzoni, F., Castagnola, M., *et al.* 2013. Proteomics of human seminal plasma: identification of biomarker candidates for fertility and infertility and the evolution of technology. *Molecular Reproduction and Development.* 5, 350-357.

Minden, J. S. 2012. DIGE: past and future. *Methods of Molecular Biology.* 854, 3–8.

Minden, J.S., Dowd, S., Meyer, H.E. and Stühler, K. 2009. Difference gel electrophoresis. *Electrophoresis.* 30, 156-161.

Mitrpant, C., Flecther, S., Iverson, P.L. and Wilton, S.D. 2009. By-passing the non-sense mutation in the 4 CV mouse model of muscular dystrophy by induced exon skipping. *Journal of Gene Medicine.* 11, 46-56.

Mitsumoto, H., Brooks, B.R. and Silani, V. 2014. Clinical trials in amyotrophic lateral sclerosis: why so many negative trials and how can trials be improved? *Lancet Neurology*. 13: 1127–38

Moat, S.J., Bradley, D.M., Salmon, R., Clarke, A., *et al.* 2013. Newborn bloodspot screening for Duchenne muscular dystrophy: 21 years experience in Wales (UK). *European Journal of Human Genetics.* 21, 1049-1053.

Mok, G.F. and Sweetman. D. 2011. Many routes to the same destination: lessons from skeletal muscle development. *Reproduction.* 141, 301–312.

Monaco, A.P., Neve, R.L., Colletti-Feener, C., Bertelson, C.J., *et al.* 1986. Isolation of candidate cDNAs for portions of the Duchenne muscular dystrophy gene. *Nature.* 323, 646-650.

Moore, C.J. and Winder, S.J. 2012. The inside and out of dystroglycan post-translational modification. *Neuromuscular Disorders.* 22, 959-965

Moriggi, M., Cassano, P., Vasso, M., Capitanio, D., *et al.* 2008. DIGE approach for the assessment of rat *soleus* muscle changes during unloading: effect of acetyl-carnitine supplementation. *Proteomics.* 8, 3588–3604.

Morrison, L.A. 2011. Dystrophinopathies. *Handbook of Clinical Neuroogy.* 101, 11–39.

Moser, J.M., Bigini, P. and Schmitt-John, T. 2013. The wobbler mouse, an ALS animal model. *Molecular Genetics and Genomics.* 288, 207–229.

Mosqueira, M., Zeiger, U., Förderer, M., Brinkmeier, H., *et al.* 2013. Cardiac and respiratory dysfunction in Duchenne muscular dystrophy and the role of second messengers. *Medicinal Research Reviews.* 33, 1174-1213.

Moss, S.B., Challoner, P.B. and Groudine, M. 1989. Expression of a novel histone 2B during mouse spermiogenesis. *Developmental Biology.* 133, 83–92.

Mouisel, E., Vignaud, A., Hourde, C., Butler-Browne, G., *et al.* 2010. Muscle weakness and atrophy are associated with decreased regenerative capacity and changes in mTOR signaling in skeletal muscles of venerable (18-24-month-old) dystrophic *mdx* mice. *Muscle Nerve*. 41, 809-818.

Muntoni, F. 2003. Cardiomyopathy in muscular dystrophies. *Current Opinion in Neurology*. 16, 577-583.

Muntoni, F., Torelli, S. and Ferlini, A. 2003. Dystrophin and mutations: one gene, several proteins, multiple phenotypes. *Lancet Neurology.* 2, 731-740.

Murgia, M., Nagaraj, N., Deshmuka, A.S., Zeiler, M., *et al.* 2015. Single muscle fiber proteomics revelas unexpected mitochondrial specialization. *EMBO Reports.* 16, 387-395.

Musaro, A. 2013. Understanding ALS: new therapeutic approaches. *FEBS Journal*. 280, 4315-4322.

Muthu, M., Richardson, K.A. and Sutherland-Smith, A.J. 2012. The Crystal Structures of Dystrophin and Utrophin Spectrin Repeats: Implications for Domain Boundaries. *PLoS ONE*. 7(7), e40066.

Nadarajah, V.D., van Putten, M., Chaouch, A., Garrood, P., *et al.* 2011. Serum matrix metalloproteinase-9 (MMP-9) as a biomarker for monitoring disease progression in Duchenne muscular dystrophy (DMD). *Neuromuscular Disorders.* 21, 569-578.

Nakamura, A., Yoshida, K., Takeda, S., Dohi, N., *et al.* 2002. Progression of dystrophic features and activation of mitogen-activated protein kinases and calcineurin by physical exercise, in hearts of MDX mice. *FEBS Letters*. 520, 18–24.

Neuer, A., Spandorfer, S.D., Giraldo, P., Jeremias, J., *et al.* 1999. Heat shock protein expression during gametogenesis and embryogenesis. *Infectious Diseases in Obstetrics and Gynecology.* 7, 10–16.

Neuhoff, V., Arold, N., Taube, D., and Ehrhardt, W. 1988. Improved staining of proteins in polyacrylamide gels including isoelectric focusing gels with clear backgrounds at nanogram sensitivity using Coomssie Brilliant Blue G-250 and R- 250. *Electrophoresis.* 9, 255-262.

Nigro, G., Comi, L.I., Politano, L. and Bain, R.J. 1990. The incidence and evolution of cardiomyopathy in Duchenne muscular dystrophy. *International Journal of Cardiology.* 26, 271-277.

Nishimura, R.N. and Sharp, F.R. 2005. Heat shock proteins and neuromuscular disease. *Muscle Nerve*. 32, 693–709.

Norris, R.A., Damon, B., Mironov, V., Kasyanov, V., *et al.* 2007. Periostin regulates collagen fibrillogenesis and the biomechanical properties of connective tissues. *Journal of Cellular Biochemistry.* 101, 695-711.

Norwood, F.L., Sutherland-Smith, A.J., Keep, N.H. and Kendrick-Jones, J. 2000. The structure of the N-terminal actin-binding domain of human dystrophin and how mutations in this domain may cause Duchenne or Becker muscular dystrophy. *Structure*. 8, 481- 491.

Nudel, U., Zuk, D., Einat, P., Zeelon, E., *et al.* 1989. Duchenne muscular dystrophy gene product is not identical in muscle and brain. *Nature*. 337, 76-78.

Nuhr, M., Crevenna, R., Gohlsch, B., Bittner, C., *et al.* 2003. Functional and biochemical properties of chronically stimulated human skeletal muscle. *European Jourbal of Applied Physiol*ogy. 89, 202–208.

O'Farrell, P.H. 1975. High resolution two-dimensional electrophoresis of proteins. *J Biol Chem.* 250(10): 4007-4021.

Offen, D., Barhum, Y., Melamed, E., Embacher, N., *et al.* 2009. Spinal cord mRNA profile in patients with ALS: comparison with transgenic mice expressing the human SOD-1 mutant. *Journal of Molecular Neurosci*ence. 38, 85–93.

Ohlendieck, K. 2013. Proteomic identification of biomarkers of skeletal muscle disorders. *Biomarkers in Medicine*. 7, 169-186.

Ohlendieck, K. 2012. Proteomic profiling of skeletal muscle plasticity. *Muscles Ligaments Tendons Journal.* 1, 119–126.

Ohlendieck, K. 2011A. Proteomic Profiling of Fast-To-Slow Muscle Transitions during Aging. *Frontiers in Physiology.* 2, 105.

Ohlendieck, K. 2011B. Skeletal muscle proteomics: current approaches, technical challenges and emerging techniques. *Skeletal Muscle.* 1, 6.

Ohlendieck, K. 2010A. Proteomics of skeletal muscle differentiation, neuromuscular disorders and fibre aging. *Expert Reviews of Proteomics.* 7, 283-296.

Ohlendieck, K. 2010B. Proteomics of skeletal muscle glycolysis. *Biochimica et Biophysica Acta.* 1804, 2089–2101.

Ohlendieck, K. 1996. Towards an understanding of the dystrophin-glycoprotein complex: linkage between the extracellular matrix and the membrane cytoskeleton in muscle fibers. *European Journal of Cell Biology.* 69, 1-10.

Ohlendieck, K., Matsumura, K., Ionasescu, V.V., Towbin, J.A., *et al.* 1993. Duchenne muscular dystrophy: deficiency of dystrophin-associated proteins in the sarcolemma. *Neurology. 43,* 795-800.

Ohlendieck, K. and Campbell, K.P. 1991. Dystrophin-associated proteins are greatly reduced in skeletal muscle from *mdx* mice. *Journal of Cell Biology.* 115, 1685-1694.

Ohlendieck, K., Ervasti, J.M., Matsumura, K., Kahl, S.D., *et al.* 1991A. Dystrophin-related protein is localized to neuromuscular junctions of adult skeletal muscle. *Neuron*. 7, 499-508.

Ohlendieck, K., Ervasti, J.M., Snook, J.B. and Campbell, K.P. 1991B. Dystrophin-glycoprotein complex is highly enriched in isolated skeletal muscle sarcolemma. *Journal of Cell Biology*. 112, 135-148.

Ohta, M., Itagaki, Y., Itoh, N., Hayashi, K., *et al.* 1991. Carbonic anhydrase III in serum in muscular dystrophy and other neurological disorders: relationship with creatine kinase. *Clinical Chemistry*. 37, 36-39.

Okumura, N., Hashida-Okumura, A., Kita, K., Matsubae, M., *et al.* 2005. Proteomic analysis of slow- and fast-twitch skeletal muscles. *Proteomics.* 5, 2896–2906.

Oliva, R., de Mateo, S., Castillo, J., Azpiazu, R., *et al.* 2010. Methodological advances in sperm proteomics. *Human Fertility (Cambridge).* 13, 263–267.

Ottenheijm, C.A. and Granzier, H. 2010. Role of titin in skeletal muscle function and disease. *Advances in Experimental Medicine and Biology.* 682, 105-122.

Özdemire, C., Akpulat, U., Sharafi, P., Yildiz, Y., *et al.* 2014. Periostin is temporally expressed as an extracellular matrix component in skeletal muscle regeneration and differentiaton. *Gene.* 553, 130-139.

Paiardi, C., Pasini, M.E., Gioria, M. and Berruti, G. 2011. Failure of acrosome formation and globozoospermia in the wobbler mouse, a Vps54 spontaneous recessive mutant. *Spermatogenesis.* 1, 52–62.

Pal, R., Alves, G., Larsen, J.P. and Møller, S.G. 2014. New insight into neurodegeneration: the role of proteomics. *Molecular Neurobiology*. 49, 1181–1199.

Pane, M., Lombardo, M.E., Alfieri, P., D'Amico, A., *et al.* 2012. Attention deficit hyperactivity disorder and cognitive function in Duchenne muscular dystrophy: phenotype-genotype correlation. *Journal of Pediatrics.* 161, 705-709.

Pansarasa, O., Rossi, D., Berardinelli, A. and Cereda, C. 2014. Amyotrophic lateral sclerosis and skeletal muscle: an update. *Molecular Neurobiology*. 49, 984–990.

Pappas, C.T., Bliss, K.T., Zieseniss A. and Gregorio C.C. 2011. The Nebulin family: an actin support group. *Trends Cell Biology.* 21, 29-37.

Paratore, S., Pezzino, S. and Cavallaro, S. 2012. Identification of pharmacological targets in amyotrophic lateral sclerosis through genomic analysis of deregulated genes and pathways. *Current Genomics.* 13, 321–333.

Parker, K.C., Walsh, R.J., Salajegheh, M., Amato, A.A., *et al.* 2009. Characterization of human skeletal muscle biopsy samples using shotgun proteomics. *Journal of Proteome Research*. 8, 3265-3277.

Parte, P.P., Rao, P., Redij, S., Lobo, V., *et al.* 2012. Sperm phospho-proteome profiling by ultra performance liquid chromatography followed by data independent analysis (LC-MS(E)) reveals altered proteomic signatures in asthenozoospermia. *Journal of Proteomics.* 75, 5861–5871.

Partridge, T.A. 2011. Impending therapies for Duchenne muscular dystrophy. *Current Opinion of Neurology.* 24, 415–422.

Partridge, T.A., Morgan, J.E., Coulton, G.R., Hoffman, E.P., *et al.* 1989. Conversion of *mdx* myofibres from dystrophin-negative to-positive by injection of normal myoblasts. *Nature*. 337, 176-179.

Pasinetti, G.M., Ungar, L.H., Lange, D.J., Yemul, S., *et al.* 2006. Identification of potential CSF biomarkers in ALS. *Neurology*. 66, 1218–1222.

Passamano, L., Taglia, A., Palladino, A., Viggiano, E., *et al.* 2012. Improvement of survival in Duchenne muscular dystrophy: retrospective analysis of 835 patients. *Acta Myological*. 31, 121-125.

Pastoret, C. and Sebille, A. 1995. *MDX* mice show progressive weakness and muscle deterioration with age. *Journal of Neurological Science.* 129, 97- 105.

Patel, V.J., Thalassinos, K., Slade, S.E., Connolly, J.B., *et al.* 2009. A comparison of labeling and label-free mass spectrometry-based proteomic approaches. *Journal of Proteome Research.* 8, 3752-3759.

Peddinti, D., Nanduri, B., Kaya, A., Feugang, J.M., *et al.* 2008. Comprehensive proteomic analysis of bovine spermatozoa of varying fertility rates and identification of biomarkers associated with fertility. *BMC Syst. Biol. 2*, 19.

Percival, J.M., Siegel, M.P., Knowels, G. and Marcinek, D.J. 2013. Defects in mitochondrial localization and ATP synthesis in the *mdx* mouse model of Duchenne muscular dystrophy are not alleviated by PDE5 inhibition. *Human Molecular Genetics.* 22, 153–167.

Perez-Victoria, F.J., Abascal-Palacios, G., Tascon, I., Kajava, A., *et al.* 2010. Structural basis for the wobbler mouse neurodegenerative disorder caused by mutation in the Vps54 subunit of the GARP complex. *Proceeding of the National Academy of Science U.S.A*. 107, 12860–12865.

Pernemalm, M., Lewensohn, R. and Lehtio, J. 2009. Affinity pre-fractionation for MS-based plasma proteomics. *Proteomics*. 6, 1420-1427.

Perrin, A., Coat, C., Nguyen, M.H., Talagas, M., *et al.* 2013. Molecular cytogenetic and genetic aspects of globozoospermia: a review. *Andrologia.* 45, 1–9.

Perrin, F.E., Boisset, G., Lathuilière, A. and Kato, A.C. 2006. Cell death pathways differ in several mouse models with motoneurone disease: analysis of pure motoneurone populations at a presymptomatic age. *Journal of Neurochem*istry. 98, 1959–1972.

Pette, D. and Staron, R.S. 2001. Transitions of muscle fiber phenotypic profiles. *Histochemistry and Cell Biology*. 115, 359–372.

Pette, D. and Staron, R.S. 2000. Muscle isoforms, muscle fibre types and transitions. *Microscopy Research and Technique.* 50(6), 500-509.

Piec, I., Listrat, A., Alliot, J., Chambon, C., *et al.* 2005. Differential proteome analysis of aging in rat skeletal muscle. *FASEB Journal.* 19, 1143–1145.

Pieper, R., Gatlin, C.L., Makusky, A.J., Russo, P.S., *et al*. 2003. The human serum proteome: Display of nearly 3700 chromatographically separated protein spots on two-dimensional electrophoresis gels and identification of 325 distinct proteins. *Proteomics*. 3, 1345-1364.

Pollin, M.M., McHanwell, S. and Slater, C.R. 1990. Loss of motor neurons from the median nerve motor nucleus of the mutant mouse 'wobbler'. *Journal of Neurocytology.* 19, 29-38

Porambo, J.R., Salicioni, A.M., Visconti, P.E. and Platt, M.D. 2012. Sperm phosphoproteomics: historical perspectives and current methodologies. *Expert Review of Proteomics.* 9, 533–548.

Pratt, A.J., Getzoff, E.D. and Perry, J.J. 2012. Amyotrophic lateral sclerosis: update and new developments. Degener Neurological and Neuromuscular Disorders. 2, 1–14.

Proenza, C., O'Brien, J., Nakai, J., Mukherjee, S., *et al.* 2002. Identification of a region of the RyR1 that participates in allosteric coupling with alpha1s(Cav1.1) 2-3 loop. *Journal of Biological Chemistry.* 227, 6530-6535.

Quinlan, J.G., Hahn, H.S., Wong, B.L., Lorenz, J.N., *et al.* 2004. Evolution of the *mdx* mouse cardiomyopathy: physiological and morphological findings. *Neuromuscular Disorders*. 14, 491-496.

Rabilloud, T., Strub, J.M., Luche, S., Dorsselaer, A., *et al.* 2001. A comparison between Sypro Ruby and ruthenium II tris(bathophenanthroline disulfonate) as fluorescent stains for protein detection in gels. *Proteomics.* 5, 699-704.

Raddatz, K., Albrecht, D., Hochgräfe, F., Hecker, M., *et al.* 2008. A proteome map of murine heart and skeletal muscle. *Proteomics.* 8, 1885-1897.

Rahimov, F. and Kunkel, L.M. 2013. Cellular and molecular mechanisms underlying muscular dystrophy. *Journal of Cell Biology.* 201, 499-510.

Rahman, M.S., Lee, J.S., Kwon, W.S. and Pang, M.G. 2013. Sperm proteomics: road to male fertility and contraception. *Int. J. Endocrinol.* 360986.

Ramasamy, P., Murphy, C.C., Clynes, M., Horgan, N., *et al.* 2014. Proteomics is uveal melanoma. *Experimental Eye Research.* 118, 1-12.

Ranganathan, S., Williams, E., Ganchev, P., Gopalakrishnan, V., *et al.* 2005. Proteomic profiling of cerebrospinal fluid identifies biomarkers for amyotrophic lateral sclerosis. *Journal of Neurochemistry.* 95, 1461–1471.

Rappsilber, J. 2011. The beginning of a beautiful friendship: cross-linking/mass spectrometry and modeling of proteins and multi-protein complexes. *Journal of Structural Biology.* 173, 530-540.

Rayavarapu, S., Coley, W., Cakir, E., Jahnke, V., *et al.* 2013. Identification of disease specific pathways using in vivo SILAC proteomics in dystrophin deficient *mdx* mouse. *Molecular and Cell Proteomics.* 12, 1061–1073.

Reddy, S. and Comai, L. 2012. Lamin A, farnesylation and aging. *Experimental Cell Research.* 318, 1–7.

Renjini, R., Gayathri, N., Nalini, A. and Srinivas-Bharath, M.M. 2012. Oxidative damage in muscular dystrophy correlates with the severity of the pathology: role of glutathione metabolism. *Neurochemistry Research.* 37, 885–898.

Richardson, M.R., Lai, X., Mason, S.B., Miller, S.J., *et al.* 2008. Differential protein expression during aging in ventricular myocardium of Fischer 344 x Brown Norway hybrid rats. *Experimental Gerontology.* 43, 909–918.

Roberds, S.L., Anderson, R.D., Ibraghimov-Beskrovnaya, O. and Campbell, K.P. 1993. Primary structure and muscle-specific expression of the 50-kDa dystrophin-associated glycoprotein (adhalin). *Journal of Biological Chemistry.* 268, 23739-23742.

Romfh, A. and McNally, E.M. 2010. Cardiac assessment in Duchenne and Becker muscular dystrophies. *Current Heart Failure Reports.* 7, 212–218.

Rouillon, J., Poupiot, J., Zocevic, A., Amor, F., *et al.* 2015. Serum proteomic profiling reveals fragments of MYOM3 as potential biomarkers for monitoring the outcome of therapeutic interventions in muscular dystrophies. *Human Molecular Genetics.* Epub ahead of eprint.

Rouillon, J., Zocevic, A., Leger, T., Garcia, C., *et al.* 2014. Proteomics profiling of urine reveals specific titin fragments as biomarkers of Duchenne muscular dystrophy. *Neuromuscular Disorders.* 24, 563-573.

Rowland, L.P. and Shneider, N.A. 2001. Amyotrophic lateral sclerosis. *New England Journal of Medicine.* 334, 1688-1700.

Rybakova, I.N. and Ervasti, J.M. 1997. Dystrophin-glycoprotein complex is monomeric and stabilizes actin filaments *in vitro* through lateral as- sociation. *Journal of Biological Chemistry.* 272, 28771-28778.

Ryberg, H., An, J., Darko, S., Lustgarten, J.L., *et al.* 2010. Discovery and verification of amyotrophic lateral sclerosis biomarkers by proteomics. *Muscle Nerve*. 42, 104–111.

Sabatelli, P., Gualandi, F., Gara, S.K., Grumati, P., *et al.* 2012. Expression of collagen VI α5 and α6 chains in human muscle and in Duchenne muscular dystrophy-related muscle fibrosis. *Matrix Biology.* 31, 187-196.

Sadoulet-Puccio, H.M. and Kunkel, L.M. 1996. Dystrophin and its isoforms. *Brain Pathology.* 6, 25-35.

Sadoulet-Puccio, H.M., Feener, C.A., Schaid, D.J., Thibodeau, S.N., *et al.* 1997. The genomic organization of human dystrobrevin. *Neurogenetics*. 1, 37-42.

Sadoulet-Puccio, H.M., Rajala, M. and Kunkel, L.M. 1997. Dystrobrevin and dystrophin: An interaction through coiled-coil motifs. *Proceedings of the National Academy of Science, USA*. 94, 12413-12418.

Sapp, J.L., Bobet, J. and Howlett, S.E. 1996. Contractile properties of myocardium are altered in dystrophin-deficient *mdx* mice. *Journal of the Neurological Sciences.* 142, 17-24.

Schiaffino, S. and Reggiani, C. 2011. Fiber types in mammalian skeletal muscles. *Physiological Reviews.* 91, 1447-1531.

Schiaffino, S., Dyar, K.A., Ciciliot, S., Blaauw, B., *et al.* 2013. Mechanisms regulating skeletal muscle growth and atrophy. *FEBS Journal.* 280, 4294–4314.

Schmitt-John, T., Drepper, C., Mussmann, A., Hahn, P., *et al.* 2005. Mutation of Vps54 causes motor neuron disease and defective spermiogenesis in the wobbler mouse. *Nature Genetics.* 37, 1213–1215.

Schreiber, D. and Ohlendieck, K. 2007. Oligomerisation of sarcoplasmic reticulum Ca^{2+}-ATPase monomers from skeletal muscle. *Protein & Peptide Letters.* 14, 219–226.

Seale, P., Sabourin, L.A., Girgis-Gabardo, A., Mansouri, A., *et al.* 2000. Pax7 is required for the specification of myogenic satellite cells. *Cell*. 102(6), 777–786.

Secciani, F., Bianchi, L., Ermini, L., Cianti, R., *et al.* 2009. Protein profile of capacitated versus ejaculated human sperm. *Journal of Proteome Research.* 8, 3377–3389.

Sedehizade, F., Klocke, R. and Jockusch, H. 1997. Expression of nerve-regulated genes in muscles of mouse mutants affected by spinal muscular atrophies and muscular dystrophies. *Muscle Nerve*. 20, 186–194.

Selbert, S., Fischer, P., Menke, A., Jockusch, H., *et al.* 1996. Annexin VII relocalization as a result of dystrophin deficiency. *Experimental Cell Research.* 1222, 199–208.

Sellers, J.R. 2004. Fifty years of contractility research post sliding filament hypothesis. *Journal of Muscle Research and Cellular Motility.* 25, 475-482.

Selsby, J.T. 2011. Increased catalase expression improves muscle function in *mdx* mice. *Experimental Physiology.* 96, 194–202.

Seo, Y., Lee, R., Park, K., Bae, K., *et al.* 2006. A proteomic assessment of muscle contractile alterations during unloading and reloading. *Journal of Biochemistry.* 139, 71–80.

Shaw, P.J. and Wood-Allum, C. 2010. Motor neurone disease: a practical update on diagnosis and management. *Clinical Medicine.* 10, 252-258.

Shevchenko, A., Tomas, H., Havlis, J., Olsen, J.V., *et al.* 2006. In-gel digestion for mass spectrometric characterization of proteins and proteomes. *Nature protocols.* 6, 2856-2860.

Shin, J., Tajrishi, M.M, Ogura, Y. and Kumar, A. 2013. Wasting mechanisms in muscular dystrophy. *The International Journal of Biochemistry and Cell Biology.* 45, 2266-2279.

Shioi, T. and Inuzuka, Y. 2012. Aging as a substrate of heart failure. *Journal of Cardiology.* 60, 423–428.

Shtilbans, A., Choi, S.G., Fowkes, M.E., Khitrov, G., *et al.* 2011. Differential gene expression in patients with amyotrophic lateral sclerosis. *Amyotrophic Lateral Sclerosis.* 12, 250–256.

Sicinski, P., Geng, Y., Ryder-Cook, A.S., Barnard, E.A., *et al.* 1989. The molecular basis of muscular dystrophy in the mdx mouse: a point mutation. *Science*. 244, 1578–1580.

Smathers, R.L. and Petersen, D.R. 2011. The human fatty acid-binding protein family: evolutionary divergences and functions. *Human Genomics.* 5, 170–191.

Smith, J.P., Hicks, P.M., Ortiz, L.R., Martinez, M.J., *et al.* 1995. Quantitative measurement of muscle strength in the mouse. *Journal of Neuroscience Methods.* 62, 15–19.

Sosa, B.A., Kutay, U. and Schwartz, T.U. 2013. Structural insights into LINC complexes. *Current Opinion in Structural Biol*ogy. 23, 285–291.

Spangenburg, E.E. and Booth, F.W. 2003. Molecular regulation of individual skeletal muscle fibre types. *Acta Physiologica Scandinavica*. 178, 413–424.

Spurney, C.F., Gordish-Dressman, H., Guerron, A.D., Sali, A., *et al.* 2009. Preclinical drug trials in the mdx mouse: assessment of reliable and sensitive outcome measures. *Muscle Nerve*. 39, 591-602.

Spurney, C.F., Knoblach, S., Pistilli, E.E., Nagaraju, K., *et al.* 2008. Dystrophin-deficient cardiomyopathy in mouse: expression of Nox4 and Lox are associated with fibrosis and altered functional parameters in the heart. *Neuromuscular Disorders.* 18, 371–381.

Stanton, P.G., Sluka, P., Foo, C.F., Stephens, A.N., *et al.* 2012. Proteomic changes in rat spermatogenesis in response to in vivo androgen manipulation; impact on meiotic cells. *PLoS One*. 7, e41718.

Staples, G.O., Bowman, M.J., Costello, C.E.,Hitchcock, A.M., *et al.* 2009. A chip-based amide-HILIC LC/MS platform for glycosaminoglycan glycomics profiling. *Proteomics*. 9: 686-695.

Staunton, L., Jockusch, H. and Ohlendieck, K. 2011. Proteomic analysis of muscle affected by motor neuron degeneration: the wobbler mouse model of amyotrophic lateral sclerosis. *Biochemicia et Biophysica Research Communication*. 406, 595–600.

Staunton, L., Zweyer, M., Swandulla, D. and Ohlendieck, K. 2012. Mass spectrometry-based proteomic analysis of middle-aged vs. aged *vastus lateralis* reveals increased levels of carbonic anhydrase isoform 3 in senescent human skeletal muscle. *International Journal of Molecular Medicine.* 30, 723–733.

Stedman, H.H., Sweeney, H.L., Shrager, J.B., Maguire, H.C., *et al.* 1991. The *mdx* mouse diaphragm reproduces the degenerative changes of Duchenne muscular dystrophy. *Nature*. 352, 536-539.

Stuckey, D.J., Carr, C.A., Camelliti, P., Tyler, D.J., *et al.* 2012. In vivo MRI characterization of progressive cardiac dysfunction in the *mdx* mouse model of muscular dystrophy. *PLoS One.* 7, e28569.

Sun, H., Liu, J., Ding, F., Wang, X., *et al.* 2006. Investigation of differentially expressed proteins in rat gastrocnemius muscle during denervation–reinnervation. *Journal of Muscle Research & Cell Motility*. 27, 241–250.

Sutovsky, P. 2009. Proteomic analysis of mammalian gametes and sperm-oocyte interactions. *Society for Reproduction and Fertility Supplement.* 66, 103–116.

Szőke, D. and Panteghini, M. 2012. Diagnostic value of transferrin. *Clinica Chimica Acta.* 413, 1184–1189.

Tanaka, F., Ikenaka, K., Yamamoto, M. and Sobue, G. 2012. Neuropathology and omics in motor neuron diseases. *Neuropathology*. 32, 458–462.

Tedesco, F.S. 2015. Human artificial chromosomes for Duchenne muscular dystrophy and beyond: challenges and hopes. *Chromosome Research.* 23, 135-141.

Tennyson, C.N., Klamut, H.J. and Worton, R.G. 1995. The human dystrophin gene requires 16 hours to be transcribed and is cotranscriptionally spliced. *Nature Genetics.* 9, 184-190.

Thanh, L.T., Man, N.T., Helliwell, T.R. and Morris, G.E. 1995. Characterization of revertant muscle fibers in Duchenne muscular dystrophy, using exon-specific monoclonal antibodies against dystrophin. The *American Journal of Human Genetics.* 56, 725-731.

Tidball, J.G. and Wehling-Henricks, M. 2007. The role of free radicals in the pathophysiology of muscular dystrophy. *Journal of Applied Physiology.* 102, 1677–1686.

Tinsley, J.M., Blake, D.J. and Davies, K.E. 1993. Apo-dystrophin 3: a 2.2 kb transcript from the DMD locus encoding the dystrophin glycoprotein binding site. *Human Molecular Genetics.* 2, 521-524.

Toigo, M., Donohoe, S., Sperrazzo, G., Jarrold, B., *et al.* 2005. ICAT–MS–MS time course analysis of atrophying mouse skeletal muscle cytosolic subproteome. *Molecular Biosyst*ems. 1, 229–241.

Tomar, A.K., Saraswat, M., Chhikara, N., Kumar, S., *et al.* 2010. Differential proteomics of sperm: insights, challenges and future prospects. *Biomarkers in Medicine.* 4, 905–910.

Torres, L.F. and Duchen, L.W. 1987. The mutant *mdx*: inherited myopathy in the mouse. Morphological studies of nerves, muscles and end-plates. *Brain*. 110, 269-299.

Towbin, H., Staehelin, T., Gordon, J. 1979. Electrophoretic transfer of proteins from polyacrylamide gels to nitrocellulose sheets, procedure and some applications. *Proceedings of the National Academy of Sciences.* 76, 4350-4354.

Trappe, S., Harber, M., Creer, A., Gallagher, P., *et al.* 2006. Single muscle fiber adaptations with marathon training. *Journal of Applied Physiology*. 101, 721–727.

Traynor, B.J., Alexander, M., Corr, B., Frost, E., *et al.* 2003. Effect of a multidisciplinary amyotrophic lateral sclerosis (ALS) clinic on ALS survival: a population based study, 1996-2000. *Journal of Neurology Neurosurgery Psychiatry.* 74, 1258-1261.

Turkheimer, F.E., Leech, R., Expert, P., Lord, L.D., *et al.,* 2015. The brain's code and its canonical computational motifs. From sensory cortex to the default mode network: A multi-scale model of brain function in health and disese. *Neuroscience Biobehavourial Reviews.* 55, 211-222.

Vainzof, M., Ayub-Guerrieri, D., Onofre, P.C., Martins, P.C., *et al.* 2008. Animal models for genetic neuromuscular diseases. *Journal of Molecular Neuroscience*. 34, 241-248.

Valentine, J.S., Doucette, P.A. and Potter S.Z. 2005. Copper-Zinc Superoxide Dismutase and Amytrophic Lateral Sclerosis. *Annu Rev. Biochem.* 74, 563-93.

Vallejo-Illarramendi, A., Toral-Ojeda, I., Aldanondo, G. and López de Munain, A. 2014. Dysregulation of calcium homeostasis in muscular dystrophies. *Expert Reviews in Molecular Medicine.* 16, e16, doi:10.1017/erm.2014.17

van Erp, C., Loch, D., Laws, N., Trebbin, A., *et al.* 2010. Timeline of cardiac dystrophy in 3-18-month-old *mdx* mice. *Muscle and Nerve*. 42, 504-513.

Verhaart, I.E.C., van Duijn, R.J.M., den Adel, B., Roest, A.A., *et al.* 2012. Assessment of cardiac function in three mouse dystrophinopathies by magnetic resonance imaging. *Neuromuscular Disorders*. 22, 418-426.

Verhaert, D., Richards, K., Rafael-Fortney, J.A. and Raman, S.V. 2011. Cardiac involvement in patients with muscular dystrophies: magnetic resonance imaging phenotype and genotypic considerations. *Circulation: Cardiovascular Imaging.* 4, 67–76.

Vidal, B., Serrano, A.L., Tjwa, M., Suelves, M., *et al.* 2008. Fibrinogen drives dystrophic muscle fibrosis via a TGFbeta/alternative macrophage activation pathway. *Genetics and Development.* 22, 1747-1752.

Walther, T.C. and Mann, M. 2010. Mass spectrometry-based proteomics in cell biology. *Journal of Cell Biology.* 4, 491-500.

Wang, G., Guo, Y., Zhou, T., Shi, X., *et al.* 2013. In-depth proteomic analysis of the human sperm reveals complex protein compositions. *Journal of Proteomics.* 79, 114–122.

Wang, J. and Pantopoulos, K. 2011. Regulation of cellular iron metabolism. *Biochemical Journal.* 434, 365–381.

Wang, K., Huang, C. and Nice, E. 2014. Recent advances in proteomics: towards the human proteome. *Biomedical Chromatography.* 28, 848-857.

Wang, Y. and Pessin, J.E. 2013. Mechanisms for fiber-type specificity of skeletal muscle atrophy. *Current Opinion in Clinical Nutrition and Metabolic Care*. 16, 243–250.

Wang, Y., Marino-Enriques, A., Bennett, R.R., Zhu, M., *et al.* 2014. Dystrophin is a tumor suppressor in human cancers with myogenic programs. *Nature Genetics*. 46, 601-606.

Waterlow, J. 1976. The relative importance of muscle protein synthesis and breakdown in the regulation of muscle mass. *Journal of Biochemistry*. 156, 185-188.

Watkins, S.C., Hoffman, E.P., Slayter, H.S. and Kunkel, L.M. 1988. Immunoelectron microscopic localization of dystrophin in myofibres. *Nature*. 333, 863-866.

Wehking-Hendrick, M., Jordan, M.C., Roos, K.P., Deng, B., *et al.* 2005. Cardiomyopathy in dystrophin-deficient hearts is prevented by expression of a neuronal nitric oxide synthase transgene in the myocardium. *Human Molecular Genetics.* 14, 1921-1933.

Weller, B., Karpati, G. and Carpenter, S. 1990. Dystrophin-deficient *mdx* muscle fibers are preferentially vulnerable to necrosis induced by experimental lengthening contractions. *Journal of Neurological Science.* 100, 9-13.

Wells, D.J. and Wells, K.E. 2002. Gene transfer studies in animals: what do they really tell us about the prospects for gene therapy in DMD? *Neuromuscular Disorders.* 12, S11-S22

Wijesekera, L.C. and Leigh, P.N. 2009. Amyotrophic lateral sclerosis. *Orphanet Journal of Rare Diseases*. 4, 3.

Wilhelm, M., Schlegl, J., Hahne, H., Moghaddas Gholami, A., *et al.* 2014. Mass-spectrometry-based draft of the human proteome. *Nature.* 509, 582-587.

Williams, I.A. and Allen, D.G. 2007. The role of reactive oxygen species in the hearts of dystrophin-deficient *mdx* mice. *American Journal of Physiology, Heart and Circulatory Physiology.* 293, H1969–H1977.

Wilson, R.C., Hughes, R.C., Flatt, J.W., Meehan, E.J., *et al.* 2009. Structure of full-length ubiquitin-conjugating enzyme E2–25K (huntingtin-interacting protein 2). *Acta Crystallographia Section F: Structural Biology Crystallization Communications.* 65, 440–444.

Wright, P.C., Noirel, J., Ow, S.Y. and Fazeli, A. 2012. A review of current proteomics technologies with a survey on their widespread use in reproductive biology investigations. *Theriogenology*. 77, 738-765.

Wu, B., Moulton, H.M., Iversen, P.L., Jiang, J., *et al.* 2008. Effective rescue of dystrophin improves cardiac function in dystrophin-deficient mice by a modified morpholino oligomer. *Proceedings of the National Academy of Sciences USA*. 105, 14814-14919.

Wu, C.Y., Whye, D., Glazewski, L., Choe, L., *et al.* 2011. Proteomic assessment of a cell model of spinal muscular atrophy. *BMC Neuroscience* 12, 25.

Xu, W., Hu, H., Wang, Z., Chen, X., *et al.* 2012. Proteomic characteristics of spermatozoa in normozoospermic patients with infertility. *Journal of Proteomics*. 75, 5426–5436.

Yin, H., Price, F. and Rudnicki, M.A. 2013. Satellite cells and the muscle stem cell niche. *Physiology Reviews.* 93, 23–67.

Yoshida, M., Noguchi, S., Wakabayashi, E., Piluso, G., *et al.* 1997. The fourth component of the sarcoglycan complex. *FEBS Letters*. 403, 143-148.

Yue, Y., Li, Z., Harper, S.Q, Davisson, R.L., *et al.* 2003. Microdystrophin gene therapy of cardiomyopathy restores dystrophin-glycoprotein complex and improves sarcolemma integrity in the *mdx* mouse heart. *Circulation.* 108, 1626-1632.

Zakeri, Z.F. and Wolgemuth, D.J. 1987. Developmental-stage-specific expression of the hsp70 gene family during differentiation of the mammalian male germ line. *Molecular and Cellular Biology*. 7, 1791–1796.

Zanotti, S., Saredi, S., Ruggieri, A., Fabbri, M., *et al.* 2007. Altered extracellular matrix transcript expression and protein modulation in primary Duchenne muscular dystrophy myotubes. *Matrix Biology.* 26, 615-624.

Zatz, M., Rapaport, D., Vainzof, M., Passos-Bueno, M.R., *et al.* 1991. Serum creatine-kinase (CK) and pyruvate-kinase (PK) activities in Duchenne (DMD) as compared with Becker (BMD) muscular dystrophy. *Journal of the Neurological Sciences*. 102, 190-196.

Zhai, J., Ström, A.L., Kilty, R., Venkatakrishnan, P., *et al.* 2009. Proteomic characterization of lipid raft proteins in amyotrophic lateral sclerosis mouse spinal cord. *FEBS Journal*. 276, 3308–3323.

Zhang, W., ten Hove, M., Schneider, J.E., Stuckey, D.J., *et al.* 2008. Abnormal cardiac morphology, function and energy metabolism in the dystrophic *mdx* mouse: an MRI and MRS study. *Journal of Molecular Cell and Cardiology.* 45*,* 754–760.

Zhao, P., Sharma, A.C. and Ren, J. 2009. Pathogenesis and therapy of autoimmunity-induced dilated cardiomyopathy. *Frontiers in Bioscience.* 14, 1708–1715.

Zolotarjova, N., Mrozinski, P., Chen, H. and Martosella, J. 2008. Combination of affinity depletion of abundant proteins and reversed-phase fractionation in proteomic analysis of human plasma/serum. *Journal of Chromatography A*. 2, 332-338.